SUBSURFACE IDENTIFICATION USING ACTIVE MASW SURVEY: RESOLUTION OF DISPERSION IMAGE

A Thesis

Submitted in Partial Fulfillment of the Requirements

for the Degree of

DOCTOR OF PHILOSOPHY

by

Jumrik Taipodia

Department of Civil Engineering

Indian Institute of Technology Guwahati

Guwahati – 781039, India

SEPTEMBER 2018

STATEMENT

I do hereby declare that the matter embodied in this thesis is the result of investigations carried out by me in and with the aid of the Department of Civil Engineering, Indian Institute of Technology Guwahati, Assam, India.

In keeping with the general practice of reporting scientific observations, due acknowledgements have been made wherever the work described is based on the findings of other investigators.

Date: **(Jumrik Taipodia)**

Place: IIT Guwahati

CERTIFICATE

This is to certify that the thesis entitled **"Subsurface Identification using Active MASW Survey: Resolution of Dispersion Image"** submitted by **Jumrik Taipodia,** Roll No. 11610401, to the Indian Institute of Technology, Guwahati, for the award of the degree of Doctor of Philosophy in Civil Engineering is a record of bonafide research work carried out by her under my supervision and guidance. The thesis work, in my opinion, has reached the requisite standard fulfilling the requirement for the degree of Doctor of Philosophy.

The results contained in this thesis have not been submitted in part or full to any other University or Institute for award of any degree.

Date:

Place: IIT Guwahati

(Dr. Arindam Dey)
Assistant Professor
Department of Civil Engineering
Indian Institute of Technology Guwahati
Guwahati-781039, India

ACKNOWLEDGEMENTS

I owe my sincere gratitude to a number of persons whose unending support and patronage enabled me to pursue my research studies and submit the thesis for PhD. First and foremost, I would like to express my heartfelt thanks and deep sense of gratitude to my thesis supervisor and research guide Dr. Arindam Dey, for his meticulous guidance, encouragement, patience and support during my entire PhD study. I am grateful to him for sparing his precious time and efforts throughout the entire work. I am highly obliged to him for all the insightful discussions, affection and kind suggestions, which helped me to complete the work successfully. I have been fortunate and blessed enough to have him as my research guide, whose able guidance and valuable advice will help me a long way in moulding my future career.

My gratitude is extended to doctoral committee members Prof. S. Sreedeep, Dr. A. Murali Krishna, Dr. Atanu Banerjee and Dr. Rohit Sinha for reviewing my work and providing their valuable inputs that helped in improving my thesis. I would also like to thank the other faculty members of Geotechnical engineering of Civil Engineering Department for their suggestions and support during my PhD. I owe great thanks to the staff of Geotechnical Engineering, particularly Mr. Hariram Upadhyay for his kind help in conducting the experiments. I thank all office staffs of Civil Engineering Department for their help and cooperation in pursuing my work.

I am extremely grateful to my family, relatives and friends for their unwavering love, encouragement and endless support throughout my education life. I cannot thank enough my well-wishers who continuously remembered me in their prayers.

My special thanks also go to Sibaji and Rajiv for helping me in MATLAB Coding for image processing.

I would also sincerely like to thank my friends Yagom, Madhurita, Jagori, Madhulatha, Milind, Paramveer, Shankar, Dipjyoti, Rajesh, Sudheer, Janarul, Rana, Romio, Chinu, Budha Ram, Shibayan and many others for their companionship, support and encouragement.

I would like to thank Dr. Mousumi Mukherjee, IIT Mandi for her valuable help in giving access to her MatLab codes for generating the analytical dispersion curves. I would also earnestly than the reviewers of the thesis, Prof. Deepankar Choudhury, IIT Bombay and Prof. Anand J Puppala, University of Texas, Arlington, for their thorough and minute scrutiny of the thesis which had led to substantial improvement in the clarity and quality of the same.

Finally, I thank the Almighty for this enriching journey.

Date: **JUMRIK TAIPODIA**

ABSTRACT

‘Multichannel Analysis of Surface Waves (MASW)’ is a non-destructive field seismic survey method used for the identification of soil stratification. The three primary steps of MASW survey comprise field data acquisition, dispersion analysis and inversion analysis. During data acquisition, the vibration signatures generated by active or passive sources are recorded by a series of geophone receivers arranged in a predefined array. In the dispersion analysis, the collected wavefield are further processed to obtain the unimodal or multimodal dispersion trends represented by the frequency-phase velocity relationships. The dispersion curve is further processed through the inversion analysis to obtain the shear wave velocity profile of the substrata in 1-D, 2-D or 3-D formats. The resolution of dispersion image plays a crucial role in governing the accuracy and reliability of the outcome. Resolution gets affected by several parameters related to data acquisition and data pre-processing. Further, a good resolution dispersion image aids in unambiguous identification of the dispersion curve which is the prime requirement for the inversion analysis. Incorrect identification of the dispersion curve will lead to erroneous subsurface stratification.

Based on the active MASW survey conducted on soil sites of varying stiffness characteristics, the thesis reports the influence of the data acquisition and pre-processing parameters to obtain a good resolution dispersion image. In this regard, raw wavefield signatures, generated by a 10 kg sledgehammer or 40 kg Propelled Energy Generator (PEG), were collected using a linear array of 12-or-24 numbers of 4.5 Hz geophones. Various receiver layouts and field configurations were considered, and wavefields were collected using various sampling frequencies and sampling lengths. The collected data were pre-processed by various filtering and muting techniques. Based on the obtained results, recommendations have been provided about the

choices of the data acquisition and data pre-processing parameters to achieve good resolution dispersion images. An exact representation of the dispersion curve is imperative to the accuracy of the shear wave velocity profile obtained from the data analysis. The quality of the dispersion trend is guided by the signal-to-noise (SNR) ratio. Conventional approach of manual extraction of dispersion curve from a dispersion image often leads to discrepancies owing to the erroneous selection of dispersion points leading to a low SNR ratio, thus leading to inaccurate subsoil stratification. Moreover, the manual extraction is subjective to the user discretion, leading to non-repeatability of the obtained outcome. This thesis reports the development of an image-processing based automated dispersion curve extraction strategy which can identify the exact occurrence of the local peak energies as the dispersion modes and overcomes the limitations of manual extraction technique. The extracted dispersion curve is subsequently subjected to inversion analysis, and the effects of various inversion parameters on the shear wave profiling have also been reported. The guidelines developed have been further used in a case study of Active MASW survey conducted along Jia Bharali river bed (a tributary of River Brahmaputra) for the proposed construction work of a 1.2 km long bridge along the new 4-lane road from Dolabari to Jamuguri connecting NH-37A with NH-52 in Tezpur, Assam. From the field study, the subsoil stratification along the proposed bridge alignment was determined which revealed top erodible riverbed sediment layer, thick soft soil layer with intermittent and perched boulder deposits, followed by deep seated bedrocks. Such findings would help in the planning and design of the foundations of the bridge piers.

Keywords: Active MASW survey; Data acquisition and preprocessing; Resolution; Dispersion image; Dispersion curve; Automated extraction; Inversion analysis; Shear wave velocity profile

TABLE OF CONTENTS

List of Figures

LIST OF TABLES

ABBREVIATIONS

MASW	Multichannel Analysis of surface waves
SASW	Spectral Analysis of Surface waves
DAQ	Data Acquisition System
SPT	Standard Penetration Test
CSW	Continuous Surface waves
PEG	Propelled Energy Generator
NEHRP	National Earthquake Hazard reduction Program
DC	Dispersion Curve
SNR	Signal to Noise ratio
1D	One Dimensional
2D	Two Dimensional
3D	Three Dimensional
MFAT	Multiple Filter Analysis Technique
PSD	Power Spectral Density
RAW	Rubber aided Weightdrop
RMSE	Root mean Square error
SODI	Selective Offset Dispersion Imaging
FODI	Full Offset Dispersion Imaging
ReMi	Refraction Microtremor
CMP	Common Midpoint
FFT	Fast Fourier Transform
lpi	Lines per inch
lpm	Lines per mm
dpi	Dots per inch

NOTATIONS

A_s	Summed up amplitude
Df	Widths of a dispersion band in terms of frequency
Dv	Widths of a dispersion band in terms of velocity
f1, f2, f3, f4	Cutoff frequencies of filters
f-c	Frequency-Phase Velocity
f-k	Frequency-wavenumber
f_s	Sampling frequency
h	Thickness of the initial model layer
L	Total length of array
M0	Fundamental Mode
M1	First order mode
n	Total number of samples recorded
N	SPT value
T	Sampling interval time
t	Time of acquisition
t-x	Time-space
V_{max}	Maximum Phase Velocity
V_{min}	Minimum Phase velocity
V_p	P-Wave velocity
V_s	Shear wave velocity
x	Inter receiver spacing
x_1	Offset distance
x_{far}	Far Offset
x_{near}	Near Offset
Z_{max}	Maximum depth of investigation
ΔV	Difference in maximum and minimum phase velocity
λ_{max}	Maximum Wave length
π-ω	Pi-omega transformation

CHAPTER 1

INTRODUCTION

1.1 General

Multichannel Analysis of Surface Waves (MASW) is a practical non-invasive seismic exploration method used for non-destructive subsurface-characterization. In comparison to the conventional borehole sounding tests, it is less expensive and provides the benefit of precision and swiftness to estimate the subsurface shear wave velocity profile over a large area within a short time. There are several non-destructive testing methodologies prevalent to identify the subsurface stratigraphy such as the Seismic Refraction Survey (Haeni, 1986), Ground Penetrating Radar (Griffin and Pippett, 2002), Nuclear Magnetic Resonance (Johnson and Hutchison, 1985) and Spectral Analysis of Surface Waves (Park *et al*., 1999). Each of the existing methods possess their inherent limitations and shortcomings. SRS is one of the earliest seismic methods that is based on the refraction of propagating waves from the interfaces of various soil layers. The major limitation of SRS in terms of its applicability is that each of the successive soil layers should have higher velocity than the shallower layer. The method proves to be improper for arbitrarily formed subsoil stratigraphy. Subsurface investigation using GPR is based on the variation of dielectric constants of various materials and reflectance of waves. Presence of higher clay content in soil increases attenuation of GPR signal, and adulterates the results. NMR is based on the excitation of protons in subsurface water by earth's magnetic field. This method proves to be ineffective in the presence of magnetic minerals in the stratum. SASW is based on the propagation of mechanically induced Rayleigh waves that operates on a two-

point receiver mechanism. This method is unable to estimate higher order of modes of vibration and the resolution of obtained data decreases beyond a depth of 10-15 m. Moreover, it is insensitive to sharp contrasts of density and velocity of stratum. With respect to these methods, MASW overcomes many of their basic deficiencies and hence, is becoming progressively popular. Unlike SRS, MASW survey can recognize and create an image for an arbitrarily formed stratigraphy, and is unaffected by the presence or absence of underlying or perched low velocity strata. Unlike NMR, MASW survey remains unaffected by the presence of magnetic minerals or alluvial clay layer. As MASW utilizes multiple geophones, unlike SASW, it aids in broader and intricate imaging of the entire terrain, with the provision to identify deeper subsurface stratifications.

The main objective of utilizing MASW as a seismic exploration method is to evaluate the 1-D, 2-D, or 3-D ground stiffness in terms of the variation of shear wave velocities. The principle of application of MASW falls within the purview of the assessment of the propagation velocity of seismic surface waves, which are recorded, analysed and processed to identify the variations of shear-wave velocity (V_s) within the surveyed area (Park *et al*. 2007). Shear wave velocity is a direct indicator of the ground stiffness and hence, can be suitably used to address various geotechnical engineering problems related to bearing capacity, dynamic response and liquefaction potential.

The depth of investigation, until which the variation of shear wave velocity is obtained, depends on the wavelengths propagating through the medium, which in turn, is governed by the technique adopted to produce the incident waves. Two techniques have been commonly employed for this

purpose, namely Active MASW and Passive MASW; the former utilizes controlled shocks, while the latter uses the uncontrolled ambient vibrations to generate the propagating waves. Any of the procedures of MASW survey consist of three basic steps: (i) Data Acquisition, the process of acquiring multichannel field records (commonly called shot gathers in conventional seismic exploration), (ii) Dispersion analysis, where the dispersion curves (describing the relation between the frequencies and phase velocities) are generated and extracted from the collected records, and (iii) Inversion analysis, which provides the spatial variation of shear wave velocity (Xia *et al*. 2000; Park *et al*. 2007). The determination of the shear wave velocity profile, however, is intricately complex from the point of view of analysing the raw signals, estimation of the dispersion images, extraction of the experimental dispersion curve, and, finally, the application of inversion analysis.

The foremost objective of using MASW technique is to obtain a high-resolution dispersion image. Resolution is significantly affected by the parameters contributing to the field surveys such as properties of the input source, parameters related to the receiver geophones such as its spacing, orientation, geometrical layout and other parameters related to the field configuration. The thesis provides a comprehensive review of Active MASW survey, with special emphasis on the parameters affecting the resolution of dispersion image. Based on the critical evaluation of the existing literature, several open issues and challenges related to the field surveys, data acquisition techniques, data processing and dispersion analyses are elucidated.

Active MASW survey is one of the geophysical seismic survey methods used for the evaluation of the elastic stiffness of the soil substrata. While conducting a MASW experiment, seismic

surface waves generated from various types of seismic or impulsive sources (e.g. sledge hammer, PEG hammer, blast and explosion) are recorded in an array of receivers placed linearly. Next, the recorded signals are analyzed as a whole to develop the dispersion image which indicates the phase velocity-frequency relationship for the particular soil strata along with the amount of energy carried by waves of particular phase velocity and frequency. The analysis for the propagation velocities of the surface waves are carried out to develop a dispersion curve by extracting the combinations of phase velocity and frequency carrying the highest energy. Finally, through a suitable inversion technique, the shear-wave velocity (V_s) variations below the surveyed area are determined (which is most responsible for the analyzed propagation velocity pattern of surface waves). Shear-wave velocity (V_s) is one of the elastic constants and closely related to shear modulus. Under most circumstances, V_s is a direct indicator of the ground strength (stiffness) and therefore commonly used to derive various geotechnical parameters and can be used in various geotechnical designs. The final V_s information can be provided in 1D, 2D, and 3D formats, depending on the conducted experimentations (as shown in Fig. 1.1). 1D analysis provides a variation of shear wave velocity over depth, while the 2D and 3D formats provide the image space depicting the spatial variability of shear wave velocity. The analysis results also help to identify the zones and demarcations of the substrata. An overview of the various steps in MASW survey, as outlined is portrayed in Fig. 1.2.

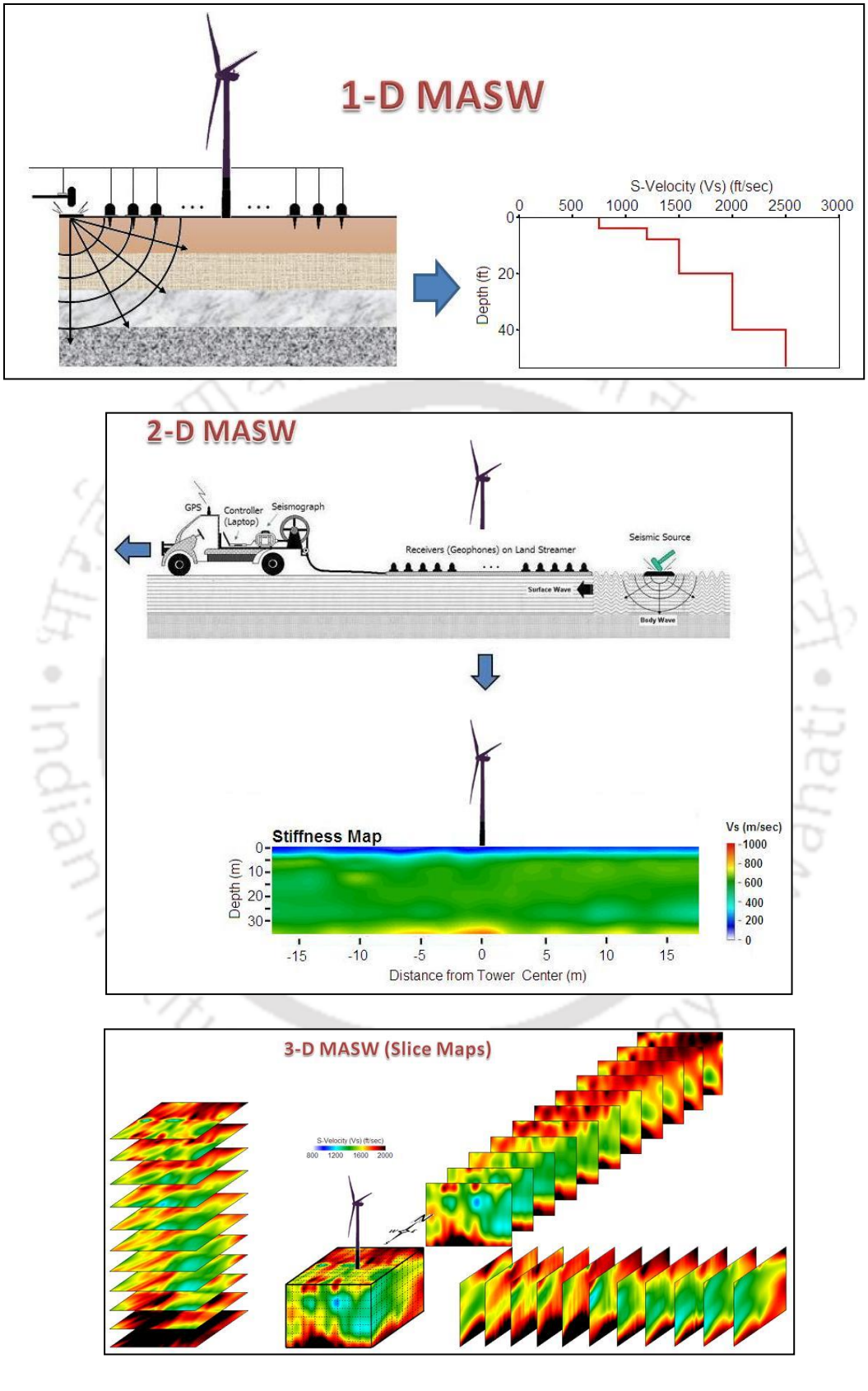

Fig. 1.1: 1-D, 2-D, and 3-D V_s mapping (Park *et al.* 2007)

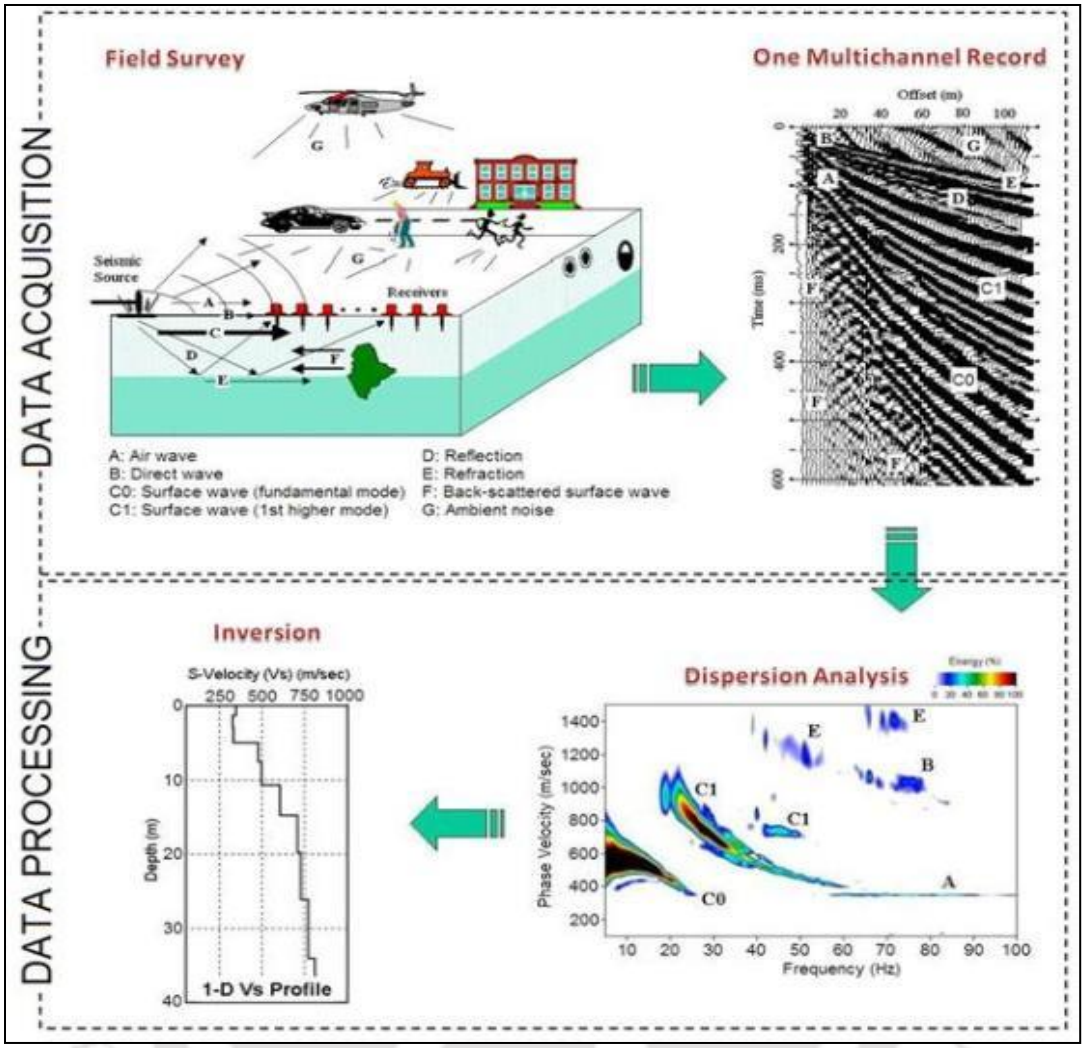

Fig. 1.2: Overall procedure of MASW survey (Park *et al.* 2007)

1.2 Motivation, Objective and Scope of the Present Study

The present work is carried out to evaluate the resolution (Park *et al*. 1998; Zhang *et al.* 2004) of the dispersion images obtained from Active MASW survey. It is realized that different field geometry/configurations yield different dispersion images and with varying resolutions. The aim is to find the most suitable dispersion images possessing the best resolution. The suitability is checked based on the visual observations and also based on the accuracy of the inverted shear

wave profile. Various data acquisition parameters affect the resolution of the images. Among data acquisition parameters, sampling frequency (Morlet *et al*. 1982; Park *et al.* 1999; Kanli *et al.* 2006; Gosar *et al*. 2008), offset distance (Park *et al*. 1999, 2002a; Park 2011), inter-receiver spacing (Dikmen *et al*. 2010; Park *et al*. 2002a), numbers of receivers (Park *et al.* 1998; Park *et al*. 1999; Park *et al*. 2001) and weight of impulse hammer (Park *et al*. 2002a) significantly affects the resolution of the dispersion images. Apart from the data acquisition parameters, the other parameter that affects the resolution are the preprocessing parameters such as filtering (Dzienwonski *et al*. 1969; Mitchell 1973; Park *et al.* 2002a; Moro *et al.* 2003), muting (Baker *et al*. 1998; Park *et al.* 2001; Ivanov *et al.* 2005) and dispersion image stacking (Louie, 2001; Schultz and Claerbout, 1978; Grandjean and Bitri, 2006; Socco *et al.* 2009, 2010).

It is observed from the critical appraisal of the literature that although there has been a significant research regarding active MASW survey, most of them are utilizing various parametric configurations in order to meet the requirements of the investigation. Very few literature attempts to provide recommendations related to the choice of various parameters in active MASW survey to enhance the reliability of the estimations. However, it is further revealed that there is a lack of consensus amongst the researchers regarding the choice of suitable parameters to obtain reliable subsurface profiles. The reliability of the outcome largely depends on the resolution of the dispersion image. Literature review revealed that, until date, the resolution of the dispersion images were primarily adjudged from visual inspection and inferences. The optimal or best suitable parameters were chosen based on visually appealing dispersion images. It is understandable that such visual identification of the characteristics is immensely subjected to user discretion, and is bound to vary with various users inspecting the same dispersion images.

Hence, it is necessary that the resolution of the dispersion images should be provided with a quantification support, and accordingly, the best suitable parameters can be chosen. Moreover, the reliability of the subsurface shear wave velocity profile also depends on the accuracy of extracted dispersion curve. SURFSEIS, used in the present, or any other commercial software available in the market concerning dispersion and inversion analysis, requires user intervention in selecting the dispersion points. As a result, shear wave velocity profiles is subjected to discrepancies, and has to face to the concerns of reliability and repeatability. Hence, it is highly necessary that an automated process be developed for the extraction of dispersion curves, so that the issues of subjectivity, reliability and repeatability can be avoided to the best possible extent. Such technique, if developed, can be integrated to the available dispersion and inversion analysis software, such as SURFSEIS, which would lead to results having more precision, accuracy and reliability.

Based on the above understanding, the primary objectives of present work are formulated as follows:

1. Determination of the suitable magnitudes of various data acquisition, preprocessing and data processing parameters, and development of guidelines and recommendations related to obtaining a good resolution dispersion image.
2. Development of an automated and precise dispersion curve extraction process to overcome the limitation of manual extraction based on visualization, and thus enhancing the reliability of the shear wave velocity profile estimates from the inversion process.

In order to meet the stated objectives, the scopes of the current work are listed as follows:

1. Conducting extensive active MASW survey at different locations in IIT Guwahati campus, comprising of different subsurface characteristics, considering varying data acquisition, preprocessing and processing parameters.
2. Application of commercial software SURFSEIS to conduct the dispersion and inversion analysis based on the collected wavefield.
3. Study the influence of data preprocessing parameters (filtering and muting) on the resolution of the dispersion images.
4. Study the influence of data acquisition parameters (sampling frequency, sample length, offset distance, inter-receiver spacing, array length, source energy, stacking, and striker plate material) on the resolution of the dispersion images.
5. Study the influence of dispersion image stacking on the generation of better resolution dispersion images
6. Utilization of the extracted dispersion curve in the inversion analysis and investigate the influence of extraction and inversion parameters (initial model, number of layers, specific frequency band selection, density of extraction points) on the accuracy of shear wave velocity (V_s) profile.
7. Establish a quantification of the resolution of the generated dispersion images to remove the subjectivity of visual inspection of resolution
8. Automate the extraction of dispersion curve from the experimental dispersion image with the aid of MATLAB 2D and 3D image processing techniques and representation.

1.3 Outline of the Dissertation

This dissertation is organized into nine chapters as per the following outline:

Chapter 1 presents the introduction to the problem and the importance of its outcome. The motivation to carry out the present work is also presented. The objectives and the scope of the research work, along with the organization of the dissertation is listed.

Chapter 2 deals with the background study and comprehensive literature review on the history and evolution of the Active MASW survey. This chapter elaborates the review related the data acquisition and data preprocessing parameters of Active MASW survey and its effects on the resolution of the dispersion images.

Chapter 3 provides the details of the experimental equipments and accessories used for the investigation. Details of the site locations used in performing the study are elucidated. The details of the software used for the analysis is also pictorially illustrated.

Chapter 4 reveals the influence of preprocessing parameters such as filtering and muting on the resolution of dispersion images. A briefing has been provided about the resolution of the dispersion images here. This chapter suggests the suitable value of filtering and muting to obtain better resolution dispersion images.

Chapter 5 highlights the influence of data acquisition parameters on the resolution of dispersion images, namely the offset distance, inter-receiver spacing, and total numbers of channels. The

most suitable values of the data acquisition parameters were reached based on the visual inspection of the resolution of dispersion image. The effect of the impulsive source and the composition of striker plate used on the obtained V_s profile are also demonstrated.

Chapter 6 discusses the influences of various inversion parameters on the accuracy of the estimated V_s profile. The effect of initial model, numbers and density of manually selected dispersion points and its corresponding frequency band have been investigated and reported.

Chapter 7 deals with the development of MatLab based image processing techniques to provide a quantification of the resolution of the dispersion image, which can be further used to identify the best suitable magnitudes of the contributing parameters. The chapter also elucidates the development of automated extraction scheme of the dispersion curve based on the image processing techniques applied on the dispersion image. The benefit and efficacy of the automated extraction scheme on the reliability of the outcomes from inversion analysis are duly explained.

Chapter 8 deals with a case study of Active MASW survey conducted along Jia Bharali river bed (a tributary of River Brahmaputra) for the proposed construction work of a 1.2 km long bridge along the new 4-lane road from Dolabari to Jamuguri connecting NH-37A with NH-52 in Tezpur, Assam. Based on the experience and knowledge gained, as reported in the preceding chapters, the field application helped to identify the shear wave velocity profiles at the pier and abutment locations along the alignment of the bridge. Moreover, 2-D V_s imaging along the entire stretch of the alignment revealed the subsurface information, with proper identification of the

perched and continuous soft and hard strata. The information will be used for the design and analysis of the proposed well foundations for the bridge piers and abutments.

Chapter 9 lists out the important conclusions and recommendations as an outcome of the present dissertation. The scope of the future work for further enhancement of research knowledge is also presented here.

The chapters are finally followed by a list of relevant references utilized for the understanding and preparation of the dissertation.

CHAPTER 2

BACKGROUND AND LITERATURE REVIEW

2.1 General

Multichannel Analysis of Surface Waves (MASW) is one of the popular and practical non-invasive seismic exploration method used for identification of subsurface stratification. The main outcome of utilizing MASW as a seismic exploration method is the evaluation of the 1-D, 2-D, or 3-D ground stiffness, in terms of the variation of shear wave velocities. The principle of application of MASW falls within the purview of the assessment of the propagation velocity of seismic surface waves, which are recorded, analysed and processed, to identify the variations of shear-wave velocity (V_s) within the surveyed area. Shear wave velocity is a direct indicator of the ground stiffness (Park *et al*. 2007) and hence, can be suitably used to address various geotechnical engineering problems related to bearing capacity, dynamic response and liquefaction potential (Andrus and Stokoe II 2000; Kayen *et al*. 2013). The depth of investigation, until which the variation of shear wave velocity is obtained, depends on the wavelengths propagating through the medium, which in turn, is governed by the technique adopted to produce the incident waves. It is worth mentioning that the amplitude/energy of Rayleigh wave decreases with depth, approximately reducing to 10% of the surface amplitude at a depth of 0.1 times the wavelength of the Rayleigh wave. Two techniques have been commonly employed for this purpose, namely Active MASW and Passive MASW; the former utilizes controlled shocks to generate the propagating waves, while the latter uses the uncontrolled ambient vibrations propagating through the medium. Any of the procedures of MASW survey consist of three basic steps: (i) Data Acquisition, the process of acquiring multichannel field

records (commonly called shot gathers in conventional seismic exploration), (ii) Dispersion analysis, where the dispersion curves (describing the relation between the frequencies and phase velocities) are generated and extracted from the collected records, and (iii) Inversion analysis, which provides the spatial variation of shear wave velocity (Xia *et al*. 2000; Park *et al*. 2007). The determination of the shear wave velocity profile, however, is intricately complex from the point of view of analysing the raw signals, estimation of the dispersion images, extraction of the experimental dispersion curve, and, finally, the application of inversion analysis.

The reliability of the outcome of the MASW survey, i.e. the subsurface shear wave velocity profile, depends largely on the resolution of the dispersion image obtained from the dispersion analysis. Resolution of a dispersion image is defined as the resolvable capabilities along both the velocity axis and the frequency axis. The resolution along the velocity axis represents the capability to discriminate a phase velocity from other velocities for a given frequency, and vice-versa (Park *et al*. 1998). A higher resolution dispersion image is instrumental in extracting a dispersion curve with higher precision, which leads to a reliable estimate of shear wave velocity profile through inversion analysis. Resolution of the dispersion image depends on the quality of collected and analysed records, which, in turn, are governed by several parameters, associated with the field data acquisition and collected data pre-processing. This chapter provides a comprehensive review of the Active MASW survey, with special emphasis on the resolution of dispersion image and its governing parameters. Based on the critical evaluation of the existing literature, several open issues and challenges related to the field surveys, data acquisition techniques, data processing and dispersion analyses are elucidated. This chapter provides a very fruitful chronological insight related to the gradual development of MASW technique, with

special emphasis on the effect of data acquisition and pre-processing parameters on the resolution of the dispersion image.

2.2 History of Surface Wave Methods

Surface-wave surveys commenced for the field of pavement engineering, to evaluate the pavement stiffness. The steady state vibration technique utilizing Rayleigh waves and employing single-receiver approach was used to find the thickness of the concrete pavement (Van der Poel 1951; Jones 1955). The pioneering steady state vibration technique was subsequently improved to make it more computationally efficient (Gordon 1997), and was, thereafter, mostly referred to as the Continuous Surface Wave (CSW) method (Matthews *et al*. 1996). The next advancement conforms to the two-receiver approach, commonly known as the Spectral Analysis of Surface Waves (SASW). Heisey *et al*. (1982) first introduced the SASW method for determining the moduli of materials used in pavements. Since then, various researchers applied the fundamental concepts of SASW for the evaluation of pavement thickness as well as for the geotechnical site characterization (Nazarian *et al*. 1987; Stokoe II *et al*. 1994). Although largely used, SASW method has several technical limitations. The primary shortcoming of the technique is its inability to identify the higher order modes-of vibration. Although SASW can provide shallow depth information, the resolution of the obtained V_s profile decreases beyond the depth of 10-15 m. It is insensitive to the sharp contrasts of density and velocity of the stratum. Difficulties also exist in evaluating and distinguishing the signal from noise with the usage of a single pair of receivers. The necessity of recording repeated shots for multiple field deployments at a given site increases the time and labour requirements to conduct a reliable SASW survey (Park *et al*. 1998).

Multichannel analysis of surface waves (MASW) overcomes many of the shortcomings of the SASW method (Park *et al*. 1999). In comparison to the SASW approach which is mostly based on the analysis of the fundamental mode (since the higher modes are nearly indistinguishable), MASW approach provides a dispersion image in which different modes can be easily identified. Unlike SASW, which is based on an active source technique, MASW has a scope of using passive sources as well, which generates low frequency waves, and thus considerably enhances the depth of investigations. Moreover, in comparison to SASW that primarily uses a single pair of geophones, deployment of multiple receivers during the MASW survey saves the labour and the time associated with the field investigation.

MASW method became popular in early 2000s among the geotechnical engineers. The term "MASW" was introduced by Park *et al*. (1999). The earliest usage of multichannel approach for surface waves was reported by Gabriels *et al*. (1987) for deducing the shear wave profile of tidal flats by analyzing the recorded surface waves using 24-channel acquisition system. Subsequently, Park *et al*. (1999) highlighted the effectiveness of the technique by detailing the advantages of multichannel acquisition and processing concepts most appropriate for the geotechnical engineering applications. The convenience in field operation and robustness in the data processing provided by diverse multichannel seismic data processing techniques were also emphasized. Soon after the concept of MASW was developed and its effectiveness was realised, the application of MASW was initiated for pavement investigation (Ryden *et al*. 2004; Forbriger 2003a, 2003b; Ryden and Lowe 2004) and site characterizations (Kanli *et al*. 2006; Xia *et al*. 2000). For data processing, various techniques have been used over the time namely the *f-k* method (Capon 1969), the π-ω transformations (McMechan and Yedlin 1981), and the phase-

shift method (Park *et al*. 1998). Xia *et al.* (1999) presented an algorithm to carry out inversion analysis to obtain the 1D shear wave velocity profile. The 1D profile obtained from a single linear array was considered most representative of the subsurface directly beneath the middle of the geophone spread. Multiple 1D plots of S-wave velocity with depth can be generated by continuously varying the position of the array. A 2D vertical cross-section of S-wave velocity is constructed by combining and suitably interpolating all the obtained 1D S-wave velocity profiles (Miller *et al*. 1999; Xia *et al*. 2000). Utilizing the 2D V_s mapping, several MASW case studies have been undertaken worldwide (Xia *et al*. 2000, 2004; Park *et al*. 2005; Kaufmann *et al*. 2005).

As the surface wave techniques gradually gained popularity among the researchers and geophysicists, a growing demand was experienced to increase the depth of investigation. Until 2000, MASW survey was carried out using an active seismic source, such as hammers, weight drops, electromechanical shakers, propelled energy generators (PEG) and bulldozers, wherein the source and rate of loading can be controlled by the user. Literature reveals that, in general, the maximum depth of investigation (governed by the wavelengths) was obtained as 20-30 m in the case of active MASW survey, since the waves generated from impacts comprise of comparatively higher frequencies, greater than 30 Hz (Park *et al*. 2002a, 2007; Gosar *et al*. 2008). In order to acquire information of deeper strata, the depth of investigation had to be increased beyond 30 m, which was attained by using low frequency surface waves (5-7 Hz). To generate waves of longer wavelengths (i.e. low frequencies) using active source, heavy weights capable of producing high impact energies have to be used so that high-energy accumulation is achieved at the lower frequency range. Application of very heavy weight systems, such as bulldozer or PEG, restricts the portability of the MASW approach, and thus renders it infeasible

and impractical. On the other hand, passive surface waves generated from natural (e.g., tidal motion, microtremors) or cultural (e.g., traffic) sources usually comprises of low-frequency waves (1–30 Hz), with wavelengths ranging beyond 30 m to several kilometres (Okada and Sakajiri 1983; Okada *et al*. 1990; Okada 2003; Park *et al*. 2007). Passive MASW utilizes such waves for subsoil survey, thus attaining larger penetration depths and allowing for deeper subsurface investigation. Application based on a similar concept originated during 1950s in Japan and was called the Microtremor Survey Method (MSM) utilizing limited number of receivers (usually 10) aided by a processing technique known as the Spatial Auto Correlation, or SPAC (Aki 1957). Later, Linear Refraction Microtremor survey (ReMi method) was introduced by Louie (2001) using a linear array of geophones, which at a stage later gave rise to the Passive Roadside MASW methods (Park *et al*. 2007).

Based on the existing literature, it can be observed that there has been a systematic development of surface wave methods starting with the Steady State vibration approach utilizing a single receiver, Spectral Analysis of Surface Waves (SASW) utilizing a two-receiver system, and the most modern Multichannel Analysis of Surface Waves (MASW) utilizing a multi-receiver array system. With the advancement in technology, the techniques of analyses have gradually evolved from the principles of surface wave refraction and, at present, include the dispersion of waves for the analyses and identification of subsurface stratification in terms of the shear wave velocity profile.

2.3 Procedure of Active MASW Survey

MASW survey primarily comprises of three stages to obtain the shear wave velocity profile viz. data acquisition from a field experimentation, dispersion analysis and inversion analysis, to obtain the shear wave velocity profile (Park *et al.* 1999, 2007). An active MASW involves impact sources (sledgehammers, bulldozers etc.) for the generation of surface waves. Multiple geophone receivers are placed on the ground surface in a linear array, wherein the motion of the soil particles generated by the propagating surface waves are captured (Park *et al*. 1998; Xia *et al*. 2004). Based on the obtained raw records, dispersion analysis is carried out to develop the dispersion image, which is a representation of the phase velocity-frequency-amplitude inter-relationship. From the obtained image, corresponding to each of the frequency magnitudes, the phase velocities with highest energy are delineated, and such plot between phase velocity and frequency is termed as the dispersion curve (Park *et al*. 1998, 2001). For an initial estimate of the shear wave velocity model, a theoretically generated dispersion curve is assumed (Schwab and Knopoff 1972), and the same is optimized towards the experimental dispersion curve through an adaptive iterative approach. During the iterations, the parameters of the earth model (*i.e.* shear wave velocity, depth of investigation, layer thickness and unit weight of the layers) are continuously updated, until the convergence criteria are satisfied. The finally obtained converged model is thereby considered as the subsurface shear wave velocity profile (Nazarian *et al*. 1983; Ganji *et al*. 1998; Xia *et al.* 1999, 2003). It is well understood that the accuracy of the inverted shear wave velocity profile is dependent upon the resolution of the dispersion image. The resolution of dispersion image, in turn, is dependent upon the data acquisition parameters such as offset distance (distance between the source and the first geophone of the array), receiver

spacing, weight of hammer, and preprocessing parameters (sampling frequency, filtering and muting parameters) (Park *et al*. 1999; Zhang *et al*. 2004).

2.4 Dispersion Analysis

Dispersion analysis is the first step of data processing in MASW (Park *et al*. 1999, 2007). Dispersion is the phenomenon related to the waves travelling with a gradually enhanced wave-front, each wave being characterized with different frequency, wavelength and phase velocity. In contrast to the earlier used wave analysis techniques (Park *et al*. 1998), the multichannel approach does not attempt to calculate the individual phase velocities corresponding to different frequencies; rather, constructs an image based on all types of propagating seismic waves, where the dispersion trends are identified from the pattern of energy accumulation. In this imaging process, with the application of Fast Fourier Transform (FFT), a multichannel record in time-space (*t*-*x*) domain is transformed into either frequency-wavenumber (*f*-*k*) or frequency-phase velocity (*f*-*C*) domain. There are three conventional transformation methods, namely: The traditional *f*-*k* method (Capon 1969), the π-ω transformations (McMechan and Yedlin 1981) and the phase-shift method (Park *et al.* 1998). It is revealed that the *f*-*k* method results in the lowest resolution image, whereas the phase-shift method (i.e. *f*-*C* method) achieves the highest resolution (Moro *et al.* 2003). To obtain a *f*-*k* spectrum, Fourier transform (FT) is applied in both time and space of the field data. The FT applied on time domain yields a good resolution in frequencies, whereas the resolution of wavenumbers obtained by FT in the space scale is comparatively low. Typically, the numbers of samples in time-domain and length of recording is sufficiently high so that good resolution is obtained in frequency domain, while the number of samples in space domain is quite limited, resulting in low resolution, and which can be

somewhat overcome by zero padding. Once the *f-k* relationship is obtained, the corresponding phase velocity is computed as the ratio of the frequency and wavenumber (Michaels *et al*. 2011; Foti *et al*. 2015). The major limitation of the *f-k* technique is that the valid frequency band for interpreting the dispersion characteristics obtained from f-k analysis techniques is limited on both sides. For low frequencies, the limitation is caused either by insufficient resolving capabilities of the chosen array layout or by the vanishing spectral energy contribution of the vertical Rayleigh wave displacements (for example related to the degenerated horizontal ellipticities around the frequency of the H/V spectral peak location). The upper limit is given by the occurrence of aliasing patterns due to insufficient spatial sampling of the wavefield. Moreover, the *f-k* transform is primarily applicable for plane-wave signal model, wherein a large offset distance and small receiver spacing are to be maintained during the test. Small receiver spacing result in lower array length, thus restricting the depth of investigation (Ohrnberger *et al*. 2004). On the other hand, phase shift method (Park *et al*. 1998) utilizes wavefield transformation method that provides images of dispersion curves directly from the recorded wavefields. With this method, different modes are separated with higher resolution even if the shot gather consists of a relatively small number of traces collected over a limited offset range. It is a simple three-step transformation method. A multichannel field record (a) is first decomposed via Fast Fourier Transformation (FFT) into individual frequency component, and then amplitude normalization is applied to the each component. Then, for a given testing phase velocity in a certain range (for example, 10 m/sec-2000 m/sec), necessary amount of phase shifts are calculated to compensate for the time delay corresponding to a specific offset, applied to individual component, and all of them are summed together to make a summed energy. This is repeated for different frequency components. Display of all summed energy in frequency-phase velocity space will show patter

of energy accumulation that represents the dispersion curve. If input field record contains multi-modal dispersion, that behavior will appear as multiple energy accumulations occur for a given frequency. With the aid of this technique, the multimodal features can be easily delineated. Moreover, since phase-shift is computed and integrated over a wide-range of phase velocities, the dispersion image covers a wide range of phase velocity and frequency, thus providing a complete picture of the energy distribution over the entire image space. The locally highest peaks for varying combinations of frequency and phase velocity can be easily identified, thus generating a good resolution dispersion curve. Thus, the highest resolution dispersion curves can be extracted from the dispersion image obtained by the *f-C* method. Accordingly, based on the identification of the corresponding frequency-phase velocity pairs having the local maximum energy accumulation, the unimodal or multimodal dispersion curves are identified (Fig. 2.1). When a wave with a particular frequency propagates with a single phase velocity possessing significant energy in the dispersion image space (measured in terms of FFT amplitude), it is stated to possess unimodal dispersion characteristics. On the other hand, if waves of a particular frequency possess multiple phase velocities traversing with significant energy, it is referred as having multimodal dispersion characteristics. The least phase velocity for any particular frequency corresponds to the fundamental mode in the dispersion image space, while the next higher velocities, for the same frequency, corresponds to the subsequent higher modes (first higher modes, and so on). The details of the algorithm and working principle of the *f-C* method can be found in standard references (Park *et al*. 1998; Park 2011). Although *f-C* method achieves the highest resolution, it is significantly affected by the data acquisition and pre-processing parameters.

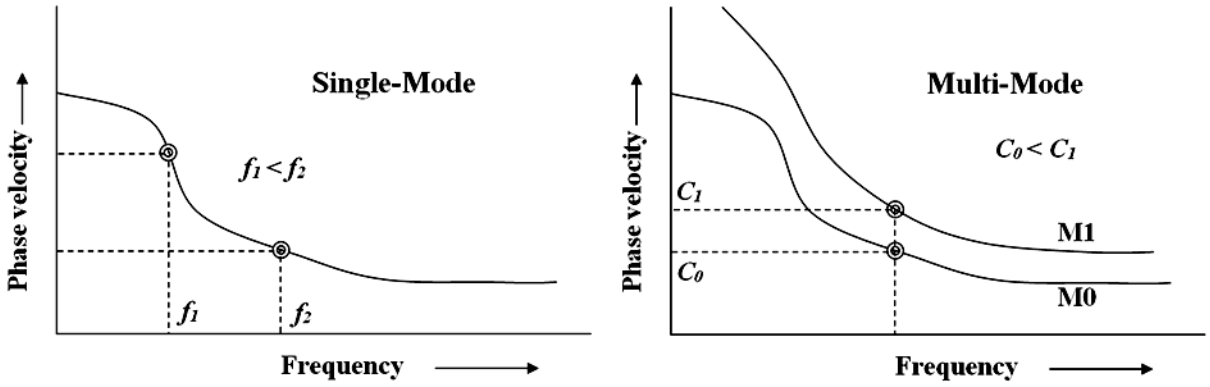

Fig. 2.1: Schematic of the unimodal and multimodal dispersion of Rayleigh waves

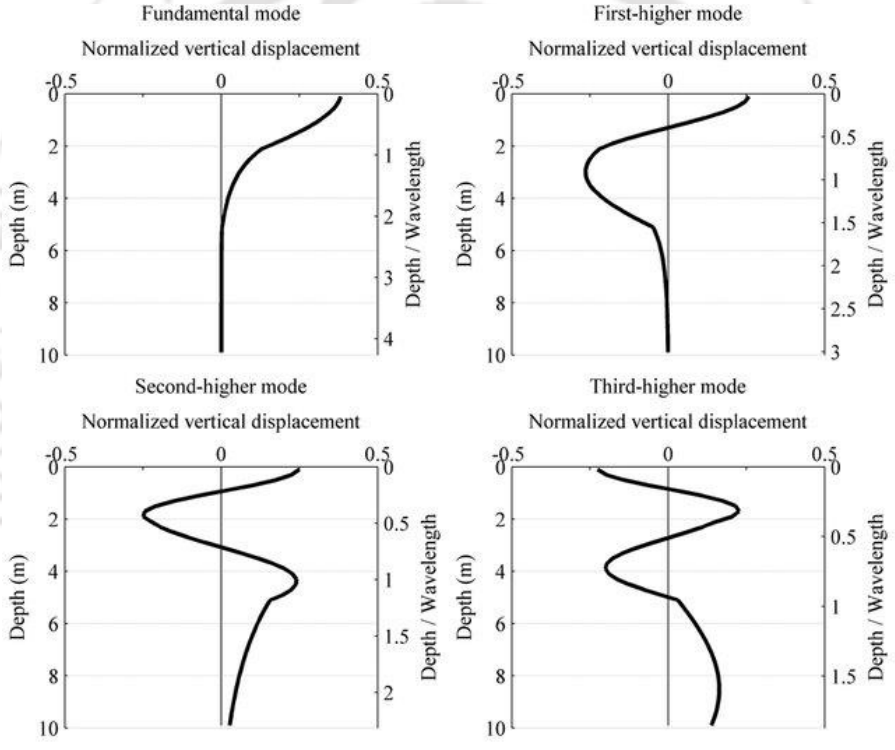

Fig. 2.2: Natural mode shapes of Rayleigh propagating at a frequency of 60 Hz (Lin 2014)

2.5 Resolution of the Dispersion Image

High resolution of dispersion image is essential to extract the fundamental or higher-order mode dispersion curves to be subsequently used in the inversion analysis. Resolution of an image

governs its sharpness and is defined by the number of pixels contained in a unit area, thus quantifying the nearness of the pixels until the limit of being visibly resolved. The same pixel resolution will be sharper on a smaller display area, and vice-versa. Resolution can be expressed in various units as lines per mm (lpm), lines per inch (lpi), and more commonly dots per inch (dpi) (https://en.wikipedia.org/wiki/Image_resolution).

A dispersion image is primarily a triaxial representation of the variation of energy for varying combinations of phase velocity and frequency of the travelling waves. Generally, such plot is provided as a biaxial representation where the energy is denoted by a colour distribution, a darker color representing higher energy. A dispersion image is stated to have a higher resolution when the higher energies are largely concentrated over thinner bands (Zhang *et al.* 2004). If the points of highest energy concentration can be easily recognised from the dispersion image trend, the dispersion curve can be directly obtained.

Park *et al.* (1998) described the resolution of a dispersion image as per two resolvable independent terms, namely resolution along the phase-velocity axis and along the frequency axis. The resolution along the velocity axis, for a given frequency, represents the capability to distinguish the particular phase velocities, having the locally highest energy, from the other adjacent phase velocities with comparatively lower energies. Vice-versa, the resolution along the frequency axis can be described in terms of a given phase velocity. Referring to Park *et al*. (1998), Zhang *et al*. (2004) explained the resolution using a dispersion spectral diagram. Analytically, it has been shown that if the integrative energy reduces rapidly with the difference

in velocity, the bandwidth would be relatively narrow; giving a relatively well-defined velocity that can be regarded as the phase velocity for a particular frequency.

2.6 Factors Governing the Resolution of a Dispersion Image

As mentioned earlier, the generation of a high-resolution dispersion image depends upon several parameters mainly associated with the data acquisition (offset distance, receiver spacing, and weight of hammer) and data pre-processing (sampling frequency, filtering and muting parameters). Moreover, stacking of dispersion images (i.e. combination of the dispersion images obtained from the analysis of repeated tests) leads to the enhancement of the energy content of different frequencies, thus resulting in the formation of a high-resolution dispersion image. The following sub-sections provide a comprehensive review of the various parameters and their effect on the resolution of the dispersion image.

2.6.1 Data Acquisition Parameters

2.6.1.1 Offset Distance and Receiver Spacing

Parameters related to the field data acquisition affects the generated dispersion image obtained for various seismic surveys involving the participation of surface waves such as SASW (Heisey *et al*. 1982; Nazarian *et al*. 1983; Stokoe and Nazarian 1983) and MASW (Park *et al*. 1999, 2002a; Park 2011). In order to obtain the suitable field parameters, different researchers have suggested different field configurations comprising of various offset distances, receiver spacing and number of geophones. Based on SASW investigations, Heisey *et al*. (1982) showed that the geophone spacing should be 1.3-2 times the maximum wavelength of the Rayleigh wave originated due to active impulse. Sanchez-Salinero *et al*. (1987) conducted the SASW survey and

theoretically calculated the condition of plane-wave propagation. It was found out that the waves with wavelengths larger than one-half the distance between receivers carry a substantial amount of body wave energy. Hence, it was recommended that the only usable wavelength is 1.5 times the receiver spacing, and that the offset distance and receiver spacing should be kept equal. Roesset *et al*. (1989) carried out a parametric study using SASW surveys to investigate the appropriate field configurations (spacing between source and receivers) required to minimize the near-field effect. It was recommended that to obtain the best resolution dispersion image, a spacing ratio d_2/d_1=1.5-2 and an offset-wavelength ratio d_1/L_R=0.5-2 should be maintained; where, d_1 is distance of source from first geophone, d_2 is distance of source from second geophone, and L_R is the propagating wavelength.

Surface waves become planar (or, stabilized) only after travelling a certain distance from the source, which is a function of its wavelength (Stokoe *et al.* 1994; Park *et al.* 1999). The surface wave method requires the analysis of the planar propagation of horizontally travelling M0 Rayleigh waves (fundamental-mode). Since the S-wave velocity profile is obtained by the inversion of the fundamental mode, the accuracy and inversion stability mainly depends upon the quality of the fundamental dispersion curve. Waves with longer wavelengths travel greater distances before they become planar, and otherwise. There are two kinds of prevalent effects that depend on the offset distance; namely, the near-field effects and the far-field effects (Park *et al.* 1999, 2002a; Park 2011). The near-field effect represents unpredictable non-planar propagation of surface waves near the source point. They are generally known to be responsible for underestimated phase velocities of relatively long wavelengths. The near-field effects are associated with the minimum distance required for surface waves to develop through the

interference of multiple reflections and mode conversions of body waves at the free surface. At the vicinity of the source, the plane-wave approximation of wave propagation is violated. Commonly, the energy of surface wave distributes in multimode. It is important to avoid recording of any non-planar components. Hence, a very close near-offset (offset distance corresponding to near-field effect) is avoided. Far-field effects (Park 2011) indicate that surface waves become relatively weak at far-offsets (offset distance corresponding to far-field effect) because of the attenuation and geometrical spreading, and are thus contaminated by noise wavefield such as the traffic noise, random ambient noise, scattered surface waves and body waves from other sources. The contamination can also be caused by higher modes of surface waves that may prevail at far offsets because of their relatively smaller attenuation. If these contaminated wavefields are included in the development of dispersion imaging, they tend to cause destructive interference on the energy of the fundamental mode and leads to its inaccurate estimation. Hence, it is important to determine a suitable offset distance so as to avoid the above-mentioned near-field and far-field effects. Park *et al.* (1999) suggested a thumb rule for the near offset, $x_1 \geq Z_{max}$, where Z_{max} is the maximum investigation depth. Park *et al.* (2002a) carried out MASW survey in two soil sites: a loose and moderately wet soil site near the Kansas Geological Survey (KGS), Lawrence, Kansas; and a fairly hard and dry soil site near Yuma, Arizona. A 10 m near-offset and 100 m far-offset was recommended to be suitable when the target depth of investigation is 30 m (i.e. the propagation wavelength is 60 m, considering the maximum investigation depth is about half of the longest wavelength) and the receiver spacing is 1 m. Zhang *et al.* (2004) proposed an suitable set of field configuration parameters, for MASW survey, in terms of the characteristics of the generated surface waves, which is expressed in Eq. (2.1).

$$x_1 = x_l,\ x_2 = 3x_l \text{ and } x_l = \frac{\lambda_{\max}.V_{\min}}{4\Delta V} \tag{2.1}$$

where, x_1 is near-offset distance, x_2 is far-offset distance, x_l is half-layout length, $\lambda_{\max}$ is maximum wavelength, $V_{\min}$ is minimum phase velocities and ΔV is difference in maximum and minimum phase velocity of the generated surface waves. To test the validity of the proposed suitable parameters, a field case study was conducted at a fill slope in Hong Kong. Stable dispersion spectra with a good resolution were obtained when the suitable acquisition parameters were employed. Based on theoretical perspective, Xu *et al*. (2006) proposed a quantitative estimation of minimum offset for active MASW survey as

$$d = \frac{2h}{\sqrt{\sigma^2 - 1}} \text{ Where, } \sigma = \frac{V_p}{V_s} \tag{2.2}$$

where, V_p is the P-wave velocity, V_s is the S-wave velocity, and *h* is the thickness of the layer.

Dikmen *et al*. (2010) suggested two offset distances for obtaining a good resolution dispersion image instead of one offset (as used in the conventional practice of MASW), which makes it easier for the determination of the dispersion curve in terms of the fundamental modes and its distinctness from the higher modes. The first offset distance is considered as 3-4 times the geophone spacing. The second offset distance is considered to be equal to or greater than one-third of the spread length depending on the power of the seismic source. Park (2011) suggested a Selective Offset Dispersion Imaging (SODI) which takes into account the wavelength-dependent far-offset (x_{far}) and near-offset (x_{near}) in the dispersion imaging scheme, as shown in Eqn. 2.3.

$$A_{s,SODI(C_T,\omega)} = \frac{1}{l_{far} - l_{near} + 1} \sum_{i=l_{near}}^{l_{far}} e^{-j\delta 1,T} R_{i,norm}(\omega) \tag{2.3}$$

where, l_{near} and l_{far} are start and end indices of traces falling in the selective offset range of $x_{near} \le x \le x_{far}$ satisfying the following relationship: $x_{near} = \xi_{near}\lambda$ and $x_{far} = \xi_{far}\lambda$, where, ξ_{near} and ξ_{far} are the minimum and maximum offset coefficients. Empirically, the suggested suitable offset (x) range for SODI is $\xi_{near}\lambda \le x \le \xi_{far}\lambda$ with $0.1 \le \xi_{near} \le 1$ and $3 \le \xi_{far} \le 7$.

The phase-shift method (Park *et al*. 1998) uses the Full Offset Dispersion Imaging (FODI) which takes into account the records from all the channels (including the near and far field offsets) in the execution of the dispersion imaging scheme. It has been noted that the dispersion image processed with SODI has better resolution than that obtained using FODI. Dikmen *et al.* (2010) have carried out the MASW survey with 9 different geophone receivers spacing. The first five linear spread geometries represent geophone spacing to be constant (C), decreasing (DE), increasing (IN), narrow-width (NW) and short-long (SL), respectively. The next four geophone spacing are symmetrical according to the spread mid-point (C_L) and represent decrease–decrease (SDD), decrease-increase (SDI), increase-decrease (SID) and increase-increase (SII), respectively. Generally, a linear spread with a constant geophone interval is used for data acquisition. However, surface waves are desired to be recorded in a wide frequency range. Geophone spacing is a variable that directly affects the resolution at the shallow depth. When the geophone spacing is increased, shallow depth resolution will be reduced. When the spread length is increased, the investigation depth will be increased, however, exhibiting low resolution. For seismic studies in which S-wave variations in shallow depths (z < 10 m) are important, identification of the dispersion image at high frequencies (e.g. 20–100 Hz) with high resolution will be important. It was observed that dispersion curve for the fundamental mode provides the widest frequency band in the SL-type spread, and the separation of the fundamental and higher

mode is best obtained for the SII-type spread. The results show that for studies investigating larger depths, the SL-type linear array is preferred, and for studies when higher modes are important, the SII-type linear array serves better.

2.6.1.2 Number of Receivers and Length of Array

The length of receiver array forms another important feature of the geometrical layout of the receivers during the field investigation. The total number of receivers or channels used, and accordingly the length of receiver array, affects the resolution of the dispersion curve. Park *et al.* (1999) highlighted the advantages of using more channels over the application of two-channel SASW approach. Park *et al.* (1998) used 24, 48 and 96 channels to determine the resolution of the dispersion image, where it was demonstrated that survey conducted with higher number of channels resulted in a higher resolution dispersion image. In general, it was stated that the utilization of higher number of channels should exhibit higher resolution, as more number of channels are involved in the collection of subsurface information. However, Park *et al*. (2001) showed that higher number of channels could result in higher-resolution dispersion image, only if it is associated with the longer receiver spread length. It was stated that no additional benefit is obtained by merely increasing the number of channels without accompanied increase in the receiver length.

2.6.1.3 Weight of the Hammer

The weight of the hammer is an important parameter that is related to the amount of energy and type of waves generated during an active MASW survey, which in turn, has an effect on the resolution of the dispersion image. Park *et al*. (2002a) carried out active MASW survey with

different hammer weights 4.5 kg (10 lb), 9.07 kg (20 lb) and rubber band aided weight drop, and obtained the dispersion images from each, based on a specific geometrical configuration. It was observed that there is a slight increase of low-frequency (< 10 Hz) energy (i.e. the resolution in the low frequency range) as the source changes from10 lb to 20 lb sledge-hammer. However, the maximum impact strength by RAWD resulted in the least amount of low-frequency energy. Instead, the higher mode energy at the higher frequencies (> 30 Hz) increased, indicating an increased resolution. This observation exhibited that a mere increase of impact strength may not ensure greater energy at lower frequencies. A consensus about the effect of impact energy to resolution of the dispersion image is to be attained.

2.6.2 Data Preprocessing Parameters

2.6.2.1 Sampling Frequency, Number of samples, Acquisition Length

Sampling frequency (f_s), or the sampling rate, is one of the important parameter, which is defined as the average number of samples recorded in one second, and is expressed in 'samples per second' (sps). It is also defined as the inverse of sampling interval (T, in s), expressed as $f_s = 1/T$. The sampling rate is defined based on the sampling theorem, which states that a signal can be exactly reconstructed if it is sampled at a rate at least twice its maximum frequency component, f_{max} (Proakis and Manolakis, 2007). As per the Nyquist-Shannon sampling theorem, $f_s = 2 f_{\max}$, where f_s is termed as the Nyquist frequency (for discrete signals) or Nyquist rate (for continuous signals). In MASW or any other geophysical surveys, the geophone records are random signatures of the effect of the propagating wave. Under such scenarios, a lower sampling frequency (i.e. higher sampling interval) fails to retrieve all the random features of the wave signature. Dispersion image developed from these records are mostly obscure, which fails to

provide sufficient information about the subsurface. Hence, for such conditions, it is imperative to use higher sampling frequencies so that all the critical features are well captured. Hence, it is suggested to use higher sampling frequency in order to obtain the best possible dispersion curve. However, there exists a suitable sampling rate (dependent on the soil site), beyond which the effect on the resolution of the dispersion image is minimal.

Time of acquisition (t), or the total sampling time, is defined as the total number of recorded samples (n) per unit sampling frequency (i.e. $t = n/f_s$). Thus, for a particular sampling frequency, higher number of recorded samples implies a higher acquisition time. If the acquisition time is low, the phase of wave propagation remains incomplete, thus providing an incomplete time-domain response. However, for a sufficiently high sampling time, not only the phase of wave propagation carrying all the significant information is completed, the additional time would undesirably record noise and unwanted signals which will lead to the contamination of the useful counterpart. Hence, it is imperative to use a suitable sampling time in order to obtain a high resolution dispersion image.

A typical Data acquisition (DAQ) system consists of predefined set of total number of samples (such as 2048, 4098, 5120, 10840, 20480) and sampling frequencies (50, 100, 500, 1000, 2000, 3750, 7500 and 15000 Hz). Based on the number of samples and the sampling frequency selected during data acquisition, the total time of sampling is decided. The signature of a particular wave can be completely recorded considering various combinations of total number of samples and sampling frequency. Under such condition, choosing the lower sampling frequency will compromise with the resolution of dispersion image due to the insufficiency in capturing all

the wave features. Hence, it is imperative to choose that particular combination which comprises of a highest sampling frequency so that most of the wave features are captured. The complete time-stamp of a record depends upon the stiffness of the propagating medium. A stiffer medium will allow for a faster passage of the wave, and hence, the time-stamp of a complete wave will be relatively lower in comparison to the same obtained for a softer site. Such observation has been reported by Morlet *et al*. (1982) where based on a sampling method for complex signal, the complex characterization of multi-layered or heterogeneous media, had been presented. Hence, the sampling frequency required to record the complete time-stamp for different sites will vary. A higher sampling frequency will be suitable for a stiffer site, and vice-versa.

Based on the field test carried out at Kansas in a site having flat surface topography and consisting of thick layered shale, Park *et al.* (1999) recommended that sampling redundancy can be obtained by relatively large number and tight spacing of geophone receivers. Kanli *et al.* (2006) carried out V_s^{30} mapping and soil classification for seismic site effect evaluation in Dinar region, SW Turkey located in the alluvial basin. A sampling interval of 0.5 ms was used for seismic refraction and surface wave surveys, employing a total acquisition time of 1024 ms and 2048 ms, respectively. Based on the comprehensive MASW study carried out in Ljubljana, Slovenia (site characterized with soft sediments and strong seismological site effects), Gosar *et al*. (2008) have mentioned the use of sampling frequency of 2000 Hz in active MASW and 128 Hz in passive MASW, utilizing sampling intervals of 0.5 ms and 2 ms for active and passive MASW survey, respectively. Eker *et al*. (2012) have carried out site classification zonation mapping in Plio-Quaternary and especially Quaternary alluvial sediments in Ankara, Turkey. For carrying out the local site characterization, total sampling length of 2 s and sampling interval of 1

ms was used. Sauvin *et al*. (2016) stated that the time of sampling should be enough to avoid aliasing. The phenomenon of aliasing is the misidentification of a signal frequency, which introduces distortion or error in the computation. Aliasing occurs when a system is measured at an insufficient sampling rate. Aliasing causes different signals to become indistinguishable from each other during sampling (Proakis and Manolakis, 2007). The problem of aliasing can be tackled by sampling at a frequency greater than Nyquist frequency. Sauvin *et al*. (2016) suggested to use 1 ms sampling interval for a total recording time of 1 s in order to tackle the problem of aliasing. However, a smaller time sampling would be necessary for processing of body waves, and a longer recording time is mandatory in cases of extremely low velocities (very soft sites) or for a long receiver spread during active MASW survey.

2.6.2.2 Filtering and Muting

To obtain a good resolution dispersion image, it is also essential to alienate and suppress the noise from the raw wavefield. Filtering is the suitable technique to separate out the noise from the signal to obtain a high signal-to-noise ratio (SNR), thus enhancing the resolution of the dispersion image. There exists different types of analog filters for the signal processing, namely high-pass, low-pass, bandpass and bandstop filters; each of which can be further classified in various subsets of Butterworth, Chebyshev, Elliptic and Linear-phase filters (Mitra 2013). The pioneering use of filters in the analysis of surface waves has been to determine the group velocities of dispersed waves based on an analytical method “Multiple Filter Analysis Technique (MFAT)” (Dzienwonski *et al*. 1969). The amplitude and phases were determined from the output of narrow bandpass digital filters. In order to determine the spectral amplitudes of the individual modes of the propagating wave, Mitchell (1973) used the peak amplitude of the envelope of the

filtered signal generated by MFAT. Hermann (1973) investigated the use of narrow band-pass filtering for determining the spectral amplitudes and group velocities of the individual modes. Gaussian filters were preferred for the analysis since the filtered signal had very small side lobes. The chronological development related to the use of filters in the seismic wave surveys is obscure. However, the recent findings show that filtering of raw record is instrumental in obtaining a good resolution dispersion image (Park *et al.* 2002a; Moro *et al.* 2003). Park *et al*. (2001) carried out the characterization of geotechnical sites near Yuma, Arizona over a dry soil within the basin using MASW survey. Near surface materials at the site consisted of thick (> 30 m) accumulation of alluvial and colluvial sediments eroded from the topographically high ridges. A special 2-D filtering scheme was developed that applies 'cut' and 'pass' operations of filtering within the frequency-phase velocity domain. Park *et al.* (2002a) specially mentioned to avoid using any low-cut analog filter during preprocessing.

Park *et al*. (2002b) introduced a new filtering technique for surface waves in the frequency-wave number (*f-k*) space by redefining the rejection zone as narrow and curved (bow-slice), instead of the familiar pie-shaped zone. Conventional pie-slice *f-k* filtering has been used to remove the noise from signals by selecting a rejection zone. The rejection (filtering) zone is defined in frequency-wave number (*f-k*) space by two fanning linear slopes (thus called pie) of S_{max} and S_{min} determined from the two limiting velocities of C_{min} and C_{max}, respectively. In bow-slice filtering, the filtering zone is defined as a thin and curved zone whose locus, $\{\omega; k_x\}$ meets the following criterion $\omega/k_x = C_\omega$, where, C_ω is the phase velocity at frequency ω of the event to be filtered, and k_x is the wavenumber. C_ω may be the phase velocity of the first higher (c_ω^1) or the fundamental (c_ω^0) mode. This locus is usually not a straight line because of the dependency of the

phase velocity (C) on the frequency (ω). It is assumed that C_ω is already known, as determined from a dispersion analysis. The actual shape of the bow slicing is of certain band (with smooth tapering applied along the boundary) instead of a true line, the width of the band being commonly set proportional to the phase velocity.

Moro *et al*. (2003) applied bandpass filters of two different configurations (0-2-20-30 Hz and 0-3-50-70Hz) on the recorded traces to compare the velocity spectra obtained from three different transformation schemes, namely the *f-k* transform, π-ω transform and *f-C* transform. When the bandpass filter with higher bandwidth was applied, the distinction between the various transformations was vividly noticed beyond a frequency of 20 Hz. For the results obtained from *f-k* and π-ω transforms, mode-mixing and higher-mode amplification in the velocity spectra was prevalent, and the fundamental-mode related signal beyond 30 Hz was highly inconceivable; while, the velocity spectra obtained from the *f-C* transform was still well defined and noise free, thus indicating the superiority of the latter transform in its application.

Muting is one of the preprocessing tasks that are aimed at suitable removal of body wave intrusions and other low amplitude noises present in the raw wavefield. It is performed by selecting two limiting scanning phase-velocities on the wave field, meant for top-muting and bottom-muting, based on which the events above and below the corresponding limits will be respectively removed. Baker *et al*. (1998) stated that the noise muting can be applied on the raw record obtained from surface wave surveys. The region of muting is commonly referred as noise cone, and thus the muting technique is known as the noise cone technique. The noise cone which is muted necessarily contains air wave and the low frequency waves which act as an incoherent

noise. Park *et al.* (2001) proposed a simple multichannel processing technique that mutes the interfering wavefields in the offset-time (*x*-*t*) domain which can significantly enhance the resolution of multimodal dispersion curves. The possibility of separation by muting is stipulated by the higher velocities of the higher modes. Ivanov *et al.* (2005) explained a simple multichannel processing technique that mutes the components of the seismic wave-field, mainly the higher modes of surface-wave energy. Careful studies of the shot record, by boosting the amplitudes, revealed two apparent phase-velocity slopes of the surface-wave energy. The two trends can be separated by an imaginary line (along which the two surface wave patterns notably change). The slope of the separation line is qualitatively determined by visually estimating for best trend separation in the phase-velocity–frequency domain.

2.6.3 Stacking of Dispersion Image

In all seismic surveys, the primary objective of data acquisition is to increase the signal-to-noise ratio (SNR), which inadvertently increases the resolution of the dispersion image. A higher SNR can be achieved in two ways: (a) Reduction of the noise level, and (b) Strengthening of the actual signal. Reduction of noise can be carried out by filtering of the raw records during the data preprocessing stage to remove the higher and the interfering modes. Alternatively, noise analysis can be carried out to identify the prevalent and ambient noise signature, which can be utilized in the muting operation (during data preprocessing) to separate the noise from the significant signals. Alternatively, the same can be achieved by choosing a geophone having a lower natural frequency, which leads to an improvement in the data acquisition obtained in the lower frequencies, and thus, eliminates noises generated due to the higher frequency bands. The choice of geophone affects the resolution of the dispersion image pertaining to the frequencies prevalent

in vicinity to the natural frequency of the geophone. Hence, a-priori information about the site and the source characteristics governs the suitability of a geophone based on the prevalent frequencies to record. Moreover, the signal can also be strengthened by using a higher energy source, thus suppressing the ambient noise content prevalent in the experimental site.

Stacking, or more commonly vertical stacking, is an alternative solution to achieve an enhanced SNR, and thus resulting in a dispersion image with enhanced resolution. It has been observed that the quality of the dispersion image obtained from the Refraction Microtremor (ReMi) method, or currently known as the Passive MASW approach, is dependent on the stacked wavefield data (Louie 2001). Conventionally, assumed hypothesis states that vertical-stacking increases the signal-to-noise ratio by the square root of the number of repetitions (Foti *et al*. 2015). Two types of stacking are possible as per its operation, namely (a) Wavefield stacking and (b) Dispersion image stacking. Wavefield stacking is the process of summing up of the multiple synchronized repetitions of the raw wavefields obtained for multiple shots with same geometrical layout of the array (Foti *et al*. 2015). Slant stacking is a type of wavefield transformation method wherein the wavefields are stacked following a particular phase velocity band (Schultz and Claerbout 1978). Enhancement of the signal-to-noise ratio can also be achieved by the stacking of the dispersion images obtained from different shots (Grandjean and Bitri 2006; Socco *et al.* 2009, 2010). Since dispersion image stacking is in frequency domain, it is more scientifically appropriate than the wavefield stacking. In wavefield stacking, if the repetitions of energy are not similar, the generated wavefields will follow non-synchronised phases, resulting in variable time of acquisition; thus, cannot be actually stacked. However, for the case of dispersion image stacking, the summing up of the energy (or Fourier amplitudes) is

conducted at the frequency domain, thus using the frequency axis as a common benchmark for the summing operation. When two or more dispersion images are combined by stacking, all the sets of image data, along with the image trends, are merged naturally to make one continuous trend of higher SNR (Park *et al*. 2007). The importance of dispersion image stacking in active MASW survey has also been reported in existing literature (Park *et al*. 2002; Foti *et al*. 2015; http://masw.com/ACQParaTables.html). Dispersion image stacking is also largely used in Passive MASW survey to increase the SNR and the resolution of the dispersion image (Park *et al*. 2006; Park and Miller 2008).

Shtivelman (2002) proposed a method for continuous representation and tracing of the dispersion patterns, based on stacking of surface waves in the common midpoint (CMP) domain. The advantages of this approach are that it defines unambiguously the surface locations of the stacked traces, and it averages the properties of all the sources and receivers participating in the given CMP gather. Moreover, the CMP stack can provide a better spatial resolution. The application of the proposed method has been reported in Shtivelman (2003). Stacking of surface waves (SSW) was tested and corroborated on a deep seismic data set where it was observed that the stacking increases the data quality and is capable to obtain higher resolution image (Neducza 2007). To demonstrate the efficacy of stacking, test was carried out in the South-East part of Hungary using 50 kg dynamite as an active impulse source. The measurement was planned for deep seismic reflection profiling and had used maximum 64 stacks for the purpose. The stacking was carried out by summing the *f-k* amplitude spectra to produce higher horizontal resolution and improved data quality.

Stacking of dispersion images from multiple impacts can suppress ambient noise significantly and is therefore always recommended, especially if the survey takes place in an urban area. The suitable number of stacking impacts can be determined when there is little change in SNR in the displayed seismic record during the stacking. The number of stacks, in general, to obtain a good resolution dispersion image is considered to be 3-5 (Park *et al*. 2007; Socco *et al.* 2009, 2010); however, there are instances where much higher number of stacking has been used to investigate deeper profiles (Neducza 2007). This number, however, should increase as the ambient noise level increases and/or total receiver array length (L) increases. Existing researches reveal that stacking increases the resolution of images, and thereby increases the signal to noise ratio of the images. However, no guidelines are mentioned about the suitable number of stacks to obtain the best resolution image, which is expected to be site dependent.

2.7 Critical Appraisal of the Literature Survey

Critical evaluation of the existing literature leads to the visioning of several open issues and challenges related to the conduct of active MASW field survey, the data acquisition techniques and the data preprocessing approaches for dispersion analysis. Based on the critical literature review, following gap areas are listed.

- From the review, it is clear that resolution of the dispersion image is very important to obtain an accurate shear wave velocity profile from an active MASW survey. However, existing literature reveals that the resolution of the dispersion image is mostly qualitative and based on the visual inspections. Very few reports in literature are available suggesting some preliminary criteria for the quantification of the resolution, achieving no conclusive consensus. It is important that extensive research must be oriented in the

direction leading to the development of the guidelines for the quantification of the resolution of a dispersion image.

- The review illustrates that variations in data acquisition parameters (receiver offset, inter-receiver spacing, total length of receiver, total number of channels, and weight of the hammer or the energy generator) during the active MASW field survey significantly affect the resolution of the dispersion image. There are certain case-specific recommendations provided about the optimum parameters to be used in the Active MASW survey to obtain a good resolution dispersion image. However, it is realized that there are no widely accepted rules that can be commonly adopted for different site conditions. There is need of in-depth and extensive study of the effect and influence of various parameters corresponding to different site conditions in order to arrive at feasible recommendations.
- The review of the literature fails to provide clarity about the recommendations for the choices of sampling frequency (or, the rate of sampling) and sampling length of the acquisitions to be adopted during an active MASW survey. Choice of sampling frequency is site dependent, since a stiffer stratum will allow for faster propagation of the waves and otherwise. It is understood that the sampling frequency will directly affect the acquisition time of the signal. If sampling length is more than the required (i.e. the acquisition time is more than that required for the phase to complete), there will be noise adulteration of the signal. This particular subject has received very less attention and needs to be thoroughly investigated to arrive at a site-specific suitable recommendation.
- Filtering of the recorded signals directly affects the SNR and the resolution of the dispersion image by suppressing the interfering modes and noise. Very few reports in

literature have discussed about the filtering of the noises recorded during the data acquisition for an active MASW survey. From the existing literature, it is not clear which type of filter should be used to yield a high- resolution dispersion image. In this regard, from the purview of digital signal processing, a thorough investigation to study the efficacy and effect of the choice of the filter on the resolution of the dispersion image has to be carried out.

- Although the effect of stacking has been highlighted in little case-study literature, there exists a lack of understanding, and recommended guidelines about the site-specific optimum number of stacking are required to obtain the best resolution image. An extensive study in this regard is highly essential.

Overall, the critical scrutiny of the literature, pertaining to the resolution of the dispersion image obtained from the active MASW survey, opens up many challenging issues which are required to be thoroughly investigated. Extensive research is required in all the sectors of data acquisition, preprocessing and stacking is the need of the hour in order to progress towards a better understanding of the subsurface characteristics using non-destructive techniques for enhanced robustness, accuracy and reliability. The subsequent chapters in the thesis reports about the studies conducted with the aim of providing the recommendations to some of the issues stated above.

CHAPTER 3

EXPERIMENTATION PROGRAM AND ANALYSIS METHODOLOGY

3.1 General

In general, there are three primary stages in an active MASW survey: Data acquisition, Dispersion analysis and Inversion analysis (Park *et al.* 1999, 2007). An array of geophone receivers are placed on the ground in order to record the vibration induced by the propagating waves emanated from an active impulsive source (Park *et al.* 1998; Xia *et al.* 2004, 2009). The time signatures are converted into the frequency domain to develop the dispersion image, and the combinations of phase velocities and frequencies with locally maximum energies are delineated to identify the dispersion curve (Park *et al.* 1998, 2001, 2004). When more than one phase velocities exist for a given frequency, the phenomenon corresponds to multimodal dispersion. The dispersion curve having the slowest phase velocities corresponds to the fundamental mode (M0), while the next faster one corresponds to the first higher mode (M1), and so on. During the inversion analysis, based on an initial estimate of the shear wave velocity earth model, a theoretically generated dispersion curve is assumed, which is subsequently optimized towards the experimental curve through an adaptive iterative approach. During the iterations, the shear wave velocity model is continuously updated. The converged model is considered to be the most probable subsurface shear wave velocity (V_s) model (Nazarian *et al.* 1983; Ganji *et al.* 1998; Xia *et al.* 1999). It is comprehensible that the accuracy of the estimated shear wave velocity profile is largely dependent upon the quality of the extracted dispersion curve, governed by the resolution of the dispersion image, which in turn, is influenced by several data acquisition, pre-processing

and processing parameters (Zhang *et al.* 2004; Dikmen *et al.* 2010). This chapter briefs about the equipments and apparatus utilized to conduct active MASW survey in the field and record the wavefields propagating from the source through the propagating medium to the geophone receivers. It also describes the working principle of SURFSEIS, the commercial software used for the purpose of pre-processing and analyzing the collected wavefield to generate the dispersion images and subsequently the inverted profiles. An indigenous MatLab code has also been developed to integrate with the SURFSEIS software, solely for the purpose of automated extraction of dispersion image, and would be described in detail in Chapter 7.

3.2 Equipments of Active MASW Survey

The various equipments used for conducting active MASW survey are primarily associated with the data acquisition stage. The apparatus used includes active or impulse source to generate the seismic or impulse shocks in the field, a set of receivers arranged in a predefined array for collecting the wavefields propagating through the medium, and a Data Acquisition System (DAQ) to act as an interface between the hardware and software used for the recording purpose. All the components play a significant role in governing the data quality which ultimately affects the estimated shear wave velocity profile. The instruments are to be chosen carefully to acquire the surface wave data of required frequency range. The source used decides the different frequency ranges to be produced with different amplitudes. The receivers have their natural frequencies below which the resolution of the acquired data becomes poor. The type of survey decides what range of receivers should be deployed. The instrumentations that were adopted for the present study are debriefed in the following sections.

3.2.1 Active Sources

For the data acquisition using active MASW survey, the sources can be classified as impulsive sources and vibrating sources. Impulsive sources include hammers, weight drops, seismic guns and explosives, whereas vibrating sources include electromechanical vibrators and Vibroseis. The impulsive sources generate energy for short span just like an impulse. Sledgehammers are the most frequently used sources for shallow subsurface investigation. Explosives require special care and permissions for its use. Only experienced practitioners use explosives as source for energy. Weight drops are also used for the purpose, but the application of the same is not as popular as sledgehammer owing to the portability issues.

Sledgehammer (Fig.3.1) is an impact source operated by single personnel. Its weight ranges from 1 kg to 15 kg, and is hit on a baseplate for good impact on the ground surface. Testing on rocks does not require baseplate and it can produce signals of very high frequency range. A light weight hammer is preferred for high frequency waves. The velocity of the hammer hitting the baseplate may be around 15 m/s, and thus the impact force may reach up to 20 kN (Foti *et al*. 2015). This energy is sufficient for an array of 50-100 m. A sledge hammer of 10 kg was considered for the surveys in the present study. Weight drop is another popular impulsive source which is used for shallow applications. It consists of a mass that is lifted to a certain height and dropped onto the ground. The weight can vary from few kilograms to few tons, and the height of drop may be few meters. Another kind of weight drop is accelerated weight drop which releases the weight with certain velocity. Thus, with the same raise in height, a greater impact can be created with this kind of active source. A 40 kg propelled energy generator (Fig 3.2) was used as the weight drop for some of the surveys in present study.

Fig. 3.1: A 10 kg sledgehammer operated by single personnel to strike the base plate

Fig. 3.2: A 40 kg Propelled Energy Generator (PEG) acts as an accelerated weight drop

3.2.2 Geophone Receivers

After generating energy in the subsurface, the waves propagating through subsurface are collected and recorded by the geophone receiver transducers. Geophones are transducers which transforms mechanical strains (vibrations) into variations in electrical current. The particle motion will be transduced into electrical signals by the receivers and then they are groomed for further analysis. The receivers are the primary recording elements in MASW survey. The ground motion can be captured as particle displacement, velocity, or acceleration. Velocimeters also called as geophones are the most used receivers for shallow surveys. Typical geophone will be moving coil type electrodynamic (electromagnetic) transducer (Fig. 3.3). It has a coil wound on a non-conducting cylinder which is place inside the magnetic field created by a circular magnet. The field around the coil restricts the movement of the spring in lateral direction and so the vertical component of the particle motion can be captured. When the coil mass moves vertically, it cuts the magnetic field around it and hence generates an electromotive force. The output voltage depends on the rate (velocity) at which the coil cuts the magnetic field. Hence they are called velocimeters. The coil is restricted to move only in vertical direction and so they are called vertical geophones. Two most important parameters for efficient working of geophones are its natural frequency and damping. Natural frequency of the geophone is the lower limit of the frequency range. Below its natural frequency, the amplitudes of the signals will be severely attenuated. The damper is used to make the response flat within in the feasible frequency range, and makes the movement of the coil smoother. The phase difference among the receivers deployed will directly affect the velocity, and will be significant if different geophones are used. Hence, identical geophones are used to obtain good quality data. Figure 3.3a shows the geophones used in the present study, and their working principle. For the present study, 4.5 Hz

geophones have been used, the characteristic response curve of which is provided in Fig. 3.4b. The output voltage in the geophone reaches its maximum level at the natural frequency of the geophone.

Fig. 3.3: (a) Geophones and their working principle

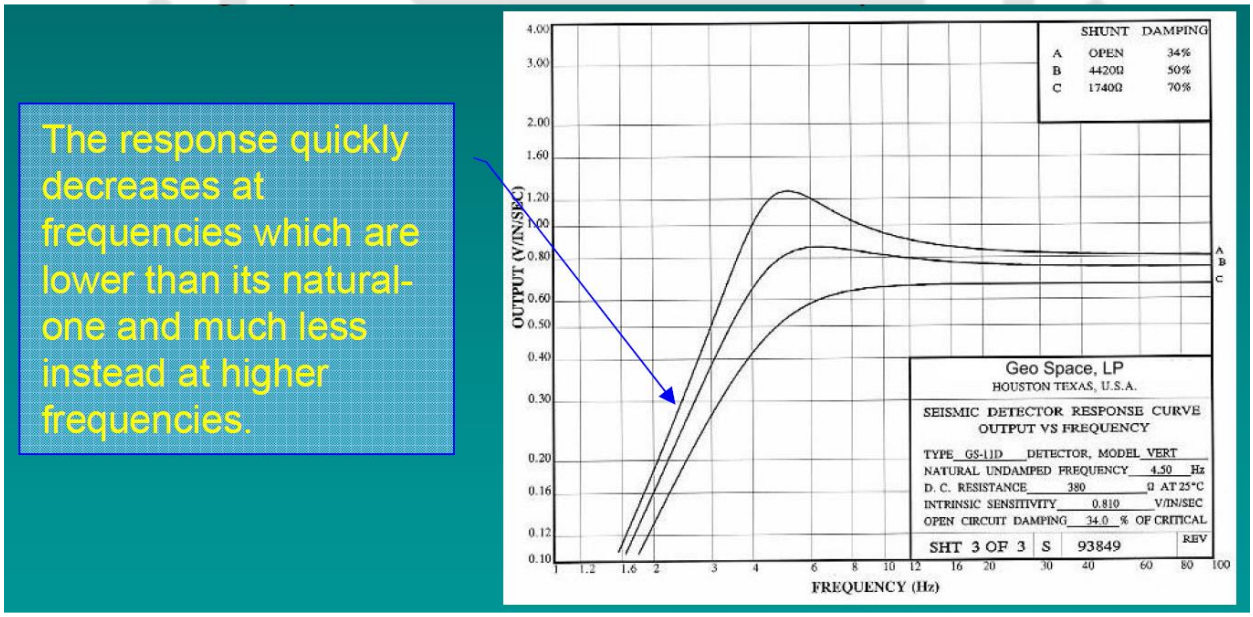

Fig. 3.3: (b) 4.5 Hz geophones and their characteristic response curve

3.2.3 Data Acquisition System (DAQ)

The particle motion converted into voltage has to be stored in a system which should be compatible for the same. DAQ seismographs are multichannel digital recorders. The primary use of these acquisition systems is to groom the raw wave field so as to be flexible for further analysis. The key parameters of a digital acquisition system (Fig 3.4) are numbers of channels, dynamic range and time sampling parameters like sampling rate and record length. Greater is the number of channels, greater will be the resolution and depth of survey (Park *et al*. 1998, 2001)**.** The data acquisition systems are compatible for expansion of number of channels. The dynamic range of seismograph affects the data quality. It is a key characteristic for analog to digital conversion of data**.** The analog-digital converter is an electronic circuit which converts electrical signals generated by sensors to numeric values. It allows transformation of analog signals to digital ones, wherein every converted value is defined as a sample of the original signal. The resolution of the converter is the number of signals it can distinguish and depends on the number of bits each sample is comprised of. For instance, a 16-bit converter distinguishes 65536 levels (2^{16}), while a 24-bit converter distinguishes over 16 million (2^{24}). The minimum sampling interval for the DAQ can be as low as 10 microseconds (Foti *et al*. 2015). This depends on the number of channels used for acquisition. The number of samples acquired multiplied with sampling interval gives record length, and thus, sampling rate is the number of samples read by the converter every second, expressed in Hertz. The bandwidth of the system indicates the frequency range up to which reliable signal can be acquired. The physical robustness of the system has to be taken care of when choosing the data acquisition system. The DAQ comes with a portable battery for uninterrupted power supply. For the present study, DAQ from MAE

(Molisana Apparachhiarature Electroniche), make A6000-S, supporting 24 channels (extendable to 36) has been used.

Fig. 3.4: 24-bit MAE Data Acquisition System (DAQ) used in the present investigations

3.2.4 Striker / Base Plate

The composition and density of the striker plate material can noticeably affect the frequency content of the generated wavefield. In the present study, striker plates made up of two different materials - cast steel and rubber, have been used. The reduction of the impact energy by the rubber plate, as used in the present tests, are not significant. Considering the fact that the thickness of both the metallic and rubber plates are approximately 3-4 cm, there would not be a substantial reduction of energy transmitted. Moreover, as the acoustic coupling has been ensured, the differences in the impact energy is not evidently influential in this case. Rather, the composition of the plates control and alter the frequency content of the transmitted waves. The use of a cast steel plate (Fig 3.5) significantly increases the higher frequency content of the

signal, while the rubber plate (Fig 3.5), being softer, absorb more of high frequency waves, thus delineating the low-frequency content of the transmitted signal (Foti *et al*. 2015). Thus, considering identical field layout and field testing configuration, a single active strike on a cast steel plate provides information for the shallow depth, while, comparatively, the rubber plates provide information for larger depths. However, due to the fatigue of the material component, rubber plate deteriorates faster and, thus, is restrictive in its use. The depth of investigation with metallic plates can, however, be significantly enhanced either by altering the field layout configurations (in comparison to the tests on asphaltic pavements, larger offset distance is suggested for testing on hard concrete pavements by Kumar and Rakaraddi 2013), or by adopting dispersion image stacking (as discussed later in Chapter 5). In order to minimize the acoustic impedance, the striker plate has been subjected to a seating impact, which led to the embedment of the plate in the ground to the extent that the top surface of the plate flushed with the ground surface. It is assumed that a full contact is established between the plate and the underlying soil so that acoustic coupling is achieved.

Fig. 3.5: Striker plates of different compositions – Cast steel and Rubber

3.3 Location of the Test Sites

Field tests were conducted at three different chosen test sites, having different substrata characteristics, within IIT Guwahati campus, Assam, India (Fig. 3.6). Site-1 is located at the Cricket Field within the campus (26°19'06.3"N, 91°69'70.28"E), Site-2 is located adjacent to the D-block faculty apartments (26°11'05.4"N, 91°41'31.8"E), and Site-3 is located in the Core-4 of the Academic Complex between M- and N-academic blocks at IIT Guwahati. As per the borehole data available, Figure 3.7 exhibits the geotechnical information available for the chosen sites. Site-1 mostly comprises of mainly soft to medium stiff clayey soil over large depths, whereas Site-2 consists of a shallow stiff soil layer of 7 m underlain by a very hard granitic stratum. Site-3 primarily comprises of heterogeneous layers of soil and crushed debris. At each site, confirmatory borehole or cross-hole tests were available which have been used to validate the findings from the MASW test. Based on the SPT-N values obtained from the bore-log, the average shear wave velocity ($V_{s,avg}$) at Site-1 varies between 80-200 m/s, while at Site-2, the same varies between 200-700 m/s. At Site-3, the information obtained from shallow depth cross-hole illustrates shear wave velocity below 100 m/s within a depth of 10 m.

Fig. 3.6: IIT Guwahati campus map showing the MASW experimentation sites

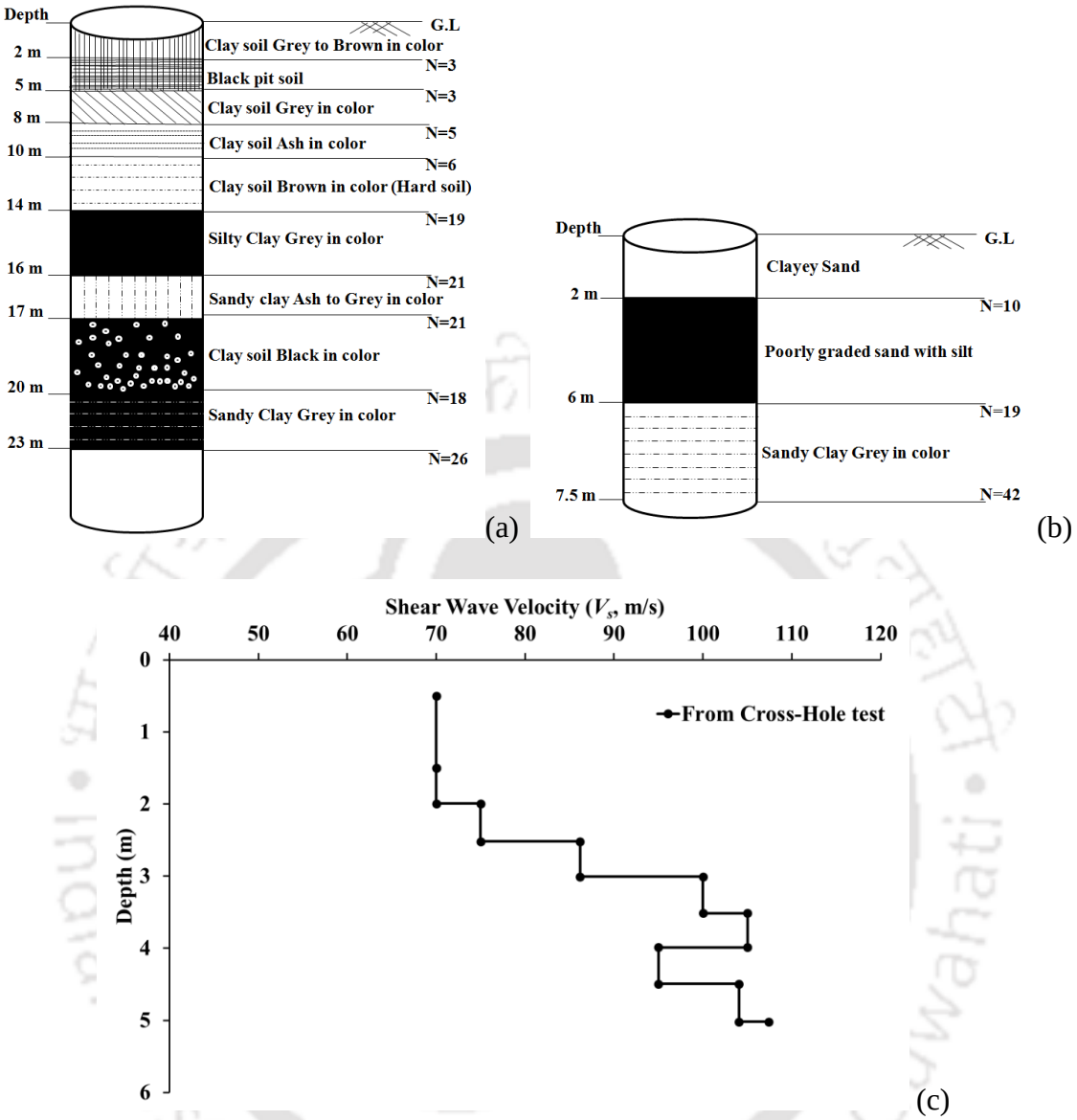

Fig. 3.7: Available geotechnical information from the test sites (a) Site-1 (b) Site-2 (c) Site-3

3.4 Test Setup and Methodology

Figure 3.8 shows the schematic diagram of an Active MASW survey conducted in the field. In general, seismic waves are generated through an impulse hammer strike, which after propagating through soil substrata, are recorded by a set of geophone receivers placed in a linear array. The receivers are connected to a Data Acquisition System (DAQ) comprising of a seismograph. In

the present study, 12 or 24 channels of 4.5 Hz geophones, placed in a linear array, have been used to record the seismic signals generated by a 10 kg sledgehammer or a 40 kg PEG. The equipments used in the present study are briefed in the previous sections.

In order to develop guidelines related to the factors influencing the resolution of the dispersion image, and accuracy of the subsurface profile, several experimental investigations were conducted with varying parameters, which are listed as follows:

- Sampling frequency - 15000 Hz, 7500 Hz, 3750 Hz, 2000 Hz, 1000 Hz and 500 Hz
- Sampling length (Total number of samples) - 5120, 10240 and 20480
- Filtering techniques – High cut, Low cut, Band cut and Band pass filters
- Muting – Different extents of muted signals
- Offset distance – Varying between 0-12 m
- Inter-receiver spacing – 1 m, 2 m, and 3 m
- Number of geophone receivers – 12 and 24
- Type of source – 10 kg sledgehammer, 40 kg Propelled Energy Generator (PEG)
- Number of stacks – 0-5 stacks, as required
- Striker plate material – Cast Steel, Rubber

Following the schematic diagram, Figure 3.8 exhibits a typical actual layout of the test setup at Site-1. A linear array of geophones is connected to the connector cable, which is further attached to the DAQ as shown in Fig. 3.4.

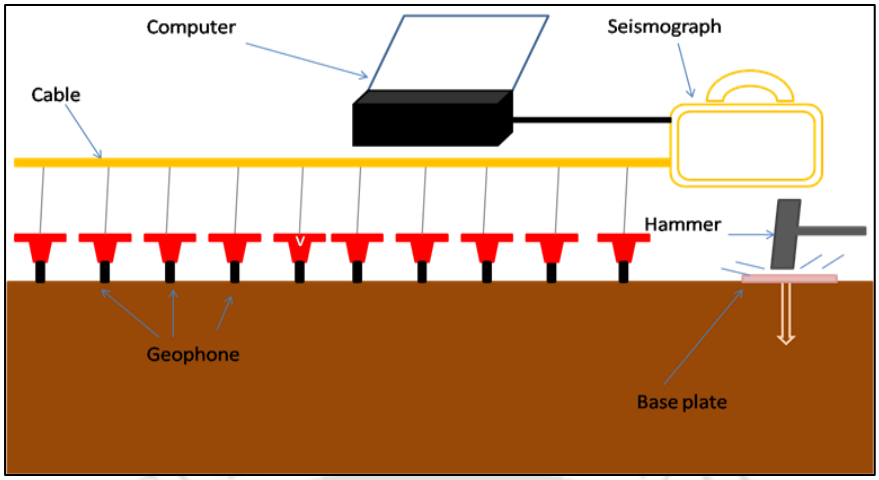

Fig. 3.8: (a) Schematic of the test setup for active MASW survey

Fig. 3.8: (b) Typical layout of linear array of geophones for active MASW survey (c) Connecting mechanism of the geophones with the connector cable

3.5 Analysis Software: SURFSEIS

Once the raw wavefields are collected through field experimentations, they are subjected to various stages of analysis namely, preprocessing, dispersion and inversion analyses. In this regard, SURFSEIS has been used in the present study to obtain the shear wave velocity profile from the raw waveforms collected from the field investigations. This section provides documentation on the software and its application for the stated purpose.

3.5.1 General Introduction

The first version of the SURFSEIS software (v 1.0) was released in 2000 for the application of the multichannel analysis of surface waves (MASW) method on seismic data. It was developed at the Kansas Geological Survey (KGS). The MASW method consists of four main components (Miller *et al*. 1999): data acquisition, dispersion-curve imaging (Song *et al*. 1989; Park *et al*. 1998; Xia *et al*. 2007; Luo *et al*. 2008, 2009), inversion of dispersion-curve to obtain a 1-D shear-wave velocity (V_s) profile (Xia *et al*. 1999), and assembling multiple 1-D results into 2-D or 3-D images (Miller *et al*. 1999, 2003) using interpolation algorithms (Matheron 1967; Olea 1974). Initially the MASW method was developed for data acquired using active seismic sources, i.e. “Active MASW” (Miller *et al*. 1999; Park *et al*. 1999). The same technique was later extended to application on seismic data from passive sources, i.e. “Passive MASW” (Park *et al*. 2004, 2005; Park and Miller 2008). The active method was introduced in the first version of SURFSEIS. It is the conventional mode of survey using an active seismic source (e.g., a sledgehammer, weight drop, explosive charges, etc.), a linear receiver array, and a data acquisition system. When there are more geophones available, it might be more efficient to collect data using a relatively larger fixed spread (Miller *et al*. 2003).

3.5.2 Working Principle of SURFSEIS

A summary of the entire procedure of a MASW survey (active or passive) is displayed in the flowchart in Fig. 3.9. The step wise procedure, as illustrated in Fig. 3.9. The detailed working principle of SURFSEIS is provided in Appendix-I.

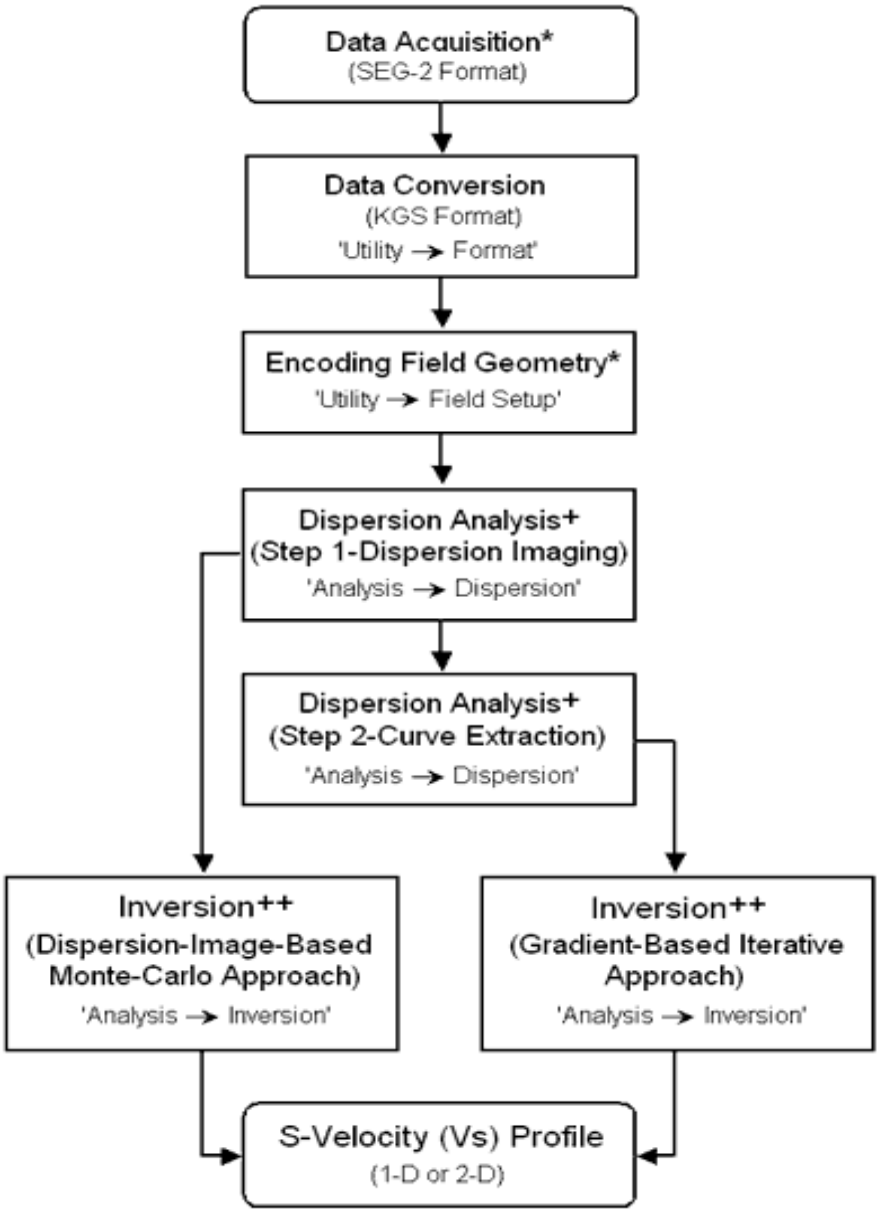

Fig. 3.9: Flowchart depicting the procedural steps of MASW survey

3.6 Summary

This chapter summarizes the experimental accessories used in active MASW survey and their working principles. It is understood that each component of the data acquisition system plays a significant role in the generation of proper signals, which eventually should result in good resolution dispersion images. Once the signals are collected, it needs to be analyzed with the aid of software. SURFSEIS has been used in the present study. This chapter provides a treatise about the important issues to be paid attention while using SURFSEIS for data preprocessing, dispersion and inversion analysis. The upcoming chapters fully portray the utility of data acquisition instrumentation units and SURFSEIS in obtaining reliable results of the subsurface profiles.

CHAPTER 4

INFLUENCE OF DATA PREPROCESSING PARAMETERS ON THE RESOLUTION OF DISPERSION IMAGE

4.1 General

MASW has been used by several researchers to determine the subsurface shear wave velocity profile (Miller *et al.* 1999; Xia *et al.* 1999; Yilmaz and Eser 2002; Tian *et al.* 2003a, 2003b; Beaty *et al.* 2002; Liu *et al.* 2004; Lin *et al.* 2004). It has been reported that the outcome of a MASW investigation is affected by the adopted data preprocessing techniques, namely involving the filtering and muting of the collected data (Dziewonski *et al*. 1969, Ivanov *et al.* 2005; Kanli *et al.* 2006; Gosar *et al.* 2008; Eker *et al.* 2012). Filtering extracts the utilizable range of wave frequencies which is further incorporated in the analysis for the construction the image space. Thus, the application of filtering reduces the noise in the signal, thereby increasing the SNR. Muting is a form of time-domain filtering, which is used to eliminate the noise adulterations from the time-stamps of the collected signals, which, in turn, reduces the noise associated with higher modes or interfering modes having higher frequencies. Hence, it is comprehensible that a proper choice of the data preprocessing parameters is required to generate dispersion images of better resolution, which subsequently increase the accuracy of the findings from a MASW test. Despite MASW being widely used for various practical applications, it is noted that there are no specific guidelines available in relation to the effect of these data preprocessing parameters on the outcome of the investigation.

Based on the data collected from a series of experimental investigations conducted on soil sites of different stiffness characteristics, the present study attempts to highlight the effect of the preprocessing parameters on the outcome of the data analysis. The outcome is manifested in terms of the resolution of dispersion image obtained from the dispersion analysis of the raw or processed signals. In order to demonstrate the typical effects of filtering and muting on the resolution of dispersion image, analysis of the MASW data, collected for a typical set of data acquisition parameters, was analyzed. The detailed effects of the influence of various data acquisition parameters on the resolution of the dispersion image will be highlighted in Chapter 5. This chapter focuses on the influence of the effects of filtering and muting on the resolution of dispersion image. Both raw data and the filtered / muted signals have been used to compare the generated dispersion image. Based on the results, suggestions have been provided about the choices of the above data preprocessing parameters during an active MASW test.

4.2 Resolution of a Dispersion Image

As mentioned earlier in the Chapter 2, a dispersion curve is the relationship between the phase velocities of the propagating waves having the highest energy of propagation with the corresponding wave frequency. During the process of analysis, MASW approach does not attempt to identify the individual dispersion curves, rather constructs an image space where dispersion trends are identified from the pattern of energy accumulation in this space (Park *et al.* 1999, 2007). Thereafter, necessary dispersion curves are extracted by following the image trends. All types of propagating seismic waves possessing any significant energy are considered in the dispersion image, thus generating a 3D contour of the energy distribution in the dispersion image space. In this imaging process, a multichannel record in time (t)-space (x) domain is transformed

into either frequency (*f*)-wave number (*k*), pi-omega (π-ω) domain, or frequency (*f*)-phase velocity (*C*) domain. The *f-k* method results in the poorest resolution in imaging, whereas the phase-shift method achieves the higher resolution than the pi-omega method (Park *et al.* 1998; Moro *et al.* 2003). Due to imaging of waves such as the air waves, scattered waves, reflected waves, refracted waves and noises, there is high probability of mode identification and mode mixing or lack of continuity of the fundamental mode image trends. Therefore, high resolution of the dispersion image is essential to extract the fundamental mode dispersion curve to be used in the inversion analysis. Park *et al.* (1998) defined the resolution of a dispersion image as the resolvable capabilities along both the velocity axis and the frequency axis. The resolution along the velocity axis represents the capability to discriminate a phase velocity from other velocities for a given frequency, and vice-versa. Zhang *et al.* (2004) stated that if the integrative energy reduces rapidly with the difference in velocity, the bandwidth would be relatively narrow; giving a relatively well-defined dispersion curve. Figure 4.1 exhibits a typical dispersion image (in grayscale), highlighting the energy bands corresponding to the fundamental mode, where *Df* and *Dv* represents, respectively, the widths of a dispersion band in terms of frequency and velocity, both of which vary along the dispersion curve.

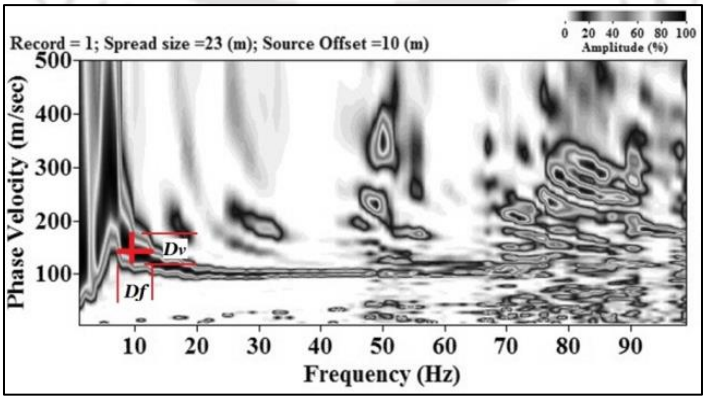

Fig. 4.1: Typical dispersion image and its resolution in terms of the thickness of energy bands

The few available documented reports about the resolution of the dispersion images focus on the resolution quality solely based on the visual inspection. To the knowledge of the authors, there is hardly any literature available that hypothesizes on the quantification of the resolution of the dispersion curve. In this context, an indigenous MATLAB code (described in detail in Chapter 7) has been developed to determine the resolution of the dispersion curves through image processing approach, in terms of the colour composition of the dispersion image, wherein the darker colours represent higher energy associated with a wave having a specific combination of frequency and phase velocity. The thickness, extent and continuity of the darkest band, aids in the quantification of the resolution, which will be further dealt in detail in Chapter 6. The interpretations reported in Chapters 4 and 5 are based on visual inspection of resolution, as has been considered conventionally in the available literature. Fig. 4.2a shows a typical dispersion image as obtained for a specific set of data acquisition and preprocessing parameters. Fig. 4.2b exhibits the corresponding dispersion band extracted from Fig. 4.2a using image processing techniques as described in Chapter 3.

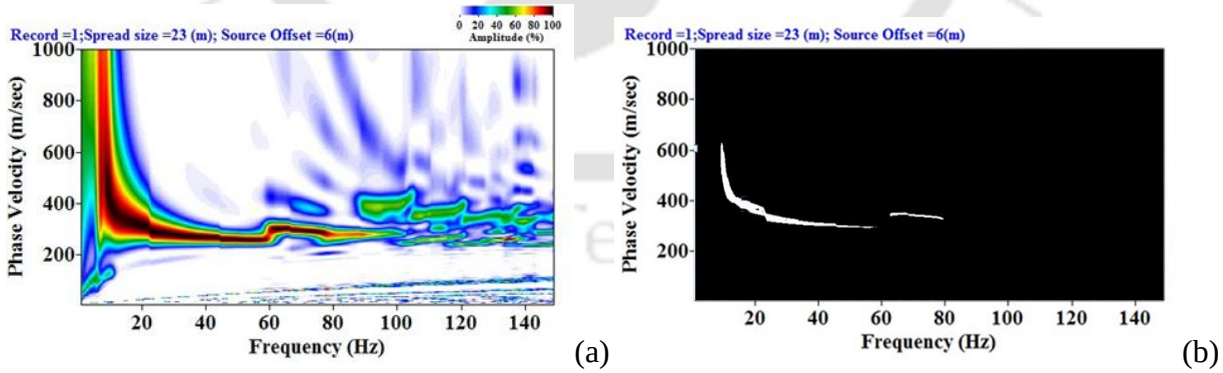

Fig. 4.2: (a) A typical dispersion image (b) Extraction of dispersion band using image processing

4.3 Results and Discussions

This section reports the outcome of application of various filtering and muting strategies on typical active MASW records collected from Site-1 (Sampling frequency – 7500 Hz, Sampling time – 683 ms, Number of channels – 24, Offset distance – 4 m, and Inter-receiver spacing – 1 m) and Site-2 (Sampling frequency – 15000 Hz, Sampling time – 341 ms, Number of channels – 24, Offset distance – 5 m, and Inter-receiver spacing – 1 m). The outcomes of the analyses are compared in terms of the visually identifiable characteristics of the generated dispersion images.

4.3.1 Influence of Frequency Filtering without Muting

As mentioned earlier, frequency filtering is a technique intended to suppress the amalgamated noise, mostly associated with higher frequencies, and subsequently enhance the resolution of dispersion image. Dziewonski *et al.* (1969) introduced the Multiple Filter Analysis Technique (MFAT) to determine the group velocities of dispersed waves, which was later applied by Mitchell (1973) to determine the spectral amplitudes of the individual modes. Raw wavefield is generally filtered and muted, aiming to create a dispersion image of high resolution. As per the conventional filtering theory, four variants of filtering are commonly applied viz. Low-cut (only high frequencies are allowed to pass), High-cut (only low frequencies are allowed to pass), Band-cut (a band of frequencies is restricted from passing) and Band-pass (only a specific frequency band is allowed to pass). Figure 4.3 portrays the various types of filters conventionally used for signal processing aspects. In the present study, commercial software SURFSEIS has been used, which has, a-priori, all the above four filtering options inbuilt in the signal processing module. In order to decide which type of filter would be best suited for the present exercise, a

thorough study was carried out to understand the functions and their efficiency of all the variants to obtain a good resolution dispersion image by processing the collected time signatures.

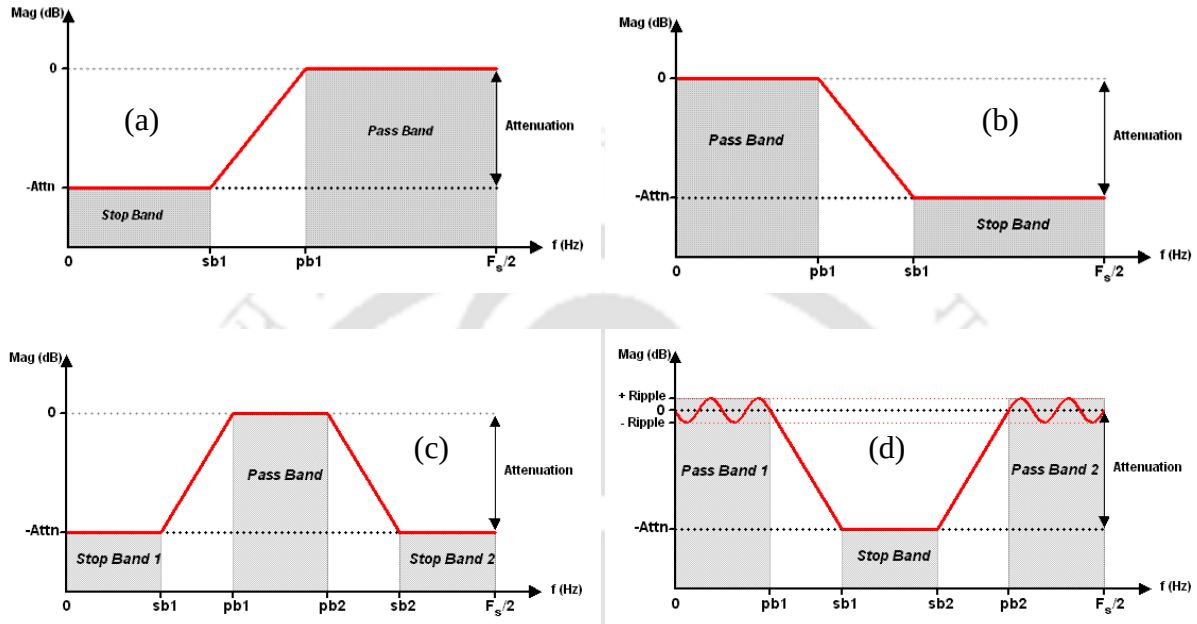

Fig. 4.3: Common types of filters conventionally used in signal processing (a) Low-cut (b) High-cut (c) Band-pass (d) Band-stop (http://www.dadisp.com/webhelp/dsphelp.htm#mergedprojects/refman2/FncrefAE/BESSEL.htm)

Filtering is carried out based on the response of the amplitude spectrum of a collected wavefield record. Figure 4.4 shows typical amplitude spectrum obtained from the two sites in consideration. The amplitude spectrum for each site is presented as an envelope developed for varying sample lengths. It can be observed that the variation of sample does not exhibit significant effect on the amplitude spectra. The amplitude spectra of MASW record, as shown in Fig. 4.3, indicates that the effective frequency content of energy ranges between 5-60 Hz for Site-1, and 5-280 Hz for Site-2. Based on the observed effective frequency content of the signal,

the frequency ranges adopted in the present study for various filtering approaches are listed in Table 4.1. In Table 4.1, f_1, f_2, f_3 and f_4 represent the cutoff frequencies of the signals. For Band-pass filter, f_2 and f_3 comprise of the practically chosen passing frequency range, while f_1 and f_4 are the theoretical pass band values. For Band-cut filter, f_2 and f_3 denote the practical stopping frequency range, whereas f_1 and f_4 denote the theoretical stopping range. For High-cut filter, f_3 is the practical cutoff value and f_4 is the theoretical value; frequencies below f_3 will pass and all other frequencies above be cut off. For low-cut filter, f_2 is the practical cutoff frequency and f_1 is the theoretical limit. A typical representation of the amplitude spectra of the filtered and unfiltered signal is portrayed in Fig. 4.5.

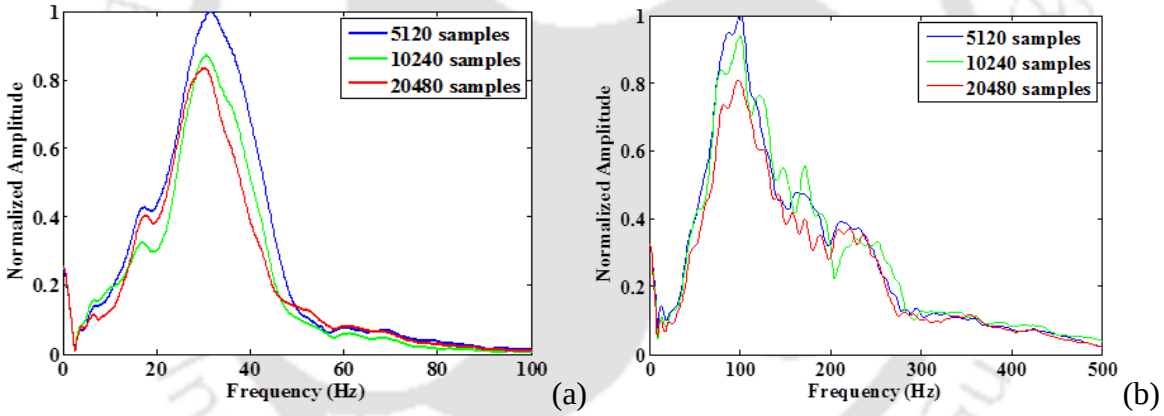

Fig. 4.4: Normalized Amplitude spectra obtained for different sample lengths (a) Site-1, using sampling frequency 7500 Hz (b) Site-2, using sampling frequency 15000 Hz

Table 4.1: Frequency ranges adopted in the present study for various filtering application

Site	Site-1				Site-2			
Filter type	f_1	f_2	f_3	f_4	f_1	f_2	f_3	f_4
Band-pass	5	10	60	80	5	10	280	300
Band-cut	5	10	60	80	5	10	280	300
High-cut	-	-	60	80	-	-	280	300
Low-cut	5	10	-	-	5	10	-	-

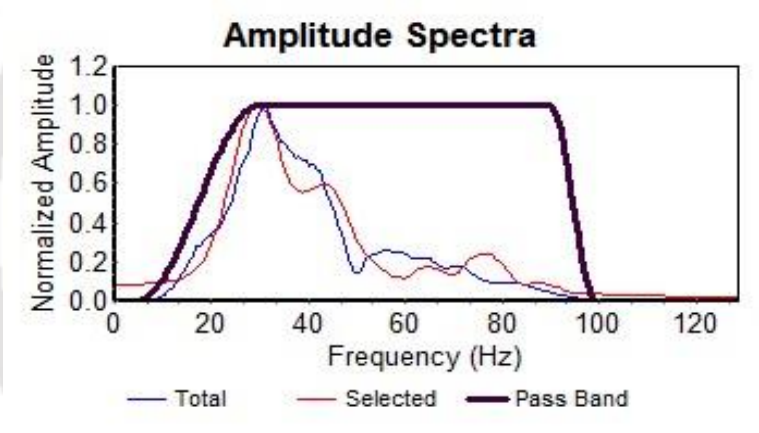

Fig. 4.5: Typical amplitude spectra of unfiltered and band-pass filtered signal

To illustrate the influence of the choice of filter, exercise has been carried out by allowing the signal to pass through all the variants of filter. Figure 4.6 shows a raw signal recorded at Site-1 and its corresponding dispersion image, obtained with a field configuration of 4 m offset, 1 m receiver spacing, and 24 numbers of geophones in a linear array having a total spread length of 23 m. Figure 4.6a shows that the unfiltered raw data is obscure in few traces, indicating noise contamination and resulting in discontinuity in the phase propagation through the geophone

array. The corresponding dispersion image (Fig. 4.6b) is low in resolution, exhibiting a thick band of dispersion trend, thus making it unreliable to extract the dispersion image. Moreover, significant energy is solely accumulated in lower frequency range (<10 Hz), indicating noise contamination originating from the low frequency waves. These observation calls for the adoption of frequency filtering.

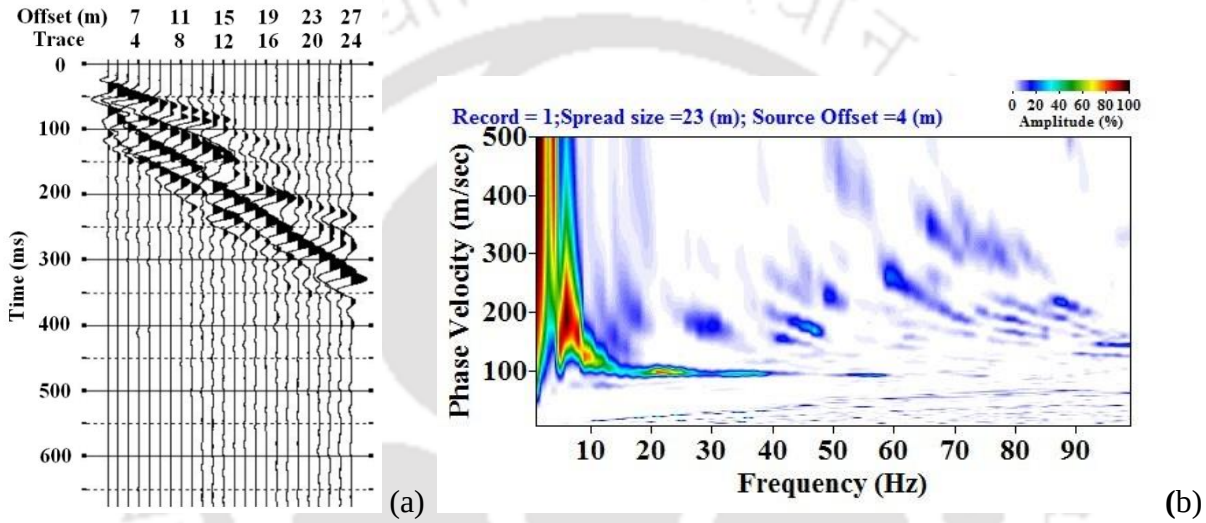

Fig. 4.6: (a) A typical unfiltered wavefield from Site-1 (b) Corresponding dispersion image.

The details of filtering effects on the collected records and the corresponding dispersion image are expressed in Fig. 4.7 and 4.8, respectively. Figure 4.7(a-d) shows the modified time records obtained after the application of various filters, namely Band-pass, Band-stop, High-cut and Low-cut, respectively. It is observed that the application of Band-stop (Fig. 4.7b) and Low-cut filter (Fig. 4.7d) significantly alters the characteristics of the original record by removing the significant energy content from the signal. Based on this observation, it is recommended to avoid the use of Band-stop and Low-cut filters to analyze the signals obtained from the Active MASW survey. The corresponding dispersion images, obtained from Band-stop and Low-cut filtering,

are shown in Fig. 4.8(b) and Fig. 4.8(d), respectively. It is observed from Fig. 4.8b that the application of Band-stop filtering results in removal of significant frequencies, indicated by the energy accumulation in the low-frequency range, thus making it difficult to identify and extract M0 dispersion curve. The dispersion image corresponding to the time-signal obtained from Low-cut filter (Fig. 4.8d) is extremely vague and fails to provide any information, and hence, is refrained from further analysis. Park *et al*. (2002) specially mentioned to avoid the used of low cut filters. Dispersion image obtained from Band-pass filtering (Fig. 4.8a) exhibits a long and distinct energy trend in the fundamental mode, uncontaminated by noise. In such case, the extraction of the M0 dispersion curve becomes easier, since it is possible to locate the peak energy points at various frequencies with greater reliability. The modified time signature of the signal obtained from the High-cut filtering (Fig. 4.7c) is nearly similar to that obtained from Band-pass filtering (Fig. 4.7a). However, the corresponding dispersion image from the High-cut filtering (Fig. 4.8c) is different than that of the latter (Fig. 4.8a), exhibiting a more truncated M0 dispersion curve trend. Moreover, the dispersion image in Fig. 4.8c exhibits a thick red zone along the y-axis which is representative of the aliasing effect, owing to the application of high-cut filter. Under such condition, it is not possible to recognize the dispersion curve in the zone of aliasing, as there would be erroneous presence of multiple phase velocities of identical or near-identical phase velocities.

Based on the above discussions, it is customary that the recorded MASW signals need to be filtered to generate good resolution dispersion curves. Out of four variants of frequency filtering, the Band-pass filter proves to be the best one to produce dispersion images with highest resolution. The choice of the frequency range is guided by the amplitude spectra of the signal.

For the present study, Band-pass filter of 5-10-60-80 Hz and 5-10-280-300 Hz specifications resulted in the best dispersion images from the tests conducted at Site-1 and Site-2 respectively.

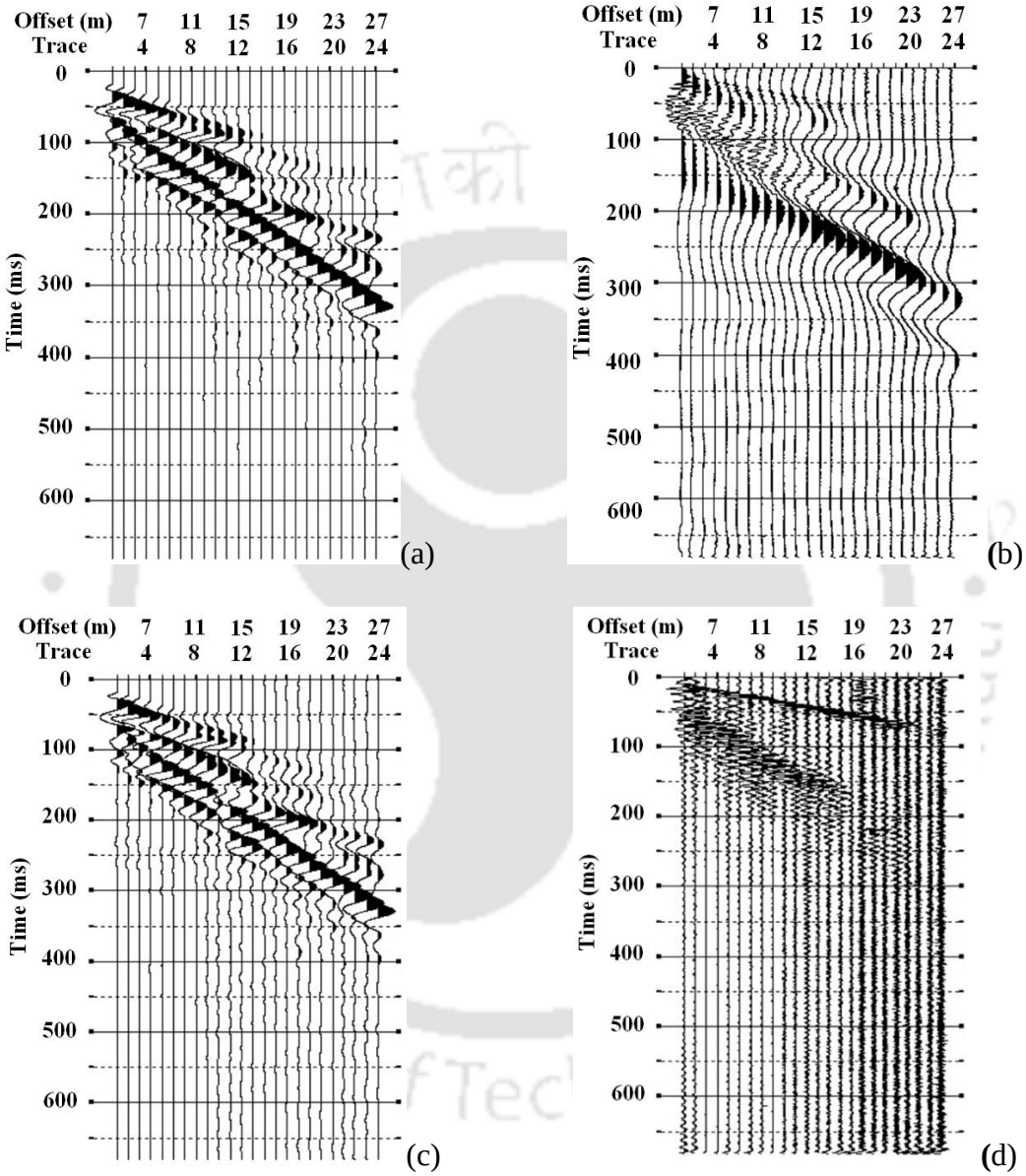

Fig. 4.7: Modified MASW records obtained from different filtering techniques (a) Band-pass (b) Band-stop (c) High-cut, and (d) Low-cut

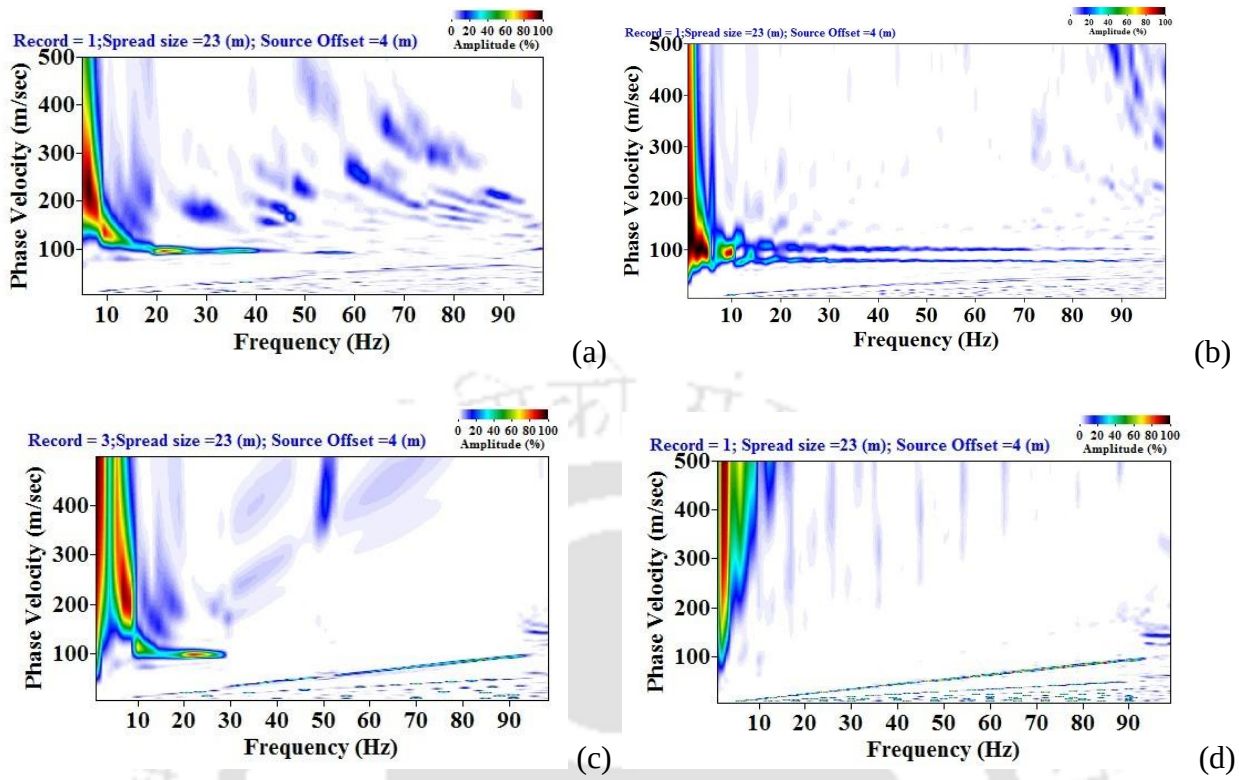

Fig. 4.8: Dispersion images obtained from different filtering techniques (a) Band-pass (b) Band-stop (c) High-cut, and (d) Low-cut

4.3.2 Influence of Muting without Frequency Filtering

Muting is a preprocessing task that is aimed at suitable removal of body wave intrusions and other low amplitude noises present in the raw wavefield. It is performed by selecting two limiting scanning phase-velocities on the wavefield, meant for top-muting and bottom-muting, based on which the events above and below the corresponding limits will be respectively removed (Park *et al.* 2001; Ivanov *et al.* 2005). Baker *et al.* (1998) stated that the noise muting could be applied on the raw record obtained from surface wave surveys. The region of muting is commonly referred as noise cone, and thus the muting technique is known as the noise cone

technique. The noise cone, which is muted, necessarily contains air wave and other low frequency waves which act as an incoherent noise.

Based on the collected raw wavefield (Fig. 4.6a), the effect of extent of muting conducted on the unfiltered record is exhibited in Fig. 4.9. Muting helps to suppress the wavefield characteristics recorded beyond specific phase velocities. Introduction of excessive muting may result in significant loss in the wavefield characteristics, and hence, muting operation should be controlled so that the best suitable energy content of the signal is maintained while removing the adulterating noises. Muting is carried out by eliminating the wave signatures which are not in phase. The muting operation is carried out along the slope of the identified prominent phases of the wavefield, as shown in figure below. Those wave signatures which are not in the phase probably originate from nearby sources which actually act as a noise. Intrusion of noise causes contamination and results in poor resolution of dispersion images. Figure 4.9 shows the extent of removal of phases which does not conform to the prominently identifiable phase velocities. Figure 4.9a is the case where the excessive muting is adopted, and only a single wavelength of the propagating phase is allowed to pass. It is seen from corresponding dispersion images at Fig. 4.10a that excessive muting eliminates the prominent signals as well, and hence, results in significant loss of information, and the corresponding dispersion image fails to provide any information. As the extent of muting decreases *i.e.* two wavelengths of the propagating wavefield are allowed to pass (Fig 4.9b), the dispersion image comparatively records more energy (Fig. 4.10b). Subsequently, three or more wavelengths are allowed to pass as shown in Fig. 4.9c, exhibiting even more energy in the dispersion image (Fig. 4.10c); a proper dispersion trend is obtained in this case in the range of 7-20 Hz, and is considered to be the best image obtained due

to various extents of muting. Finally, a minimal muting is carried out to remove only the uneven phases, as shown in Fig. 4.9d. However, in this case, the corresponding dispersion image (Fig. 4.10d) becomes difficult to ascertain a significant concentration of energy. This can be observed at the low frequency range, which is mostly attributed to the accumulation of noise.

The dispersion images of the corresponding muted records (Fig. 4.9) of unfiltered wavefields are presented in Fig. 4.10. It can be observed that when the excessive muting was undertook (Fig. 4.9a), significant energy was lost, and hence, the corresponding dispersion image (Fig. 4.10a) fails to provide any information. As the extent of muting decreases (Figs 4.9b-d), the corresponding dispersion images (Figs 4.10b-d) exhibit an energy concentration at the lower frequency region. However, at the same time, the dispersion images clearly indicate the aliasing effect in the very low frequencies arising due to the consideration of unfiltered wavefield. Aliasing effect is related to Nyquist frequency and sampling frequency. For the present study, several tests have been conducted with varying sampling frequency, which satisfies the requirement of Nyquist theorem. However, it is to be noted that the concepts regarding the Nyquist frequency are based on unadulterated signal records. Records collected from MASW survey will always be contaminated with field or ambient noises, and it is possible to remove the noise only to a particular extent. Hence, even though a suitable Nyquist and sampling frequency is chosen, there would always be chances to experience recognizable aliasing effect. It can noted that Fig. 4.10 represents the dispersion images obtained from the unfiltered wavefields, which indicates that even though best suitable muting is adopted, unfiltered wavefields will contain noise contamination leading to aliasing effects as experienced in this case. These observations

suggest that muting alone cannot lead to the generation of a dispersion image with sufficient information and good resolution. Hence, muting on the filtered wavefield is recommended.

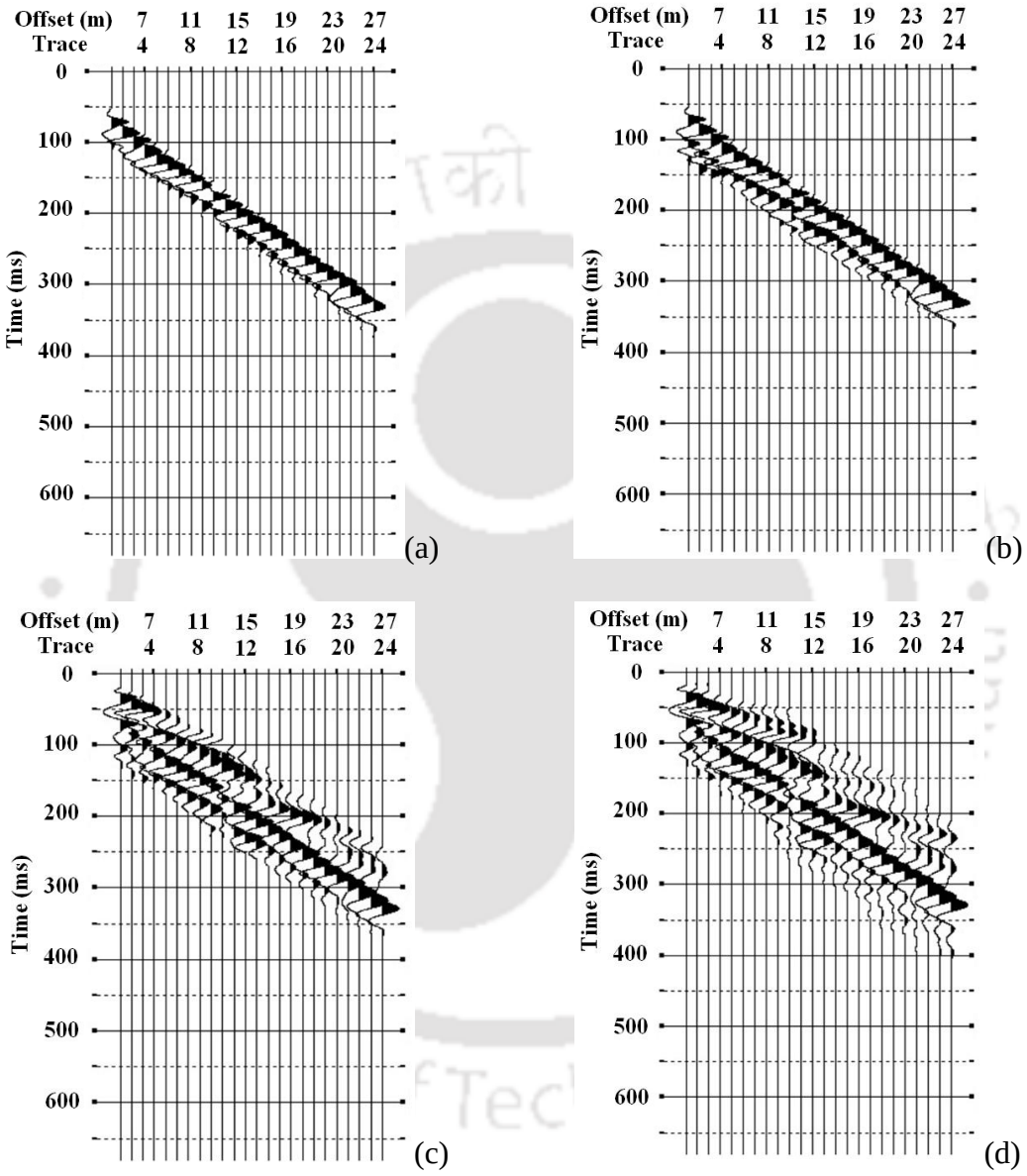

Fig. 4.9: Effect of different extent of muting on the wavefield pattern (a) Excessive muting allowing only one wavelength to pass (b) Moderate muting allowing two wavelengths to pass (c) Best suitable muting allowing three or more wavelengths to pass (d) Minimal muting to remove the uneven phases

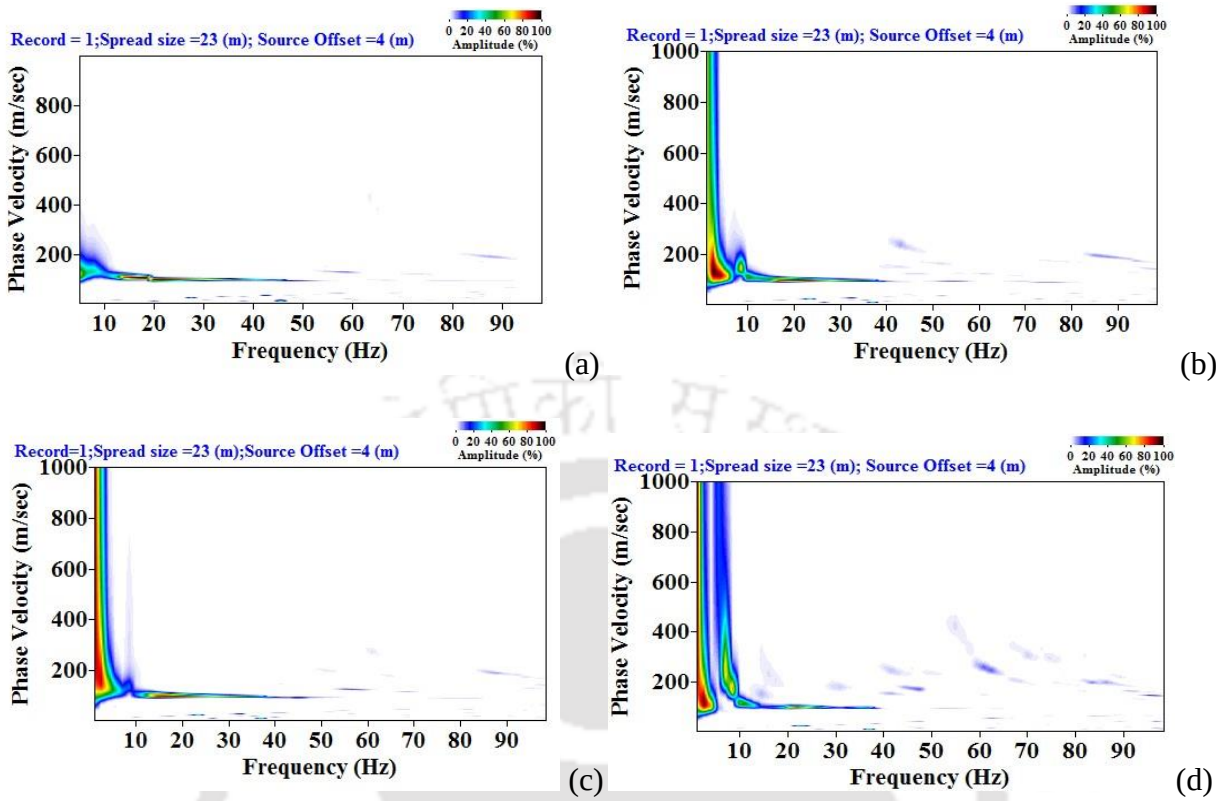

Fig. 4.10: Dispersion images from variably muted unfiltered wavefield records (a) Excessively muted (b) Moderately muted (c) Best suitably muted (d) Minimally muted

It should be noted that there exists no criteria for determining the suitable extent of muting until date, and the procedure is enacted based on the visual decision, engineering judgment and the expertise of the analyst. Since the process of muting conforms to the pre-processing of signal operations, it would not be possible for making the comparisons with a correct dispersion curve, which would be unknown at this stage. A methodology may be developed to decide for the best suitable extent of muting based on the resolution of dispersion images, as the best suitable muting would likely to produce a good resolution dispersion image having a narrow dispersion band that is continuous over a wide frequency band. It is worth noting that wavefields obtained from various tests would have different extents of noise adulteration depending upon the test

location. Hence, it would be difficult to reach a consensus or a general guideline about the suitable extent of muting, even while relying on the resolution-based determination of optimal parameters. However, such study can be conducted as a future application of the developed methodology to explore the possibility of developing criteria for best suitable extent of muting.

4.3.3 Combined Effect of Band-Pass Filtering and Muting

From the above sections, it is clear that band-pass filter is required for obtaining a good resolution dispersion image. However, attempt has been made to further refine the resolution of the dispersion images by muting the uneven phases in the filtered MASW record. The earlier section has revealed that a suitable muting is necessary to prevent excessive loss of information. Figure 4.11a shows data raw wavefield record obtained from Site-1, where the phases lack clarity from noise contamination. Figure 4.11c-d depicts the modified wavefield records after processing through only muting (Fig. 4.11c), only band-pass filtering (Fig. 4.11d), and both filtering and muting (Fig. 4.11d). It can be observed that application of both filtering and muting techniques produces the best quality wavefield records.

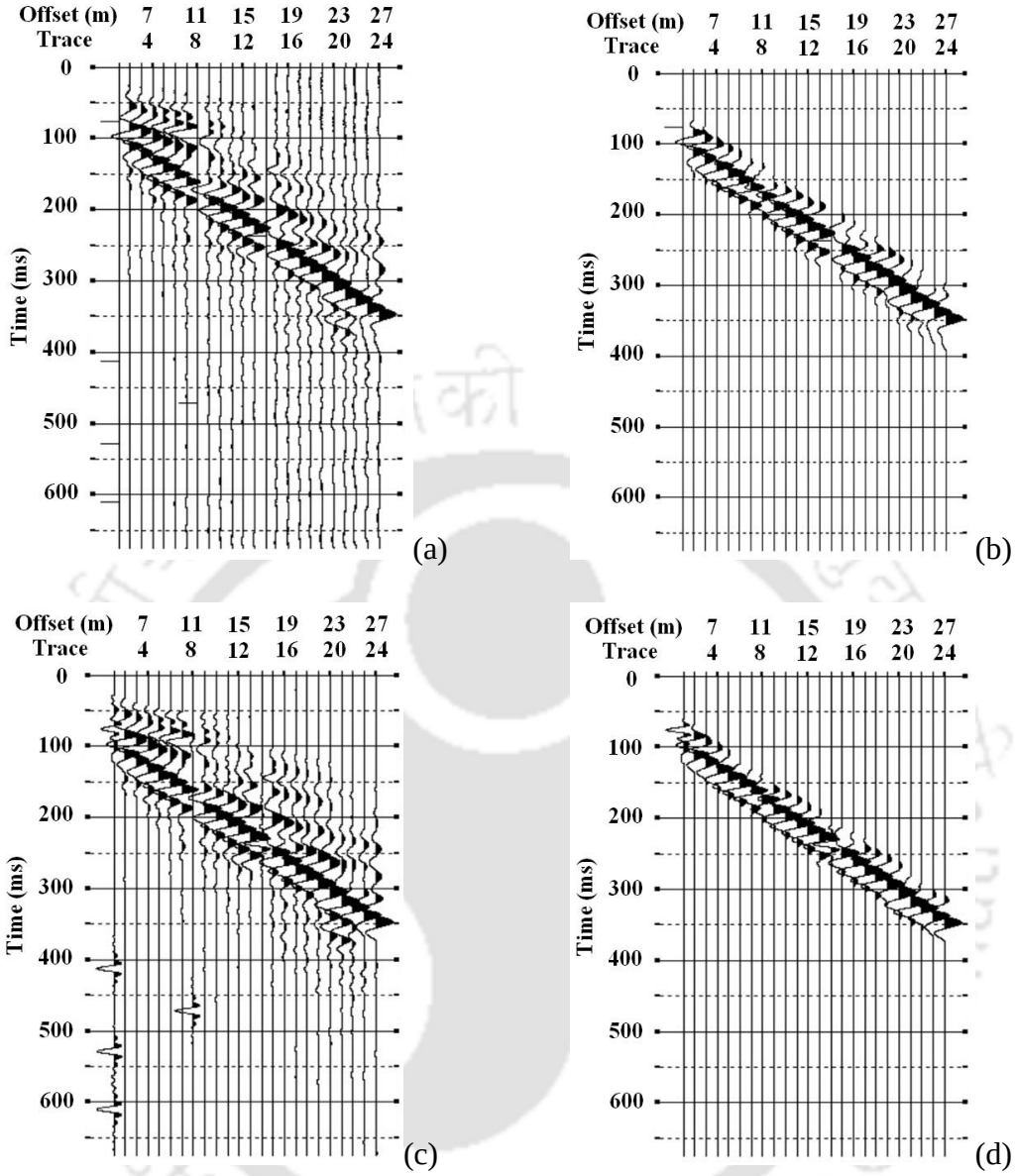

Fig. 4.11: Typical wavefield records from Site-1: (a) Raw wavefield (b) Only muted wavefield (c) Only filtered wavefield (d) Combined filtered and muted wavefield

Figure 4.12 exhibits the dispersion images corresponding to the filtered wavefields obtained from varying extent of muting operation (as exhibited in Fig. 4.9). Compared to the dispersion images obtained from unfiltered wavefields (Fig. 4.10), it can be clearly observed that the same obtained from the filtered and muted wavefields exhibit superior resolution, since most of the

noise has been eliminated in the process. As observed earlier, excessive muting results in significant information loss and renders a very poor resolution dispersion image. Based on the obtained dispersion images, the suitable extent of the muting of the filtered wavefield can be suitably decided.

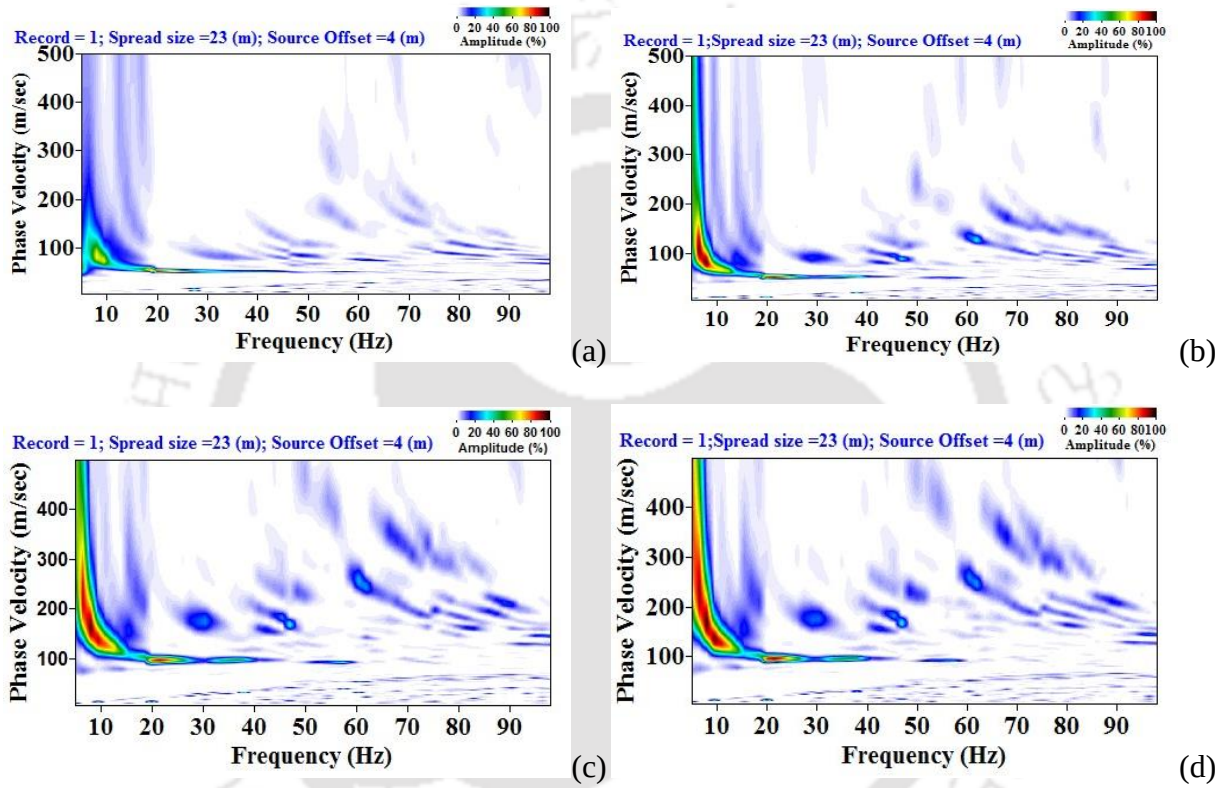

Fig. 4.12: Effect of extent of muting on dispersion image obtained from band-pass filtered wavefield records (a) Excessively muted (b) Moderately muted (c) Best suitably muted (d) Minimally muted

Typical MASW raw wavefields obtained from Site-2 has also been subjected to the combined filtering and muting processes, as shown in Fig. 4.13. It can be observed that the raw wavefield possess recognizable noise adulteration (Fig. 4.13a), which has been suppressed by the

application of Band-pass filtering and muting (Fig. 4.13d). For the sake of comparison, Fig. 4.13b and Fig. 4.13c show the wavefield records obtained by subjecting the raw wavefield to 'only muting' and 'only Band-pass filtering' operations, respectively. It is observed that, in this case as well, the best result is obtained when the raw wavefield is subjected to 'combined muting and Band-pass filtering' operations. The corresponding dispersion images are highlighted in Fig 4.14. As Site-2 has the presence of a very hard granitic stratum (N≥42) at a shallow depth of 7 m, the energy band corresponding to the M0 dispersion curve was obtained to be very prominent even when the raw wavefield was processed (Fig. 4.14a). A minute scrutiny reveals that Fig. 4.14(a) contains the aliasing effect and energy accumulation in the very low frequencies of the dispersion image, which is absent from the image obtained from signal processed with simultaneous muting and Band-pass filtering (Fig. 4.14d). The dispersion images obtained from the other preprocessing operations fail to provide appropriate information. Dispersion image obtained from 'only muting' operation leads to significant low-frequency aliasing (Fig. 4.14b), while the same obtained from 'only Band-pass filtering operation' shows reduced resolution. Hence, it can be observed that the influence of combined Band-pass filtering and muting process is also effective for the shallow soil sites underlain by stiffer stratum.

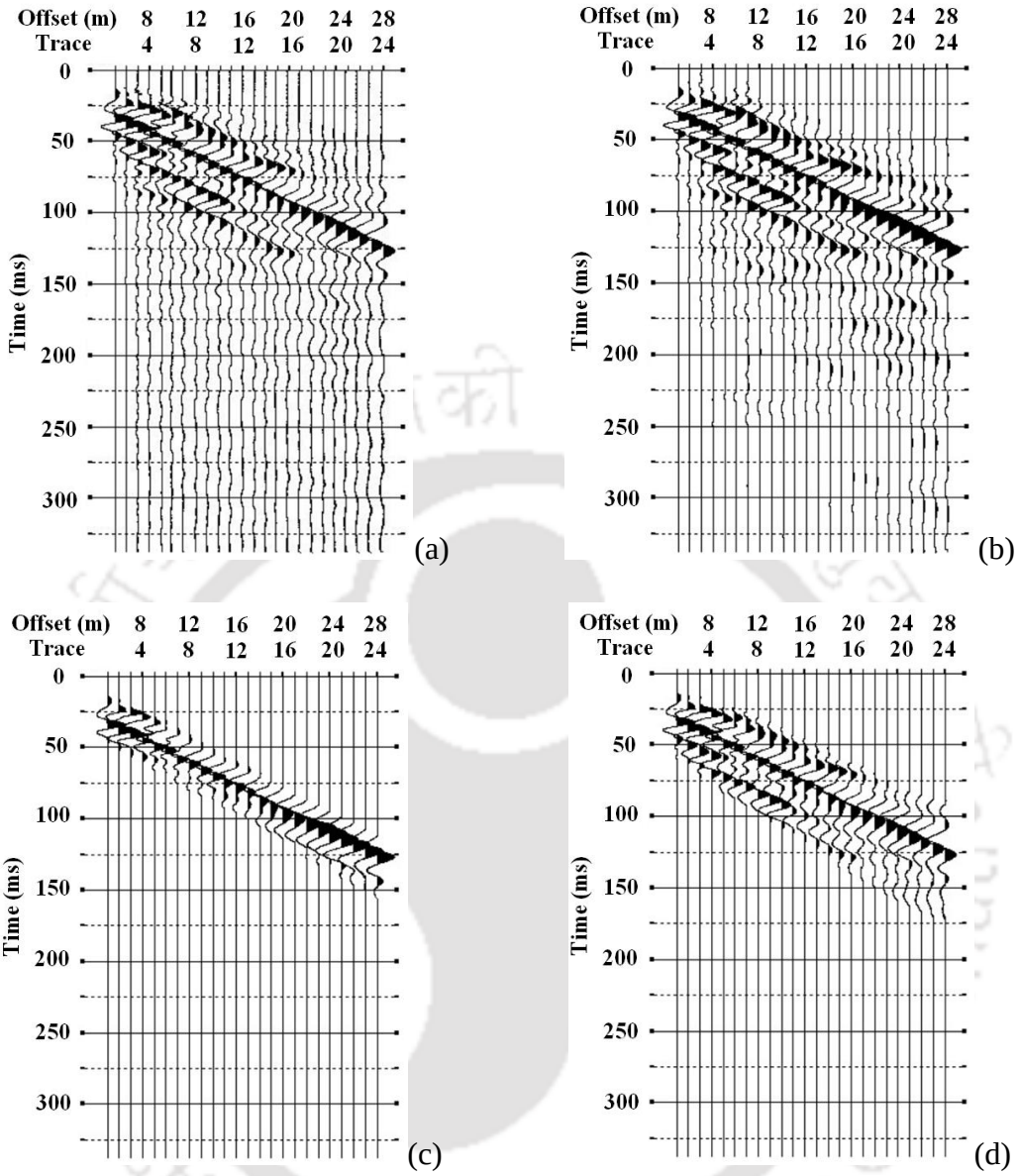

Fig. 4.13: Typical wavefield records from Site-1: (a) Raw wavefield (b) Only muted wavefield (c) Only filtered wavefield (d) Combined filtered and muted wavefield

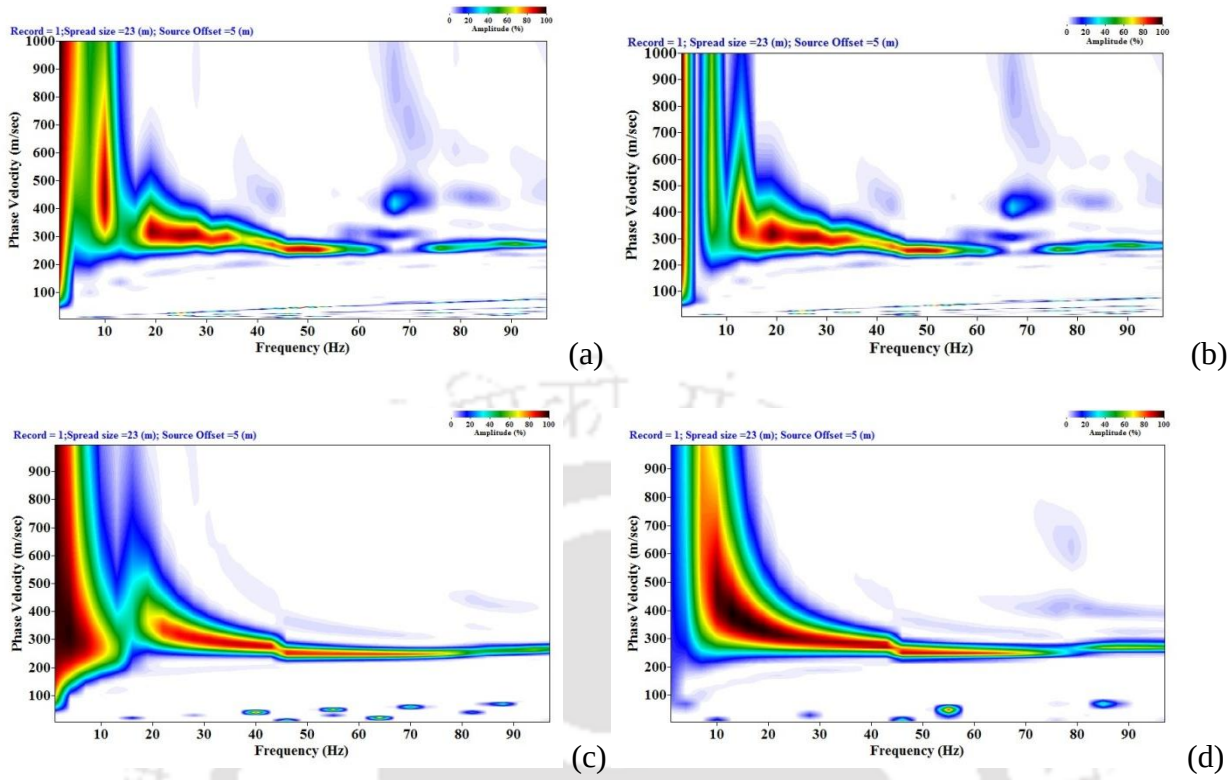

Fig. 4.14: Typical dispersion images from Site-2 based on (a) Raw wavefield (b) Band-pass filtered wavefield (c) Muted wavefield (d) Combined band-pass filtered and muted wavefield

4.4 Summary

This chapter highlights the influence of preprocessing parameters on the resolution of the dispersion images obtained from active MASW survey. Based on the conducted experimental investigations, the following salient points are noted:

- It is observed that the significant frequency range to be filtered is site dependent, and can be obtained from the normalized amplitude spectra of wavefield records. The filtering frequency range for soil sites underlain by a shallow depth stiffer stratum is higher (approx. 5-280 Hz) in comparison to that of softer sites (approx. 5-80 Hz).

- Band-pass filter with proper choice of filtering frequency range results in the best resolution of the dispersion image. High-cut filter produces a dispersion image with energy concentrations truncated in the lower frequency range. Dispersion images obtained from Low-cut and Band-stop filters are undecipherable, and are not recommended. Muting should be suitable so that the significant energy of the propagating wavefield is obtained.
- Excessive muting results in loss of information and resolution of the dispersion image. Application of muting on unfiltered wavefields produces aliasing effects on the low frequency range of the dispersion images.
- For active MASW survey conducted at any site, combined preprocessing using suitable muting on Band-pass filtered wavefield records provides the best resolution wavefield images and results in the dispersion images devoid of aliasing effects.

CHAPTER 5

INFLUENCE OF DATA ACQUISITION PARAMETERS ON THE RESOLUTION OF DISPERSION IMAGE

5.1 General

To obtain an accurate shear wave velocity profile, it is necessary to extract the dispersion curve with highest signal-to-noise ratio (SNR). However, the extraction process becomes difficult if the resolution of the obtained dispersion image is not sufficient. Several data acquisition parameters affect the resolution of the dispersion image, namely the effect of sampling parameters (sampling time and sampling frequency), offset distance, inter-receiver spacing, total number of channels, the type of source energy and the striker or base plate (Morlet 1983; Miller *et al*. 1999; Xia *et al.* 1999; Beaty *et al*. 2002; Yilmaz and Eser 2002; Tian *et al*. 2003a, 2003b; Liu *et al*. 2004; Lin *et al*. 2004; Sauvin *et al.* 2016). In this regard, considering various combinations of data acquisition parameters, a series of active MASW surveys were carried at three different locations (of different subsurface characteristics) within IIT Guwahati campus. To study the influence of the source energy and striker plate, experiments were carried out at Site-1 and Site-3, while the influence of the rest of the data acquisition parameters are deducted based on the experiments conducted at Site-1 and Site-2. The effects of these parameters are described in terms of the visual inspection of the resolution of the generated dispersion images and the corresponding shear wave velocity profiles. The aim of this study is to highlight influence of these parameters and frame some guidelines for generating good resolution dispersion images from an Active MASW survey.

5.2 Results and Discussions

This section documents the influence of various data acquisition parameters of active MASW survey on the visually identifiable characteristics of the generated dispersion images. The forthcoming sections elaborate on the influence of sampling parameters, offset distance, inter-receiver spacing, total number of channels, the type of source energy and the composition of striker or base plate. For the said purpose, a series of experimentations were conducted at all the three sites (Site-1, Site-2 and site-3) at IIT Guwahati, considering varying combinations of the above-mentioned parameters.

5.2.1 Influence of Sampling Parameters

Sampling frequency or the sampling rate, f_s, is the average number of samples obtained in one second (samples per second, sps), thus f_s= 1/T, where, T is the sampling interval (seconds). The sampling rate is chosen by considering the sampling theorem, incorporating the desired highest frequency of the signal (f_{max}). Frequencies greater than 100 Hz are rarely recorded. As per sampling theorem, a signal can be reconstructed exactly if it is sampled at a rate at least twice the maximum frequency component in it. Thus, f_s=2f_{max} is the desired condition, where, f_s is known as the Nyquist frequency (for discrete signals) or Nyquist rate (for continuous signals) (Proakis and Manolakis 2007). Any sampling frequency lower than the fails to retrieve the critical features of the wave signature. It is to be remembered that Nyquist-Shannon theorem was developed and is perfectly applicable to pure harmonic or superposed harmonic signals, as it was primarily developed for the conversion of analog signals to digital signals, and the reconstruction of the otherwise, wherein the waves being converted is free from noise contamination (Marks 1991). However, with increasing noise adulteration in the signals, as recorded by the geophones

during MASW survey, Nyquist-Shannon theorem is used only to decide the limiting or minimum sampling frequency so that the minimal random features of the wave signature can be captured. However, the choice of the actual sampling frequency, which is to be adopted for the survey, depends upon several factors such as the site characteristics and the prevalent noise fields, which contaminates the actual signals with stochastic or non-stochastic noise overlays. Hence, the choice of the Nyquist frequency as the sampling frequency, although theoretically acceptable, fails to achieve the desired resolution of the dispersion image constructed at a later stage. Hence, in order to obtain the best resolution dispersion images, the sampling frequency to be adopted differs for different sites having varying stiffness characteristics (as reported in the thesis), although for both the sites, the Nyquist frequency remains to be 200 Hz, as it has been already mentioned that signals with frequency greater than 100 Hz are rarely recorded. Sauvin *et al.* (2016) stated that time sampling should be small enough to avoid aliasing, and suggested to use a sampling interval of one-millisecond with a 1 second recording time. The time window length has to be long enough to record the whole surface wave on all the traces. If the recorded traces are truncated in time due to too short a window, a portion of the low velocity energy is lost and velocities can be overestimated with the reduction in the associated energy. If the sampling frequency is substantially higher, more than of the required information will be collected, and hence, eventually retrieve too less information from the impulse wave propagating through the geophone. In active survey, the waves produced due to impact are mostly high frequency waves penetrating smaller depths in the subsurface. For these waves, low sampling frequency proves to be insufficient, and hence, results in an obscure dispersion image, which fails to provide reasonable information. Hence, it is suggested to use higher sampling frequency in order to obtain the best possible dispersion curve.

Time of acquisition (t), or the total sampling time, is defined as the total number of recorded samples (n) per unit sampling frequency (*i.e.* $t = n/f_s$.). The higher is the number of samples, the more is the acquisition time. However, if the time of sampling is too high not only the phase of wave propagation carrying all the significant information is completed, the additional time would undesirably record noise and unwanted signals which will lead to the contamination of the useful counterpart. Hence, it is imperative to use a suitable sampling time in order to obtain a high resolution dispersion image. Different researchers have used different sampling frequencies and time of sampling, without providing a sound scientific reasoning. Kanli *et al.* (2006) carried out V_s^{30} mapping and soil classification for seismic site effect evaluation in Dinar region, SW Turkey, where sampling rate of 0.5 ms was used along with 1024 ms and 2048 ms sampling lengths. Gosar *et al.* (2008) have mentioned the use of sampling frequency of 2000 Hz in active MASW and 128 Hz in passive MASW for comparative study of active and passive multichannel analysis of surface waves carried out in Ljubljana, Slovenia. The sampling interval was 0.5 ms for active and 2 ms for passive MASW surveys. Eker *et al*. (2012) have mentioned the use of total sampling length of 2 s and sampling interval of 1 ms for carrying out the local site characterization.

For the present study, varying length of the samples, available in the MAE Seismograph, have been used i.e. 5120, 10240, 20480, along with different sampling frequencies (15000 Hz, 7500 Hz, 3750 Hz, 2000 Hz, 1000 Hz, 500 Hz, 100 Hz, and 50 Hz). The choice of sampling frequency and the number of samples is based on the time of sampling, which is in turn, governed by the site characteristics. Stiffer stratum lets the wave propagate faster in comparison to that of a softer

stratum, and hence requires a lesser time of acquisition. For Site-1, Fig. 5.1(a-h) illustrates the MASW raw records collected for different sampling frequencies corresponding to a fixed sample length of 5120 samples (Number of channels – 24, Offset distance – 7 m, Inter-receiver spacing – 1 m).

From the Figs. 5.1(a-f), it is clear that time of sampling is dependent upon the choice of sampling frequency. From Fig. 5.1a, exhibiting the results for a sampling frequency 15000 Hz, it can be observed that all the predominant waves have not been completely recorded by the geophone array, thus generating missing information in the collected record. The sampling time (ratio of total length of samples to sampling frequency) for the same is found to be 5120/15000=341 ms, which has not been sufficient for the phases to complete. Figure 5.1b, which is raw data for sampling frequency 7500 Hz, the sampling time is 5120/7500=683 ms, exhibits the recording time just appropriate enough for all the dominant phases to completely pass the geophone array. For the other cases (Figs. 5.1c-f), with lesser sampling frequencies, it can be observed that although the dominant phases gets completed, unnecessary increase of sampling time becomes redundant in acquiring any further beneficial information, rather becomes detrimental to the signal quality due to unwanted noise adulteration.

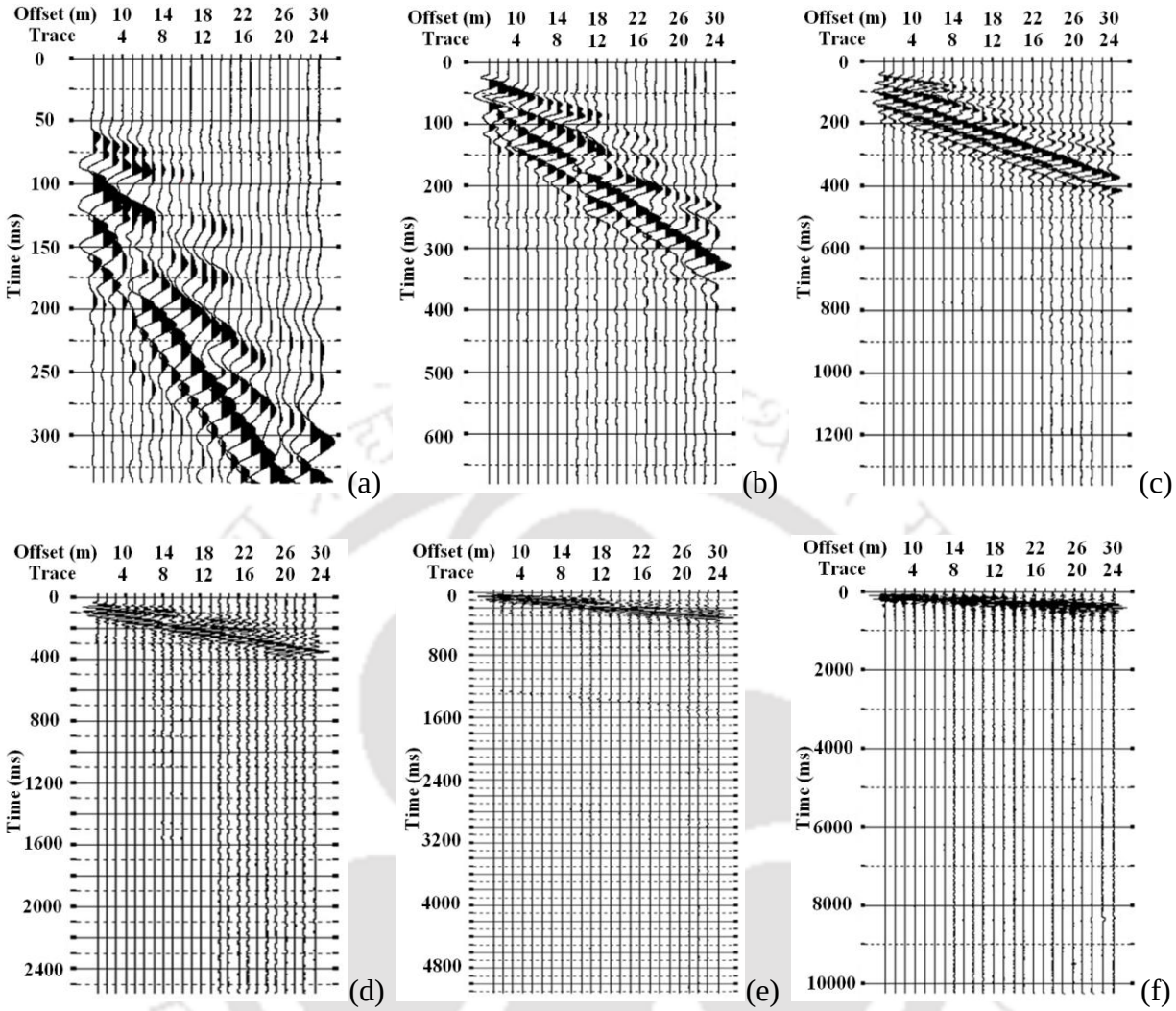

Fig. 5.1: Effect of sampling frequency on time records obtained from Site-1 for 5120 samples (a) 15000 Hz (b) 7500 Hz (c) 3750 Hz (d) 2000 Hz (e) 1000 Hz (f) 500 Hz (Number of channels – 24, Offset distance – 7 m, Inter-receiver spacing – 1 m)

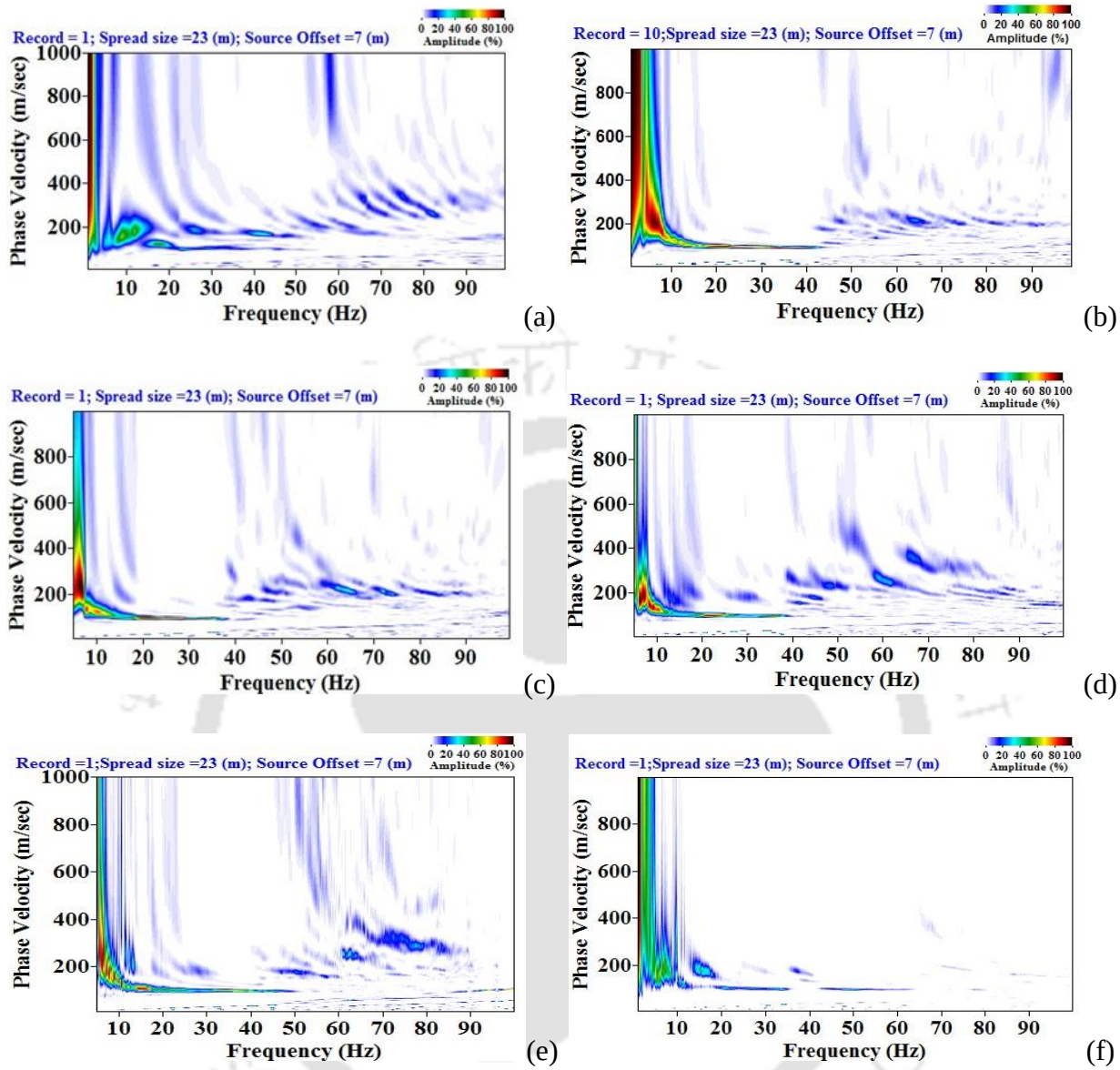

Fig. 5.2: Dispersion images corresponding to 5120 samples having different sampling frequencies (a) 15000 Hz (b) 7500 Hz (c) 3750 Hz (d) 2000 Hz (e) 1000 Hz (f) 500 Hz (Number of channels – 24, Offset distance – 7 m, Inter-receiver spacing – 1 m)

Corresponding to the collected time-stamps exhibited in Fig. 5.1, the dispersion images for different sampling frequencies (15000 Hz, 7500 Hz, 3750 Hz and 2000 Hz) are shown in Fig. 5.2 (a-d). It can be seen that the dispersion image with 15000 Hz sampling frequency does not contain any significant information, owing to the incomplete time stamps collected from field survey. Moreover, dispersion image corresponding to the sampling frequency of 2000 Hz produces noise adulteration near the fundamental dispersion curve, and does not produce a good resolution dispersion image. This behavior is attributed to the noise adulteration in the recorded signals due to unnecessary larger time of sampling. The dispersion images generated by using 7500 Hz and 3750 Hz sampling frequencies possess good resolution; better resolution being exhibited by the former as observed by the presence of a prominent energy band till a frequency of 40 Hz. Dispersion images for the sampling frequencies 1000 Hz and 500 Hz were beyond consideration for any useful information due to excessive noise adulteration in the time stamps. As mentioned earlier, the best suitable length of sampling, allowing for the completion of the propagation of the dominant phases, although not overshooting them to a large extent, is immensely important for obtaining a good resolution dispersion image.

Figure 5.3 exhibits the time stamps of the recorded signals obtained for a sampling frequency of 15000 Hz, having various lengths of samples. It is observed from Fig. 5.3a that sampling time (341 ms) obtained for a sample length of 5120 is insufficient to capture the complete phase propagation. This observation required increasing the length of the sample. Figures 5.3b and 5.3c show the raw data collected based on sample lengths of 10240 and 20480, thus having an enhanced sampling time 10240/15000=682 ms and 20480/15000=1365 ms, both of which are sufficient for the phase to complete.

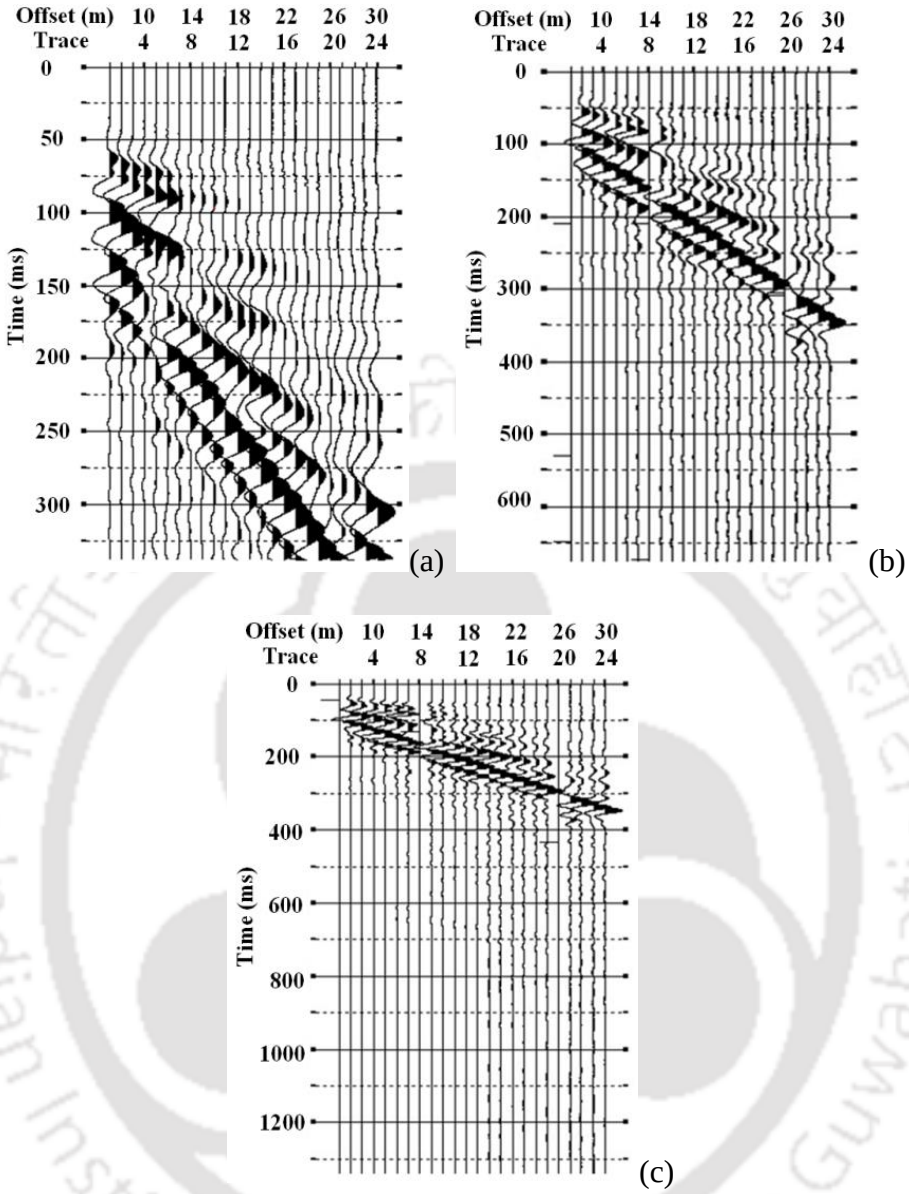

Fig. 5.3: Collected time records having sampling frequency 15000 Hz with varying number of samples (a) 5120 (b) 10240 (c) 20480 (Number of channels – 24, Offset distance – 7 m, Inter-receiver spacing – 1 m)

Figure 5.4 exhibits the corresponding dispersion images, from which it can be observed that a good resolution dispersion image is obtained when a suitable phase completion is attained for 10240 samples (Fig. 5.4b). For the other cases, when either the phase is not complete (5120

samples) or unwanted noise is recorded due to unnecessary sampling (20480 samples), the obtained dispersion images are poor as can be Fig. 5.4a and Fig. 5.4c, respectively.

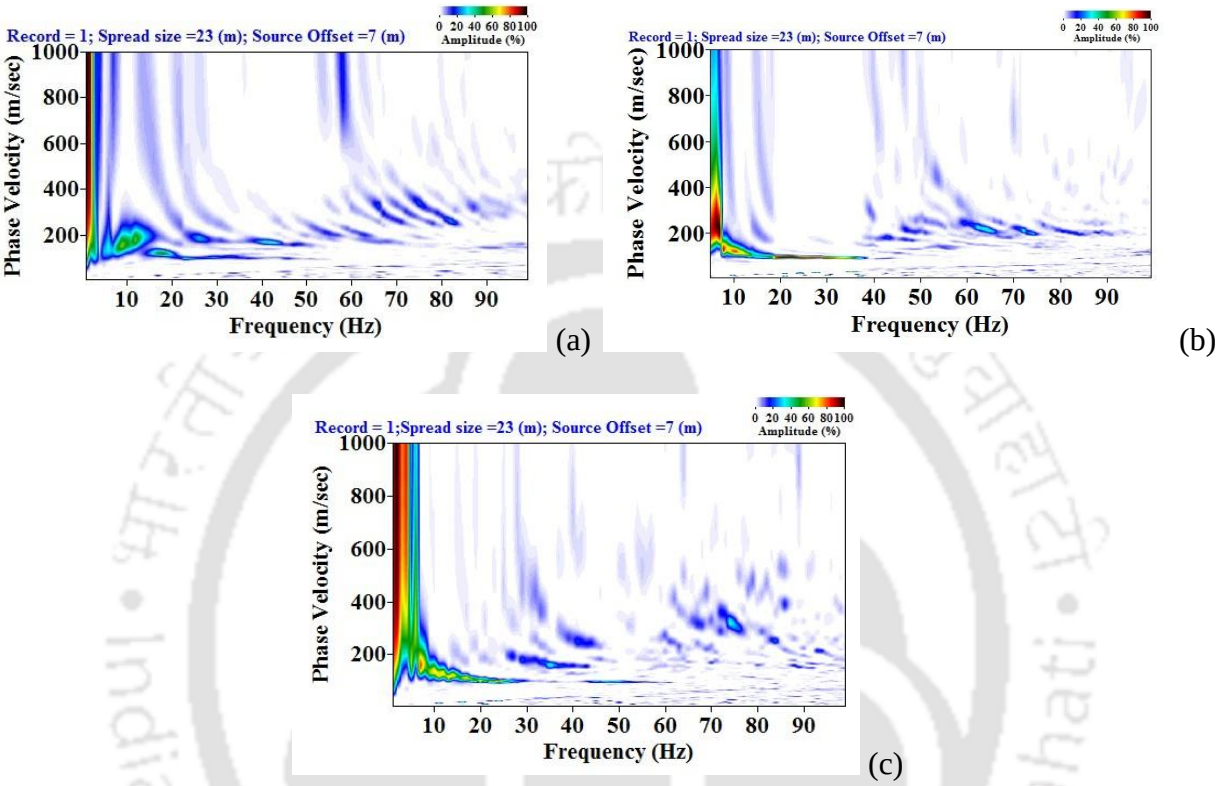

Fig. 5.4: Dispersion images developed from the collected time records having sampling frequency 15000 Hz with varying number of samples (a) 5120 (b) 10240 (c) 20480 (Number of channels – 24, Offset distance – 7 m, Inter-receiver spacing – 1 m)

Figure 5.5 exhibits the results for various sampling time for the record collected based on 7500 Hz sampling frequency. It can be observed that for this case, 5120 samples are sufficient to capture the completion of the wave propagation through the array; increase in the number of samples increased the sampling time, leading to noise adulteration. In this case as well, the best dispersion image is obtained for the suitable sampling with 5120 samples (Fig. 5.5a), while, for

the excess time records, the quality of the dispersion images gradually becomes inferior due to significant noise adulteration (Fig. 5.5b-c). Figure 5.6 shows the corresponding dispersion images, which reconfirm that 5120 samples with sampling frequency of 7500 gives the best resolution.

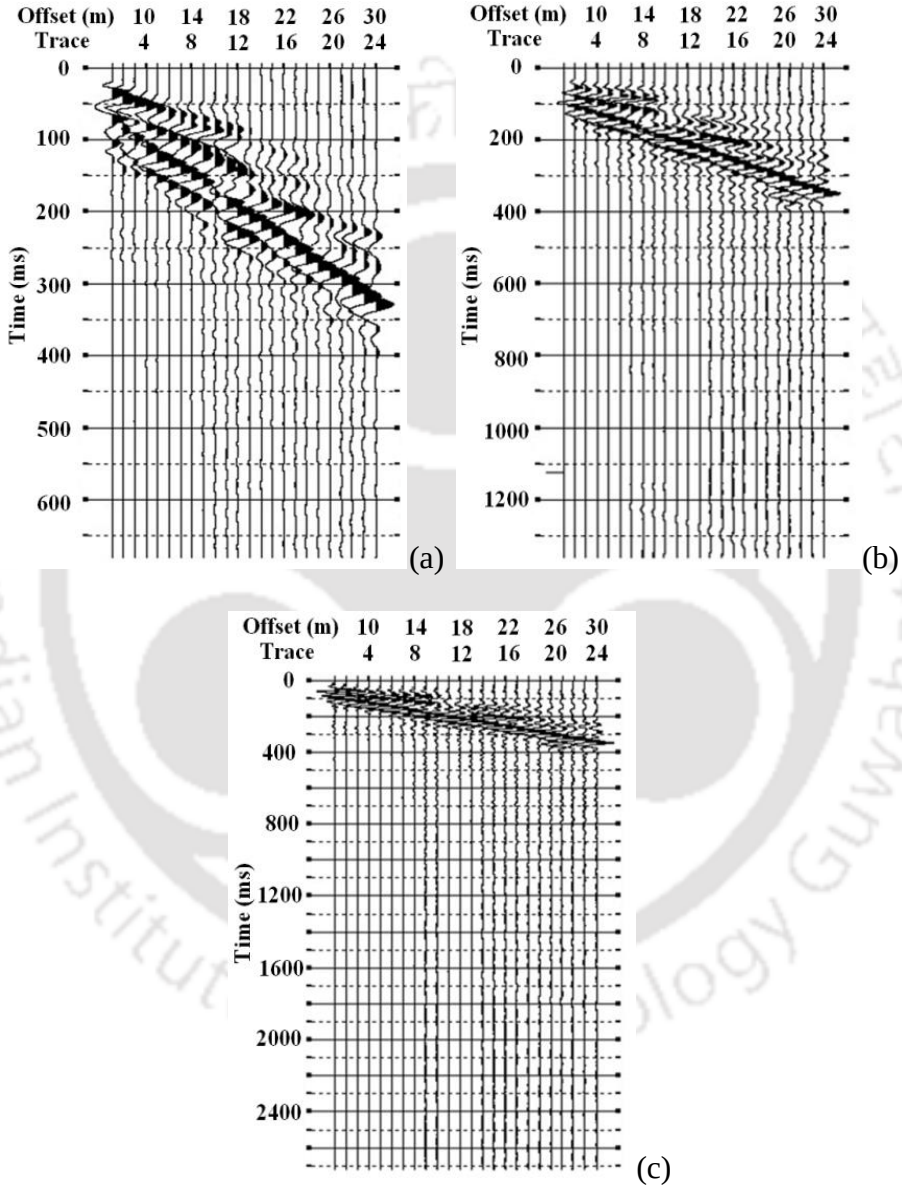

Fig. 5.5: Collected time records having sampling frequency 7500 Hz with varying number of samples (a) 5120 (b) 10240 (c) 20480 (Number of channels – 24, Offset distance – 7 m, Inter-receiver spacing – 1 m)

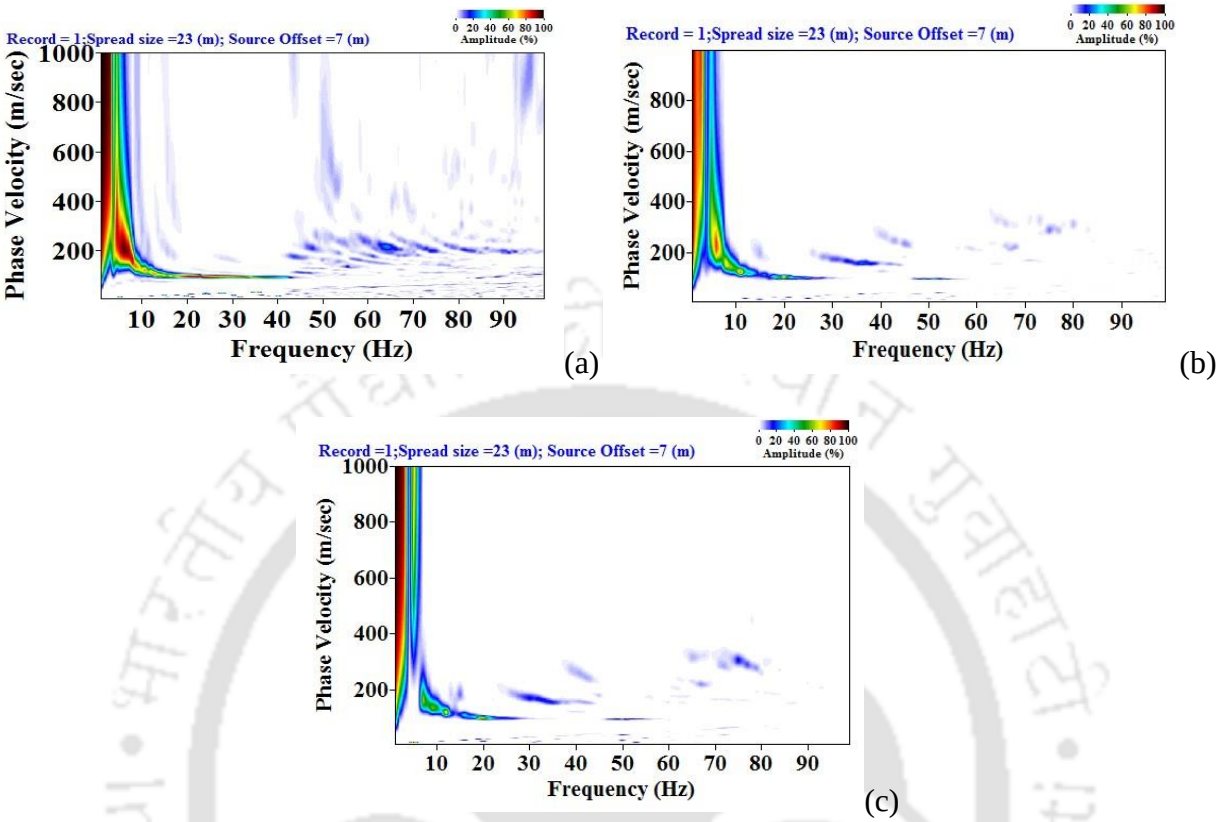

Fig. 5.6: Dispersion images developed from the collected time records having sampling frequency 7500 Hz with varying number of samples (a) 5120 (b) 10240 (c) 20480 (Number of channels – 24, Offset distance – 7 m, Inter-receiver spacing – 1 m)

The effect of sampling frequency was also checked for Site-2, which consists of stiffer substrata located at shallow depth, in contrary to Site-1. Figure 5.7 exhibits the collected time stamps from varying sampling frequencies. In this case, considering 5120 samples, sampling frequency of 15000 Hz is found to be sufficient enough to trace the complete phase propagation through the geophone array. The minimum time of sampling required in this case is obtained to be 5120/15000=341 ms.

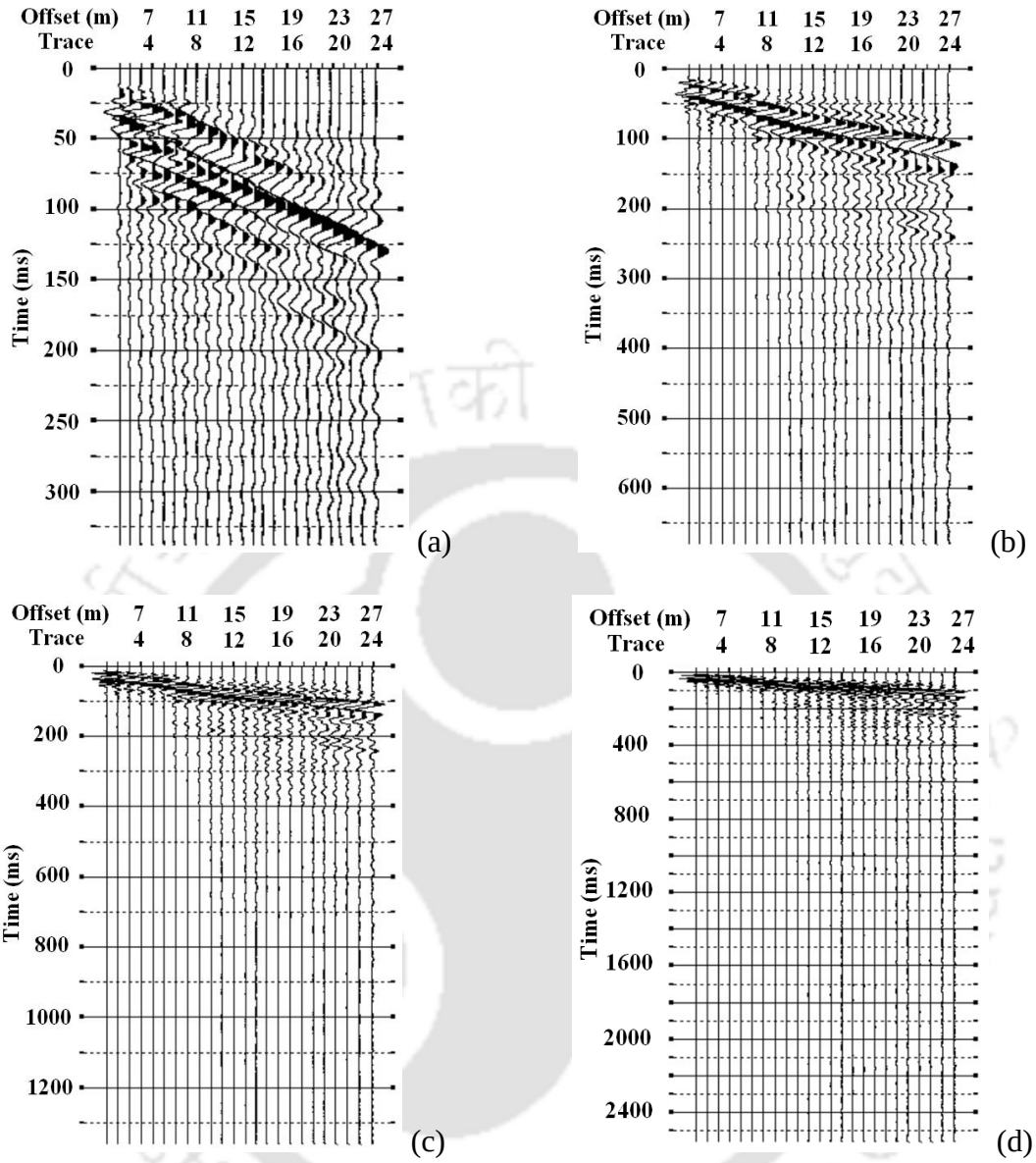

Fig. 5.7: Effect of sampling frequency on time records obtained from Site-2 for 5120 samples (a) 15000 Hz (b) 7500 Hz (c) 3750 Hz (d) 2000 Hz (Number of channels – 24, Offset distance – 4 m, Inter-receiver spacing – 1 m)

Hence, based on the present study, it can be stated that compared to the softer soil site, for stiffer substrata, the time required for complete waveform to propagate is lesser, which can be achieved by comparative lower number of samples recorded with relatively higher sampling frequency.

The dispersion images corresponding to the time stamps (Fig. 5.7) is shown in Fig. 5.8, from which it can be observed that the resolution decreases with the increasing sampling time. Hence, it can be confirmed that undesirable sampling of the noises beneath the significantly suppress the resolution, and hence the utility, of the dispersion image.

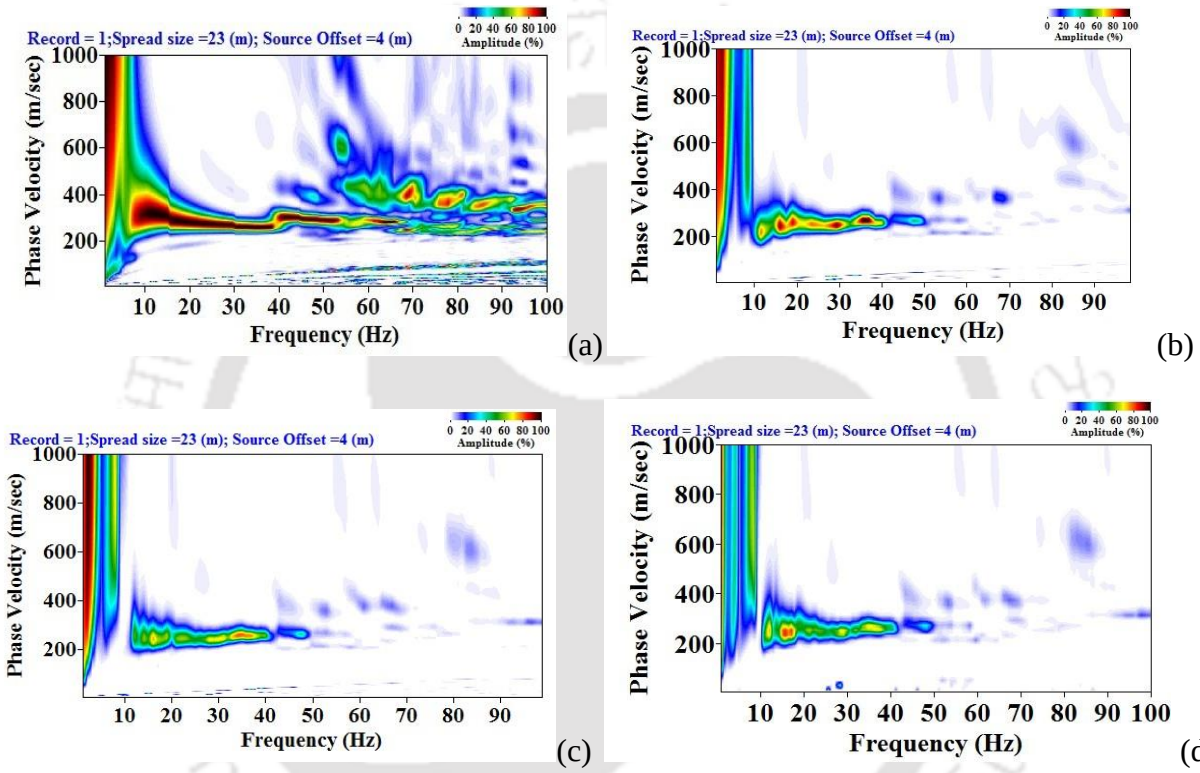

Fig. 5.8: Effect of sampling frequency on the dispersion images obtained from Site-2 for 5120 samples (a) 15000 Hz (b) 7500 Hz (c) 3750 Hz (d) 2000 Hz (Number of channels – 24, Offset distance – 4 m, Inter-receiver spacing – 1 m)

Based on the above observations, it can be stated that for any particular site, the complete phase of wave propagation through the geophone array can be tracked by various combinations of sampling frequency and sampling length. Among the possible combinations, choosing the one

with higher sampling frequency provides a higher resolution dispersion image, as under such condition, more information can be collected from the recorded signal per unit time.

Figure 5.9 portrays the amplitude spectra obtained for the Site-1 and Site-2. It can be understood that the length of the samples does not have a significant effect on the quality of the collected record, provided the phase of wave propagation is completely captured. It can be seen that for a particular site, the normalized amplitudes are tolerably same for different length of the samples.

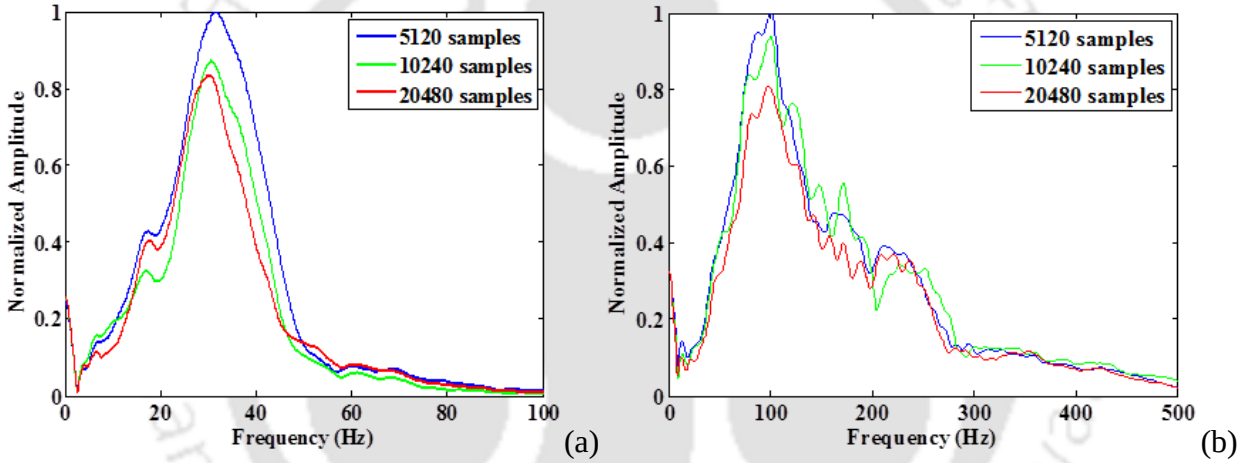

Fig. 5.9: Normalized Amplitude spectra obtained for different sample lengths (a) Site-1 with sampling frequency 7500 Hz (Number of channels – 24, Offset distance – 7 m, Inter-receiver spacing – 1 m) (b) Site-2 with sampling frequency 15000 Hz (Number of channels – 24, Offset distance – 4 m, Inter-receiver spacing – 1 m)

Based on the above study, a sample length of 5120 samples for sampling frequency 7500 Hz was found suitable and chosen for the Site-1 for further processing. Site-2 being stiffer, relatively lesser sampling time proved to be sufficient. Hence, a length of 5120 samples for sampling frequency 15000 Hz was chosen. Figure 5.9 also indicates the range of frequencies over which

the energy of wave propagation is concentrated. For Site-1, the range is between 20-40 Hz, whereas in the relative stiffer Site-2, the same is obtained around 50-150 Hz. It has been observed that the records collected using 50 Hz sampling frequency are insufficient to produce a dispersion image with clarity due to the violation of the basic sampling theorem. Lower sampling frequencies have higher sampling intervals, and hence, record too less number of bits of information from the wave propagating through the geophone array, and hence, are unable to represent the characteristics of the propagating medium.

In the absence of any previous subsurface exploration data, trial tests are invariably necessary even to get the basic information about the stiffness characteristic of the site. As mentioned in Chapter 4, it is imperative that the geophone array records the entire wavefield generated by the impulse source. Fig. 4.7a exhibits such a typical record, which primarily indicates the propagation of the waves from the source to multiple geophone receivers with a phase lag. The recognizable maximum and minimum slope of the wavefield provides the idea of the range of shear wave velocity accommodated in the study. The dominant, or the average, slope of the wavefield approximately represents the average shear wave velocity of the site. For example, in the typical wavefield shown in Fig. 14(b), it can be visually observed that a dominant wave requires approximately 250 ms to travel from the source to the last geophone (27 m) while passing through the substrata, thus illustrating an approximate velocity of 110 m/s, which is conforming to the approximate shear wave velocity of Site-1 as mentioned in Chapter 3. Although sampling frequency and sampling interval are site dependent, the approximate idea of the shear wave velocity at the site can be estimated as described herein, and accordingly, the

recommendations for the sampling frequency can be adopted to reduce the number of initial trial and errors during the field investigation.

From the above study, it can be concluded that proper choice of sampling frequency is necessary for obtaining good resolution dispersion image. The conventional notion that the resolution of the dispersion image increases with the increase in sampling frequency is not always necessarily true. In fact, the choice of sampling frequency is dependent upon the time of sampling and the total length of the sample. Before carrying out any rigorous experimentation at a particular site, it is recommended to check whether the chosen sampling frequency is appropriate by reading the recorded phase propagation pattern. It is important that only a suitable acquisition time is chosen so that the collected records are complete and devoid from the adulterating noise to the highest possible extent.

5.2.2 Influence of Offset Distance

Surface waves become planar (or sometimes termed 'stabilized') only after travelling a certain distance from the source (Stokoe *et al.* 1994; Park *et al.* 1999). Qualitatively, a longer wavelength traverses a greater distance before it becomes planar. Offset distance is defined as the linear distance between the source and the first receiver geophone. There are two kinds of effects due to offset distance i.e. the near-field effect and the far-field effect (Park *et al.* 1999; Park 2011). The near-field effect represents the unpredictable non-planar propagation of surface waves near the source point caused by generation of excess stresses, which are generally responsible for underestimated phase velocities of relatively long wavelengths. The near-field effects are associated with the minimum distance required for planar surface waves to develop,

and is governed by the interference of multiple reflections and mode conversions of body waves at the free surface. Since, the surface wave method requires the analysis of horizontally travelling plane waves, it is important to avoid recording of any non-planar components. Far field effects indicate that surface waves either become relatively weak at larger distances because of attenuation and geometrical spreading, or are contaminated by prevalent undesirable noise wave field such as traffic noise, random ambient noise, scattered surface waves and body waves (Park 2011). The contamination can also be caused by higher modes of surface waves that may prevail at far offsets because of their relatively smaller attenuation. If these contaminated wave fields are included in the analysis for dispersion imaging, they tend to cause destructive interference (due to superposition of out-of-phase waves) on the computation of the phase velocity-frequency relationship, and hinder from obtaining large amplitude in the image space. Park *et al.* (2002) proposed field parameters for conducting active MASW survey, in which source offset is provided as a function of different field conditions such as receiver source, receiver spread and depth of investigation. Zhang *et al.* (2004) proposed an optimized set of measurements parameters in MASW survey, given as

$$x_1 = x_l,\ x_2 = 3x_l \text{ and } x_l = \frac{\lambda_{\max}.V_{\min}}{4\Delta V} \tag{5.1}$$

where, x_1 is nearest receiver offset and x_2 is farthest receiver offset, x_l is half-layout length, $\lambda_{\max}$ is maximum wavelength, $V_{\min}$ is minimum phase velocity and ΔV is difference between maximum and minimum phase velocities. Based on simple experimental data, Xu *et al*. (2006) proposed a quantitative estimation of minimum offset for active MASW survey as

$$d = \frac{2h}{\sqrt{\sigma^2 - 1}} \tag{5.2}$$

where, $\sigma = V_p / V_s$, V_p is the P-wave velocity, V_s is the S-wave velocity and *h* is the thickness of the layer. For easier determination of the dispersion curve in terms of the M0 mode (based on its distinctness from the higher modes), Dikmen *et al*. (2010) suggested two offset distances for obtaining a good resolution dispersion image instead of one offset (as used in the conventional practice of MASW). The first offset distance is considered as 3-4 times the inter-receiver spacing. The second offset distance is considered to be equal to or greater than one-third of the spread length depending on the energy of the seismic source. Park (2011) suggested a trial-and-error technique and recommended an initial of value of 0.5 m as nearest offset distance and 3 m as farthest offset distance.

In the present study, in order to check the far-field and near-field effect on the resolution of dispersion image, experiments were carried out with different offsets (varying in the range of 0-15 m), sampling frequencies (7500-15000 Hz), and receiver spacing (1-3 m), accompanied by varying number of receivers (12 and 24). All the collected field records were treated with Band-pass filtering and suitable muting to remove the noise adulterations to the best possible extent. Three vertical stacking of the dispersion image have been used to increase the resolution of the images obtained for Site-1. Site-2 being a stiffer ground, single stack was found to be sufficient in obtaining good resolution dispersion images. Figure 5.10 shows the effect of offset distance, where it can be clearly observed that a larger offset distance result in a higher time-lag for the receivers to commence recording the signals.

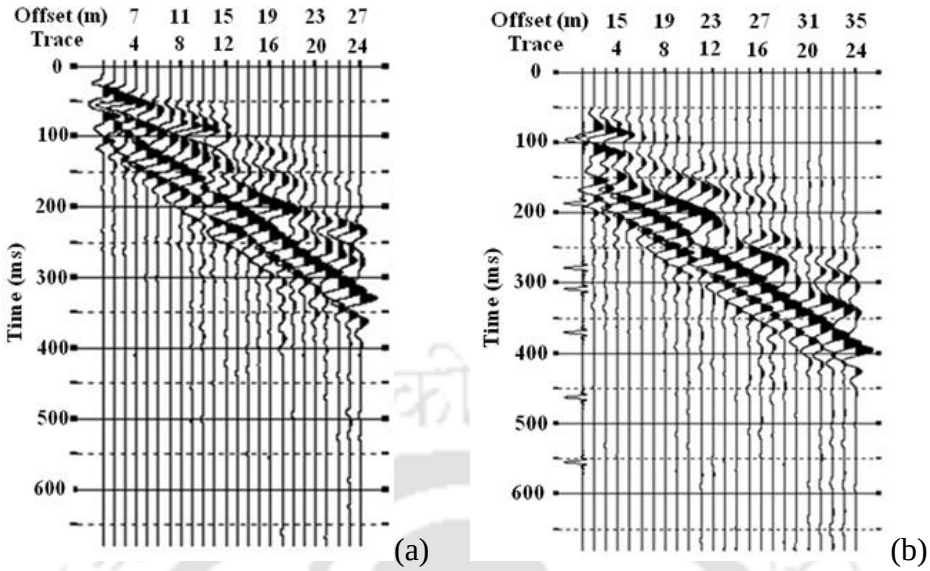

Fig. 5.10: Typical wavefield records obtained at Site-1 for different offsets (a) 4 m (b) 12 m (Sampling frequency – 7500 Hz, Inter-receiver spacing – 1 m)

Figure 5.11 shows the effect of the near-field and far-field offsets on the obtained resolution of dispersion image. Figure 5.12 shows the corresponding inverted shear wave velocity profiles. It can be observed that due to significant interference from body waves, the M0 dispersion images obtained using near offsets, 0 m (i.e. when the source is just adjacent to the first receiver) and 4 m (Fig. 5.11a-b), does not exhibit a distinct energy trend; rather, displays a discontinuous trend with an unnaturally high accumulation of energy at low frequencies. Dispersion curves, extracted by image processing technique, when inverted, resulted in extremely shallow depth (5 m) shear wave velocity profiles (Fig. 5.12a-b). The trend of M0 dispersion image becomes distinguishable and continuous for surveys conducted with 6 m offset and beyond (Fig. 5.11c-f). Although the dispersion curves for 6 m and 8 m offsets (Fig. 5.11c-d) are visually recognizable, the shear wave velocity profiles are obtained only up to the depths of 10-11 m (Fig. 5.12c-d). Shear wave velocity profiles obtained with a 10 m offset exhibited the agreeably best match with that

obtained from a previously conducted field borehole survey. From Fig. 5.11(c-f), it is also recognized that with the increase in the offset distance, the dispersion images gradually becomes adulterated due to the far offset effect.

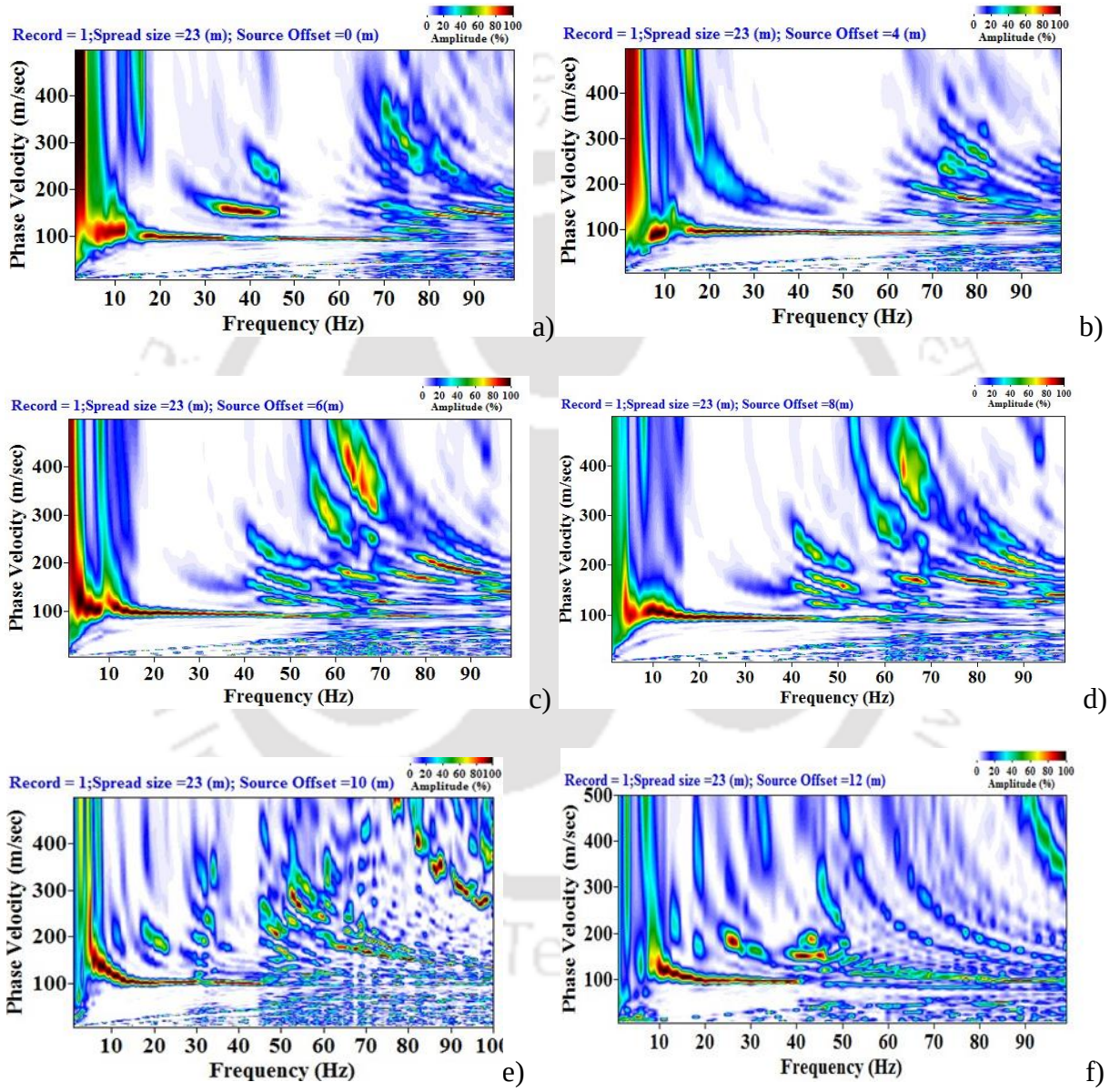

Fig. 5.11: Dispersion image obtained from active MASW survey at Site-1 conducted with various offset distances (a) 0 m (b) 4 m (c) 6 m (d) 8 m (e) 10 m (f) 12 m (Sampling frequency – 7500 Hz, Sample length – 5120, Inter-receiver spacing – 1 m, Number of channels - 24)

The findings for the offset distance conform and agree well with the recommendations of the previous researchers. It has been recommended that in order to achieve subsurface information until a depth of 30 m using 4.5 Hz geophones, 3-18 m offset distance is suitable. It has also been stated that the recommended values are not definitive and can possess a tolerance of ±20%, and requires continuous updating based on the tests conducted at various regions comprising various soils (Park *et al*. 2002; http://masw.com/ACQParaTables.html).

For 12 m offset and beyond, the resulting dispersion images exhibit dominant adulteration throughout the significant frequency range of analysis. Such adulteration, due to far offset effect, results in low SNR for the extracted dispersion curve, as a result of which shear wave velocity profile is obtained for a significantly curtailed depth of investigation, 5 m for this case. The aim of the present study is to identify a reasonable value of offset distance which provides a good resolution dispersion image with a distinguishable M0 dispersion curve, spread over a wide frequency range, and at the same time, is able to effectively portray the substrata characteristics through the inverted profiles. In this regard, an offset of 10 m proves to be the best choice for Site-1. However, keeping in mind the practical uncertainties, a choice of 6-10 m offset can be stated to be sufficient to obtain a good resolution dispersion image for sites comprising of soft strata ($V_{s,avg}$ < 200 m/s)**.** The averaged power spectrum was also calculated for all the offset distances to check the amount of sustained energy content.

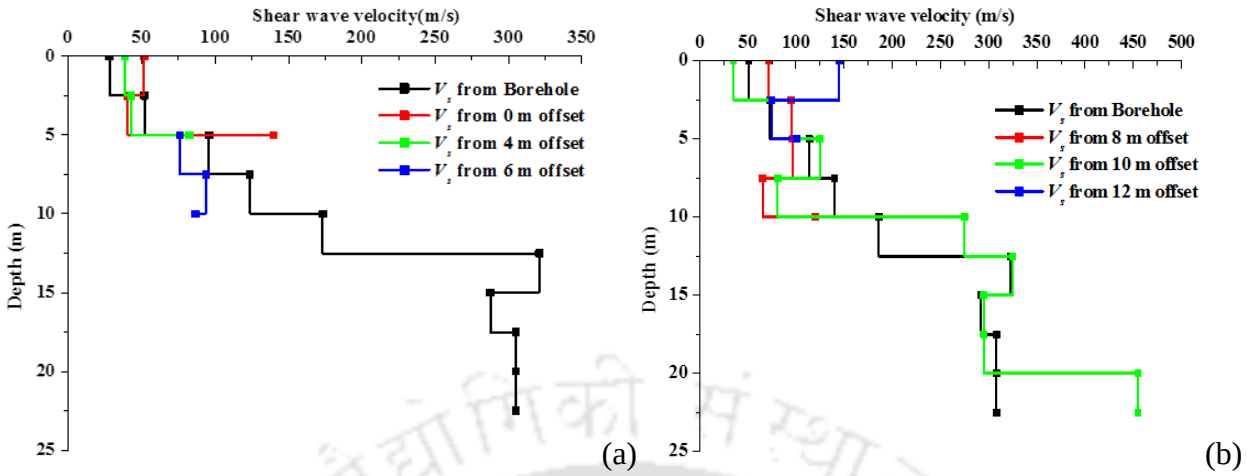

Fig. 5.12: Comparison of shear wave velocity profiles obtained from borehole survey at Site-1 and that obtained from MASW survey considering various offset distances (Sampling frequency – 7500 Hz, Sample length – 5120, Inter-receiver spacing – 1 m, Number of channels - 24)

Dikmen *et al.* (2010) manifested the application of averaged power spectrum in order to determine the spectral properties of different types of linear spreads. In the present study, similar concept has been used to determine the spectral properties based on different configurations of linear spreads with varying offsets. Power Spectral Density (PSD) is a measure of a signal's power intensity and distribution in the frequency domain. In practice, the PSD is computed from the Fourier spectrum of a signal. The unit of power spectra is energy (variance) per frequency (width). The energy within a specific frequency range can be obtained by integrating the Power Spectra within the said frequency range. By Parseval's Theorem, Power spectrum is defined as $P=[abs(FFT(signal)]^2$. Using the stated theorem, the normalized average power spectra from 15 different linear arrays with varying offset distances was calculated, the inter-receiver spacing being 1 m for each case. The average power spectrum from each test was estimated by averaging the Fourier power spectra of all the 24 traces of each MASW record. Figure 5.13 represents such a set of averaged power spectrum for an active MASW survey conducted at Site-1.

It is observed that a configuration with 0 m and 1 m offsets resulted in power spectrum with incomparably high peak energy as compared to the same obtained with other offsets. Such observation is common due to the significant body wave intrusion in the wavefield owing to the prevalent near-offset effect, and hence, further details of these observations are discarded herein. The PSD obtained from the configurations having offsets of 1-3 m also exhibits high energy, although it quickly degrades for higher frequencies beyond 50 Hz, thus showing the incapability of small offsets to track the effect of higher frequencies in the collected records. Configurations with offsets within the range of 7-12 m recorded significant energy for a very wide frequency band, which inadvertently states that these are the favorable offset ranges that are prone to pick up the Rayleigh wave propagation. Increment of offset beyond 12 m resulted in the incomplete wavefield propagating through the geophone array, owing to the attenuation of energy towards the far end of the array, thus revealing the far-offset effect. Under these conditions, the total energy of the recorded wavefield significantly reduces.

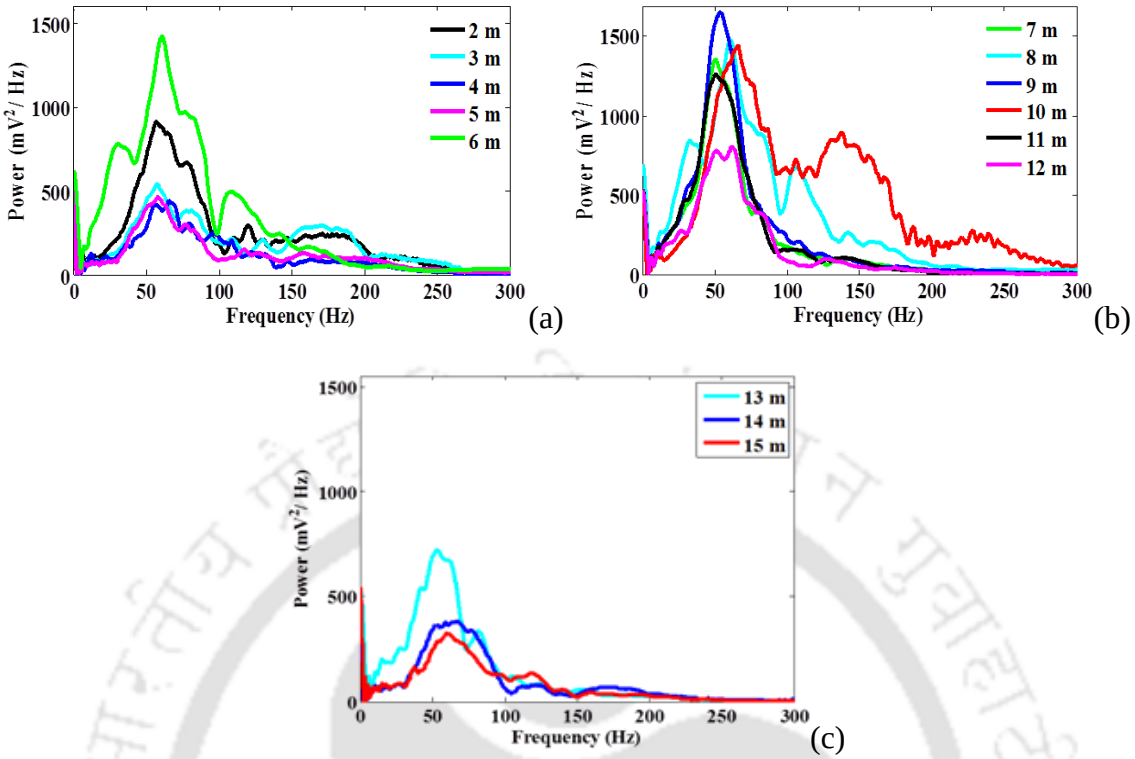

Fig. 5.13: Averaged power spectrum estimated from the wavefield records for active MASW survey conducted at Site-1 with various offset distances (Sampling frequency – 7500 Hz, Sample length – 5120, Inter-receiver spacing – 1 m, Number of channels - 24)

Figure 5.14a illustrates the total energy of the signal, obtained as the area under the average power spectrum curves. It can be observed that the area under the average power spectrum curve is comparatively high in the range of offsets 6-10 m, where the wavefield recorded for the 10 m offset exhibits highest energy. Correspondingly, Fig. 5.14b shows that the frequency bandwidth, containing the significant energy of the signal, is also highest for the wavefield recorded with 10 m offset. This signifies that at Site-1, not only the total energy of the signals recorded with 10 m offset is highest; it is also distributed over a wide frequency band resulting in the development of high resolution dispersion images.

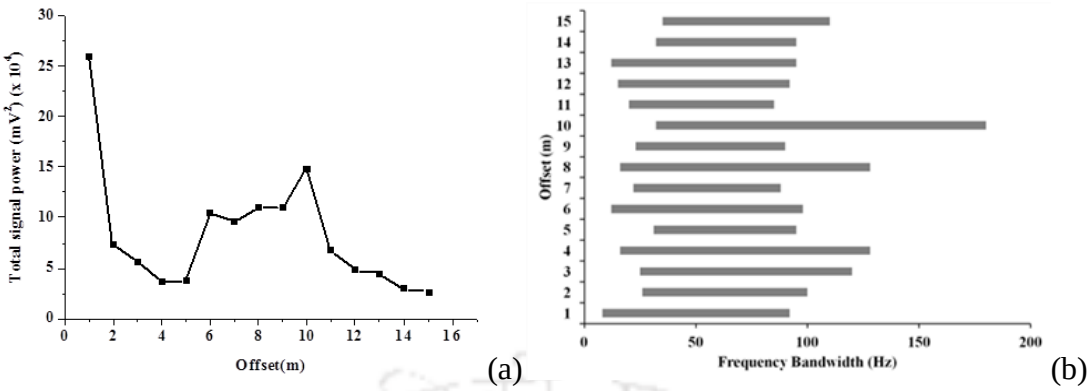

Fig. 5.14: (a) Total power of wavefield records collected at Site-1 for various offset distances (b) Frequency bandwidth of significant energy content of the collected wavefields records (Sampling frequency – 7500 Hz, Sample length – 5120, Inter-receiver spacing – 1 m, Number of channels - 24)

The near field and far field effect of offset was also checked for Site-2. The sampling frequency used for data acquisition at Site-2 is 15000 Hz, having 5120 number of samples; thus, rendering the sampling time to be 341 ms. Single stack was used for the analysis of the raw data at Site-2. Figure 5.15(a-h) shows the effect of offset on resolution of dispersion images. The dispersion curve extracted using image processing technique indicated that active MASW surveys conducted with 4-6 m offsets resulted in generating the best resolution dispersion images. Since Site-2 is founded on a stiffer substrata, a large offset distance was not necessary to obtain good resolution dispersion images. Moreover, for offset distances of 0-2 m, the M0 dispersion curve was observed to be exceessively thick due to larger extent of body wave intrusion.

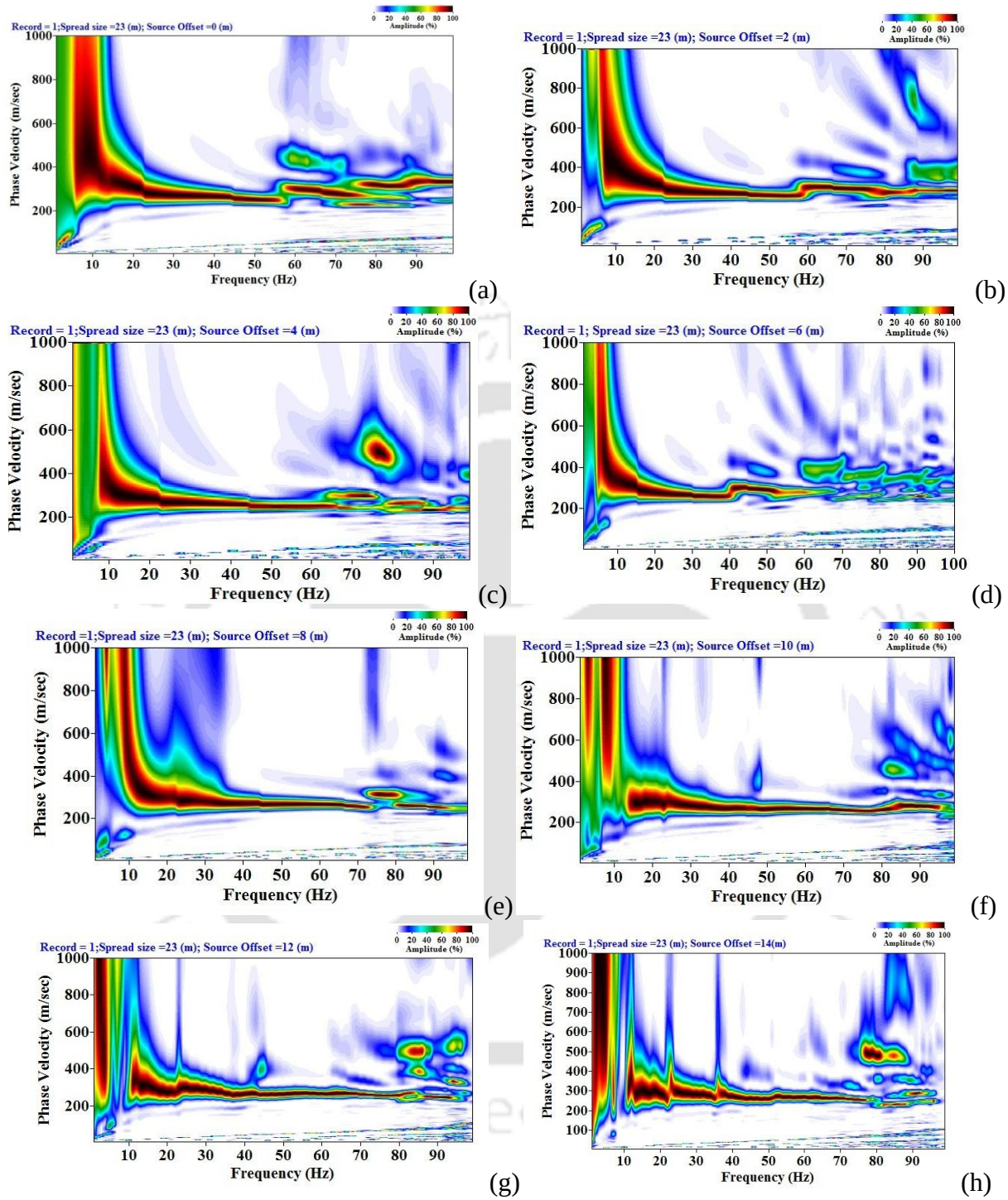

Fig. 5.15: Dispersion image obtained from survey at Site-2 conducted with various offset distances (a) 0 m (b) 2 m (c) 4 m (d) 6 m (e) 8 m (f) 10 m (g) 12 m (h) 14 m (Sampling frequency – 15000 Hz, Sample length – 5120, Inter-receiver spacing – 1 m, Number of channels - 24)

The comparison of the V_s profiles obtained from the borehole survey and active MASW survey is shown in Fig. 5.16. Due to the presence of hard stratum, it was possible to conduct the borehole survey only up to a depth of 7.5 m. From the results, it can be seen that, not only the V_s profile obtained from the MASW survey with 6 m offset produced the best match; it also provided the information of much deeper strata which could not be investigated from the borehole survey. The results of 8 m offset survey are also comparable in terms of the depth of investigation, although the results do not particularly agree the profile obtained from borehole survey. Thus, keeping in mind the practical uncertainties, a choice of 4-6 m offset can be stated to be sufficient to obtain a good resolution dispersion image for sites comprising of soft strata ($V_{s,avg}$ greater than 200 m/s).

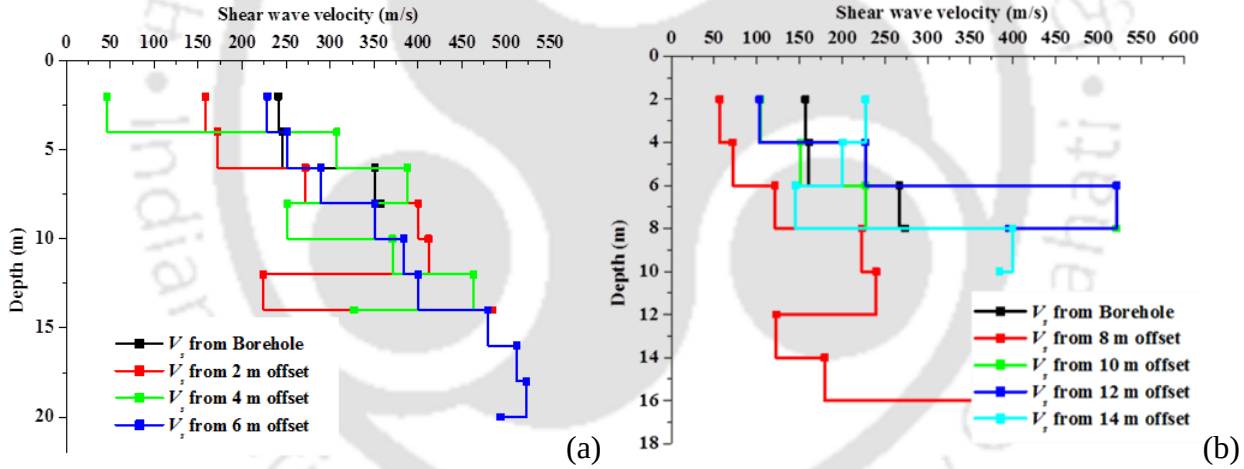

Fig. 5.16: Comparison of shear wave velocity profiles obtained from borehole survey and active MASW survey at Site-2 (Sampling frequency – 15000 Hz, Sample length – 5120, Inter-receiver spacing – 1 m, Number of channels - 24)

Figure 5.17 shows the averaged power spectra of the wavefield records at Site-2 for various offsets. It is observed that the records with 1-2 m offset distances exhibit very high spectral densities due to body wave intrusions, portraying the near-offset effect as could be seen from the

corresponding dispersion images (Fig. 5.15a-b). The spectral densities for wavefields with offsets greater than 9 m shows low spectral densities, indicating the far-offset effect due to prevalent noise adulteration, as can be seen from the dispersion images exhibited in Fig. 5.15(f-h). The total power of the recorded wavefield is provided in Fig. 5.18, which exhibits that the highest energy is obtained for surveys with offset distances in the range of 4-7 m.

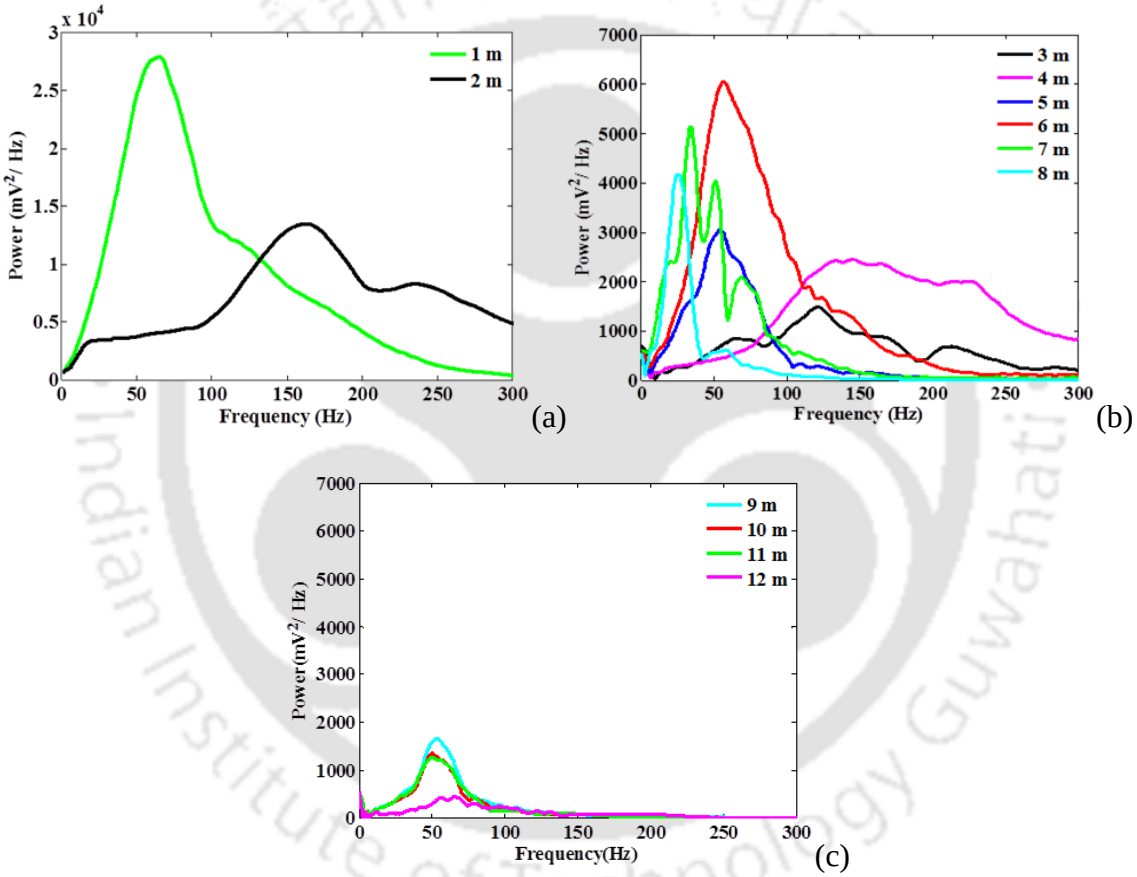

Fig. 5.17: Averaged power spectrum estimated from the wavefield records collected for active MASW survey with various offset distances conducted at Site-2 (Sampling frequency – 15000 Hz, Sample length – 5120, Inter-receiver spacing – 1 m, Number of channels - 24)

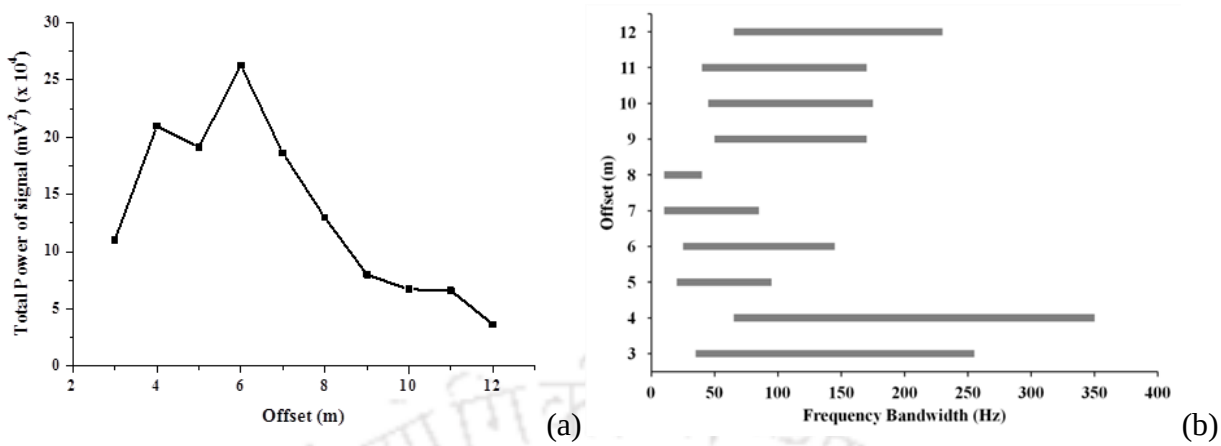

Fig. 5.18: (a) Total power of wavefield records collected at Site-2 for various offset distances (b) Frequency bandwidth of significant energy content of the collected wavefields records (Sampling frequency – 15000 Hz, Sample length – 5120, Inter-receiver spacing – 1 m, Number of channels - 24)

5.2.3 Influence of Receiver Layout

The properties of the shallower layers are obtained from the velocity associated to the shorter wavelengths. The minimal wavelength is usually associated to the highest recorded frequency. Small geophone spacing controls the high-frequency range of the dispersion image, and is, therefore, related to the resolution at shallow depths. This observation is more important particularly at the low velocity sites (sites comprising of relatively less stiff strata, $V_{s,avg}$ < 200 m/s). For the higher velocity sites (sites comprising of stiff substrata, $V_{s,avg}$ > 200 m/s), lesser geophone spacing induces lesser phase difference, thus leading to the recording of incomplete wavefield. Hence, it is necessary to increase the receiver spacing for accommodating larger wavelengths in the analysis. However, uncontrolled increase in the receiver spacing or the array length may lead to the development of far-field effects, which may lead to the attenuation of the signals and unwanted adulteration from the prevalent noise wavefields. Hence, it is understood

that there should exist a reasonable receiver spacing, in accordance to the site characteristics, which will lead to achieving the best resolution dispersion image.

The inter-receiver spacing has a significant influence on the collected wavefield, and hence affects the resolution of dispersion image. Considering various receiver spacing, Figure 5.19 exhibits a typical set of wavefield recorded in the field for an experiment conducted with sampling frequency 15000 Hz and comprising of 5120 samples (i.e. sampling time of 341 ms). It can be observed that, for higher receiver spacing, the waves could not reach to most of the geophones at the far side of the array, resulting in significant noise adulteration and rendering a poor and diffused dispersion image. As shown in Figure. 5.19c, for an inter-receiver spacing 3 m, from the 9^{th} channel onwards, there are practically no active signals, and the traces are substantially contaminated with the prevalent noise. Similar phenomenon can be observed beyond the 20^{th} channel for a spacing of 2 m. Hence, it can be stated that as the inter-receiver spacing increases, larger numbers of geophones fail to participate in providing a proper trace record of the propagating active waves. Figure 5.19 exhibits a typical condition when the sampling time (341 ms) proves to be insufficient for recording the complete wave propagation through the geophone array. Similar experiment conducted with sampling frequency 7500 Hz and 5120 samples (i.e. a sampling time 682 ms) exhibit a complete wavefield propagation in the trace records (Fig. 5.20). However, in this case as well, it can be observed that for higher receiver spacing (e.g. 3 m), beyond 15^{th} channel, the recorded signals are mostly noises due to the attenuation and non-arrival of the active signals with recognizable energy.

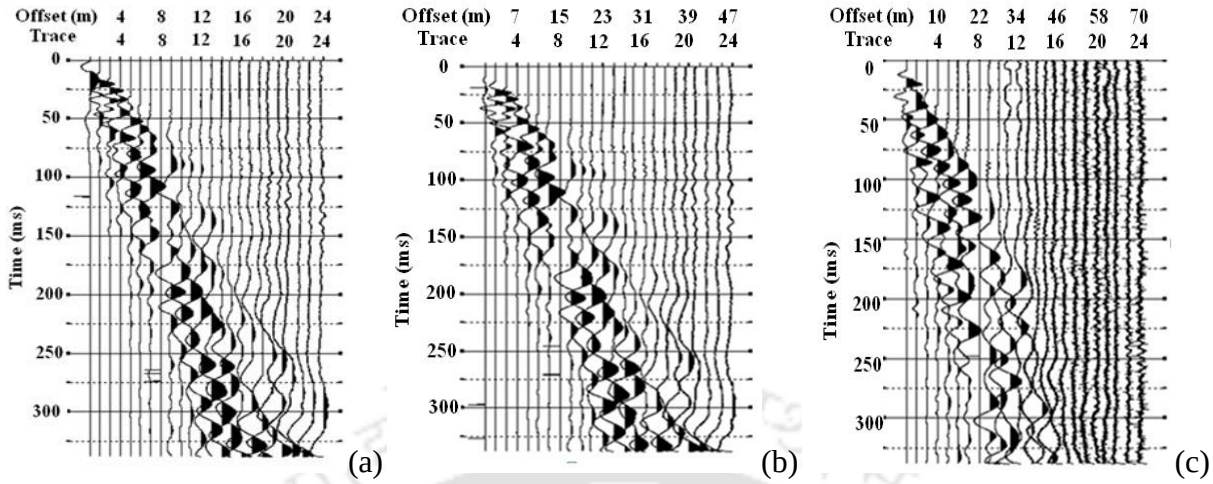

Fig. 5.19: Traces obtained for survey with 15000 Hz sampling frequency, 5120 samples, 1 m offset distance and receiver spacing of (a) 1m (b) 2 m and (c) 3 m

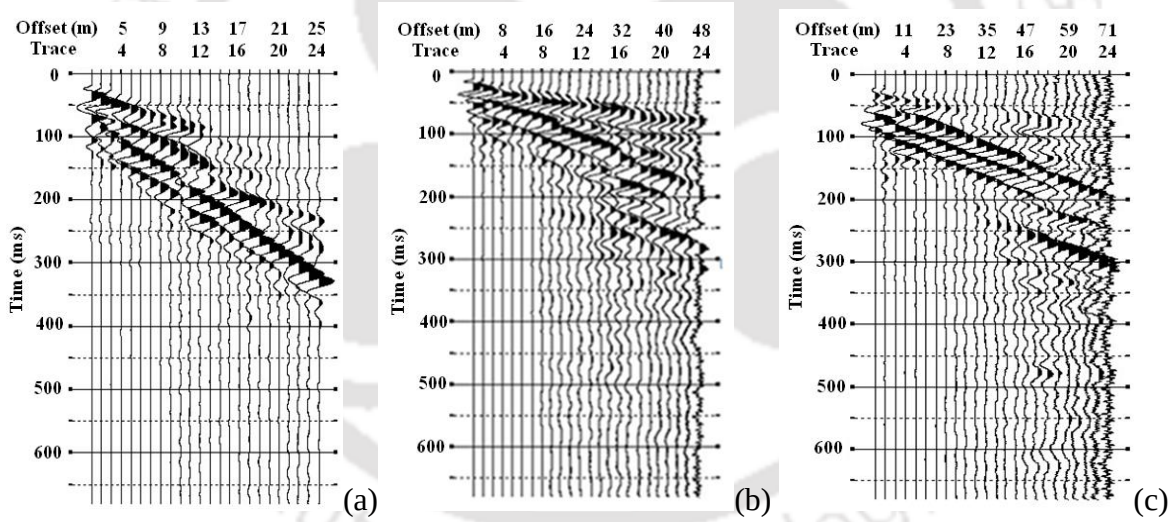

Fig. 5.20: Typical traces obtained for survey with 7500 Hz sampling frequency, 5120 samples, 2 m offset distance and receiver spacing of (a) 1 m (b) 2 m and (c) 3 m

Figure 5.21 shows a set of typical dispersion images developed from the wavefields collected at Site-1, with 10 m offset, and for varying receiver spacing of 1 m, 2 m and 3 m. It is observed that as the receiver spacing increases, there is a significant attenuation of energy leading to loss of

information. This is especially noted in the case of dispersion image created with a receiver spacing of 3 m, exhibiting minimal energy spread over the image without portraying any proper dispersion trend. It is aptly clear that 1 m inter-receiver spacing provided the best resolution image for the study conducted at Site-1.

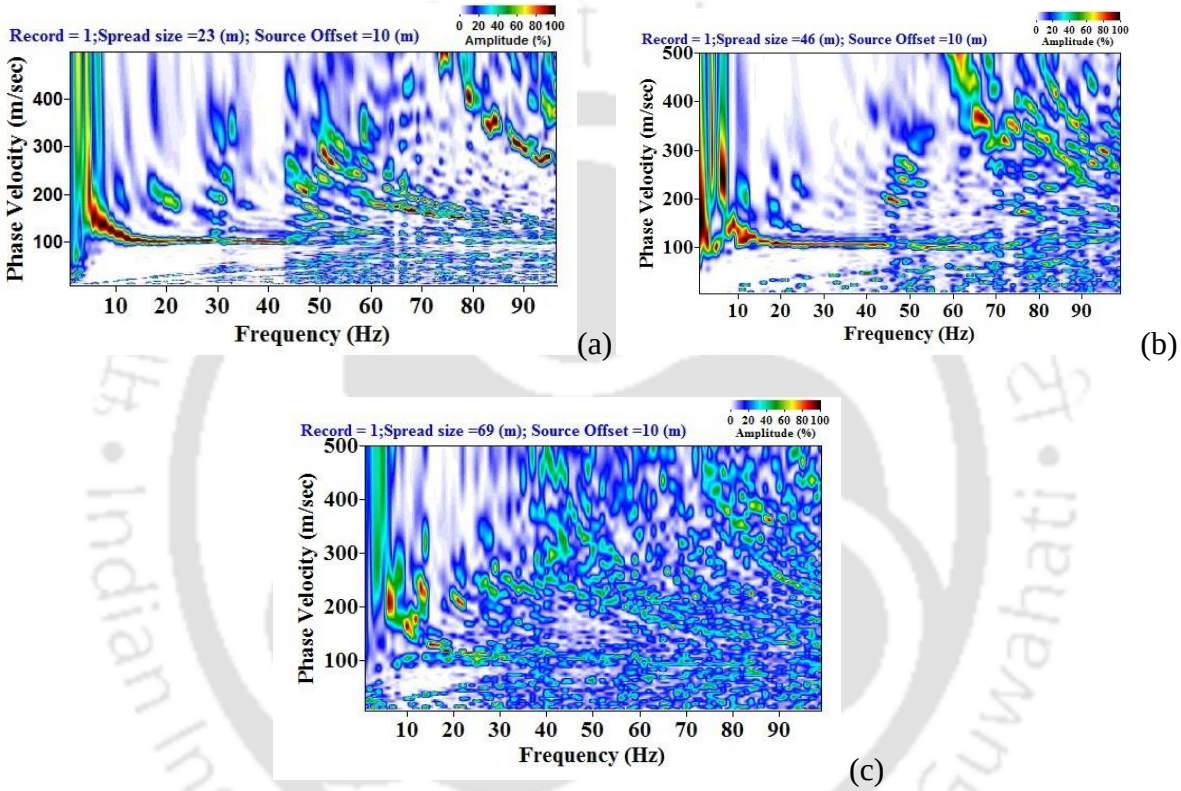

Fig. 5.21: Typical dispersion images obtained from survey at Site-1 conducted with 10 m offset for a sampling frequency of 7500Hz and 5120 samples, for varying receiver spacing (a) 1 m (b) 2 m (c) 3 m

It is a common notion that an increase in the spread length can accommodate larger quantities of the longer wavelengths, thus aiding in attaining the information of the deeper strata. In general, spectral analysis portrays that the maximum wavelength recorded should be equal to the array

length. However, for a given receiver layout, it is easily possible to perform the analysis considering wavelengths greater than the array length, without violating any sampling theorem. From any trace record, the time shift can be computed, for instance, by means of the cross correlation between the two traces, and the smaller identifiable time shift is equal to one time sample. For a fixed frequency *f*, if the spacing between the two traces is Δx, and the sampling rate is Δt, then, the maximum velocity can be computed as $V_{\max} = \frac{\Delta x}{\Delta t}$, and the maximum wavelength is given by $\lambda_{MAX} = V_{\max} / f = \frac{\Delta x}{f.\Delta t}$. It can be observed that there is no upper limit on the wavelength imposed by the array length, and it is worthwhile to mention that the maximum wavelength depends more on the site conditions, and the frequencies that can propagate through the medium.

Figure 5.22 shows the inverted V_s profile obtained from surveys with 1 m, 2 m and 3 m receiver spacing, *i.e.* a total spread length is 23 m, 46 m and 69 m. In case of 23 m and 46 m array length, the depth of investigation is up to 25 m and 70 m, respectively. However, with receiver spacing 3 m total depth of investigation is 12.5 m, which is due to the fact that at 3 m spacing, there is no energy accumulation in the lower frequency range. From the present study, it is observed that the recorded wavelengths (manifested by the depth of investigation) do not merely depend on the maximum spread length. The recorded maximum wavelength is found to be primarily dependent on the frequency characteristics of the substrata medium and the generating source. The dependence of the maximum wavelength on the array length is not as pressing as it is commonly considered.

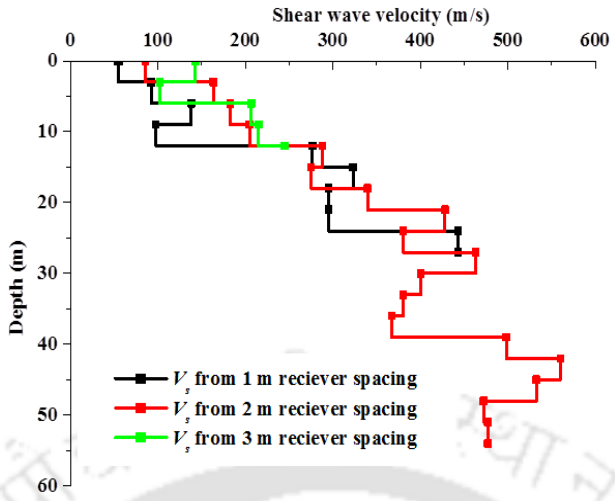

Fig. 5.22: Shear wave velocity profile obtained from surveys conducted at Site-1 with offset 8 m and varying receiver spacing of 1 m, 2 m and 3 m (Sampling frequency – 7500 Hz, Sample length – 5120, Number of channels - 24)

Another aspect in the field data acquisition is the total number of receiver geophones used in the active MASW survey. It is normally assumed that higher the total number of receiver, the better is the resolution of dispersion images (Park *et al*., 1998; Moro *et al*., 2003). However, the present study shows that increase of the total number of receivers should be accompanied by increase of array length to get the good resolution dispersion image. Figure 5.23 shows typical wavefield recorded by 12 and 24 numbers of geophone at Site-1, having an array configuration comprising of 7 m offset with 1 m receiver spacing. The corresponding dispersion images are shown in Fig. 5.24. It can be observed that the dispersion images are nearly similar, although the 24-channel record exhibits more distinctness due to the accumulation of the higher energy in the record.

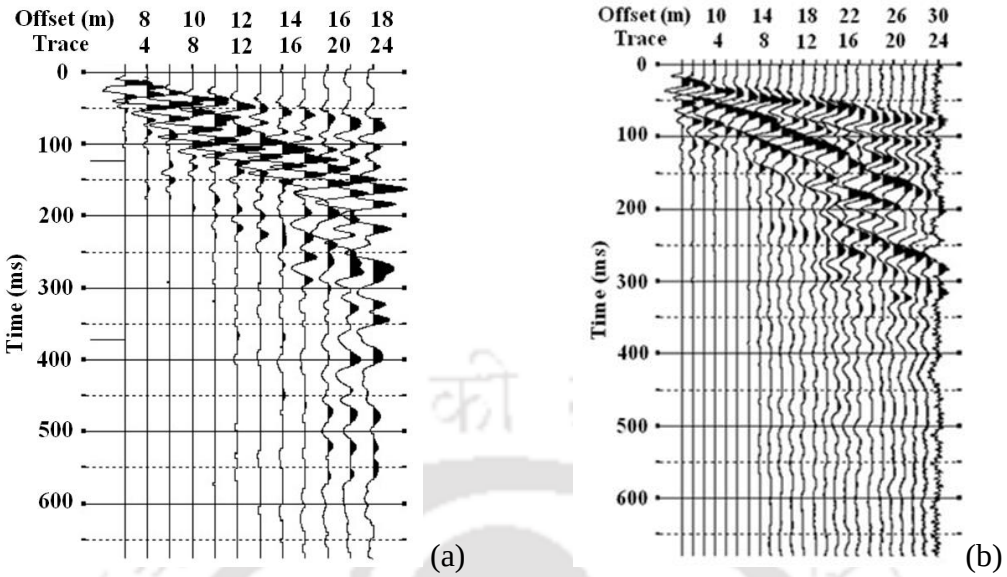

Fig. 5.23: Typical wavefields collected from Site-1 with 7 m offset and 2 m receiver spacing using (a) 12 channels (b) 24 channels (Sampling frequency – 7500 Hz, Sample length – 5120)

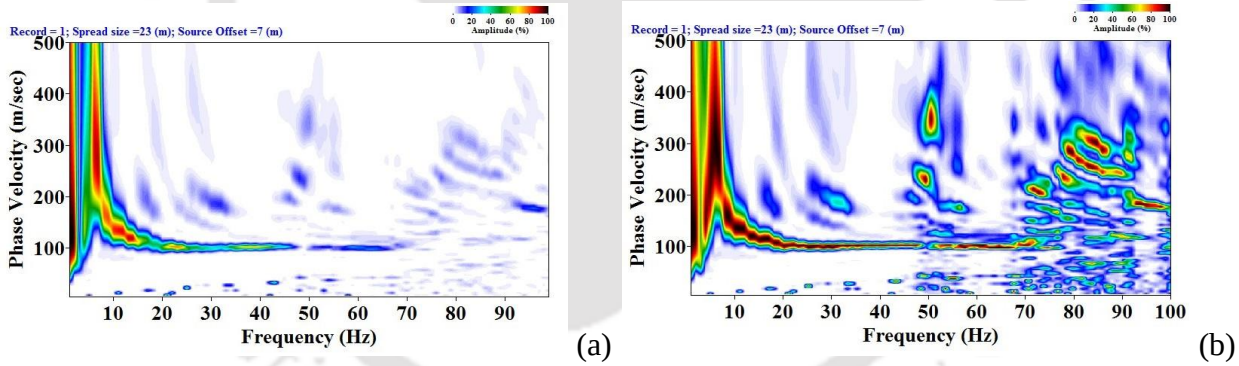

Fig. 5.24: Dispersion image for active MASW survey conducted at Site-1 with 7 m offset and 1 m receiver spacing using (a) 12 channels (b) 24 channels (Sampling frequency – 7500 Hz, Sample length – 5120)

Figure 5.25 exhibits the dispersion images obtained for a configuration with 2 m receiver spacing. It can be seen that in this case as well, the 24 channel record provides a comparatively better resolution dispersion image than the 12-channel record, and aids to obtain relatively better

information of the substrata. Hence, it can be stated that higher number of channels can result in higher-resolution dispersion image, if and only if it is associated with a longer receiver spread. There is no benefit in a mere increase in the number of channels without an increase in the array length.

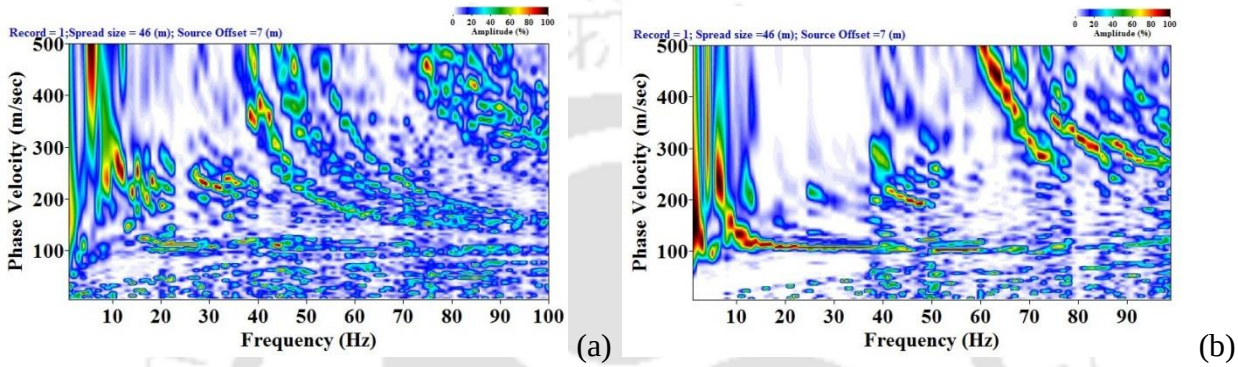

Fig. 5.25: Dispersion image for active MASW survey conducted at Site-1 with 7 m offset and 2 m receiver spacing using (a) 12 channels (b) 24 channels (Sampling frequency – 7500 Hz, Sample length – 5120)

5.2.4 Influence of Source Energy

A seismic source generates surface waves (as well as body waves) when it makes an impact on the ground surface. Its impact energy is directly related to the range of wavelengths of the generated surface waves, which determines the maximum depth of investigation (Z_{max}). A more powerful source is always needed as a foremost condition to increase investigation depth. A sledge-hammer (e.g., ≥ 10 kg) is the most common type of impact source for achieving $Z_{max} \leq 30$ m. An accelerated weight-drop source can increase Z_{max} by 30% under the most favorable conditions. A projectile source (e.g., Buffalo Gun) can increase Z_{max} by generating more energy at low frequencies (long wavelengths). Apart from the choice in terms of the Z_{max}, selection of a

proper energy source for active MASW survey should also consider other factors such as convenience of use, cost effectiveness, and other regulation issues. Table 5.1 lists different sources commonly used for the conduct of an active MASW survey.

Table 5.1: Details of the various sources of MASW

Source	Maximum depth (m)	Type of active energy
Sledgehammer (10 kg)	20-30	Impulsive
Weight drop (40 kg)	50	Impulsive
Rubber aided weight drop (80 kg)	60-90	Impulsive
Electromechanical Vibrator	Varying depth depending on generated frequency	Harmonic or random
Bulldozer (in tons)	100	Semi-impulsive
Blast	Varying depth	Strong impulsive

(Sledgehammer**- (Park *et al*. 1999: Park *et al*. 2002; Shtilveman 2003; Zhang *et al*. 2004; Ivanov *et al*. 2005; Xia *et al*. 2000; Xia *et al*. 2007; Park *et al*. 2007; Gosar *et al*. 2008; Dikmen *et al*. 2010; Eker *et al*. 2012; Wood and Cox 2012; Srinivas *et al*. 2014; Sauvin *et al*. 2016) **Weight drop**- (Stephenson *et al*. 2005; Park *et al*. 2005; Sauvin *et al*. 2016), **Rubber aided weight drop**-(Park *et al*. 2001, 2002a), **Electromechanical Vibrator**- (Park *et al*. 1999, 2001; Xia *et al*. 2000; Xu *et al*. 2006; Wood and Cox 2012), **Bulldozer**-www.masw.com, **Blast**- Tian *et al*. 2003a, 2003b; Kaufmann *et al*. 2005; Neducza 2007).

Energy of different impact sources can be calculated on the basis of their delivered kinetic energy at the point of impact. If m is the mass of the source (in kg), and v is the velocity of fall of the weight on the ground surface (m/s), the impact energy can be calculated as the $\text{Kinetic energy} = 0.5mv^2$ (J). As an example, if the velocity of the fall of hammer is 10 m/s,

accordingly, the kinetic energy will be estimated as 250 J for the 10 kg sledgehammer and 2000 J for the 40 kg PEG.

In active MASW, the source, so chosen, is supposed to produce surface waves with a high SNR in a wide frequency band. This task of obtaining a high SNR in the low frequency ranges is difficult, thus limiting the resolution at the higher investigation depths. Inadvertent to the type of active source used, the spectral power distribution over the frequency band is primarily site dependent. The spectrum of the source is related to the frequency content of the generated signal; however, the site characteristics play a dominant role in altering the spectrum of the propagating signals. Different sites exhibit different frequency bands with spectral energy concentrations. At certain sites, the substrata characteristics strongly eliminate particular frequency bands. Under such condition, the change in the source spectrum merely helps in increasing the signal quality received by the geophones.

Figure 5.26 shows the typical energy spectrum from the acquisitions made by the 10 kg sledgehammer at all the three sites considered in the present study. Site-2 shows the highest energy spectrum as it is the stiffest site considered in the present study. It can be observed that Site-3 shows the relatively lesser spectral energies, while, in its comparison, Site-1 shows comparatively higher energy spectra given its relatively stiffer characteristics. It can also be noted that even though the same 10 kg sledgehammer has been used for all the sites, each of spectra exhibit different significant frequency bandwidths of energy concentration, governed by the prevalent substrata characteristics. The spectrum of the recorded wavefield, generated during an active MASW due to the usage of a specific impact source, is primarily site dependent. The

spectral energy obtained from sites comprising of relatively stiffer substrata ($V_{s,avg}$ > 200 m/s) is nearly 3-6 times higher than the sites comprising of less stiffer substrata ($V_{s,avg}$ < 200 m/s). Correspondingly, the effective frequency bandwidth of the energy distribution for the stiffer sites is approximately 2-4 times higher than the sites having relatively softer substrata.

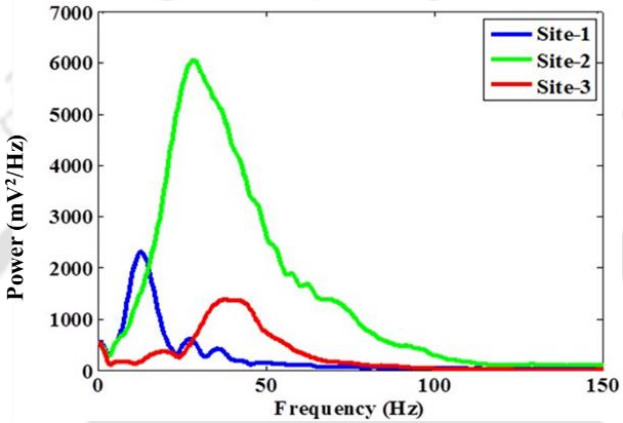

Fig. 5.26: Typical comparative spectrum of signal produced by a 10 kg sledgehammer at three different test sites

The use of an adequate source is primarily governed by the desired depth of investigation. It is worth mentioning that the low frequency content of the signal is necessary to have a larger penetration depth. Figure 5.27 depicts typical dispersion images obtained from a single strike of a 40 kg PEG and a 10 kg sledgehammer for the tests conducted at Site-1. It can be observed that the dispersion curve generated by the PEG has significant energy content in the low frequency ranges, as compared to the image obtained from the strike of a 10 kg sledgehammer. Along with the higher energy imparted, it had been observed that PEG is able to generate significant low frequency waves (longer wavelengths), thus aiding in larger investigation depths. The weight of the hammer preconditions the frequency content of the generated pulse, and thus, a hammer with

lighter weights striking on rigid steel plates produces mostly the high-frequency waves, and hence, provides information only of the relatively shallower depths.

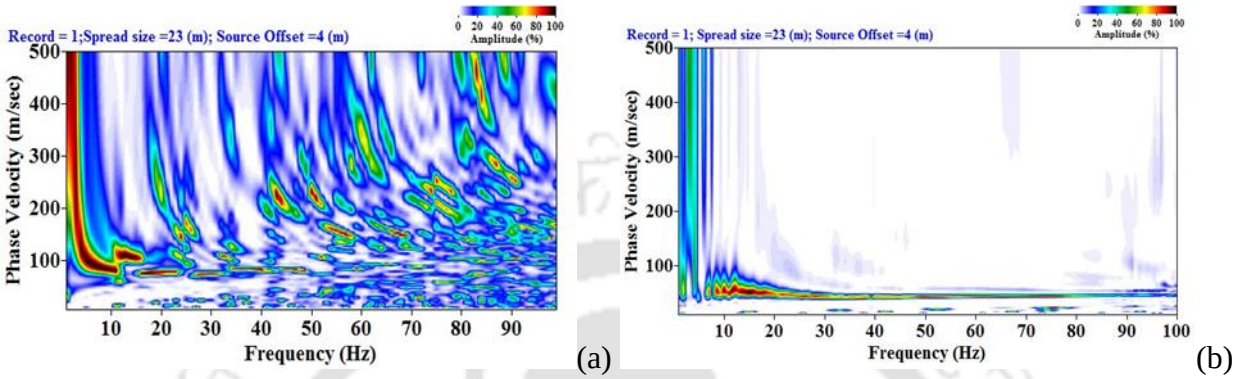

Fig. 5.27: Typical dispersion images obtained at Site-1 from the single strike of a (a) 40 kg PEG (b) 10 kg sledge hammer (Sampling frequency – 7500 Hz, Number of samples – 5120, Number of channels – 24, Offset distance – 4 m, Inter-receiver spacing – 1 m)

Figure 5.28 shows the typical power spectra obtained for a single shot of the 10 kg sledgehammer and that of a 40 kg PEG. It can be easily recognized that a single shot with a 40 kg weight dropping PEG has substantially more energy than a sledge hammer. Even at lower frequencies, the presence of high energy renders the heavy-weight PEG to be suitable to provide information of much deeper substrata.

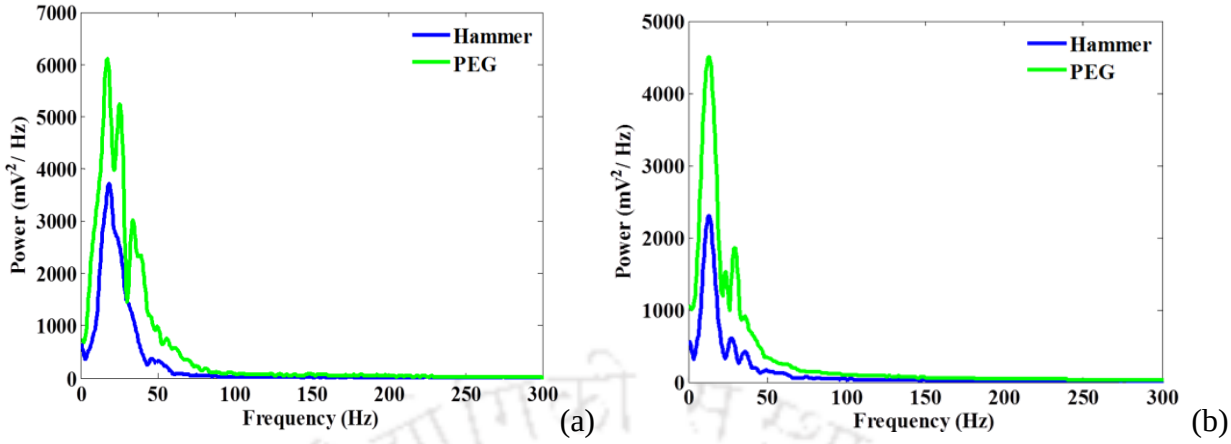

Fig. 5.28: Typical power spectrum of the signals recorded with 10 kg sledgehammer and 40 kg PEG (a) Site-1 (b) Site-3 (Sampling frequency – 7500 Hz, Number of samples – 5120, Number of channels – 24, Offset distance – 7 m, Inter-receiver spacing – 1 m)

Increasing the SNR is a primary objective of the acquisition, and it can be achieved either by reducing the level of noise or by increasing the level of signal. Increasing the signal level can be done by increasing the energy of the source. Possible strategies for increasing the signal level include using sources that are more powerful or combining different sources for different frequency ranges. An alternative approach is the 'vertical stacking' or summation of the multiple synchronized repetitions of the test. Stacking is a process of combining the dispersion images of various shots so that the resulting dispersion image has higher energy at different frequencies. The signals acquired during the field investigation is mostly contaminated with two different noise phenomena. The contaminating noise may be coherent which consists of deterministically reproducible events. Typically, these are source-generated events that are not associated with the signal of interest. In this case, increasing the power of the source or summing multiple repetitions does not increase the SNR, as the noise also is equally summed up. These events increase their power proportionately or repeat themselves with the same character. Such noises

are removed to the best possible extent during the pre-processing of the recorded wavefield through muting and filtering techniques. The other type of noise that results in contamination is the incoherent noise, which arises due to the effect of the background vibrations at the site produced natural and anthropogenic sources related to traffic, vibrating or moving machines, wind, and the movements of surface or ground water. They are often dominated by the surface waves, which are, however, incoherent with respect to the data acquisition experiment. They are generated by sources whose position and time of activation are unknown. Other types of incoherent noise are electric or electronic noise in the receivers or cables and in the acquisition system. These noises may be generated by power lines and other external sources and by imperfections in the recording system. The amplitude spectrum of such incoherent noises are mostly spatially stationary, and the average of the noise tends to zero even with the increase in the stacks. If the incoherent noise is not deterministically reproducible and has a random phase component, stacking increases the SNR by the square root of the number of repetitions ($\sqrt{n}$). The signal, when perfectly reproducible among multiple repetitions, increases its amplitude with proportionally to the number of stacked signals (n). Thus, considering a stationary amplitude spectrum of the incoherent noise, the SNR increases as $n/\sqrt{n} = \sqrt{n}$ (Foti *et al*. 2015). In this process, even the energy at the lower frequencies can be substantially increased, so as to obtain shear wave velocity profiles exhibiting higher depths of investigations. Figure 5.29 exhibits the stacked dispersion images obtained from various numbers of shots the 10 kg sledge hammer at Site-3. It can be observed that the dispersion image becomes more distinct with the increasing number of stacks, or shot gathers. In general, if it is assumed that the velocity of fall is identical for both the impulsive sources in consideration (sledge hammer and PEG), the potential energy imparted by a single shot of PEG is nearly 3-4 times higher than a single shot of sledge hammer.

In this regard, stacking up the dispersion images from multiple shot gathers of the sledge hammer can be an alternative, yet efficient, approach to generate dispersion images of higher energy. Figure 5.30 exhibits that the dispersion images obtained from a single shot of PEG and 3-stacked shots of the sledge hammer are very similar in terms of the distribution of the energy along the significant frequencies.

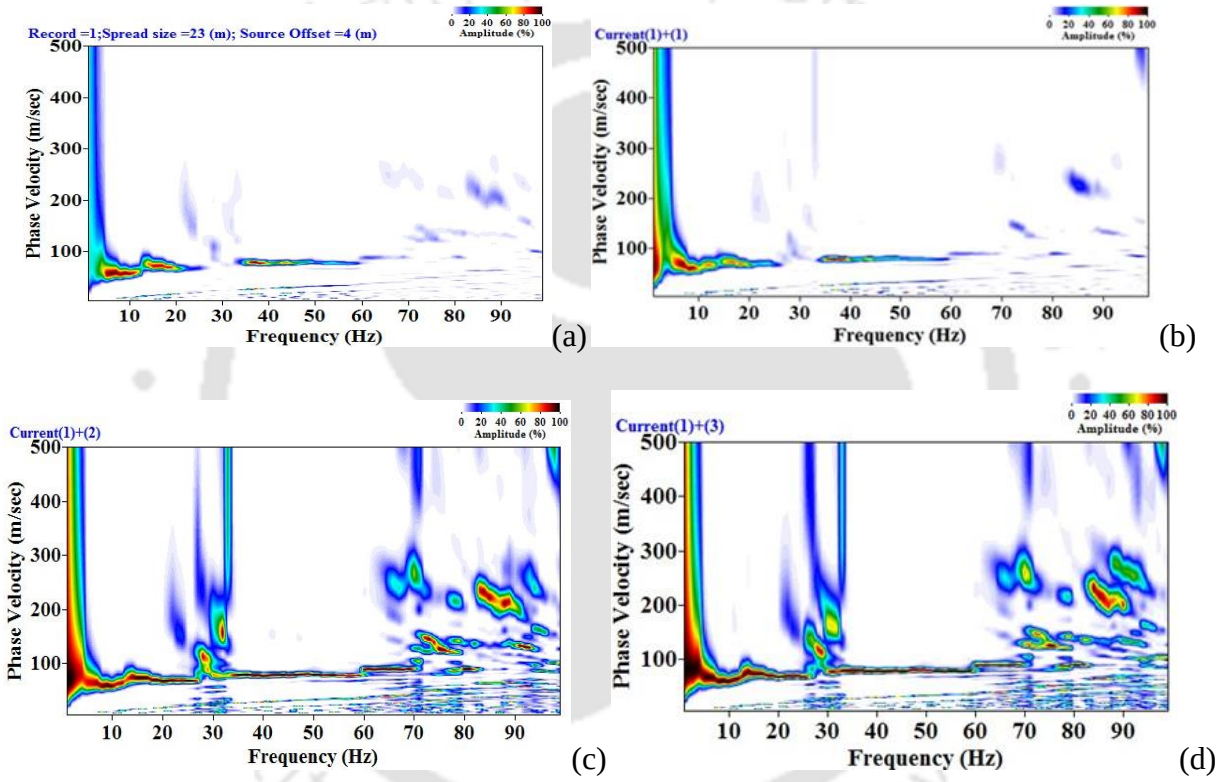

Fig. 5.29: Typical dispersion images obtained Site-3 obtained from stacking of 10 kg sledge hammer records (a) No stack or single shot (b) Single stack (c) Two stack (d) Three stack (Sampling frequency – 7500 Hz, Number of samples – 5120, Number of channels – 24, Offset distance – 4 m, Inter-receiver spacing – 1 m)

Based on the depth of investigation obtained from various stacks, Fig. 5.31(a) depicts that the V_s profile obtained from the 3-stacks of the sledge hammer is nearly similar to the same obtained from a single shot of the PEG. Similar observation is reflected from the inverted V_s profile obtained from the stacked records at Site-3 (Fig. 5.31b). It can also be observed that with the increase in the number of stacks, the depth of investigation increases. This observation, thus, establishes that stacking results in an overall increase in the energy content, even at low frequencies, thus rendering larger investigation depths. Hence, from an overall understanding, it can be stated that the energy of the signals recorded at the same site with a single shot of 40 kg PEG can be achieved by 3-4 stacks of the same obtained by the use of a 10 kg sledge hammer. This ensures the applicability of a comparatively lightweight sledge hammer in harnessing the information of deeper substrata using multiple shots and utilizing the strategy of dispersion image stacking.

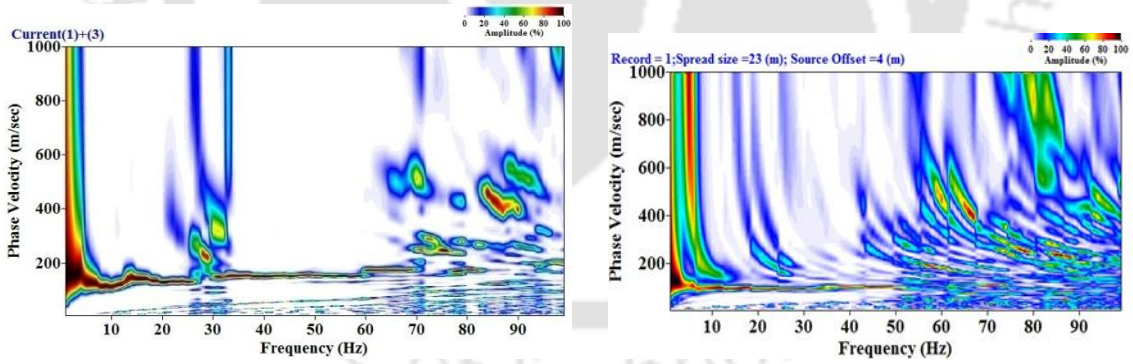

Fig. 5.30: Comparative of the typical dispersion image obtained for Site-3 from (a) 3-stacked 10 kg sledge hammer record (b) Single shot of 40 kg PEG (Sampling frequency – 7500 Hz, Number of samples – 5120, Number of channels – 24, Offset distance – 4 m, Inter-receiver spacing – 1 m)

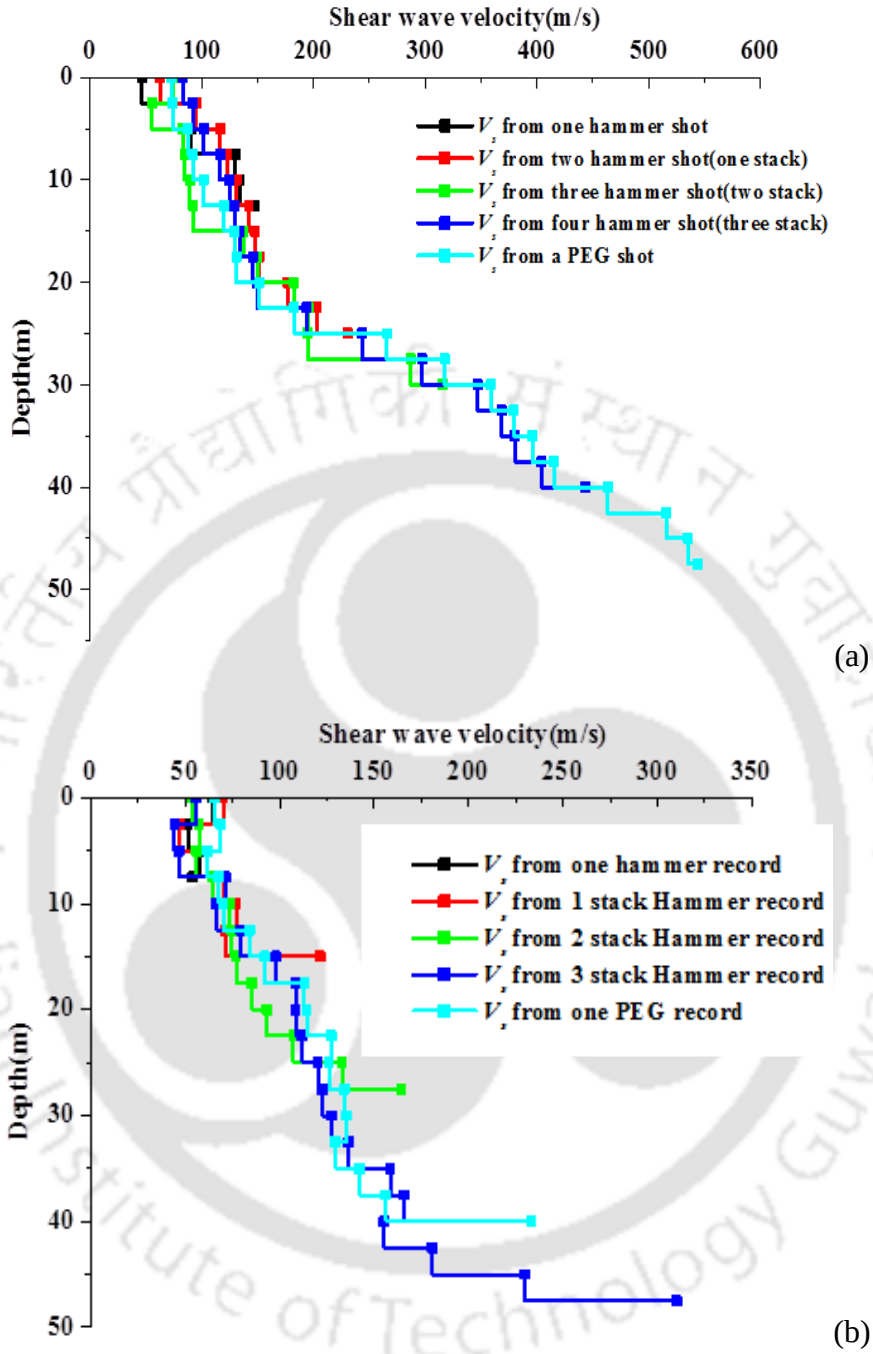

Fig. 5.31: Comparative of the shear wave velocity profiles obtained from a single shot of 40 kg PEG with different stacks of 10 kg sledge hammer records for (a) Site-1 (b) Site-3 (Sampling frequency – 7500 Hz, Number of samples – 5120, Number of channels – 24, Offset distance – 4 m, Inter-receiver spacing – 1 m)

The influence of stacking has also been checked for Site-2, the outcome of which is provided in 5.32 in terms of the dispersion image. The primary objective of stacking is to improve the resolution of the dispersion image so that the dispersion curve can be efficiently extracted to the best possible accuracy. It can be observed that at Site-2, which is a relatively stiffer site, a single stack record is sufficient to produce a good resolution dispersion image, especially due to the presence of a very hard granitic stratum in a shallow depth of 7 m. It is observed that even with the single stack, the dispersion trend is prominent enough to obtain the dispersion curve with sufficient accuracy, along with the identification of the multimodal feature. Hence, further stacking does not necessarily contribute in the identification of further utilizable dispersion features.

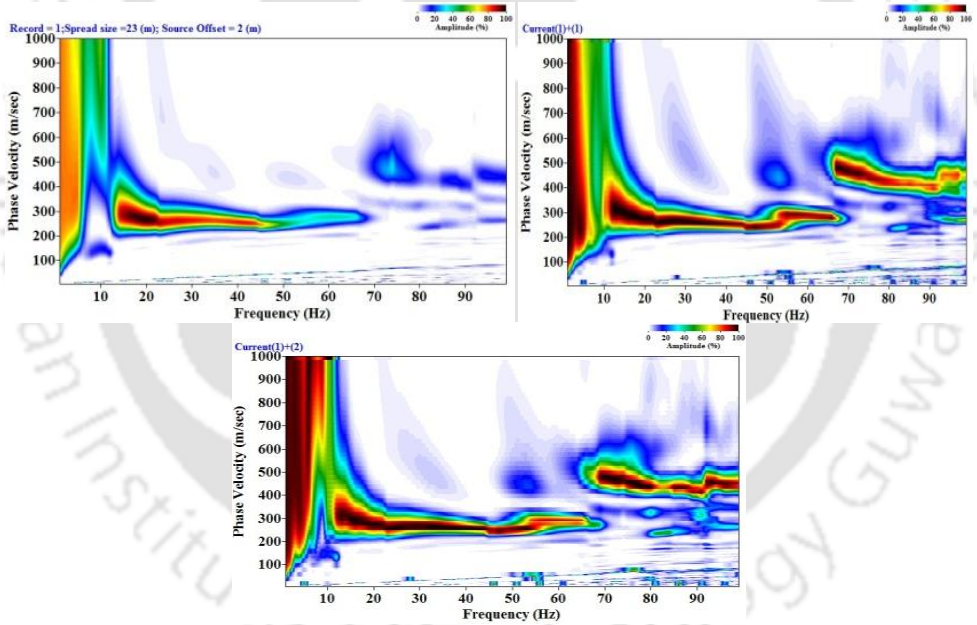

Fig 5.32: Typical dispersion images for Site-2 obtained from stacking of 10 kg sledge hammer records (a) No stack or single shot (b) Single stack (c) Two stack (Sampling frequency – 15000 Hz, Sample length – 5120, Inter-receiver spacing – 1 m, Number of channels - 24)

5.2.5 Influence of the Striker Plate

The composition and density of the striker plate material can noticeably affect the frequency content of the generated wavefield. In the present study, striker plates made up of two different materials, cast steel and rubber, have been used. The use of a cast steel plate significantly increases the higher frequency content of the signal, while the rubber plate, being softer, produces wavefield records with low frequency content. Figure 5.33 shows typical wavefield records obtained from a 10 kg sledge hammer strike on a steel plate and a rubber plate, exhibiting typically different patterns of wave propagation through the array. Figure 5.34 shows the typical dispersion image obtained using rubber plate, which exhibits the M0 dispersion curve possessing only low frequency content (< 15 Hz), whereas the use of cast steel striker plate resulted in obtaining the M0 dispersion curve extending approximately till 50 Hz, along with multimodal information in the dispersion image. Figure 5.35 shows that V_s profile obtained from a single strike on a cast steel plate terminates at the depth of 5 m, since the generated wavefield mostly consist of higher frequencies; however, it shows an agreeable match with the V_s obtained from the borehole survey for shallow depths. V_s profile obtained from a single strike on rubber plate agrees well with that of the borehole survey results beyond a depth of 5 m. It fails to show an agreeable match at shallower depth as practically no information is available at the high frequency region. Hence, for a particular impulse source, the choice of the striker plate should be made on the basis of the target depth of investigation. Therefore, cast steel striker plates are recommended to be used for field investigations where it is required to achieve higher resolution for shallow depth investigations. However, if the specific target is to obtain information for the low frequency range, a rubber plate can be suitably used, although it is prone to substantial wear and tear. It is worth mentioning that the same striker plate (e.g. cast steel plate) will result in

higher investigation depths provided a heavier impulse source is utilized, or using higher numbers of dispersion image stacking (as shown in Fig. 5.31b).

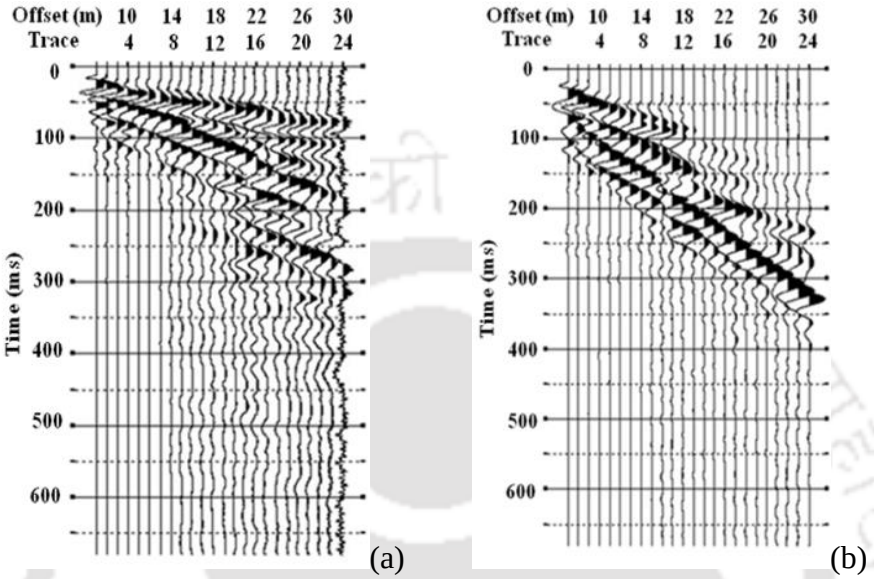

Fig. 5.33: Typical wavefield records obtained at Site-3 from a single strike on a (a) Rubber plate (b) Cast steel plate (Sampling frequency – 7500 Hz, Number of samples – 5120, Number of channels – 24, Offset distance – 4 m, Inter-receiver spacing – 1 m)

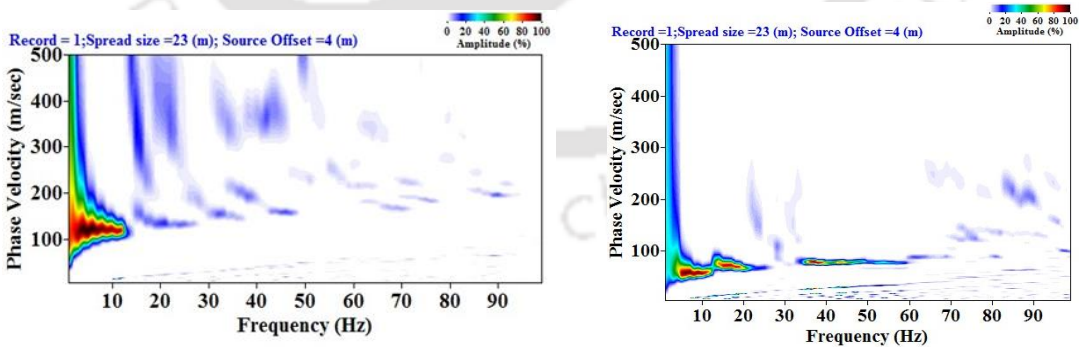

Fig. 5.34: Typical dispersion images obtained at Site-3 from single strike on a (a) Rubber plate (b) Cast steel plate (Sampling frequency – 7500 Hz, Number of samples – 5120, Number of channels – 24, Offset distance – 4 m, Inter-receiver spacing – 1 m)

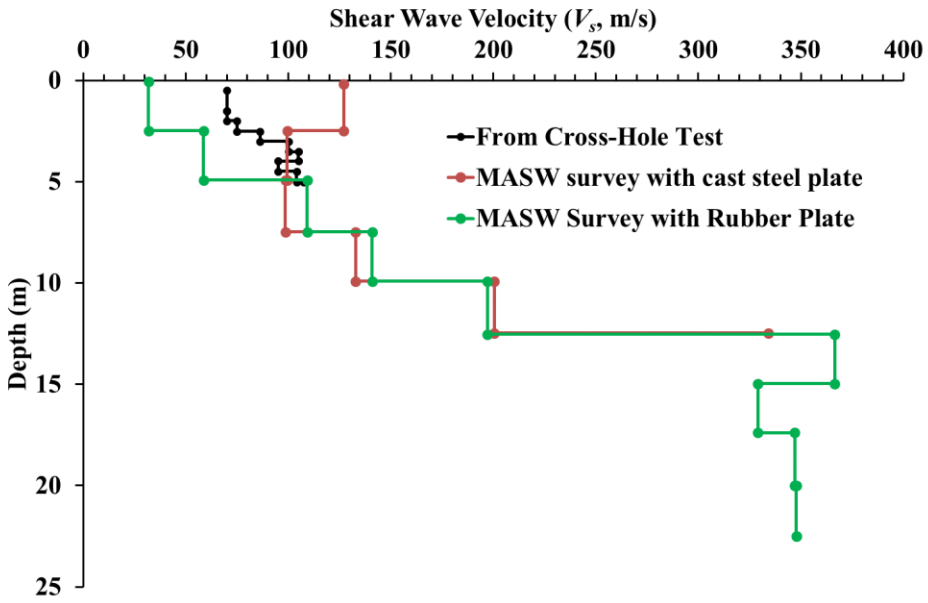

Fig. 5.35: Comparison of the typical V_s profiles obtained from SPT results and that obtained from single strike on rubber plate and a cast steel base plate at Site-3 (Sampling frequency – 7500 Hz, Number of samples – 5120, Number of channels – 24, Offset distance – 4 m, Inter-receiver spacing – 1 m)

5.3 Validation of the Experimental Dispersion Curve

Several computational techniques can be used to generate dispersion curves. Some of the techniques use the feed-forward earth model to determine the theoretical dispersion curves (Schwab and Knopoff 1972; Ke *et al*. 2011), which are further used in the inversion algorithms to estimate the best possible shear wave velocity profile of the subsurface considering minimum error between the theoretical and experimental dispersion curves. Some techniques use analytical solutions to generate dispersion curves directly from the collected wavefield records (Mukherjee and Prashant 2009, 2013; Kumar and Naskar 2015, 2017). Such a typical comparison of DCs (for Site-1) is presented as shown in Fig. 5.36. It can be observed that although the trends of the

dispersion curves are similar, there are appreciable differences between the DC obtained from experimental and analytical procedures. It is worth mentioning that the analytical solutions have been primarily developed for SASW two-receiver surveys. Material damping has been neglected in the analytical solutions (Kumar and Naskar 2017). An extremely large source offset is maintained so that the recorded wavefields are not affected by the high frequency body waves (Kumar and Naskar 2015). In such technique, the time-domain records of the two geophones are used to generate the dispersion curves following a sequence of Fourier transformation of time domain signals, estimation of power spectra, cross-spectra, coherency and phase unwrapping. During the phase unwrapping, a large part of the transformed record is eliminated which does not suit the desired coherent signals. As damping is neglected, in general, the estimated dispersion curves indicate a stiffer subsurface behavior, especially in the lower frequencies, as can be seen in the figure. In case of MASW survey, owing to the utilization of closer offset, multiple geophones and longer recording array, several types of waves (surface waves and body waves of fundamental and higher order modes, scattered waves, reflected and refracted waves, even waves newly developed as a result of the interaction with the soil interfaces and change of stiffness) are accounted in the dispersion analysis, as it is believed that all types of waves carry a part of the generated energy. In such case, the mixing of various wave characteristics yield multimodal dispersion characteristics, which distribute the total energy over the wide frequency band. Moreover, due to the inclusion of material damping, unit weight and Poisson's ratio of propagating medium, realistic dispersion characteristics conforming to the field conditions are obtained which are substantially different from that obtained from analytical solutions. As the energy inevitably decreases over higher frequencies, the DCs approach closer, while a substantial difference exists in the lower frequencies (below 8 Hz). Considering these issues, the analytical

DC obtained for a two-receiver approach is not suitable to validate or compare the results obtained from MASW techniques that account for more complex dispersion phenomenon. Rather, the comparison with the dispersion curve generated from the feed-forward earth model, proposed by Ke *et al.* (2011), show better promise of validation. One such example is illustrated in Fig. 5.36.

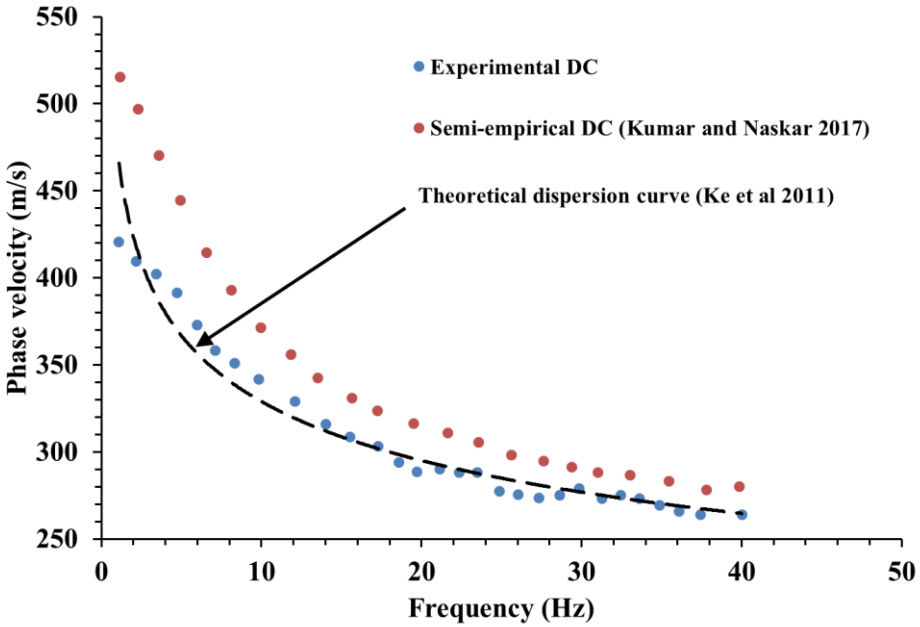

Fig. 5.36: Validation of the a typical experimental dispersion curve obtained for Site-1 with respect to the analytical and theoretical dispersion curves

5.4 Summary

This chapter highlights the influences of various data acquisition parameters on the resolution of dispersion image obtained from active MASW surveys. The geophysical investigations have

been conducted at three locations of varying substrata characteristics. Based on the experimental investigations, some salient observations have been made.

- The investigations highlighted that suitable sampling frequency is site dependent. Suitable sampling time depends on the completion of phase propagation through the receiver array without inducing noise adulteration in the wavefield record. Out of the several combinations sampling frequency and sampling time which allows for the suitable completion of phase propagation, the maximum sampling frequency is recommended.
- The offset distance should be so chosen that the requirement of planar wave propagation is satisfied and the best resolution dispersion image is obtained. Smaller offset distance induces high accumulation of energy at low frequencies resulting in indistinct dispersion trends and shallow depth shear wave velocity profiles (near-field effect). Large offset distance results in dominant adulteration of the records due to the prevalent noises, resulting in dispersion curves with low SNR (far-field effect).
- The choice of suitable offset distance is site dependent. In lieu of the fact that it is difficult to state an universally suitable offset distance due to the geotechnical and geophysical variations of the site, it is recommended to follow the offset limits stated in the text, accompanied by few preliminary trials of active MASW survey in the site to determine the workable offset distance.
- Large receiver spacing should be avoided as it leads to significant attenuation of active energy traversing the array, leading to incomplete wave propagation through the array. Even if the entire wave front passes through the array, significant noise signals are

recorded in the farthest receivers. This leads to obscure dispersion images with substantially indistinct dispersion trend.

- Inter-receiver spacing and the numbers of receivers used in active MASW survey governs the total length of array. It is found that in contrary to the conventional notion, merely increasing the length of the array will not enhance the depth of investigation. The depth of investigation, governed by the maximum wavelength recorded by the receiver, is primarily dependent on frequency characteristics of the site substrata and the wave generating source. Even if the source generates long wavelengths, the same can get curtailed depending on the site characteristics, and the receivers will be left with shorter wavelength records leading to shallow investigation depths. Mere increase in the number of receivers will not enhance the resolution of the dispersion image. An increase in the array length accompanied by an increase in the number of receivers will provide higher resolution dispersion images.
- The spectrum of the recorded wavefield, generated during an active MASW due to the usage of a specific impact source, is primarily site dependent. The spectral energy obtained from sites comprising of relatively stiffer substrata ($V_{s,avg}$>200 m/s) is nearly 3-6 times higher than the sites comprising of less stiffer substrata ($V_{s,avg}$<200 m/s). Correspondingly, the effective frequency bandwidth of the energy distribution for the stiff sites is approximately 2-4 times higher than the otherwise. Heavier source such as 40 kg PEG imparts higher impulse energy, nearly 3-4 times that produced by a 10 kg sledgehammer, thus generating wavefields containing longer wavelengths, allowing for higher depths of investigation.

- Since stacking results in the enhancement in the energy of the frequency spectra, dispersion image stacking can be used as an effective means of achieving higher depths of investigation using low weight 10 kg sledgehammers, thus overcoming the difficulty of portability of heavy weight drops for the purpose of active MASW survey. In order to obtain a good resolution dispersion image, it is recommended to use 3-4 dispersion image stacks for sites with $V_{s,avg}$<200 m/s, while single stack is recommended for sites with $V_{s,avg}$>200 m/s.
- Wavefields generated by striking a rubber base plate produces waves of low frequency content (<15 Hz), and hence is recommended for large-depth investigations using single shot results. Cast steel plates are recommended for high resolution shallow depth investigations since the generated wavefield consists of significant high frequency content (till 50 Hz). Owing to the rapid deterioration of the rubber strike plate from continuous usage and for avoiding the recurring replacement, cast steel plate is recommended to be used for all practical purposes accompanied by dispersion image stacking depending on the site substrata characteristics

CHAPTER 6

INVERSION ANALYSIS

6.1 General

Inversion analysis forms the third and final module of a MASW survey through which the shear wave velocity profile along the depth of the subsurface can be deciphered from the wavefield records collected from the field, after duly subjecting them to dispersion analysis and dispersion curve extraction. The surface wave inversion process does not have a direct solution, and requires an iterative or an optimization technique following a deterministic, probabilistic or a hybridized approach (Menke and Abbott 1989; Yuan and Nazarian 1993; Ganji *et al* 1998; Xia *et al.* 1999; Lai *et al*. 2002; Xia *et al*. 2003; Lu and Zhang 2006; Song *et al*. 2007; Socco and Boiero 2008). The conventional practice utilizes the fundamental-mode (M0) dispersion curve in the unimodal inversion analysis, assuming that the fundamental mode dominates the field records. For inversion analysis to be carried out, an initial earth model considering horizontal subsurface layers are chosen. The initial earth model, defined by its elastic parameters (namely, primary and shear wave velocities, V_p and V_s, the unit weight of the stratum material and the stratum thickness), is subjected to theoretical dispersion analysis using the algorithm proposed by Schwab and Knopoff (1972). A theoretical dispersion curve for the fundamental mode is obtained, which is then compared with the measured, or experimental, dispersion curve. The root mean square error (RMSE) or the 'mismatch' between the two curves is computed, and accordingly, the earth model is refined (i.e. at each successive iterations). The theoretical dispersion curve based on the refined model is optimized towards the experimental dispersion curve. The RMSE is usually used as an indicator of the closeness between the two dispersion

curves. The optimization can be carried out by local search and global search methods available. The process is terminated when the RMSE reaches the tolerance criterion, and the corresponding model is granted as the shear wave velocity profile corresponding to the experimental records. The inversion technique, as described herein, is schematically represented in Fig. 6.1.

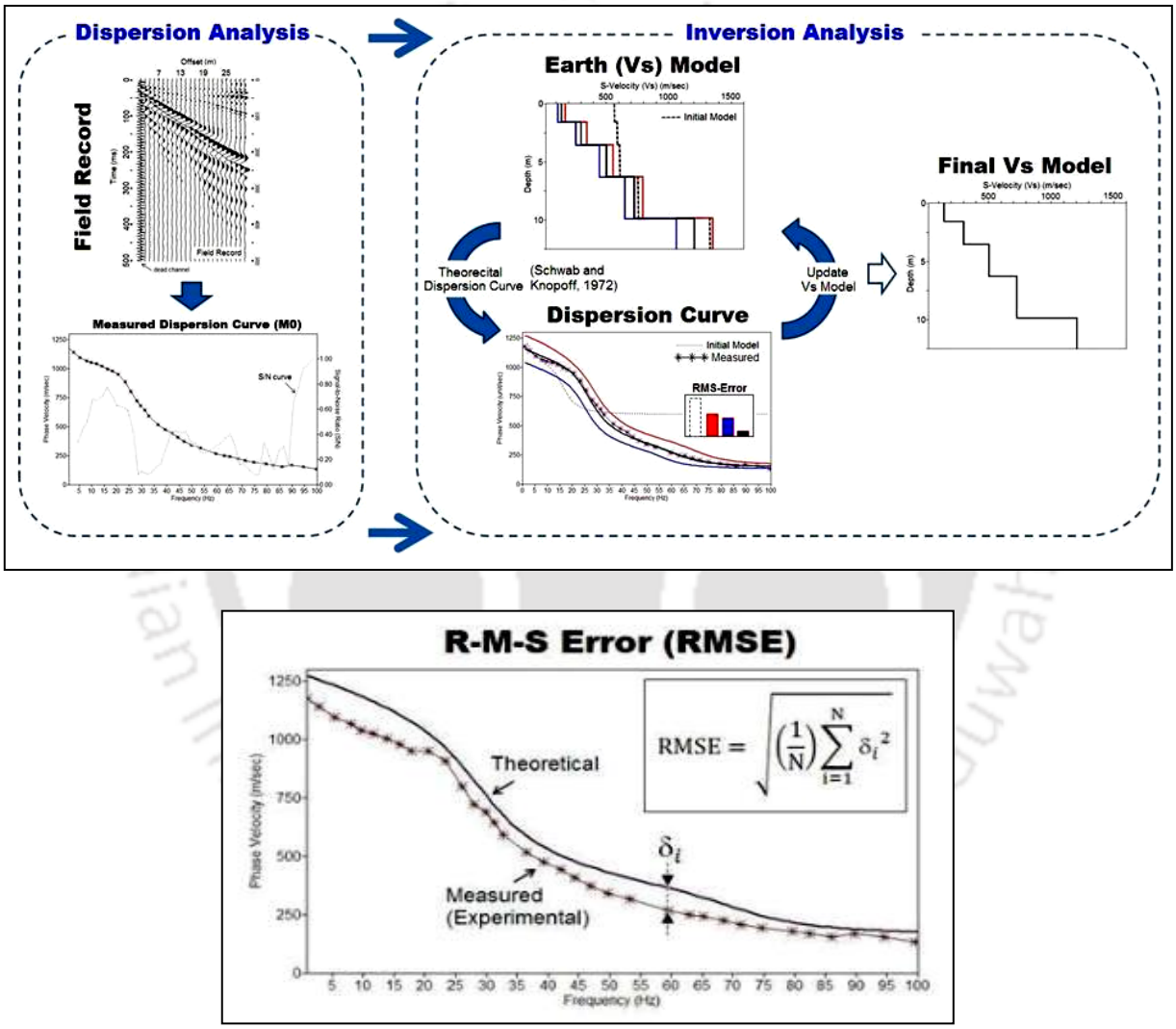

Fig. 6.1: Schematic representation of the inversion analysis (www.masw.com)

Inversion analysis performed with the extracted dispersion curve is associated with different numerical pitfalls. One of the major concerns is the termination criterion adopted to stop the

iterative process of reduction of RMSE and refinement of the earth model. One such case is encountered when the stopping criteria is chosen to be sufficiently low, and even with lower RMSE, the final earth model although numerically correct, may not be realistically true. An example of the same is highlighted in Fig. 6.2. The solution conforming to Point B, although reflects an improved RSME, might not be realistic if checked with the soil profile and geology available in the region of experimentation. In such case, it is always recommended to validate the obtained result with the available confirmatory test.

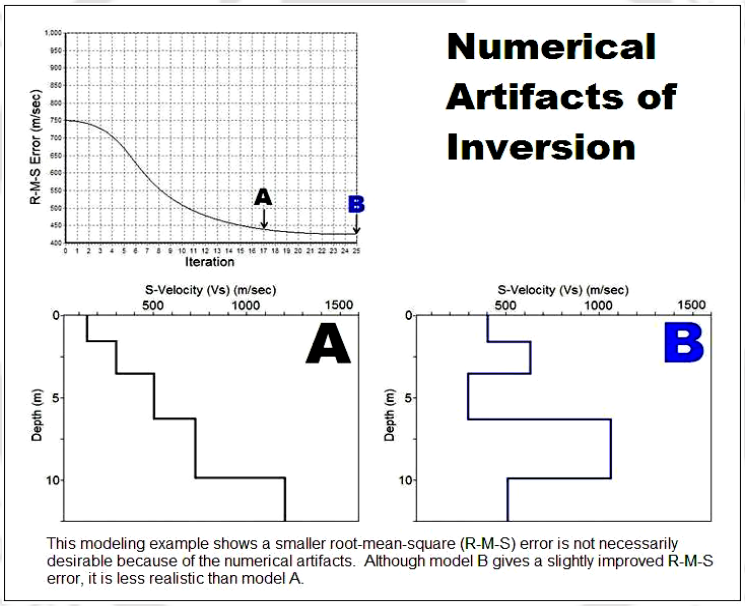

Fig. 6.2: Numerical pitfalls of achieving too low RMSE values (www.masw.com)

In most of the cases, the experimental dispersion image functions will be multimodal, while the theoretical dispersion image curve will be developed from a unimodal perspective. Hence, the experimental dispersion space will contain numerous local energy peaks, out of which only one will correspond to the global energy peak for the fundamental mode, while the rest will conform to higher order multi-modes. Thus, application of any classical optimization algorithm will suffer

from the problem of the solution getting converged and trapped to a local minimum, leading to the misidentification of the shear wave velocity profile of the substrata. This phenomenon is pictorially represented in Fig. 6.3. A possible technique of overcoming such problems is to adopt non-traditional and evolutionary optimization algorithms such as Genetic algorithms (GAs), Particle Swarm Optimization (PSO), Cuckoo Search Optimization (CSO), etc. Literature reveals the existence of some advanced inversion concepts, although the numbers of documentation are extremely few and mostly conceptual and based on hypothesis.

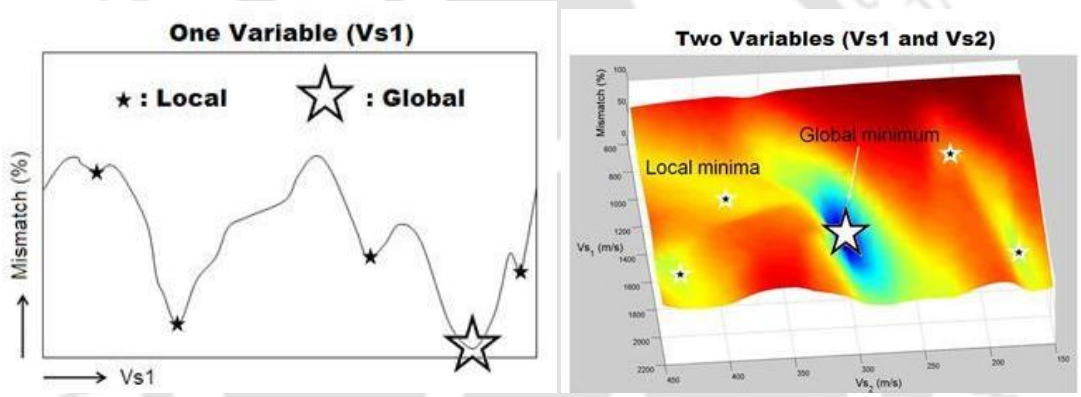

Fig. 6.3: Trapping into local minima for multimodal functions (Ryden *et al*. 2004)

***Multimodal Inversion*:** This type of inversion uses not only the M0 curve but also higher-mode curve(s) for the inversion. The motivation is to increase the accuracy (resolution) of the final 1D V_s profile by narrowing the range of possible solutions of 1D V_s profiles otherwise equally well suited if only the M0 curve is used (Fig. 6.4). This approach somewhat disposes of many possible solutions and attempts to reduce the intrinsic problem associated with the non-uniqueness of inversion analysis.

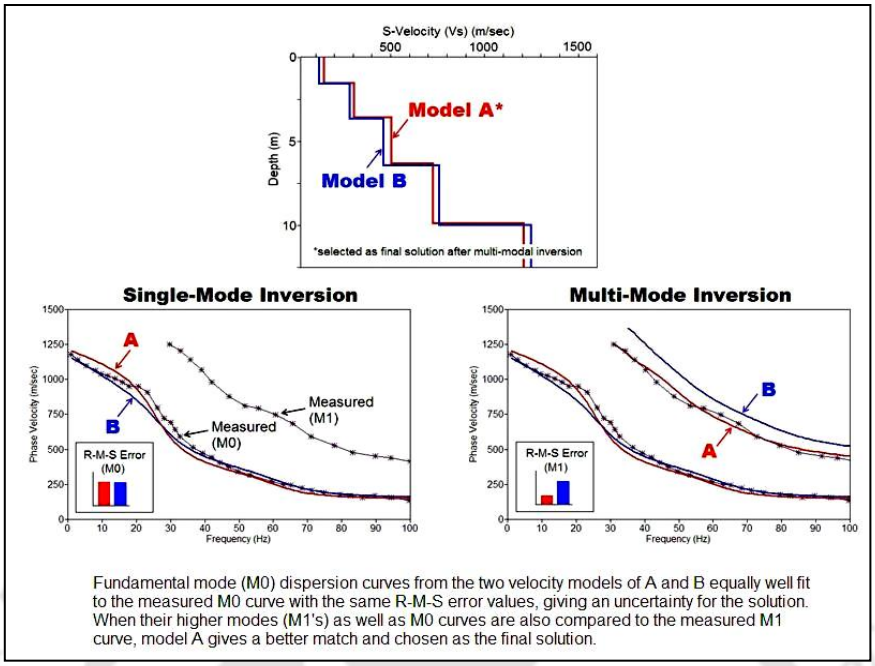

Fig. 6.4: Multimodal inversion using fundamental and higher modes (www.masw.com)

***Dispersion Image Inversion*:** This type of inversion includes the use of dispersion image data (also called phase velocity spectra) instead of dispersion curve(s) (Ryden and Park 2006; Forbriger 2003a, 2003b) (Fig. 6.5). This approach eliminates drawbacks of mode-misidentification and mode-mixing commonly associated with the modal-curve-based inversion techniques.

***Raw Data Inversion*:** This inversion approach uses the raw multichannel field record as obtained from the field experimentation, without any further processing such as dispersion imaging (Forbriger 2003b) (Fig. 6.6). This technique basically tries to compare the whole seismic waveforms observed at different distances from the source with synthetic waveforms generated from a proper forward modeling scheme. This approach may have the advantage of eliminating bias caused by subsequent data processing such as dispersion imaging or curve extraction. It,

however, has to simultaneously solve the difficulty of handling the attenuation and excitability issues, as well as layer parameters, as all of these can contribute to the shaping of a seismic waveform.

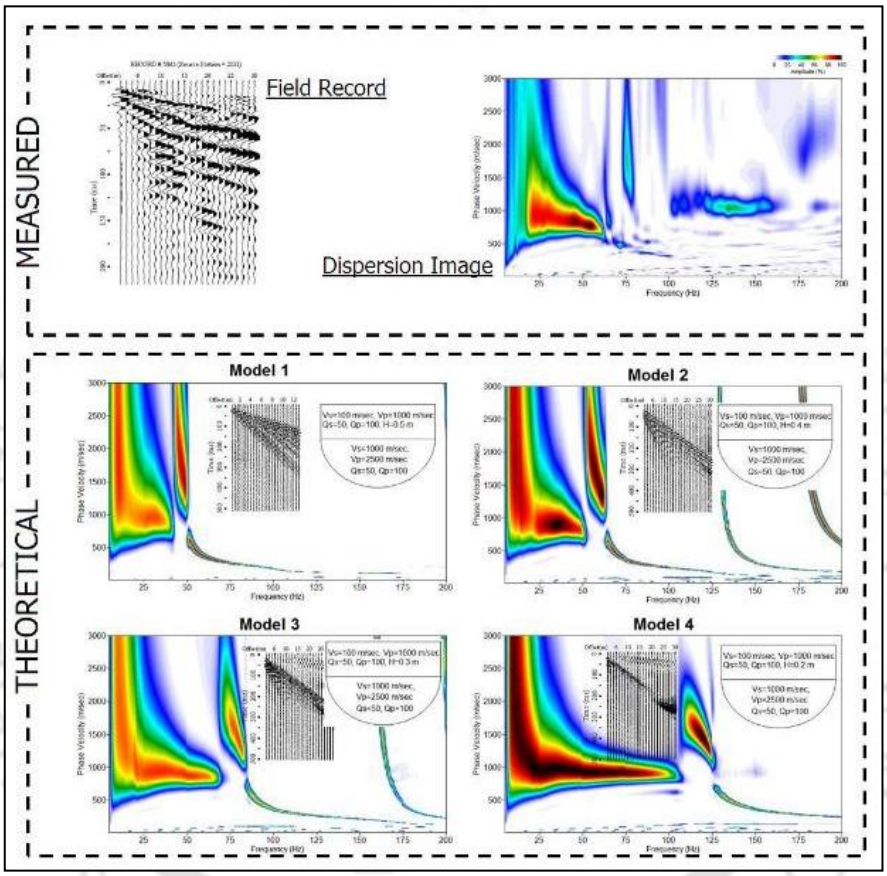

Fig. 6.5: Dispersion image inversion (Forbriger 2003a)

-

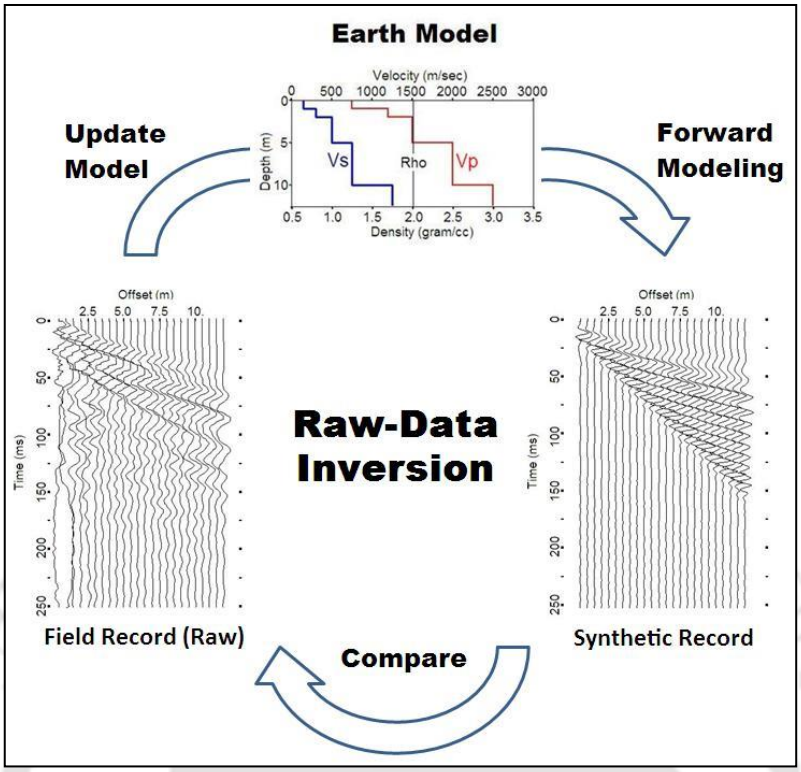

Fig. 6.6: Raw data inversion (Forbriger 2003a)

In absence of sophisticated algorithms and techniques to attempt the advanced inversion techniques, the present study utilizes the inversion of the fundamental mode dispersion curve to obtain the shear wave velocity profile of the subsurface. SURFSEIS has been used for the desired purpose of obtaining the dispersion image, from which the fundamental dispersion curve is extracted through visual inspection and manual selection. The fundamental dispersion band is visually identified, and a set of points from the band is manually selected to define the dispersion curve. In this process, the dispersion curve extraction is user-dependent, and gets subjected to errors. In actuality, the dispersion points (which represent the fundamental dispersion curve) should be the combination of frequency and phase velocity having the highest energy. In most cases, such energy peaks are sharp and are associated with steep downhill gradient. Hence, any minuscule error in the selection of the dispersion point selection actually leads to the choice of

point which remains in the adjacent low energy region, and hence, the fundamental dispersion curve gets misrepresented. However, such error cannot be avoided through manual selection, and needs the development of an automated dispersion picking algorithm which can extract the dispersion curve points with local peak energies. Such an approach will be discussed in detail in Chapter 7. However, it is understandable that in the commercially available softwares used for dispersion imaging and inversion analysis, such automated extraction algorithms are not inbuilt, and they still rely on the user intervention and subjectivity for manual extraction of the dispersion curve. Such technique of extraction is subjected to variation in the selection process adopted by the user, and thus affects the outcome of the inversion analysis. This chapter highlights the influence of such various choices made by the user on the obtained shear wave velocity profiles.

6.2. Results and Discussion

There are several parameters that affect the outcome of the inversion analysis, primarily governed by the subjectivity of the user in choosing the dispersion points corresponding to the fundamental curve. In this regard, the influence of the numbers of dispersion points selected and the frequency band from which it is selected is investigated. Apart from the issue of dispersion point selection, subjectivity also arises from the choice of the initial earth model which his necessary for the initiation of the optimization algorithm, In this regard, the influence of the chosen initial model and numbers of stratification layers of the earth model have been investigated. For each case, comparative plots have been presented to highlight the influence of each of the above parameters on the outcome.

6.2.1 Influence of Initial Model

The initial model has an important role on inversions (Tarantola 2005). The final inverted model determined by iterative inversions inherently depends on an assumed initial model due to the existence of locally suitable solutions (Yamanaka and Ishida 1996). When an appropriate initial model can be generated using a priori information about subsurface structure, inversions may find a suitable solution that is the global minimum of a misfit function. If a priori information is either scant or unavailable, the inversion may find a local suitable solution. Luke *et al*. (2003) showed that linear inversion yields excellent dispersion results for simple profiles. However, for more complex profiles, multiple solutions with equally good data fits are possible. As far as the initial model is concerned, three types of model definitions are available in SURFSEIS: Equal thickness model, Variable thickness model and User-defined thickness model. In Equal thickness model, initial models in Surfseis are generated based on the recommendations of Park *et al.* (1999). Selection of equal thickness model has been carried out in the present study, wherein the selected depth of half-space will be equally divided into the selected number of layers. However, in variable thickness model, the initial models are generated as per the algorithm of Xia *et al.* (1999). In this regard, a typical investigation has been attempted using 10 layers of substrata with a total depth of analysis being considered as 20 m. In both types of models, 'equal thickness model' and 'variable thickness model', the total depth and numbers of layers in the substrata are maintained constant during the entire analysis. The variable thickness model allows the pre-assumed thickness of substrata to change during the iterative optimization process. For the 'variable thickness model', the optimization algorithm is provided with the information that the thickness of layer is also a variable and needs to be optimized. Thus, in the latter case, there are *n* (*n* – number of layers) numbers of additional variables to be optimized (the thickness of *n*

layers). However, as the numbers of the layers are constant, the optimization scheme leads to nearly equivalent shear wave velocity profiles. It can be observed from Fig. 6.7 that there is no significant difference in V_s profile obtained with either of the initial profile definitions. However, the 'variable thickness model' provided same shear wave velocity for the 3rd and 4th layers, thus indicating the depth of investigation comprises 6 soil layers, while the 'equal thickness model' provides 8 layers, although the velocities are nearly equal.

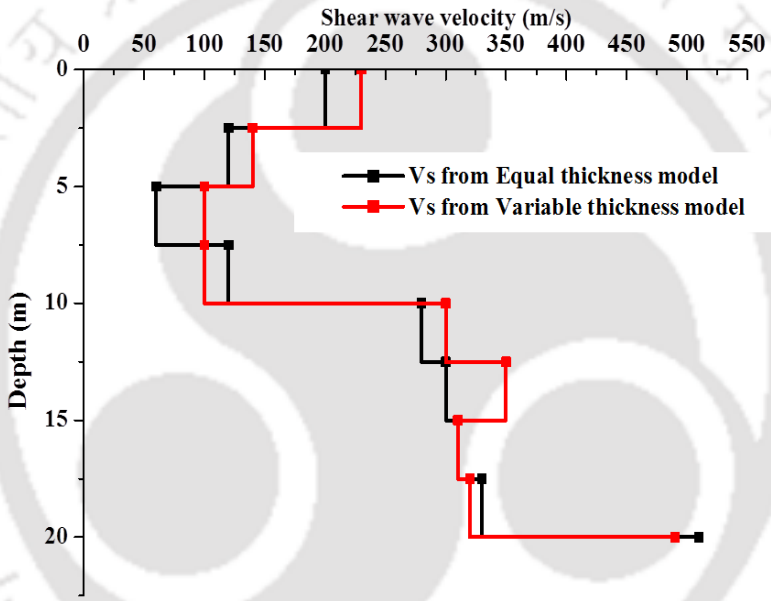

Fig. 6.7: Influence of initial model definition on typical shear wave velocity profile for Site-1

6.2.2 Influence of the Stratification of Initial Model

As far as the layer stratification is concerned, it was not known a-priori how many number of layer in the initial model would best represent the given site. Therefore, parametric study was carried out to check the influence of the numbers of layers on the shear wave velocity profile. In this regard, various numbers of layers were considered for the analysis (2, 4, 6, 8, 10, 12, 14, 16, 18, and 20). The initial profile for all the cases is adopted as 'variable thickness model', based on

the algorithm proposed in Xia *et al.* (1999). It was found out that the 2 layer give the highest RMSE error, rendering the practical infeasibility of the obtained solution. With the increase in the numbers of layers, the RMSE values decreased, and it was observed that beyond 10 numbers of the layers, all the outcomes are nearly similar and practically feasible. Figure 6.8 shows the parametric effect of the variation of numbers of layers in the computed RMSE. When the number of layers are increased, more complex earth models are created which aided in close match of the theoretical dispersion curves to the experimental one, thus reducing the RMSE values. Figure 6.9 portrays the V_s profiles obtained with various numbers of layers in the initial model, which indicates that beyond 10 layers, the profiles obtained are approximately similar to each other. Hence, the investigation shows that beyond 10 or 12 layers, the solution becomes stable and can be considered as a stable model definition. If more number of layers is considered, then it will take longer time for inversion process without significant improvement in the RMS error and the obtained solution. However, it is worth mentioning that a choice for higher number of layers (say, 20) might be useful when there is no a-priori information available. If in actual case, the number of distinct layers is lesser, the obtained solution would automatically indicate the same, showing nearly similar shear wave velocities for successive layers. In case of a-priori information from previous borehole surveys, the numbers of layers of the initial model can be adopted based on the known stratifications, thus reducing the computation time.

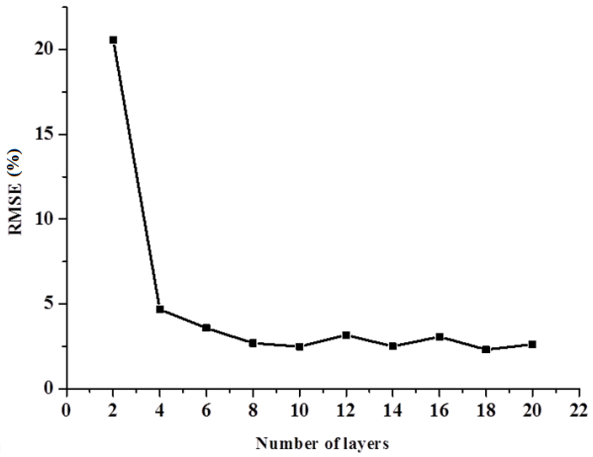

Fig. 6.8: Influence of numbers of layers in the initial model on the RMSE of typical shear wave profile obtained for Site-1

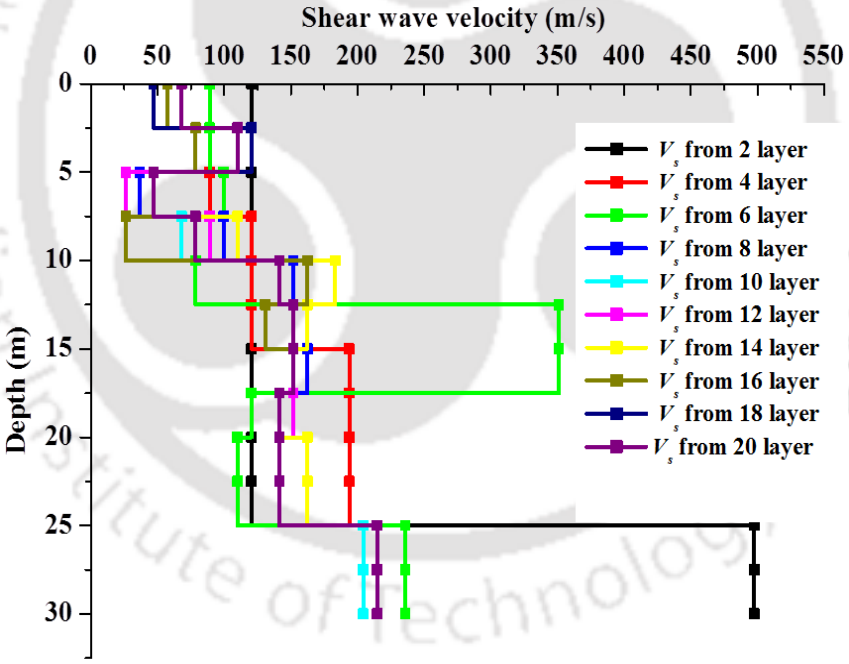

Fig. 6.9: Influence of numbers of layers in the initial model on the typical shear wave velocity profile for Site-1

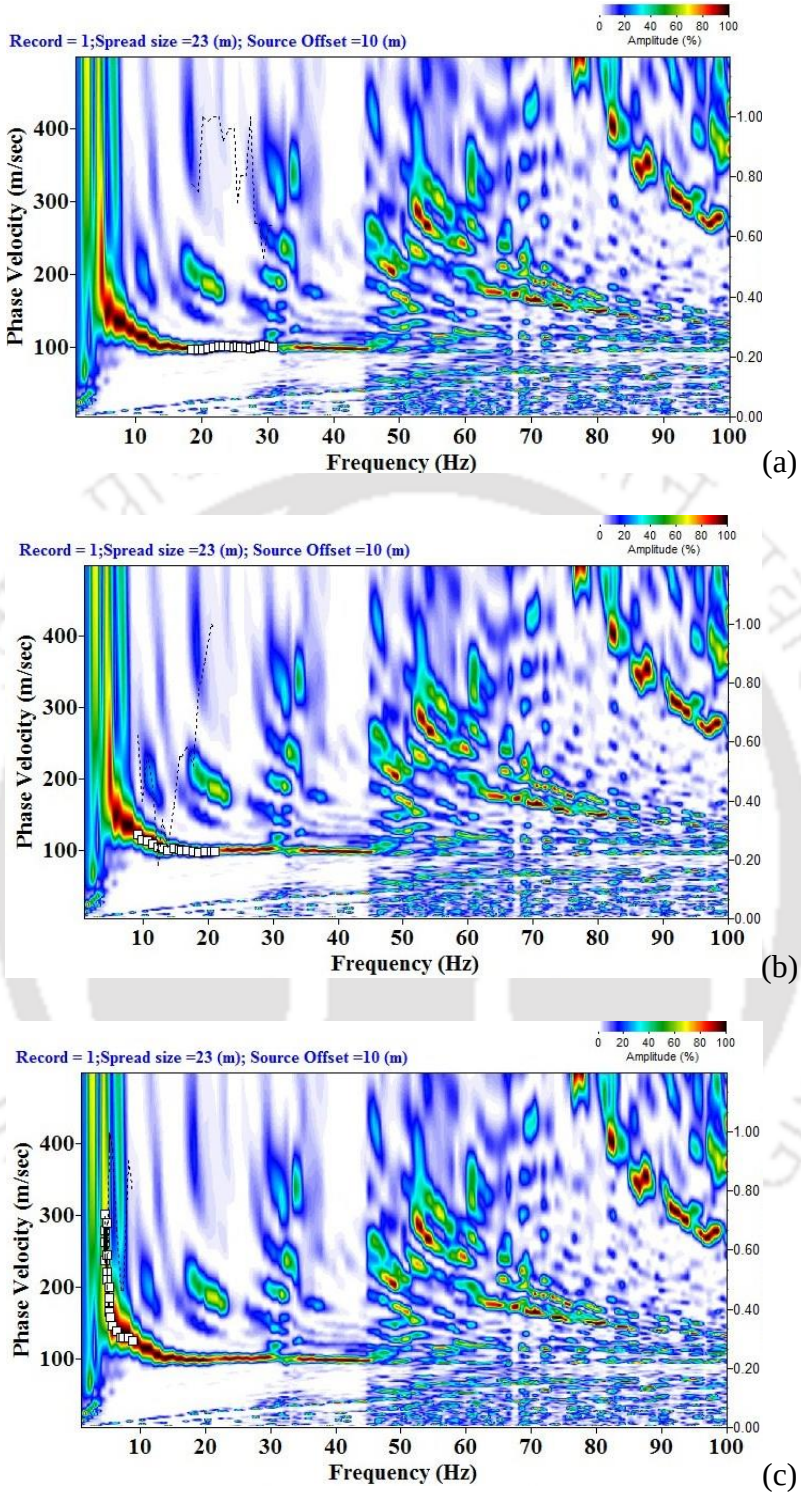

Fig. 6.10: Extraction of dispersion points from different frequency bands of a typical dispersion image for Site-1 (a) 20-30 Hz (b) 10-20 Hz (c) 5-10 Hz

6.2.3 Influence of Frequency Band Density of Dispersion Points

The extent of the dispersion curve in the frequency domain significantly affects the outcome of the inversion analysis. A dispersion curve incorporating the lower frequency ranges will be informative on the shear wave profiles of the deeper strata, while a dispersion curve will provide information about the shallow strata if it is encompassing the higher frequencies. In this regard, attempts have been made to select the dispersion points from various frequency bands and study their effects in the shear wave velocity profile. In each case 15 dispersion points were selected from the fundamental dispersion curve, where the points belong to different frequency bands namely, 20-30 Hz, 10-20 Hz and 5-10 Hz, as shown in Figure 6.10.

Figure 6.11 depicts the shear wave velocity profiles obtained from the inversion analysis of the dispersion curved selected from different frequency bands (Fig. 6.10). It can be observed that with the increasing magnitude of the frequencies in a band, the depth of investigation becomes lower. It is an obvious finding since higher frequencies are associated with lower wavelengths, which can penetrate lower depth in the subsurface for revealing its information. It can also be observed that selection of lower frequency band produces erroneous results in the shallow depth. Hence, it is imperative that the dispersion points should be selected from all along the dispersion curve so that the complete information of the substrata can be simultaneously obtained.

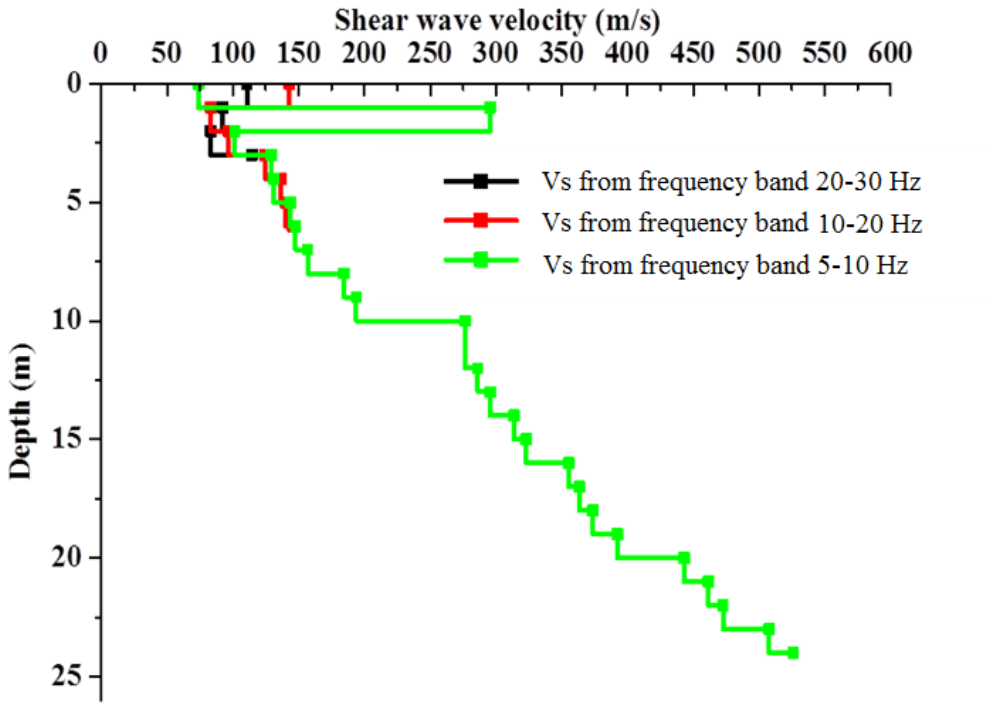

Fig. 6.11: Comparative of typical V_s profiles for Site-1 obtained from the dispersion curves selected from different frequency bands

6.2.4 Influence of Number of Dispersion Points

As has been shown in the previous section, the dispersion points should be selected from all along the fundamental dispersion curve in order to obtain a best suitable profile of the substrata. One can select varying number of dispersion points to represent the extracted dispersion curve. Figure 6.12 portrays a typical representation of the fundamental dispersion curve using varying number of dispersion points. It is recommended that the number of dispersion points should not be too low, as the heterogeneity of the substrata cannot be evenly recognized. Picking of more number of points does not necessarily increase the accuracy of the shear wave velocity profile. However, the integrity in the data points i.e. the continuity and trends of the points in regular or irregular fashion, affects the inversion results. In the present study, all the dispersion curve points

were picked in regular trends, as the irregular picking gives very low SNR and inaccurate results. As mentioned earlier, the accuracy depends on the exact identification of the locations of peak energy in the dispersion image. Hence, mere increase in the manually selected dispersion points is bound to increase the error accumulated due to the selection. In most cases, manual selection will miss the exact peak, and end up with an adjacent low energy point incorrectly selected as a point on the fundamental dispersion curve. Hence, in case of manual extraction of the dispersion curve, there lies a trade-off between the number of selected points and the error associated with the inverted profile. Table 6.1 shows the RMSE with different number of points. It can be observed that lower RMSE values can be achieved when 10-30 dispersion points were chosen to represent the dispersion curve. The RMSE was high for sparse selection of dispersion points as it failed to represent the critical variations in the subsurface profile, while higher number of selected points resulted in error accumulation. Although the manual selection of 10-30 points is site-specific (Site-1 for this case), 30 points are suitable enough for most of the sites. . More than stating it to be site-specific, the choice depends on the quality and resolution of the dispersion image, as the latter depends on several site-dependent and experimental parameters. Lesser number of points are required for dispersion images with better resolution. Independent on the number of points being selected, the primary requirement would always be to select those points whose SNR is high, so that the representative dispersion curve has an overall high SNR. The SNR of the selected dispersion points should not be compromised under any condition; otherwise, the final shear wave velocity would become ambiguous. However, maintaining such high SNR for all the dispersion points being manually selected is not possible, hence, is the necessity for the automated dispersion curve extraction, where the maximum SNR can be maintained. Since the points selected are assumed to be linearly connected, too less numbers of

dispersion points would fail to represent the actual curvilinear dispersion trend and result in an incorrect piece-wise linear dispersion characteristic, further leading to incorrect shear wave velocity profile (Fig. 6.12f).

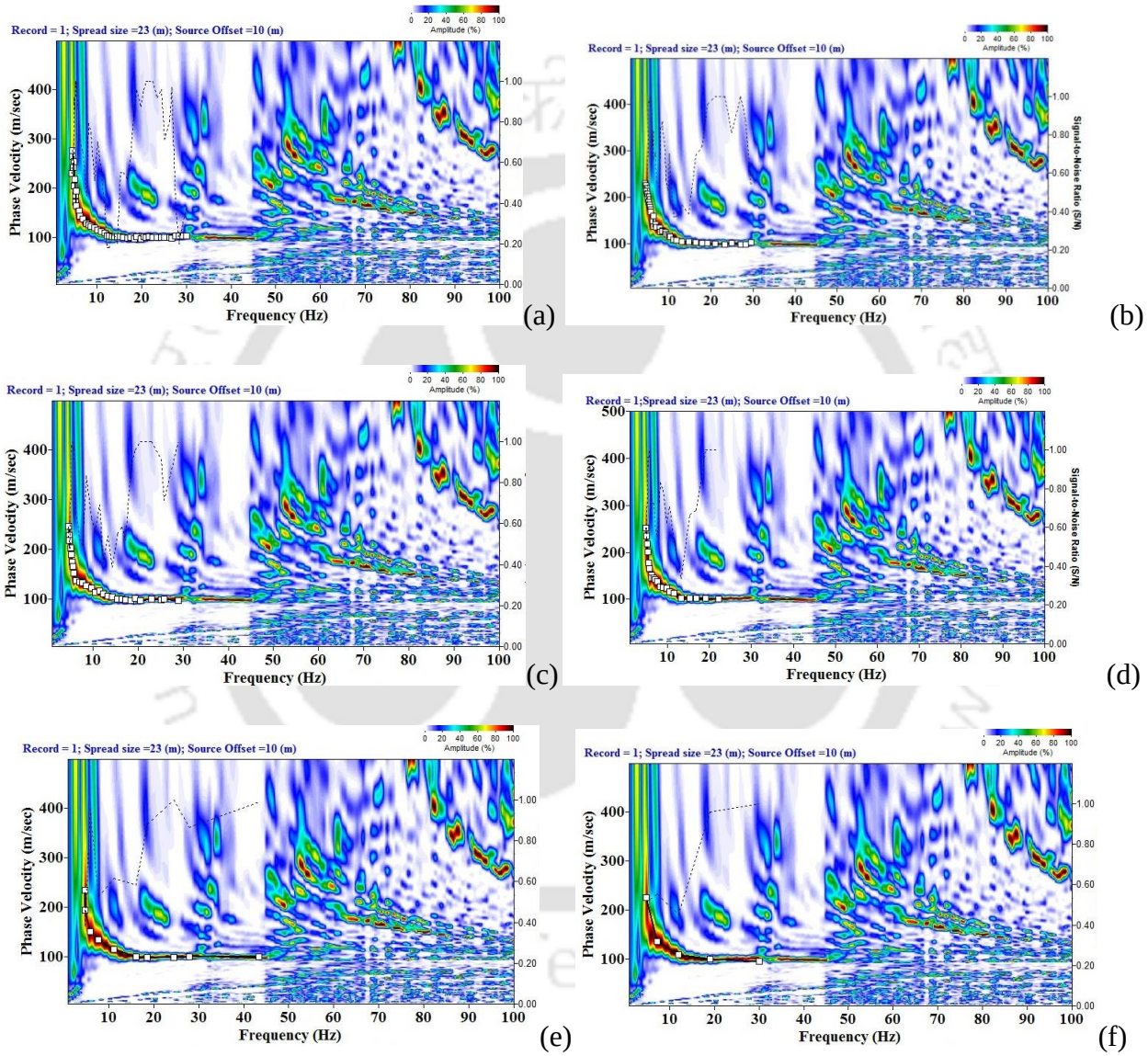

Fig. 6.12: Representation of fundamental dispersion curve of a typical dispersion image for Site-1 obtained by varying numbers of dispersion points (a) 50 (b) 40 (c) 30 (d) 20 (e) 10 (f) 5

Table 6.1: Comparison of the number of selected dispersion points with the RMSE

No. of Points representing the fundamental dispersion curve	50	40	30	20	10	5
RMSE	15.49	1.11	0.82	0.76	0.9	1.58

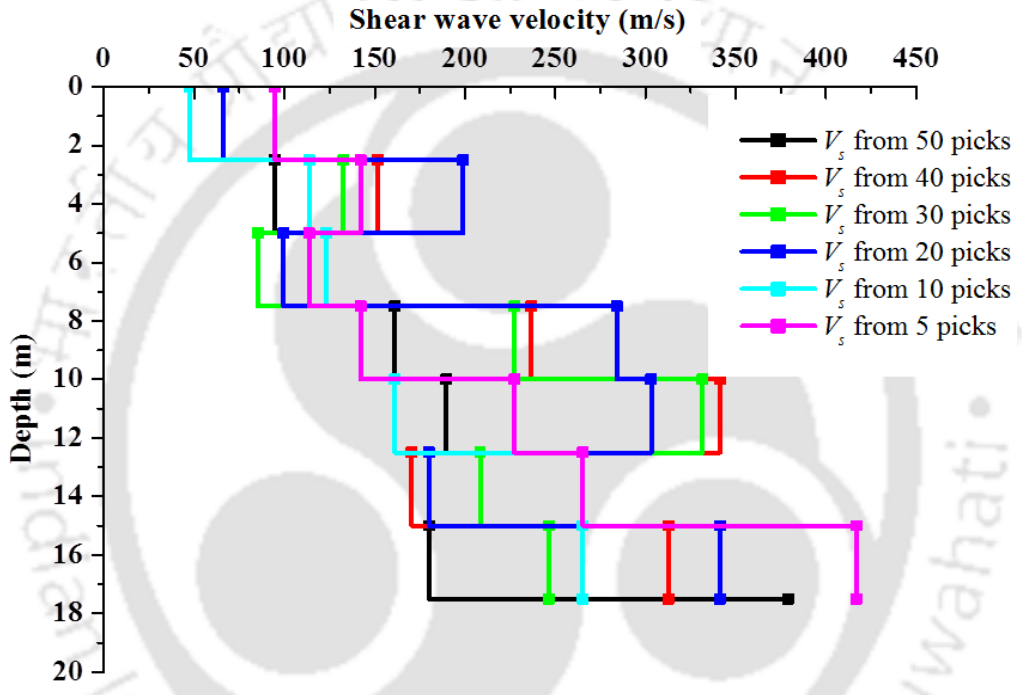

Fig. 6.13: V_s profiles for Site-1 obtained from the inversion of fundamental dispersion curve represented by varying numbers of dispersion pickup points

Figure 6.13 shows the V_s profile obtained from the inversion of fundamental dispersion curve represented by varying numbers of dispersion points. It can be observed that there is a lack of convergence in the velocity profiles with the variation in the number of points. Although the RMSE error obtained from selecting 10-30 points are comparable (Table 6.1), still the velocity profiles are far from reaching a favorable comparison. Hence, it is amply clear that mere increase

in the number of dispersion points would not be enough for a proper representation of the subsurface. It is highly essential that the points possessing the highest local energy are only selected, which is not possible in manual selection. Hence, there is an utmost necessity of automated selection of the dispersion points following the locally highest energy trends. Such a technique has been developed and will be dealt in Chapter 7.

Based on the observations and discussions presented above, in order to obtain the subsurface profile to a sufficient depth, the following combination of parameters were found to be suitable and are suggested to be applied for an inversion process involving manual extraction of dispersion curve: (a) Initial earth model as per the Variable Thickness scheme and comprising a minimum of 10 numbers of layers, and (b) An average of 20 dispersion points to represent the fundamental dispersion curve, where the dispersion points should be regularly distributed along the entire dispersion curve and definitely incorporating the lower frequency regions, if available. In this regard, following the stated suggestions, inversion analyses were carried out to obtain the V_s profile with depth for all the three sites (Site-1, Site-2 and Site-3).

Figure 6.14 reveals the comparative variation of shear wave velocity profile of Site-1 obtained by the analysis of active MASW survey records and that obtained from *N*-value from a borehole log carried out at the same site. The experimental dispersion curve for Site-1 was obtained from the best suitable field parameters as had been already described in detail in Chapters 4 and 5 (*i.e.* Sampling frequency – 7500 Hz, Numbers of samples – 7500 Hz, Source offset – 10 m, Inter-receiver spacing - 1 m, Numbers of channels – 24, Combined band-pass filtering and suitable muting). The borehole log obtained provided the variation of N-values from Standard

Penetration Test (SPT). The corresponding variation of shear wave velocity (V_s) was estimated using the relationship provided by Imai and Tonouchi (1982), expressed as, V_s=97N$^{0.314}$. It canbe observed that the velocity profiles obtained from the field geotechnical (SPT) and geophysical (MASW) investigations are sufficiently agreeable to each other, with some tolerable variation to each other. The mean deviation is computed to be 27 m/s, which is considerably low. This observation indicates the efficacy of the suggested parameters in conducting a rational inversion analysis. Figures 6.15 and 6.16 shows similar appreciable agreements between the shear wave velocity profiles of Site-2 and Site-3 respectively obtained from SPT and MASW tests.

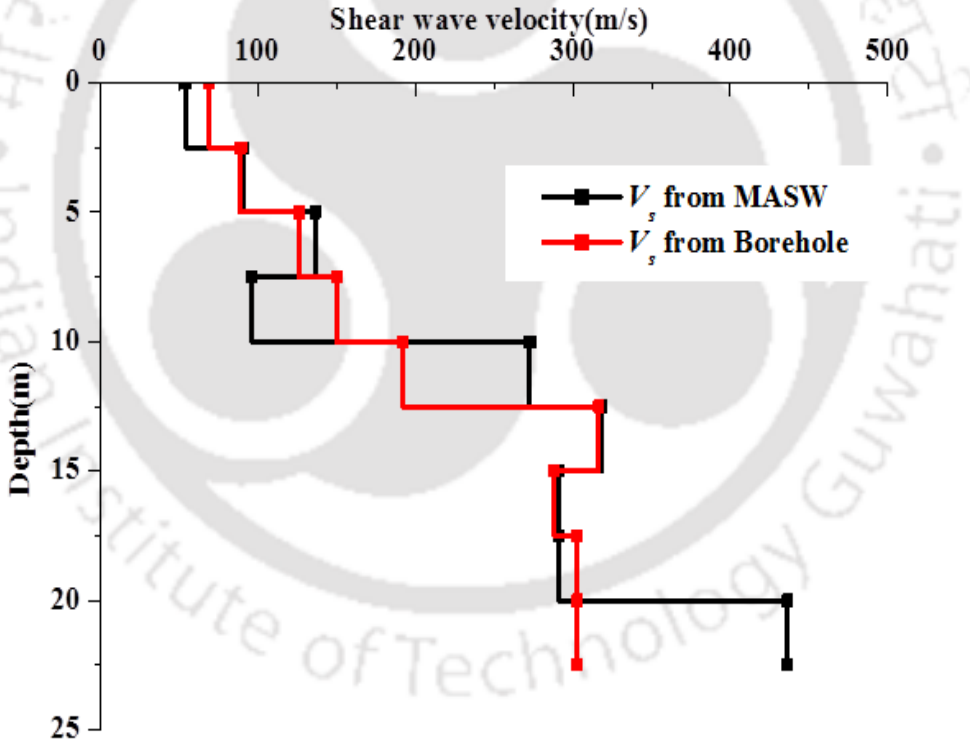

Fig. 6.14: Comparison of V_s profiles obtained from SPT and MASW investigations for Site-1

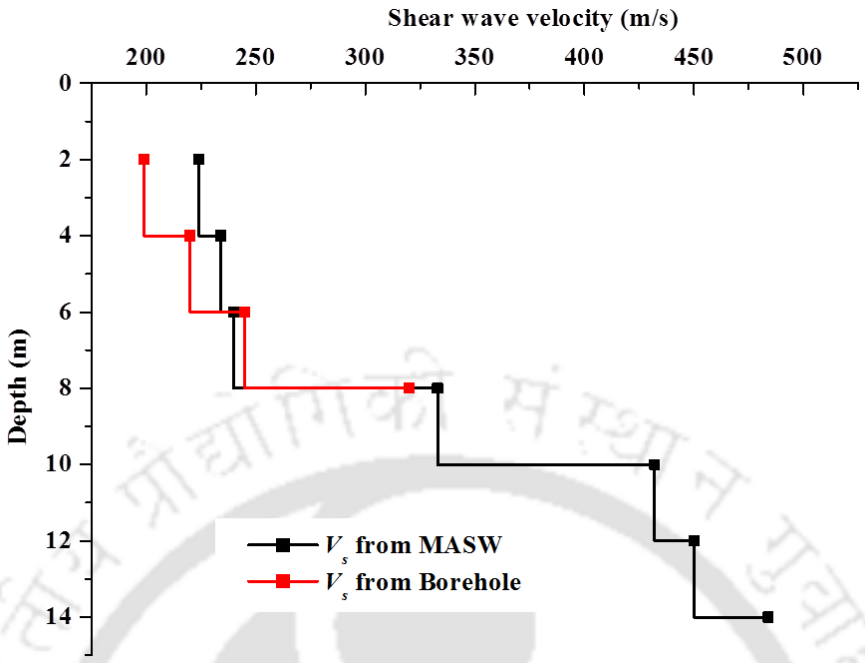

Fig. 6.15: Comparison of V_s profiles obtained from SPT and MASW investigations for Site-2

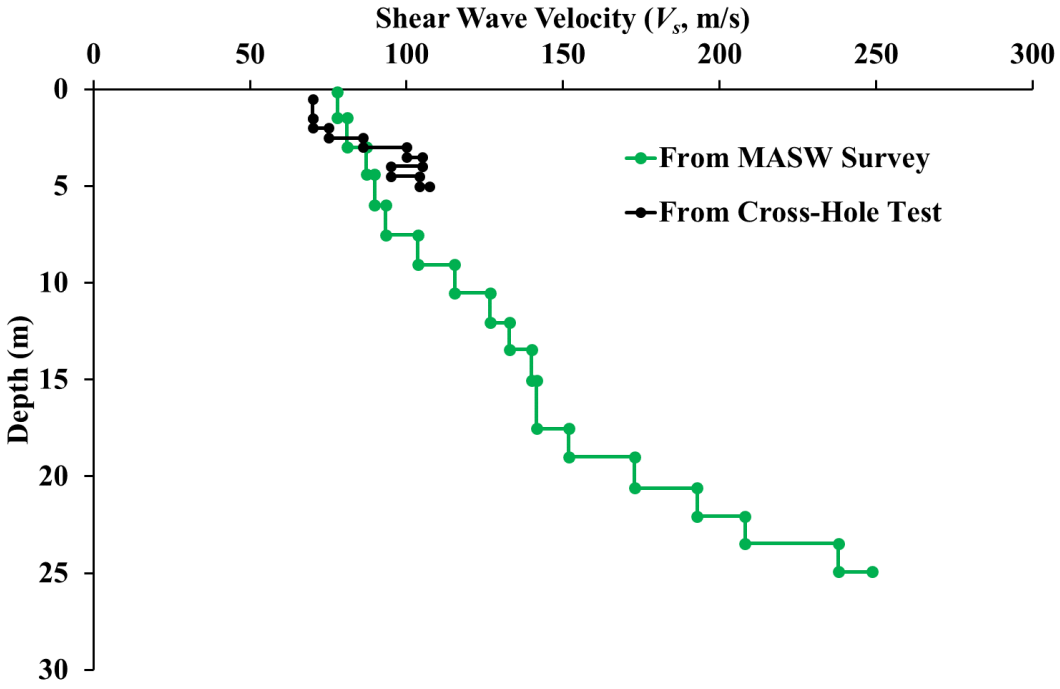

Fig. 6.16: Comparison of V_s profiles obtained from SPT and MASW investigations for Site-3

6.3 Summary

This chapter highlights with the parameters that affect the accuracy of the shear wave velocity profiles obtained from inversion analysis. Factors such as the choice of initial model and its type, numbers of stratigraphy layers in the initial model, number of manually selected dispersion points representing the fundamental mode dispersion curve and the frequency band from which the dispersion points are selected play a significant role on the accuracy of the obtained V_s profile. Based on the above study, the following salient points are highlighted:

- There is no significant difference in V_s profile obtained from the Initial thickness model and the Variable thickness model.
- Number of layers in the initial model affects the accuracy of V_s profile. The variations of RMSE with the increasing numbers of layers indicate that a choice of more than 10 layers in the initial model is sufficient to obtain a fairly accurate shear wave velocity profile. Choosing larger numbers of layers might increase computational time without significantly increasing the accuracy of the obtained profile.
- Making a manual selection of 10-30 dispersion points is sufficient in representing the fundamental dispersion curve. Shear wave velocity profiles obtained from these selections would be fairly precise, if the selection has been made carefully enough to identify the dispersion points as the points of locally highest peak energy.
- Selection of dispersion points should be so made that the points remain regularly scattered along the entire length of the fundamental dispersion band, so that most of the information of the subsurface shear wave velocity can be deciphered. Dispersion points belonging to the low frequency region should be given special attention since these points are instrumental in providing information of deeper substrata.

CHAPTER 7

QUANTIFICATION OF RESOLUTION OF DISPERSION IMAGE AND AUTOMATED EXTRACTION OF DISPERSION CURVE

7.1 General

Dispersion of waves is the phenomenon related to a cylindrical or hemispherical wave front travelling through a medium, where each of the propagating wave frequencies can possess multiple phase velocities, and vice-versa. The collected wavefield records, after preprocessing with frequency filtering and required temporal muting, is subjected to dispersion analysis, in order to establish the relationship between the frequency (*f*) and the phase velocity (*C*) of the waves present in the wavefield. In contrast to the earlier used wave analysis techniques to directly estimate the dispersion curve (Park *et al*. 1998), the multichannel approach does not attempt to estimate the individual phase velocities, rather constructs an image space where the dispersion trends are identified from the pattern of energy accumulation in *f*-*C* space. The dispersion image is generally obtained by applying Fast Fourier Transform (FFT), or similar techniques, on the time-stamp of a recorded wavefield to achieve the power spectral amplitude in the frequency domain, which indicates the distribution of the recorded energy over a frequency band. All types of propagating seismic waves are eventually imaged if they possess considerable energy. For the construction of the dispersion image, a multichannel record in time-space (*t*-*x*) domain can be transformed into either frequency-wavenumber (*f*-*k*) or frequency-phase velocity (*f*-*C*) domain. It is generally known that the *f*-*k* method results in dispersion images with the lowest resolution, whereas the phase-shift method (*f*-*C* domain) renders the same of highest

resolution (Park *et al*. 1998; Moro *et al*. 2003). From any dispersion image, the necessary dispersion curves are extracted by following the image trends of localized maximum energy accumulation. When more than one phase velocities exist for a given frequency, the phenomenon corresponds to multimodal dispersion. The dispersion curve having the slowest phase velocities corresponds to the fundamental mode (M0), while the next faster one corresponds to the first higher mode (M1), and so on (Fig. 7.1).

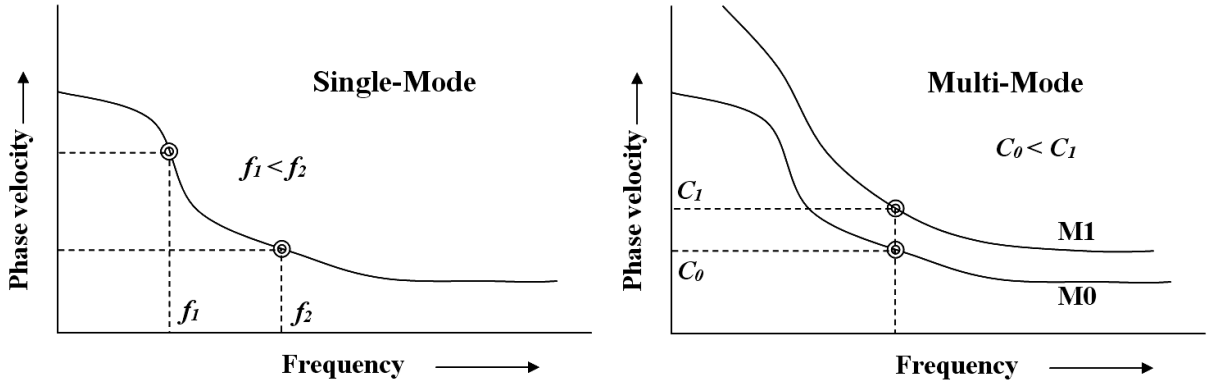

Fig. 7.1: Schematic dispersion curves featuring unimodal and multimodal characteristics

Dispersion is a property of surface waves that is defined as the dependence of phase velocity (or, the propagating velocity of each wave) on its frequency content (Park *et al.* 1998). In this manner, different frequencies are expected to have different phase velocities owing to the fact that they travel through different numbers of layers having varying characteristics. In dispersion imaging scheme, the normalized propagating energy is imaged on a 2D plane of phase velocity and frequency. Theoretical dispersion curve obtained from any of the standard methods (Schwab and Knopoff 1972; Ke *et al*. 2011) is optimized towards experimental dispersion curve, through sequential and iterative model parameter updating scheme. A common practice is to reduce the

root-mean-square (RMS) error between the theoretical and experimental dispersion curve to a minimal. As the tolerance is satisfied, the optimized theoretical dispersion curve is decided to be the final dispersion model to be further used in inversion analysis for ascertaining the field subsurface stratigraphy profile. However, the efficacy and accuracy of the inversion analysis depends on the precision of extracting the fundamental or higher order dispersion curves from the corresponding dispersion image, which, in turn, is dependent upon the resolution of the dispersion images. The effects of various data pre-processing and data acquisition parameters on the resolution of the dispersion image have already been discussed in Chapter 4 and Chapter 5, respectively. However, the resolution of the images was merely qualitatively described based on visual inspection and classification, while the quantification of the resolution of the dispersion images was omitted.

Chapter 6 had employed the manually extracted dispersion curve to inversion analysis in order to decipher the shear wave velocity profile of the subsurface. Commercially available software extracts the dispersion curve for inversion process based on the user discretion. As had been clearly mentioned earlier, such manual extraction of dispersion points of the fundamental or higher order modes is subjected to human discrepancies. Such discrepancies originate due to the lack of unambiguously identifying the exact location of the locally highest peak energy occurrences in the dispersion image. Hence, any minuscule error in locating the peak energy point would erroneously lead to choosing an adjacent point with lower energy, which would be misread as a point representing the fundamental or higher order modes. Such erroneous inclusions of the dispersion points in defining the dispersion curve to be subsequently used in inversion would result in a inaccurate or imprecise shear wave profile. Hence, it is extremely

necessary to unambiguously locate the locally highest energy peaks through an automated process so that the subjectivity of the inversion results can be eliminated.

This chapter describes the attempts which has been made to address the above two problems, namely (a) quantification of the quality of the generated dispersion image, and (b) automated extraction of precise fundamental or higher order mode dispersion curves as per the exact peak energy trends of the dispersion image. In order to address the problems, MatLab codes have been developed and have been integrated with SURFSEIS, wherever necessary. The following sections provide a detailed description of the approaches.

7.2 Quantification of the Resolution of Dispersion Image

Resolution of an image governs its sharpness and is defined by the number of pixels contained in a unit area, thus quantifying the nearness of the pixels till the limit of being visibly resolved. The same pixel resolution will be sharper on a smaller display area, and vice-versa. Resolution can be expressed in various units as lines per mm (lpm), lines per inch (lpi), and more commonly dots per inch (dpi). From various literatures as described in Chapter 2, it can be concluded that good resolution dispersion image indicates a distinguishable trend of dispersion curve, with clearly identifiable fundamental and/or higher modes within a wide frequency band. The image should exhibit narrow bandwidth of the energy so that, based on the highest energy accumulation at fundamental mode, the extraction of dispersion curve becomes simpler and can be subsequently used for inversion analysis. In this study, image processing techniques have been used to identify the highest energy accumulations in the dispersion image space for the proper identification and extraction of the dispersion curve.

Park *et al.* (1998) defined the resolution of a dispersion image as the resolvable capabilities along both the velocity and frequency axes. The resolution along the phase velocity axis represents the capability to discriminate the phase velocity for a particular frequency from the same for any other adjacent frequencies, while vice-versa along the frequency axis. Till date, resolution is based on the visual identification of the observer and hence an attempt has been made in the present study to quantify the resolution of the dispersion images. In the present study, the concept provided by Park *et al*. (1998) is applied through MatLab based image processing framework.

7.2.1 MATLAB based Image Processing to Quantify Resolution

Image Processing Toolbox provides a comprehensive set of reference-standard algorithms and workflow apps for image processing, analysis, visualization, and algorithm development. Image segmentation, image enhancement, noise reduction, geometric transformations, image registration, and 3D image processing can be efficiently performed using the toolbox command menu. Hence, in this regard, a MatLab coding has been developed to extract the dispersion band and provide a quantification of the resolution of the dispersion image in terms of the numbers of pixels per unit area, the pixels being counted when they exceed a specified energy threshold. Figure 7.2 depicts a typical input 2D dispersion image (as obtained from Surfseis) and the corresponding output from the image processing which is used to quantify the resolution.

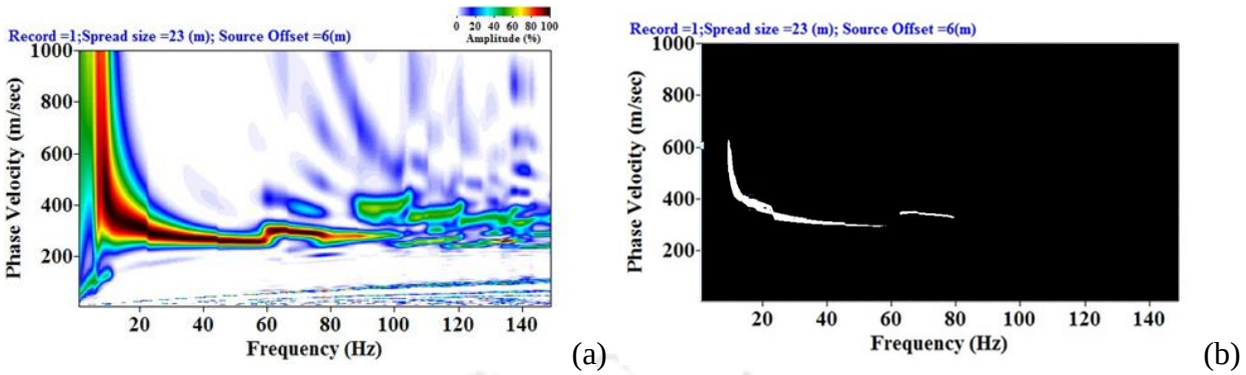

Fig. 7.2: (a) A typical 2D dispersion image as obtained from SURFSEIS (b) Extracted dispersion band through MatLab based image processing approach

The algorithm of the extraction of the dispersion band(s), developed as a MatLab code, is described step-wise as follows:

- The 2D dispersion image generated from Surfseis is read into MatLab code using the command ***imread***. The command converts the dispersion image into Red-Green-Blue (RGB) color model. The obtained RGB image is resized into a convenient size using the command ***imresize***, and then further converted into the Luminance-Chrominance (YCbCr) color model using the command ***rgb2ycbcr***.
- A binary mask is created using the command ***createmask***, by which the color-mode converted image is stored in black and white (BW) pixels. The command actually thresholds the RGB or YCbCr image into a BW mode using auto-generated code from ***colorthresholder app***. The colorspace and minimum/maximum values for each channel of the colorspace were pre-coded in the app, which leads to the segregation in the binary mask, and a composite masked RGB Image is created which shows the original RGB image under the mask BW. The darker sections (defined by the color thresholds as per

the percentage of the amplitude/power) are allotted white color, while the rest of the sections which does not meet the threshold are allotted black color.

- The created masked image is further smoothened an operated upon by the commands ***im2bw*** and ***bwareaopen***.
- The BW image is then displayed with the aid of the command ***imshow*** where each of the pixels with are displayed as black dot if the value is zero, while the rest are shown as white images.
- The number and density of white pixels are counted with the aid of ***nnz*** command and a script code. The white pixels represent the extracted dispersion band.

The above technique can be successfully implemented to quantify the resolution of the dispersion band. Moreover, based on the resolution of the dispersion bands generated from the parametric variations of the contributory factors, the best suitable or optimal magnitude of the parameter can be recognized which produces the best resolution dispersion image. In this regard, a typical example is presented herein wherein the resolution of the dispersion bands, generated on the basis of varying offset distances, are quantified, and accordingly the optimal optimal offset distance is recognized. Figure 7.3 shows a set of typical dispersion images obtained through SURFSEIS. As per the normal practice referred in several literatures, a subjective visual identification concluded that 6 m offset gives the best resolution dispersion images. In the present study, the resolution is quantified based on the density of white pixels (in dpi) present in the binary image (the white pixels represent the localized energy points having more than 99% normalized energy). Quantification is also made of the average thickness and the width (spread) of the dispersion band.

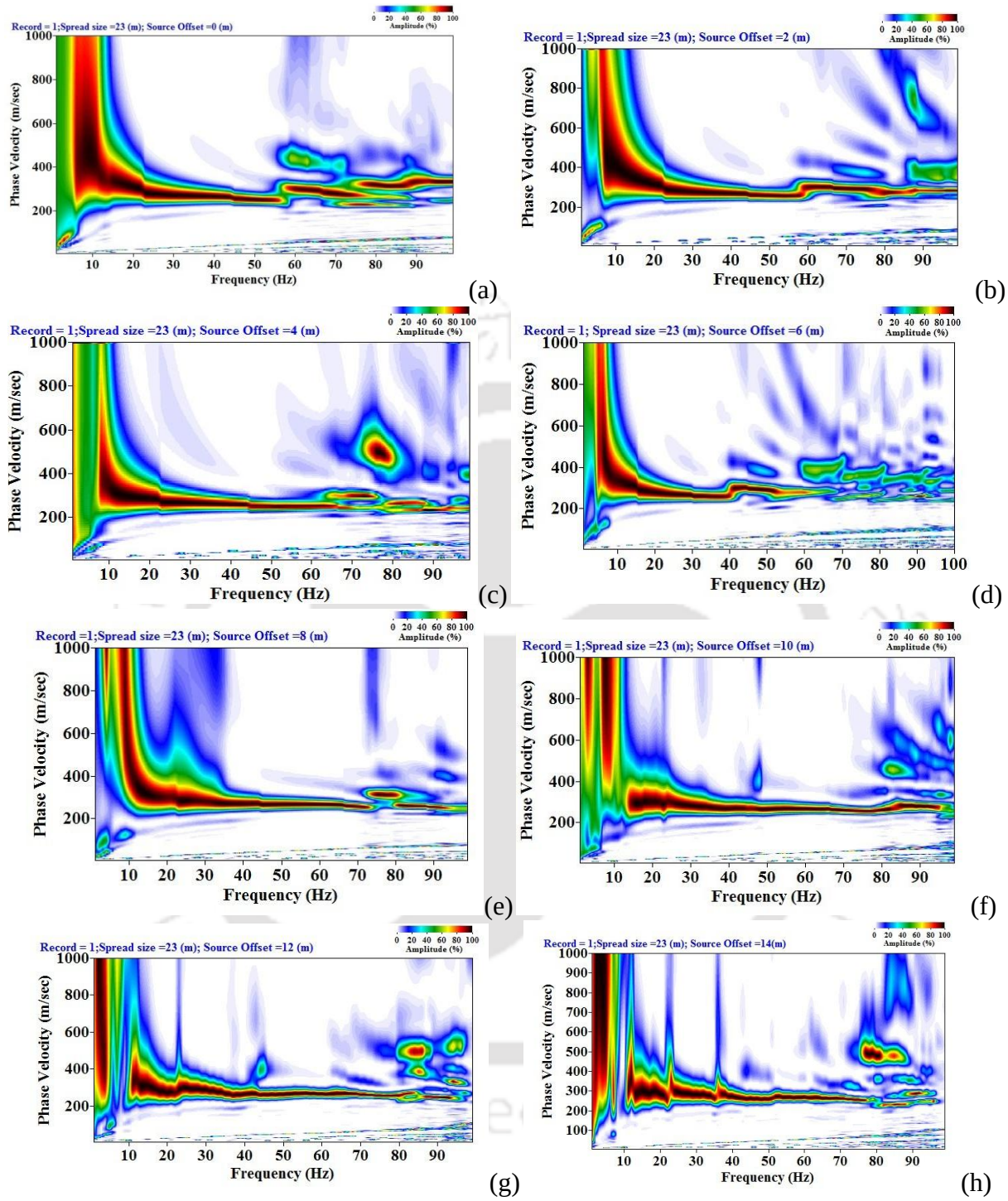

Fig. 7.3: Dispersion image obtained from survey at Site-2 conducted with various offset distances (a) 0 m (b) 2 m (c) 4 m (d) 6 m (e) 8 m (f) 10 m (g) 12 m (h) 14 m (Sampling frequency – 15000 Hz, Sample length – 5120, Inter-receiver spacing – 1 m, Number of channels - 24)

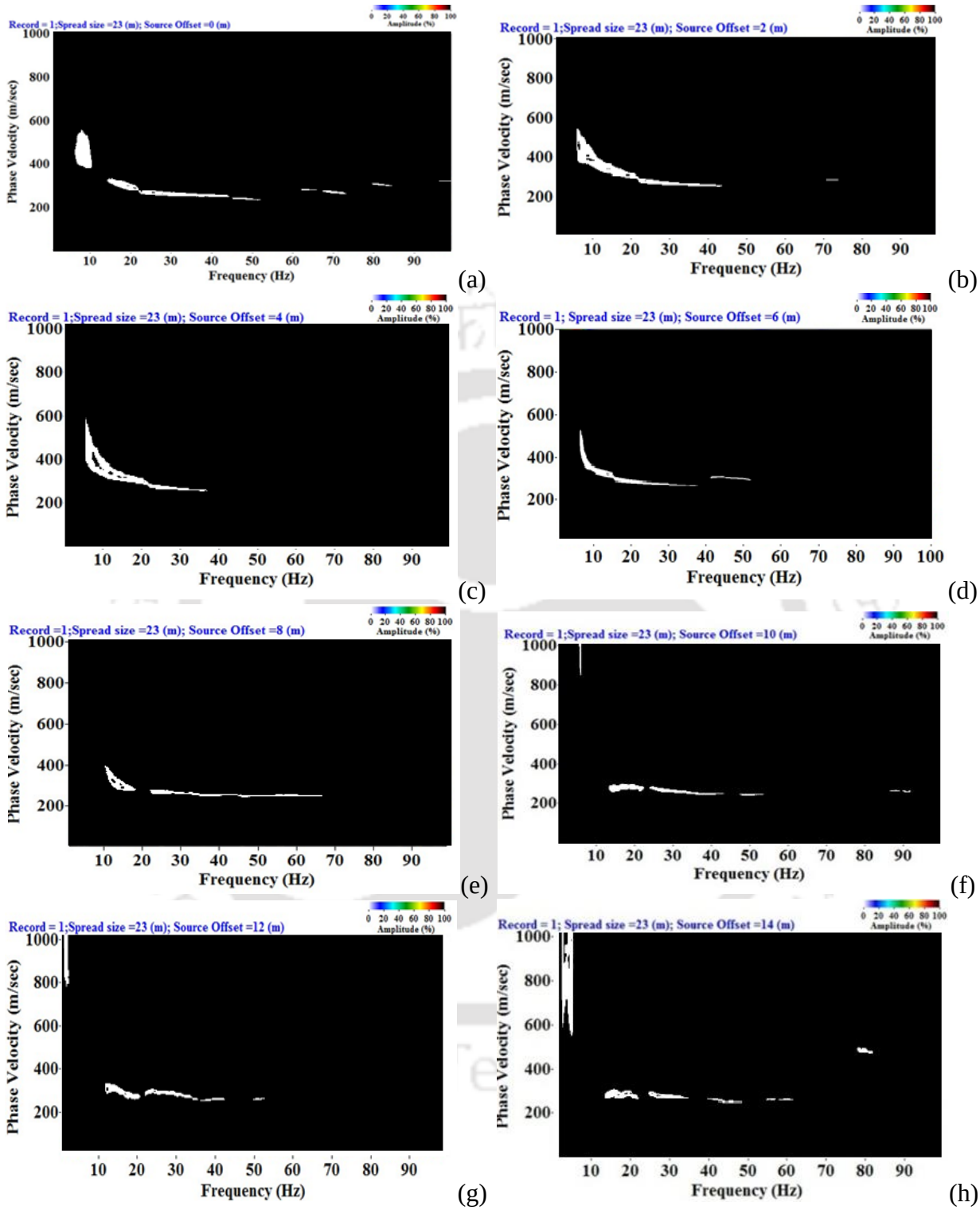

Fig. 7.4: Extracted dispersion band using image processing algorithm considering various offsets (a) 0 m (b) 2 m (c) 4 m (d) 6 m (e) 8 m (f) 10 m (g) 12 m (h) 14 m (Sampling frequency – 15000 Hz, Sample length – 5120, Inter-receiver spacing – 1 m, Number of channels - 24)

From the fundamental definition, resolution is number of pixels contained in a unit area, thus quantifying the nearness of the pixels till the limit of being visibly resolved. Based on the extraction of the white colored pixels from the Fig.7.3, Fig. 7.4(a-h) illustrates the white bands as the congregation of the points of highest energy, which is an indicator of the dispersion bands of fundamental or higher order modes. The dispersion curve is expected to belong to this white-shaded band. The Red and Yellow color shades (Fig. 7.3) also contains some information and attributes to 60-80% of energy. However, consideration of these points lead to a compromise in accuracy, and hence, only the darkest colored pixels, representing 99.9% normalized energy, are extracted.

Table 7.1 lists the variation of the resolution in dpi (dots per inch) for different offset distances, as obtained from the MATLAB image processing. The corresponding average thickness of the white band, denoted as *dv* in present case, is also reported. The lesser the thickness of the band, higher is the resolution, and lesser is the possibility to pick the lowest energy dispersion points. From the table, it can be noticed that beyond 6 m offset, the dispersion bands are quite narrow, thus indicating good resolution dispersion images. It can be noted that the dispersion bands corresponding to 10 m, 12 m and 14 m offsets possess significant discontinuity in the dispersion band, as well as the information related to the lower frequency region is almost negligible. Dispersion image corresponding to the 6 m offset show the highest resolution of 3220 dpi and the band thickness is only 20 m/s, and thus the same can be convincingly concluded as the suitable or optimal offset distance. Hence, in this manner, to the author's knowledge, this is the first instance of quantification of the resolution of dispersion image, which has been achieved by MATLAB image processing. In a similar manner, the suitable magnitudes of the other

influencing parameters can also be determined. For the sake of brevity, the details of each of them are not presented here.

Table 7.1: Resolution of dispersion bands extracted through image processing

Offset (m)	Resolution - Number of white pixel count (dpi)	Band thickness *dv* (m/s)
0	2485	50
2	1462	100
4	1195	80
6	3220	20
8	1766	40
10	1706	20
12	1875	20
14	2492	10

Figure 7.4 shows the dispersion bands which contains the dispersion curve. However, depending upon the thickness of the band, it will be difficult to decipher the exact dispersion curve, (represented by the localized peak energy points) which is to be further used for the inversion analysis. Hence, with a bit of trade-off to accuracy, under such circumstances, the dispersion curve is considered to be represented by the average of the upper and lower limits of the dispersion band. Fig 7.5 represents the corresponding dispersion curves obtained by the averaging of the limits of the extracted dispersion bands, already shown in Fig. 7.4.

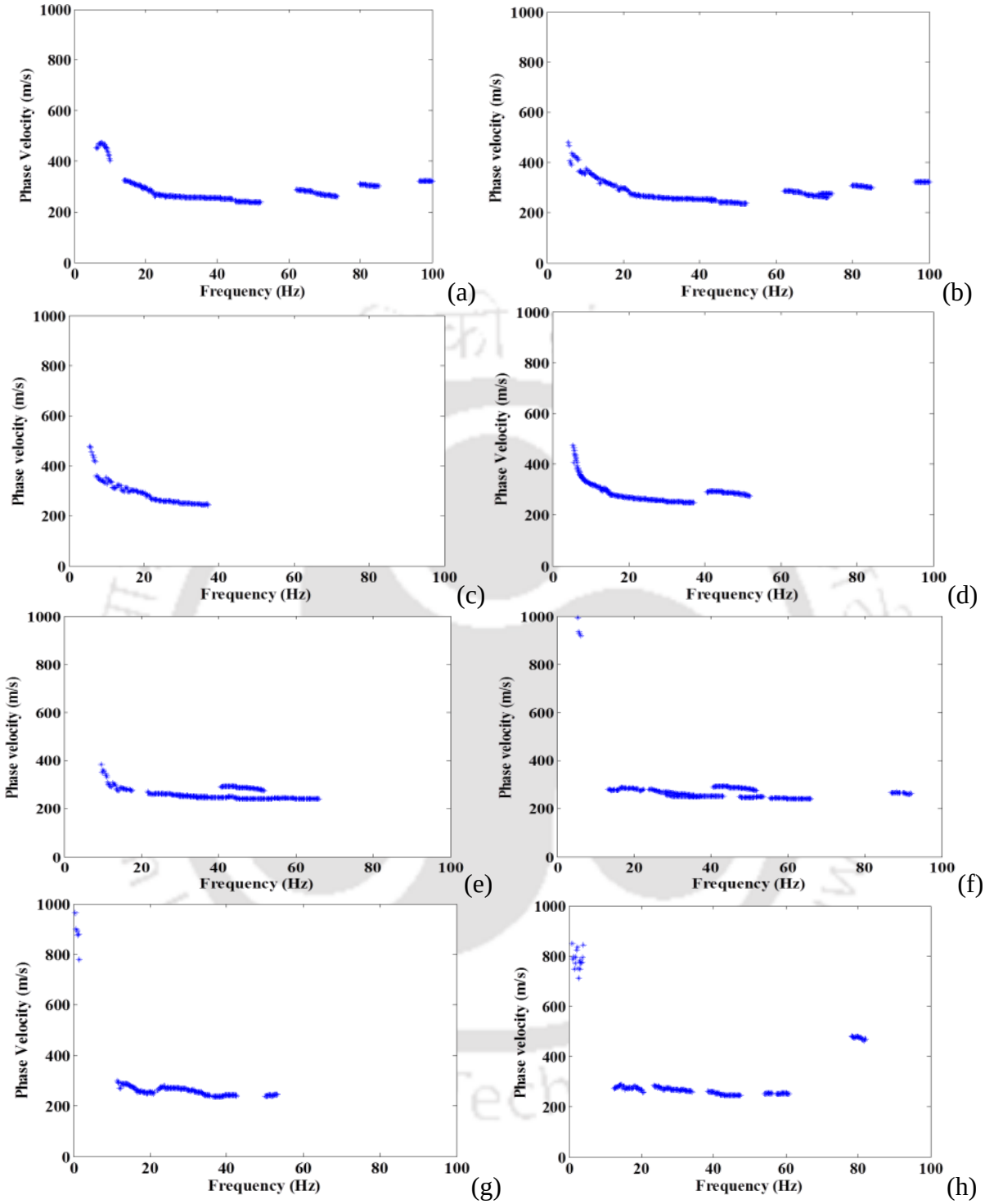

Fig. 7.5: Dispersion curve represented by the averaging of the lower and upper limit of the dispersion band obtained for varying offsets (a) 0 m (b) 2 m (c) 4 m (d) 6 m (e) 8 m (f) 10 m (g) 12 m (h) 14 m (Sampling frequency – 15000 Hz, Sample length – 5120, Inter-receiver spacing – 1 m, Number of channels - 24)

7.3 Automated Extraction of Dispersion Curve from Dispersion Image

Section 7.2 exemplifies the application of image processing in order to extract the dispersion band from a SURFSEIS dispersion image, and further defined the dispersion curve as the average of the upper and lower limits of the extracted dispersion curve. In such an exercise, a trade off is made on the accuracy since the exact location of the peak energy points (representing the dispersion curve) might not exactly coincide with the averaged limits. The technique of averaging the limits of the extracted dispersion band will be justifiable only if the energy dispersion trend, along the frequency or the phase velocity axis, follows a Gaussian or Normal distribution. Under such case, the average of limits of energy threshold will correspond to the location of the peak energy. However, if the energy distribution follows a Lognormal or any other skewed distribution, the coincidence of the location of the average of the limits and the peak energy will not be valid. Under such circumstance, the average values might actually conform to lower energy points, thus misrepresenting the dispersion curve. Figure 7.6 illustrates the deficiency in the averaging approach.

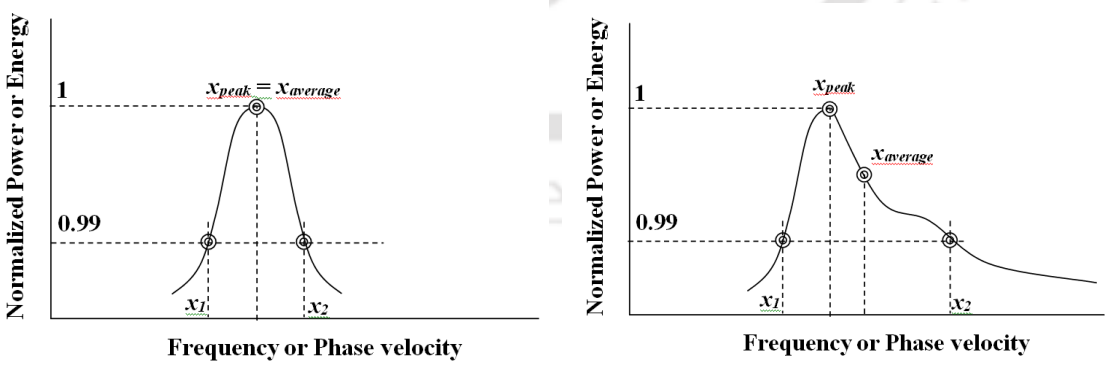

Fig. 7.6: Illustration showing the justification of the averaging technique only when the energy distribution follows a Gaussian or Normal distribution over frequency or phase velocity

7.3.1 MatLab based Automated Extraction Technique

It is now well understood that depending on several geometrical and physical parameters, the dispersion image can be a fuzzy and obscure one. Dispersion curve, as stated earlier, represents the distribution of localized highest energy over a wide range of phase and frequency. The energy accumulations are represented as peaks and ridges in such an image. Any dispersion image will be marked by one or more such ridges, illustrating the unimodal or multimodal nature of dispersion of the propagating surface waves. Extraction of dispersion curve involves the choosing of the peak energy points from such dispersion image space. The image processing and the determination of the dispersion curve, described in the Section 7.2, will be more reliable if the dispersion band is sufficiently narrow, i.e. the resolution of the dispersion image is significantly high. In practice, obtaining a very thin dispersion band will not always be possible, and under such cases, the averaging technique used in 2D image processing might be questionable. If the dispersion band is sufficiently thick, it would be judicious to exactly decipher the highest energy points from the dispersion image.

In this regard, to overcome the subjectivity of the 2D image processing representation technique to extract the dispersion curve, a MATLAB based coding for the automated extraction of the dispersion curve from a 3D dispersion image representation has been developed, and the outcome is illustrated in Fig. 7.7. The dispersion images, obtained from SURFSEIS, are always represented in a 2D format. Such a typical image is as shown in Fig. 7.7a. The step-by-step algorithm required to exactly extract the dispersion curve (fundamental or higher modes) from a 2D dispersion image from SURFSEIS is described as follows:

- The 2D dispersion image generated from Surfseis is read into MatLab code using the command ***imread***. The command converts the dispersion image into Red-Green-Blue (RGB) color model. The obtained RGB image is resized into a convenient size using the command ***imresize***, and then further converted into the Hue-Saturation-Value (HSV) color model using the command ***rgb2hsv***.
- The obtained HSV image is then subjected to multi-colour masking considering different colour bins comprising varying thresholds for each of the HSV components based on the histogram settings. This adaptation results in a 3-D image matrix where the different colour entities are provided with a mathematical value as per the segregation adopted.
- The obtained image is subjected to 2D median filtering using the command ***medfilter2***. Neighborhood averaging can suppress isolated out-of-range noise, but the side effect is that it also blurs sudden changes such as line features, sharp edges, and other image details all corresponding to high spatial frequencies. The median filter is an effective method that can, to some extent, distinguish out-of-range isolated noise from legitimate image features such as edges and lines. Specifically, the median filter replaces a pixel by the median, instead of the average, of all pixels in a neighbourhood. The outcome of median filtering is plotted as a filled up contour map using the command ***contourf***.
- The 3D structure of the dispersion image is further constructed using the ***struct*** command. In this section, varieties of colours are selected in terms of the HSV component for segregation in the 3D image. In the present study, red, black, ultramarine, bronze and greyed lavender colours have been used in order to portray the 3D image. The ***struct*** command actually creates a 3D matrix where the energies at various combinations

of frequency and phase velocity can be differentiated on the basis of the colour intensities. The 3D image is plotted with the aid of ***surf*** command.

- At the final step, the 3D matrix is subjected to ***findpeaks*** command to identify all the localized maximum energy peaks in the dispersion image neighbourhood. Further, a filter is applied on the results obtained so as to identify only the peaks corresponding to the energy value greater than 99.9% of the global maximum energy (i.e. the maximum energy in the whole domain of the dispersion energy). The target is to extract this highest energy trend which will be used as input to inversion analysis. The outcome is plotted as a scatter plot to get the dispersion curves. Further filtering on the frequencies are conducted if is required to segregate the higher order modes from the fundamental mode.

The application of the above stated algorithm is exemplified through an illustration in Fig. 7.7. Figure 7.7a portrays a typical 2D dispersion image obtained from the dispersion analysis by SURFSEIS. Accordingly, as per the indigenously developed MatLab coding, the 3D dispersion image structure is constructed, as shown in Fig. 7.7b. Using the local peak finding search technique, all the local peaks are identified as shown in Fig. 7.7c. Further, an energy threshold filtering is used to select the energy peaks conforming to 99.9%, or more, of the global maximum energy. The output of such an activity is represented in Fig. 7.7d, which shows the existence of fundamental mode and a single higher order mode. This process provides the exact demarcation of the fundamental and significant higher order modes which can be used in the inversion analysis.

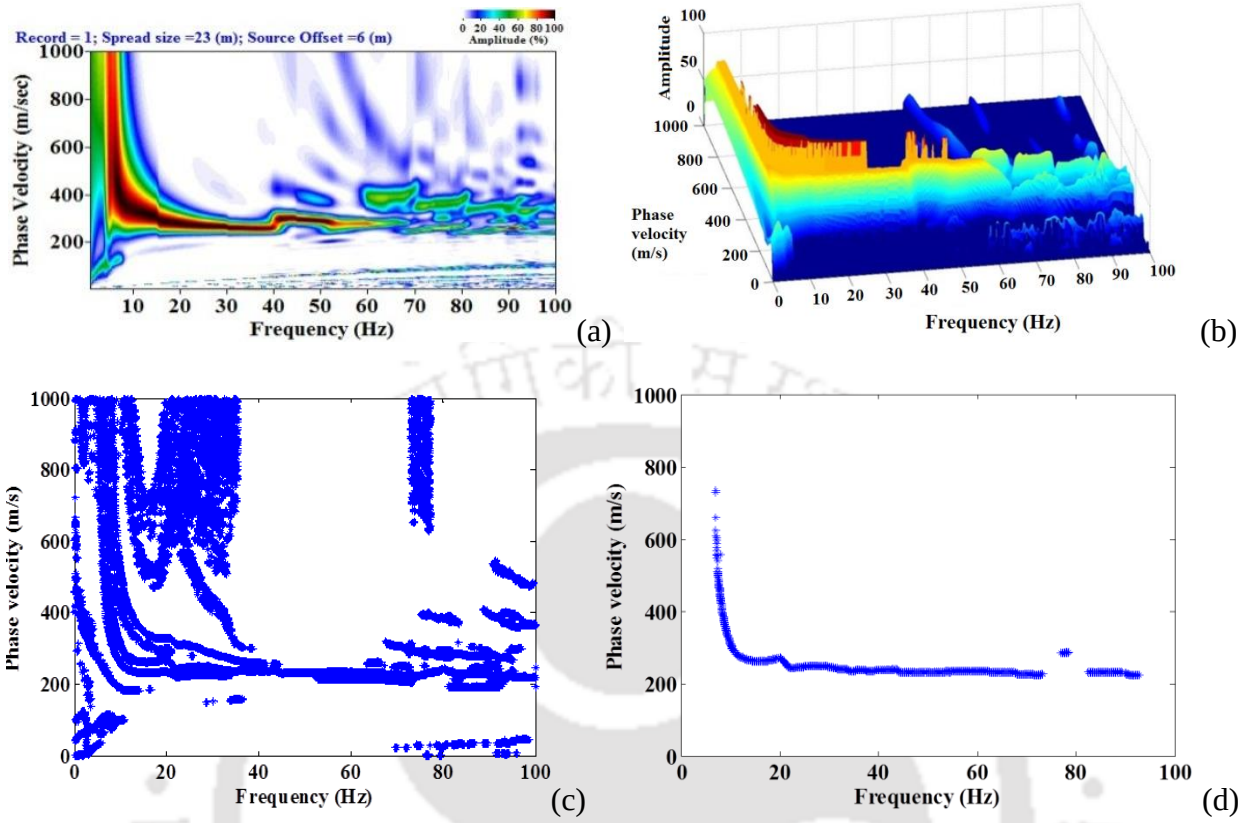

Fig. 7.7: (a) A typical 2D dispersion image obtained from SURFSEIS (b) 3D dispersion image representation obtained from MATLAB based coding related to color intensity / energy concentrations (c) Extraction of all possible local peaks from the 3D dispersion image (d) Identification of the fundamental and higher mode dispersion curves (local highest energy peaks)

It has already been mentioned that SURFSEIS facilitates only manual selection of the dispersion points in order to extract the dispersion curve from the dispersion image. As had been pointed out earlier, such manual selection may lead to the improper selection of the dispersion points misrepresenting the desired fundamental dispersion curve. Once the dispersion points are selected, the information about the same are stored in a text (*.txt) file in the form of combination of the frequency and phase velocity of each selected point. Such a screenshot of a

*.txt file is portrayed in Fig. 7.8a, which highlights the data comprising of 28 data points and corresponding to the dispersion points manually extracted directly from SURFSEIS to represent the fundamental dispersion curve. It can be observed that the 2nd and 3rd column provides the magnitudes of frequencies and phase velocities. The third column provides the corresponding signal-to-noise ratio (SNR). The SNR is an indicator about the goodness of the extracted dispersion curve. A high SNR for any data point indicates high signal content with lesser participation of the noise. The maximum value of SNR is 1, which indicates a pure signal without any noise adulteration. If the obtained SNR for various data points is substantially less than 1, it is imperative that the selected dispersion point does not conform to the locally highest energy peaks and is attributed with significant noise adulteration. It can be observed from Fig. 7.8a that several of the manually selected dispersion points possess SNR substantially less than 1, indicating all such points are improperly selected and do not conform to the locally highest or near-highest energy peaks, and hence, misrepresent the fundamental dispersion curve. Utilization of such misrepresented dispersion curve will lead to deviated outcomes from the inversion analysis. Another important aspect of the utilization of manually selected dispersion curve involved the repeatability issues. Since the manual extraction is subjected to user intervention and user discretion, the selected values in all the three columns of the *.txt file are subjected to change each time based on the extraction of points chosen by the user. Thus, the possibility of obtaining the dispersion trend will vary at each attempt, which will subsequently affect the obtained shear wave velocity profile from inversion, wherein each attempt of inversion will produce a different V_s profile.

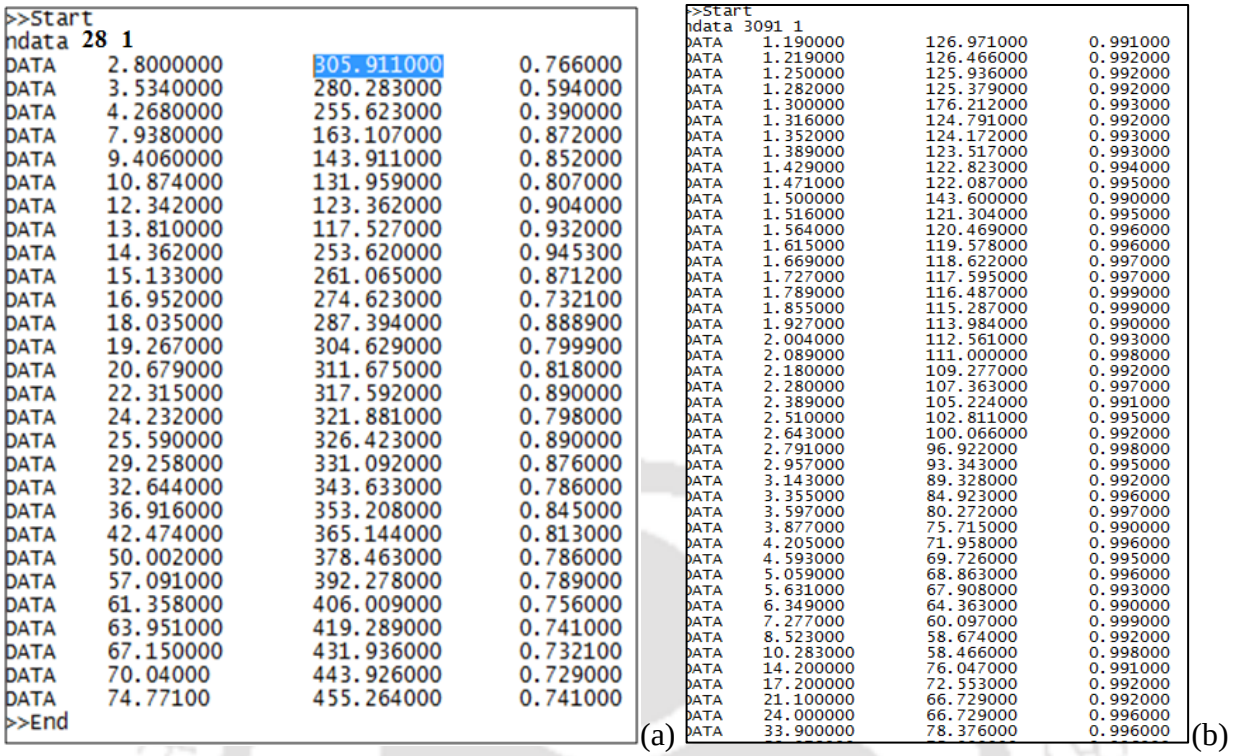

Fig. 7.8: Dispersion curve points obtained with (a) Manual extraction (b) Automated extraction

In this regard, the automated extraction of the dispersion curve, as discussed in this chapter aids to overcome these problems with the manual extraction. The dispersion points conforming to the fundamental dispersion curve as extracted through automation (using MatLab coding) are imported to the *.txt file as produced by SURFSEIS through post-dispersion analysis. Since the automated extraction precisely identifies and utilizes the dispersion points of localized highest energy, the SNR of all the automated points remains substantially high and approaches the magnitude of 1. Thus, each of the points conforms very closely to the fundamental dispersion curve. Figure 7.8b highlights the screenshot of such an imported *.txt file. It can be observed that the number of points used for inversion, in this case, is substantially higher (3091 for this case) as the automated process precisely selects all the points with locally highest energy, and flanking a very wide frequency band, which was not possible to obtain from manual extraction.

Moreover, the SNR values of all the extracted points can be found to have SNR greater than 0.99, which indicates an extremely good quality of the extracted dispersion curve. Moreover, since the dispersion curve is extracted through automation, it is repeatable at every possible instant, thus nullifying the concerns with the repeatability of the obtained shear wave velocity profiles from inversion analysis. This technique is, thus, successful in removing any subjectivity arising from user discretion. Hence, such automated technique thus renders the estimation of the shear wave velocity profiles to be more reliable than that obtained from manual process and user discretion.

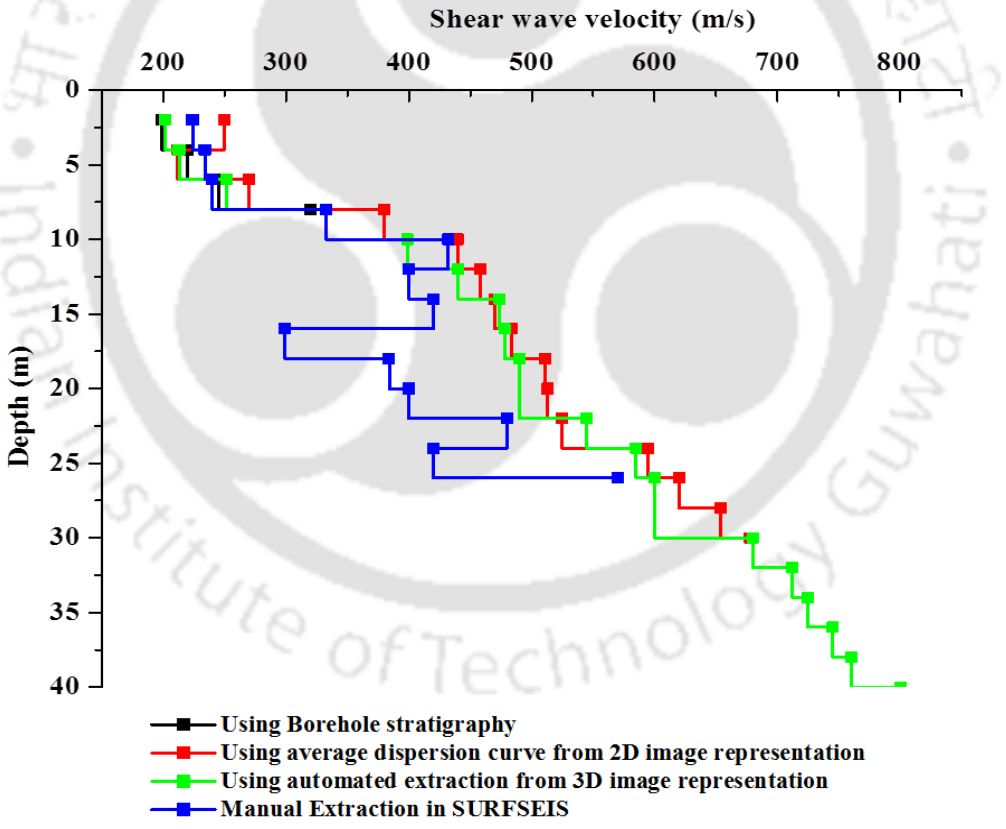

Fig. 7.9: Comparison of V_s obtained from borehole stratigraphy, average dispersion trend from 2D representation, automated extraction from 3D image representation and Manual extraction from SURFSEIS dispersion image

Figure 7.9 shows a typical comparison of the V_s profiles obtained for Site-1 using fundamental model dispersion curves developed through various techniques: (a) manual extraction from SURFSEIS, (b) averaging of limits of dispersion curve from 2D representation of dispersion image, and (c) automated extraction from 3D representation of dispersion image. The V_s profile developed using field SPT-N values, obtained from borehole stratigraphy at Site-1, is also plotted for the sake of comparison. Since the soil stratum was stiff, the borehole could be advanced only up to 7 m depth, and hence, the stratigraphy information beyond 7 m was not available. It can be observed that the shear wave velocity profile (up to a depth of 22 m) obtained using manually extracted dispersion curve produces the largest deviation from that obtained from field SPT-N values as well from those obtained using automated extractions. Moreover, use of the manually extraction dispersion curve revealed anomalous shear wave velocities at any intermediate stratum (12-15 m in this case). This is due to the imprecise choice of the fundamental mode dispersion points through manual selection as indicated in Fig. 7.8a. The profiles obtained using dispersion curves using both 2D and 3D image representations exhibit significant agreement with the profile obtained from borehole stratigraphy. The depth of investigation from the automated extractions is found to be substantially larger than that obtained from manual extraction, owing to the precision in the extraction of fundamental mode information from a wider frequency band, and due identification and incorporation of the lower frequency band in the extraction process. The V_s profile obtained using automated extraction from 3D image representation exhibited larger depth information than that obtained usnign the averaging technique from 2D image representation. This is attributed to the enhanced precision of identifying the fundamental dispersion curve using the 3D automation. Though borehole reading terminated at 7 m depth due to practical difficulties, the imaging techniques have aided

in deciphering the large depth shear wave velocity profiling due to selection of low frequency dispersion points, which was not possible through manual extraction. Thus, it can be conclusively stated that the imaging and automated techniques developed in this regard are highly efficient to identify large-depth subsurface V_s profiles.

7.4 Summary

This chapter highlights about the quantification of resolution of the dispersion image obtained as a result of dispersion analysis using SURFSEIS. An indigenously developed MatLab code, encompassing image processing techniques, has been used to characterise the resolution of the dispersion image in terms of the thickness of the dispersion band, its frequency extent and continuity over a frequency band. It has been illustrated that the quantification of the resolution of the dispersion image can be instrumental in justifiably identifying the best suitable, or optimal, data pre-processing and data-acquisition parameters. This chapter also highlights the automated dispersion curve extraction techniques from 2D and 3D representations of the dispersion image. Simultaneous utilization of the image processing technique and threshold energy filtering in an indigenously developed MatLab code helped in successful identification of the dispersion curve. From the 2D image representation, the dispersion curve has been defined as the average of the upper and lower phase velocity limits of the dispersion curve for its entire extent. The limitations of this technique have been explained in terms of the pattern of energy distribution over the frequency or phase velocity. For more precise extraction of the dispersion curves conforming to the best suitable identification of the localized maximum energy peaks, an automation process has been developed and explained based on the 3D representation of the dispersion image. In this regard, comparisons have been drawn based on the V_s profiles obtained through manual and

automated extraction of the dispersion curves. It is observed that the dispersion curves developed from automate extractions led to more precise shear wave velocity profiles extending over to larger depths; the depth of investigation being higher for dispersion extracted from 3D image representation. The automated extractions have been found successful in obtaining precise and reliable dispersion curves, and overcome the issues of repeatability occurring due to manual extraction using user discretion of choosing dispersion points.

CHAPTER 8

CASE STUDY: SUBSURFACE IDENTIFICATION USING ACTIVE MASW SURVEY ALONG 1.2 KM STRETCH OF JIA BHARALI RIVER BED

8.1 Introduction and Background of the Investigation Work

This chapter presents the case report of Active MASW survey conducted along Jia Bharali river bed (a tributary of River Brahmaputra) for the proposed construction work of a 1.2 km long bridge along the new 4-lane road from Dolabari to Jamuguri connecting NH-37A with NH-52 in Tezpur, Assam. The location of the site is encircled and exhibited in Fig. 8.1. The proposed bridge is supposed to consist of 25 spans, and resting on 24 numbers of piers and 2 abutments (Fig. 8.2). All the piers and abutments have been planned to support on well foundation. Borehole stratigraphy tests were conducted along the alignment of the bridge in few selected locations. While conducting the field SPT tests, at some pier locations, within a depth of 20-25 m, the boring had to be stopped due to the detection of an existent very hard stratum, probably consisting of gravel and boulder formations. At some pier locations, the boring continued to larger depths (~ 35 m) without any hindrances. Since, well foundation had been planned for the entire bridge, for its piers and abutments, it is imperative to properly identify the subsurface stratification which would govern the geotechnical design of the foundation in terms of the settlement, bearing capacity, tilt and shift, depending upon different load criteria. Hence, active MASW survey work was conducted for identifying the subsurface stratification and stiffness characteristics along the alignment of the bridge. Several tests were conducted in the locations of the bridge piers and the abutments, as well as in between of the piers. Both spot survey and roll-

along surveys were conducted to meet the project requirements. Variations of the data acquisition and preprocessing parameters have been checked to obtain complete phase propagation through the geophone array. Good resolution dispersion images are obtained, providing significant depth of analysis. The results obtained from MASW survey have shown considerable agreement with the shallow depth borehole profiles.

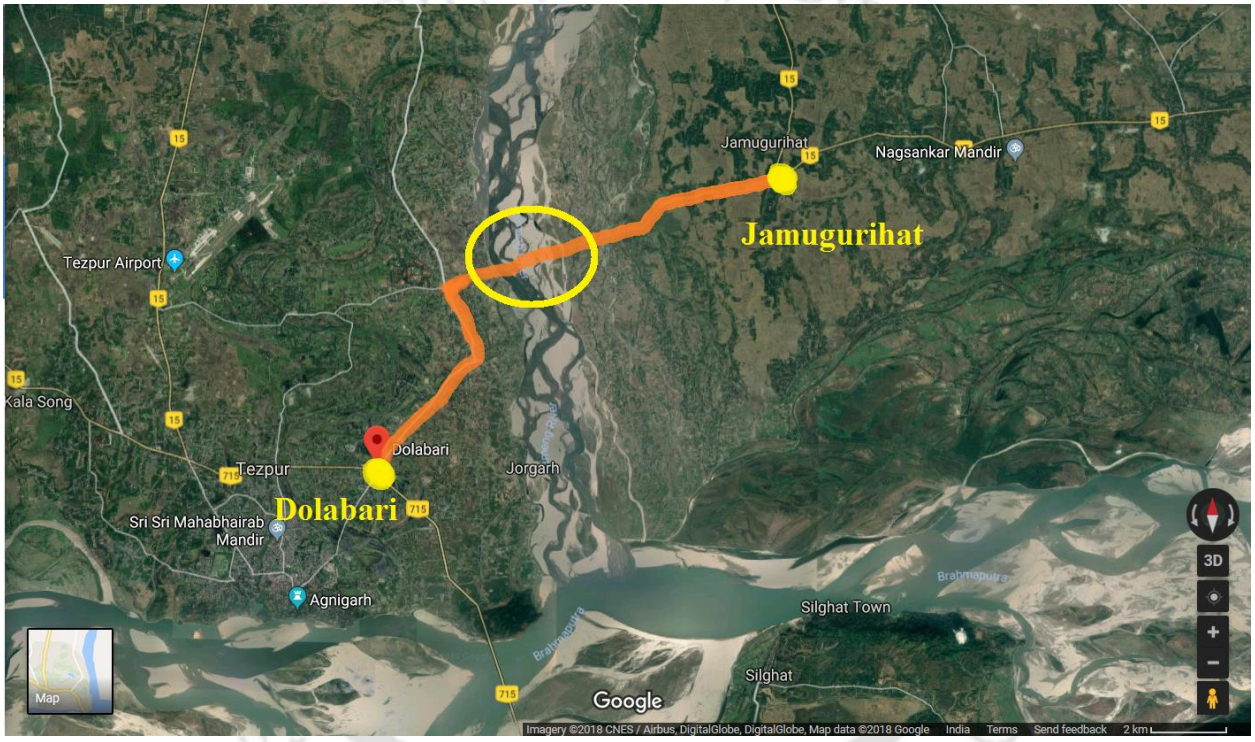

Fig. 8.1: Location of Jia Bharali River bed site for the proposed bridge

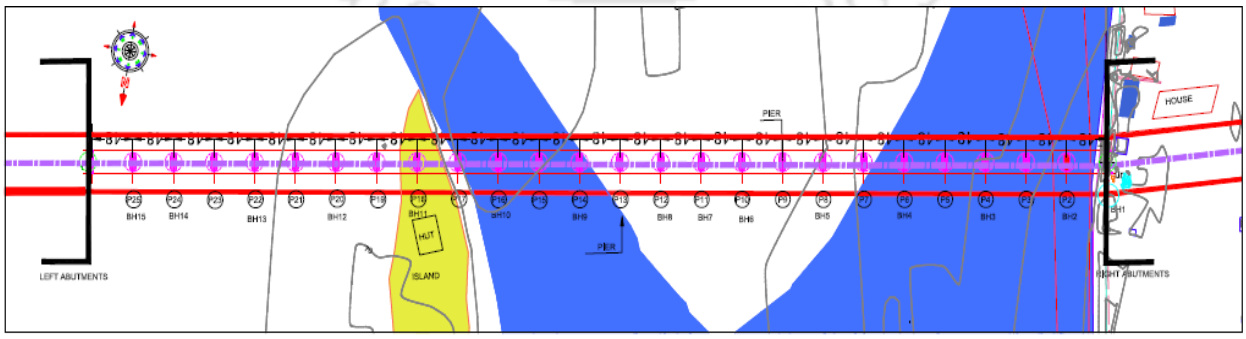

Fig. 8.2: Section profile of the proposed bridge showing the locations of abutment and piers

8.2 Active MASW Testing Methodology adopted at site

As per the preliminary designs, the bridge is supported by 24 numbers of piers and one abutment on either side of the river bank. Well-foundations were proposed for all the piers (P1-P24). The spacing between the piers was approximately 48 m. Geophysical tests were conducted at the locations of Abutment 1, P5-P24 and Abutment 2. As the piers P1-P4 were in submerged locations, the tests were not conducted at these locations. P16 was located on an inhabited river bed island with moderate vegetation.

The MASW test was carried out in Active mode using a 10 kg sledge hammer impact as seismic source and the corresponding surface wave signals were recorded by an array of 4.5 Hz Geophones. The test was conducted using 24-channel array with 1 m receiver spacing and 4 m offset distance (source to first geophone) from A1-P11. Further tests, (at P12-A2) have been carried out using 12 channel arrays with 2 m receiver spacing keeping offset as constant. The best suitable geometric configurations as used in the site were chosen based on the quick trials conducted in the field and based on the understanding detailed in Chapter 5. The time of sampling (no. of samples / sampling frequency) was adopted to be around 680 ms, ensuring that the complete phase of wave energy being captured. Thus the sampling frequency of about 7500 Hz with 5120 no. of samples was chosen as best suitable for this site. The raw record was obtained for 4-shots (hammer impact) in order to stack the records for ensuring good quality of dispersion image which can provide the deep strata V_s profile. The 1D shear wave velocity was obtained (after rigorous data processing and analysis) at the center of the 24/12 channel array where the pier/abutment is supposed to be built. Figure 8.3 shows typical layouts of the geophones and MASW setup in the field nearby pier locations P6 and P16.

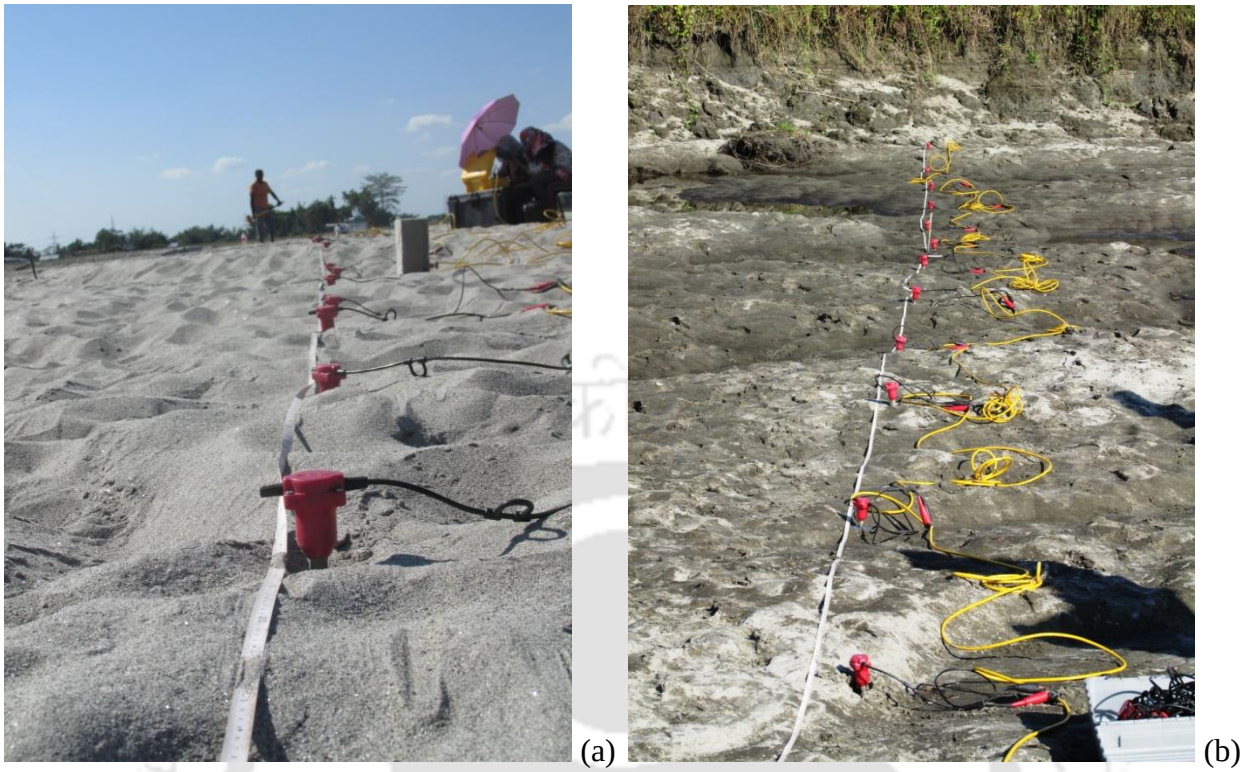

(a) (b)

Fig. 8.3: Typical layouts of geophones at locations of (a) Pier P6 (b) Pier P16

8.3 Data Processing and Analysis

The processing of raw data to obtain V_s profile was performed in 4-stages such as: Filtering, Muting, Dispersion Curve or DC extraction (using automated code) and Inversion. Filtering of raw data was carried out using band-pass filter which allowed the targeted frequency range, containing significant energy, to pass through. As the raw data obtained was of good quality (with minimum noise), muting was performed to a minimal extent. The dispersion image had been obtained containing peak energies at lower frequencies. The trend of peak energies variation with the phase velocity and the frequency was identified and the dispersion curve was extracted. The extraction of DC points had been made using advanced processing code developed in Matlab, as described in Chapter 7. The DC, thus extracted, is termed as

measured/experimental DC. The last stage of data analysis i.e. inversion, had been performed through iterative forward modeling with back-feeding of the error in the misfit function. In this process, initially the soil model had been assumed with 10 layers of varying thickness, and the theoretical DC was extracted for the initial model. After performing successive number of iterations, the V_s profile based on the least mismatch (least RMSE) between the measured and theoretical DC was selected to be the final profile. The data was of good quality at this site, except for few pier locations which were unavoidable. Among such circumstances, one was Pier-5 which was located almost at the edge of river bank i.e. nearer to the river channel. The data collected at this particular location contained some sort of noise effect attributed to river-water currents and eroding banks. In this case, the data was processed for excessive muting and filtering to suppress the high frequency noises due to water currents. At another location at Pier-15, the soil was in almost soft state due to seeping water. Hence the data processing and analysis has been carried out extensively to obtain soil stiffness up to best possible deeper strata. The data collected at Pier-16, which was located on the top of high landmass as a different elevation to that of the river bed, was affected by the surrounding inhabitation and moderate vegetation cover. Nevertheless, 12-channel geophone array had been maintained in a linear fashion with some obstructions (trees) in between the receivers. Thus, the data obtained at this location is of not so good quality, attributed to unwanted wave reflections from undulations and obstructions on the ground. Finally the dispersion image of good quality with significant peak energy with proper trend has been identified after 4 stacks of raw data.

8.3.1 Sampling Frequency and Numbers of Samples

For the present study, since the previous borehole exploration at the site indicated the presence of hard strata, initially a sampling length of 5120 samples with a sampling frequency of 15000 Hz and 7500 Hz were collected and analyzed. The choice of sampling frequency and the number of samples is based on the time of sampling, which is in turn, is governed by the site characteristics. Stiffer stratum lets the wave propagate faster in comparison to that of a softer stratum, and hence requires a lesser time of acquisition. Fig. 8.4 illustrates the MASW typical raw records collected for different sampling frequency of 15000 Hz and 7500 Hz corresponding to a fixed sample length of 5120 samples.

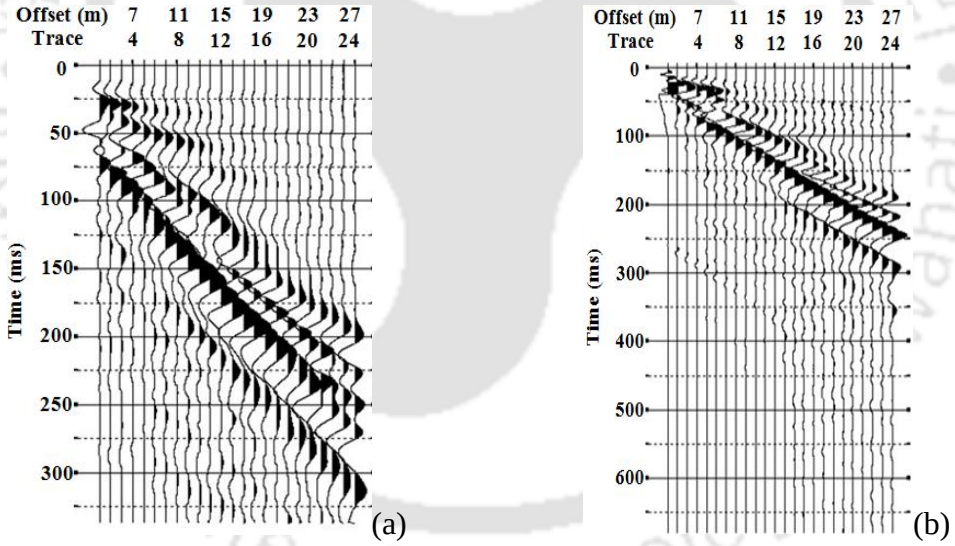

Fig. 8.4: Typical wavefield records collected at the site for 5120 samples with sampling frequency (a) 15000 Hz (b) 7500 Hz (Offset distance – 4 m, Inter-receiver spacing – 1 m, Numbers of channels – 24)

The corresponding dispersion images are shown in Fig. 8.5. From the figures, it is clear that although the image trend in both the figures are similar, the energy content obtained with the 15000 Hz sampling frequency is more than that obtained with 7500 Hz sampling frequency. This is attributed to the recording of noises due to higher time of sampling. Hence, a sampling frequency of 15000 Hz with 5120 samples is chosen for the rest of the investigation at the present site.

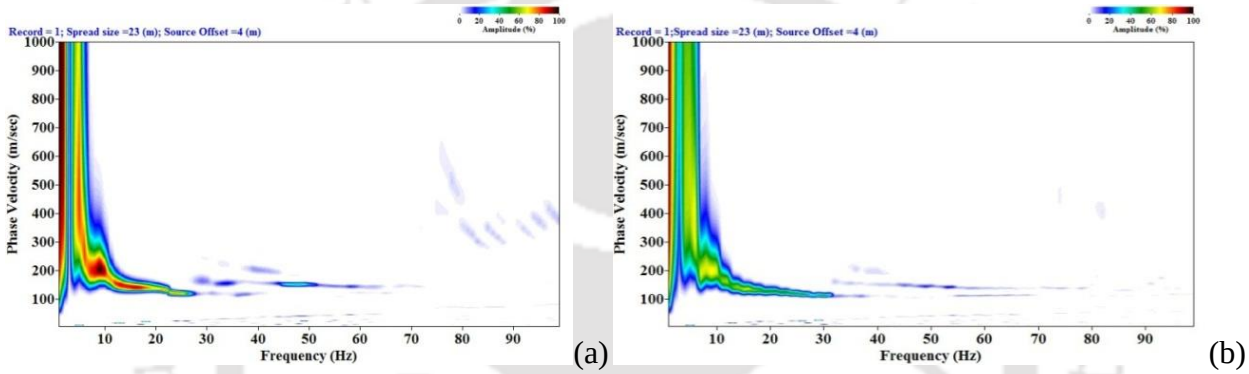

Fig. 8.5: Dispersion images obtained at the site for 5120 samples with sampling frequency (a) 15000 Hz (b) 7500 Hz (Offset distance – 4 m, Inter-receiver spacing – 1 m, Numbers of channels – 24)

8.3.2 Filtering without Muting

Filtering was carried out based on the response of the amplitude spectrum to the applied filter (as explained in detail in Chapter 4). The effective frequency content of energy ranges between 5-90 Hz for present site. As explained in Chapter 4, Band-pass filter proved to be more efficient than the other options for filter available in SURFSEIS. Therefore, Band-pass filter was directly applied on the raw record. Based on the observed effective frequency content of the signal, suitable frequency ranges were adopted. Figure 8.6 shows a typical Band-pass filtered record and

the corresponding dispersion image. It can be noticed that there is a change in the dispersion image, the heavy accumulation of low frequency energy is removed as compared to the unfiltered dispersion image (Fig 8.4a).

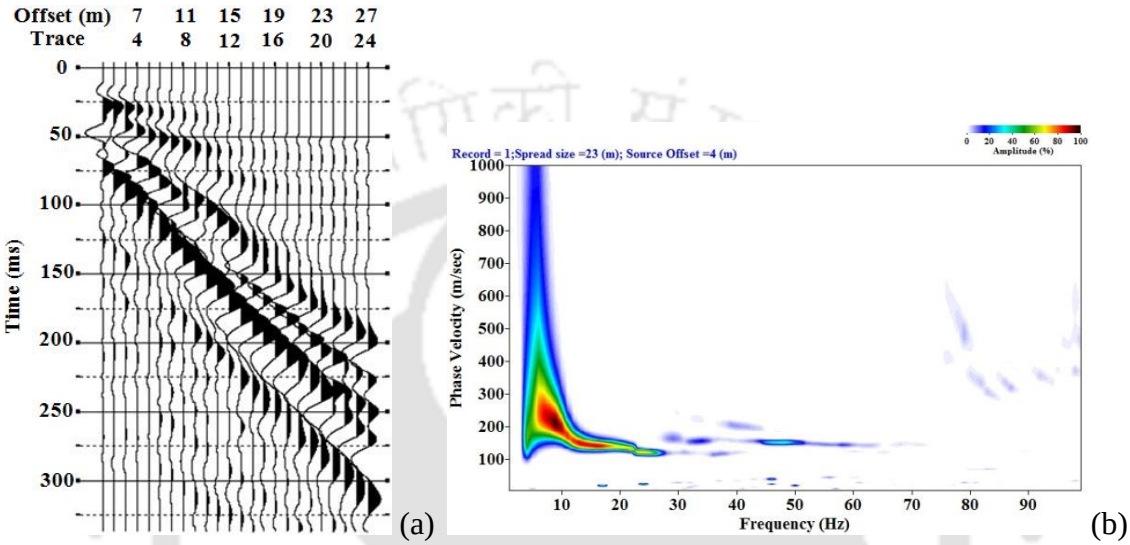

Fig. 8.6: (a) Typical Band-pass Filtered record (b) Corresponding dispersion image (Sampling frequency – 15000 Hz, Numbers of samples – 5120, Offset distance – 4 m, Inter-receiver spacing – 1 m, Numbers of channels – 24)

8.3.3 Muting without Filtering

Based on the collected raw wavefield (Fig. 8.4a), the effect of various extents of muting conducted on the unfiltered record is exhibited in Fig. 8.7. Muting helps to suppress the wavefield characteristics recorded beyond specific phase velocities. Introduction of excessive muting may result in significant loss in the characteristics, and hence, muting operation should be controlled so that a suitable energy content of the signal is maintained while removing the adulterating noises. Figure 8.7a shows the outcome of excessive muting which have resulted in a

modified wavefield with a single wavelength of the original record; similarly, Fig. 8.7c shows the result when minimal muting is carried out to remove the noise adulterations.

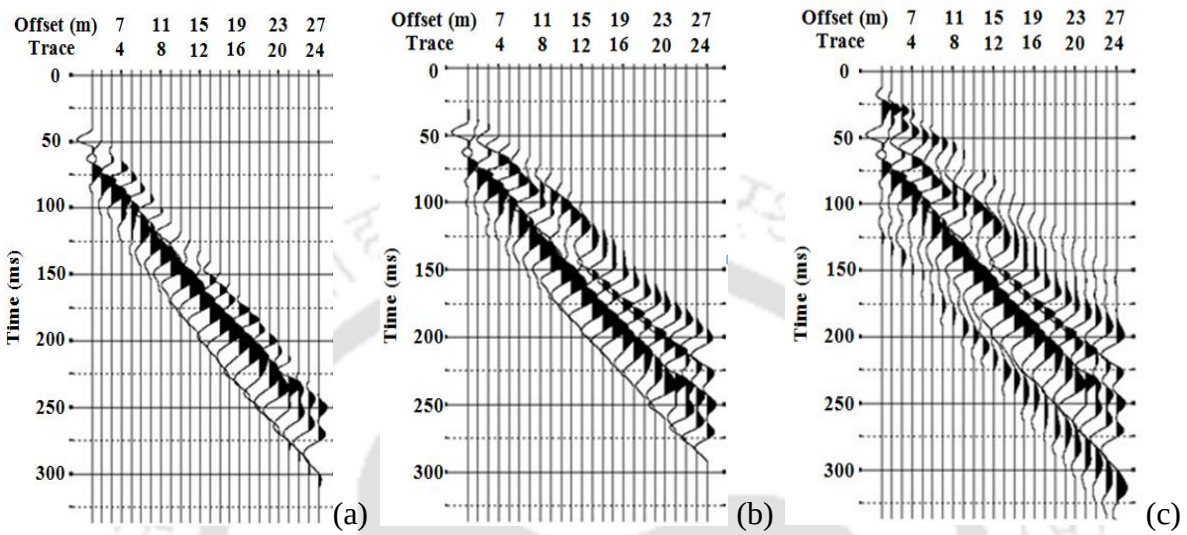

Fig. 8.7: Influence of extent of muting on raw data (a) Excessive muting (b) Moderate muting (c) Minimal muting (Sampling frequency – 15000 Hz, Numbers of samples – 5120, Offset distance – 4 m, Inter-receiver spacing – 1 m, Numbers of channels – 24)

The dispersion images of the corresponding muted records (Fig. 9.6) are presented in Fig. 9.7. It can be observed that when the excessive muting is undertook (Fig. 9.6a), significant energy is lost, and hence, the corresponding dispersion image (Fig. 9.7a) fails to provide any information. As the extent of muting decreases (Figs 9.6b-c), the corresponding dispersion images (Figs 9.7b-c) exhibit an energy concentration at the lower frequency region. However, at the same time, the dispersion images clearly indicate the aliasing effect in the very low frequencies arising due to the consideration of unfiltered wavefield. These observations suggest that muting alone cannot lead to the generation of a dispersion image with sufficient information and good resolution. Hence, muting on the filtered wavefield is recommended.

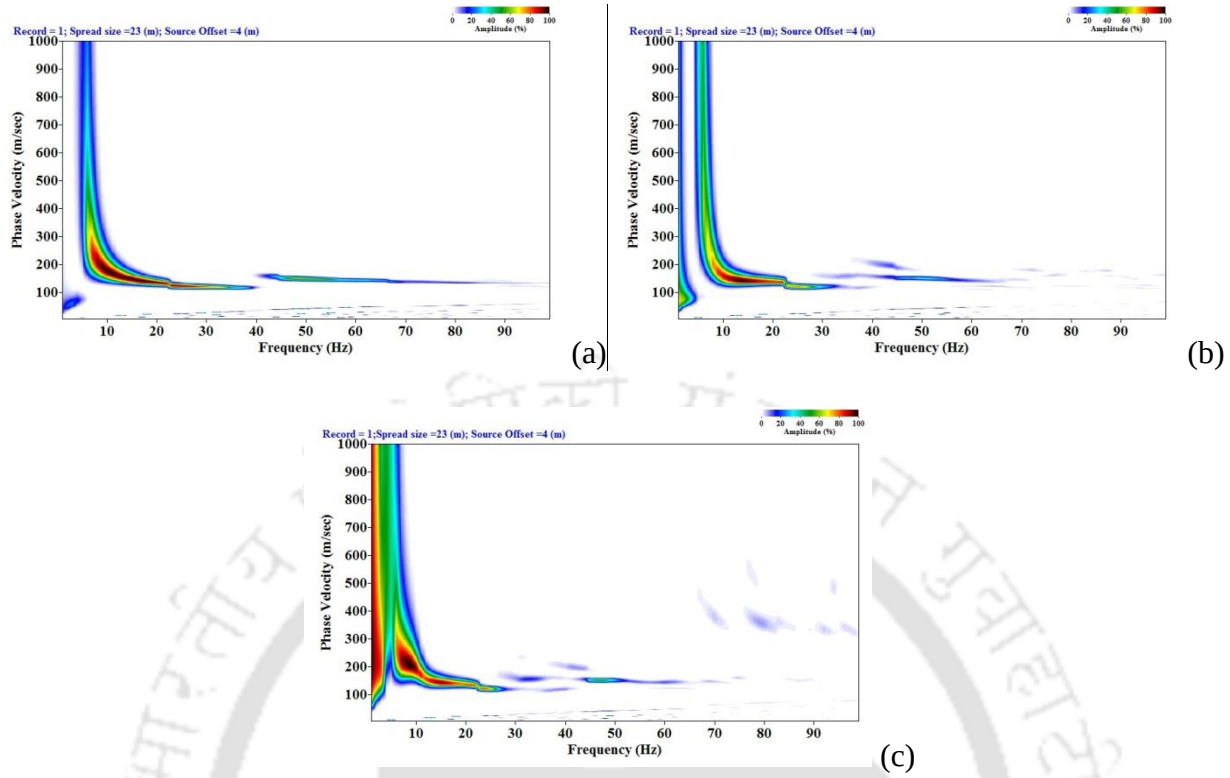

Fig. 8.8: Influence of extent of muting on dispersion image (a) Excessive muting (b) Moderate muting (c) Minimal muting (Sampling frequency – 15000 Hz, Numbers of samples – 5120, Offset distance – 4 m, Inter-receiver spacing – 1 m, Numbers of channels – 24)

8.3.4 Combined Muting and Filtering

From the above sections, it is clear that Band-pass filter is required for obtaining a good resolution dispersion image. However, attempt has been made to further refine the resolution of the dispersion images by muting the uneven phases in the filtered MASW record. The earlier section has revealed that a suitable muting is necessary to prevent excessive loss of information. Figure 8.9a shows a typical raw wavefield record obtained from the site, where the phases lack clarity due to noise contamination. Figure 8.9b-d depicts the modified wavefield records after processing through only muting (Fig. 8.9b), only filtering (Fig. 8.9c), and combined filtering and

muting (Fig. 8.9d). It can be observed that application of both filtering and muting techniques produces the best quality wavefield records.

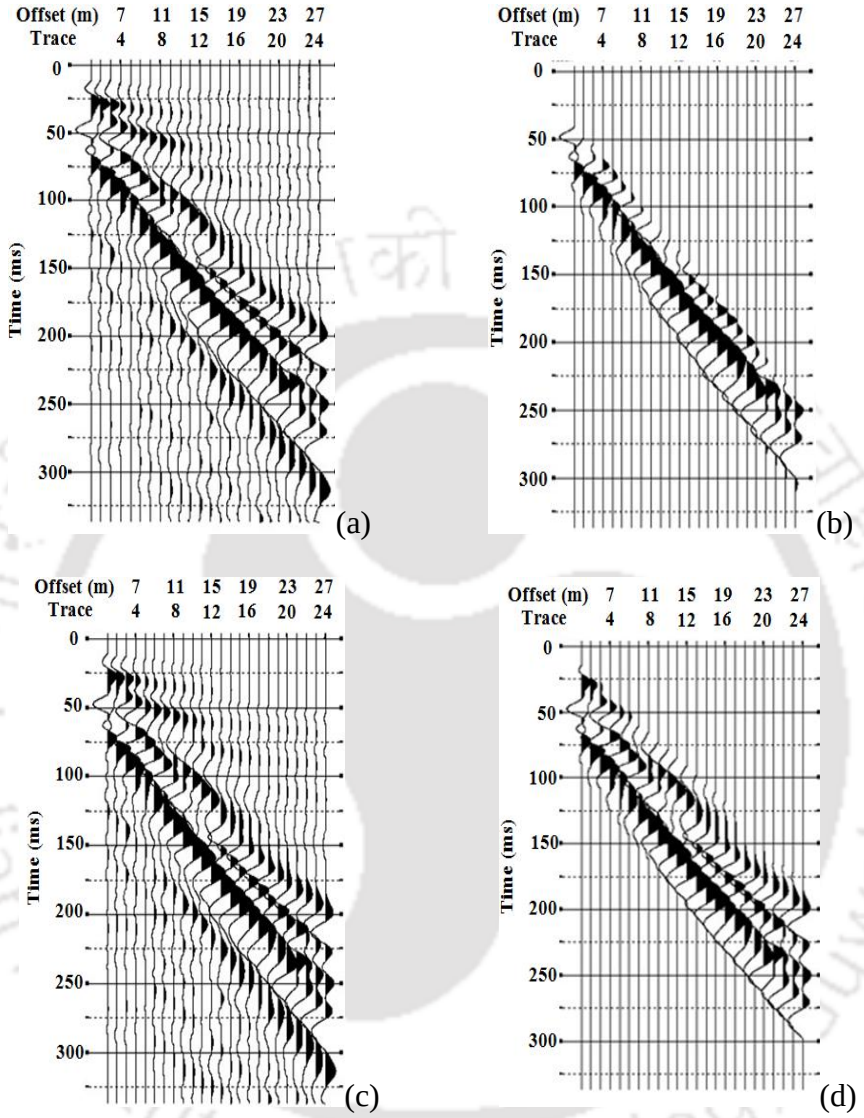

Fig. 8.9: Typical wavefield records (a) Raw (b) Only muted (c) Only filtered (d) Combined filtered and muted (Sampling frequency – 15000 Hz, Numbers of samples – 5120, Offset distance – 4 m, Inter-receiver spacing – 1 m, Numbers of channels – 24)

Figure 8.10 exhibits the dispersion images corresponding to the filtered wavefields obtained from varying extent of muting operation. Compared to the dispersion images obtained from

unfiltered wavefields (Fig. 8.10a); it can be clearly observed that the same obtained from the filtered and muted wavefields exhibit superior resolution, since most of the noise has been eliminated in the process. As observed earlier, excessive muting results in significant information loss and renders a very poor resolution dispersion image (Fig. 8.10b). Based on the obtained dispersion images, the suitable extent of the muting of the filtered wavefield can be suitably decided.

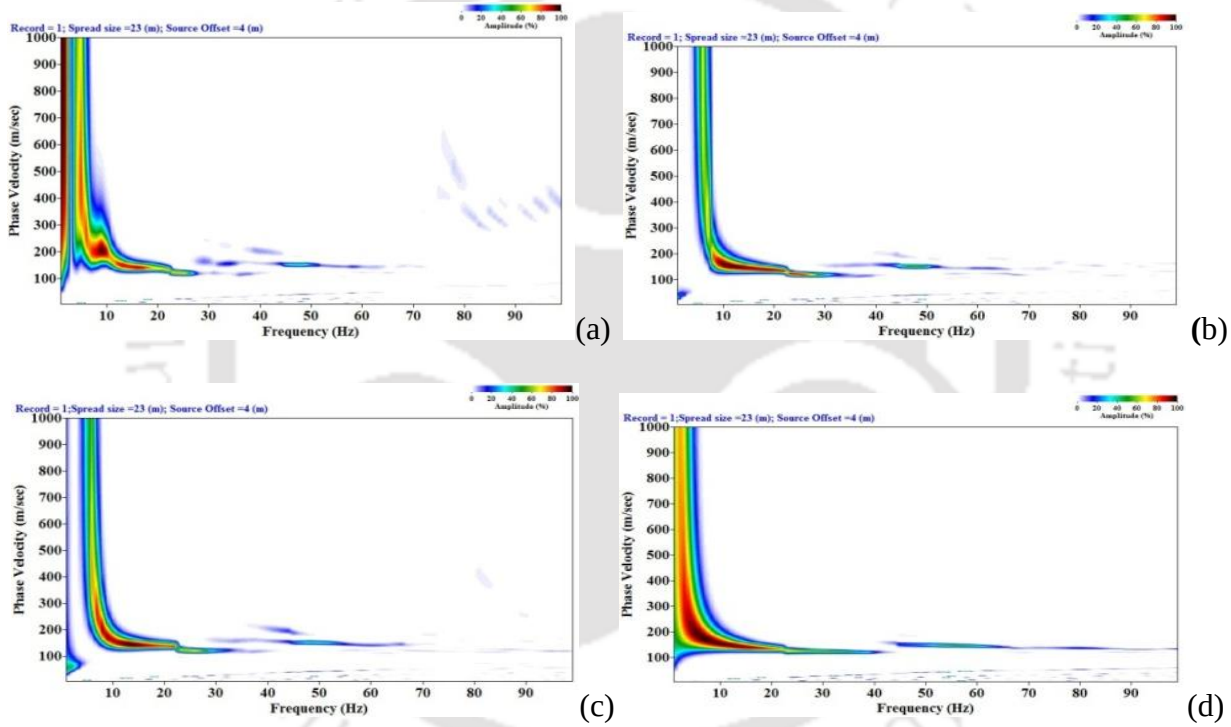

Fig. 8.10: Effect of extent of muting on dispersion image obtained from filtered wavefield (a) Only Filtered (b) Filtered with excessive muting (c) Filtered with moderate muting (d) Filtered with minimal muting (Sampling frequency – 15000 Hz, Numbers of samples – 5120, Offset distance – 4 m, Inter-receiver spacing – 1 m, Numbers of channels – 24)

8.3.5 Offset distance

Based on the experience gained as described in Chapter 5, at the Jia Bharali site, the influence of offset distance was checked with 0 m and 4 m offset distances. Typical raw records for 0 m and 4 m offset distance are shown in Fig. 8.11, and the corresponding dispersion images are provided in Fig. 8.12. It can be clearly seen from the dispersion images obtained for 0 m exhibits a curtailed fundamental dispersion band with energy content accumulated at low frequency region, exhibiting near offset effect. The fundamental dispersion band obtained with 4 m offset was found to be more distinct and flanking over a much wider frequency band. Hence, 4 m offset was chosen for the further investigations.

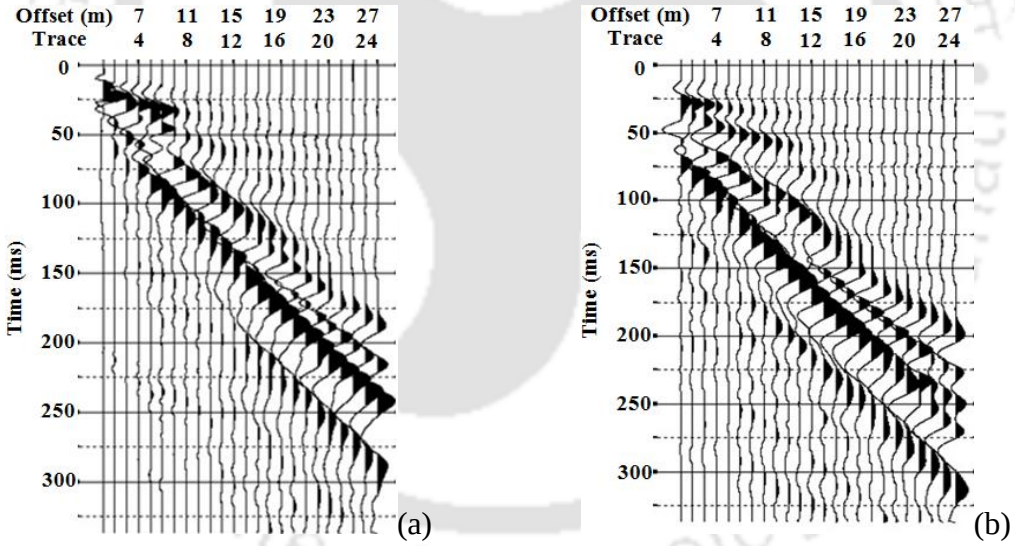

Fig. 8.11: Typical wavefield records with varying offsets (a) 0 m (b) 4 m (Sampling frequency – 15000 Hz, Numbers of samples – 5120, Inter-receiver spacing – 1 m, Numbers of channels – 24)

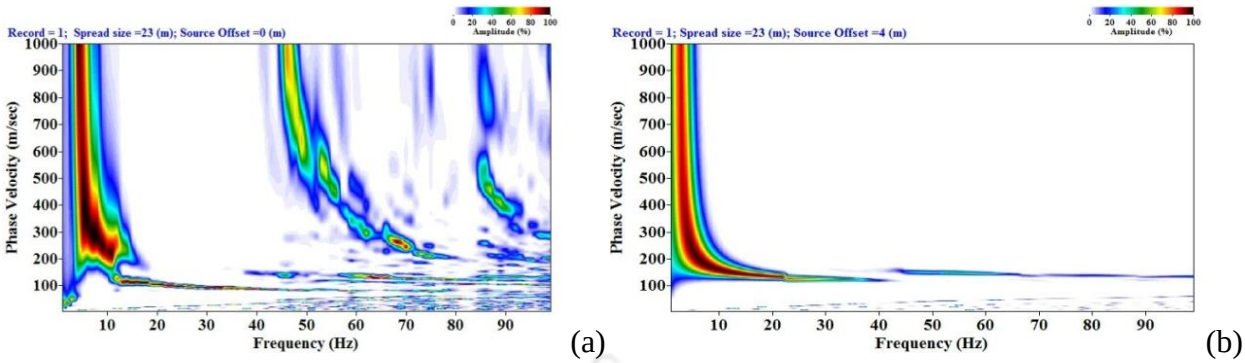

Fig. 8.12: Dispersion images for varying offsets (a) 0 m (b) 4 m (Sampling frequency – 15000 Hz, Numbers of samples – 5120, Inter-receiver spacing – 1 m, Numbers of channels – 24)

8.3.6 Dispersion Image Stacking

Stacking is a process of combining the dispersion images of various shots so that the resulting dispersion image has higher energy at different frequencies. In this process, even the energy at the lower frequencies can be substantially increased, so as to obtain shear wave velocity profiles exhibiting higher depths of investigations. Figure 8.13 exhibits the stacked dispersion images obtained from various numbers of shots of 10 kg sledgehammer. It can be observed that the dispersion image becomes more distinct with the increasing number of stacks, or shot gathers. For the present site, 3 stacks of dispersion image have been considered for the rest of the investigation.

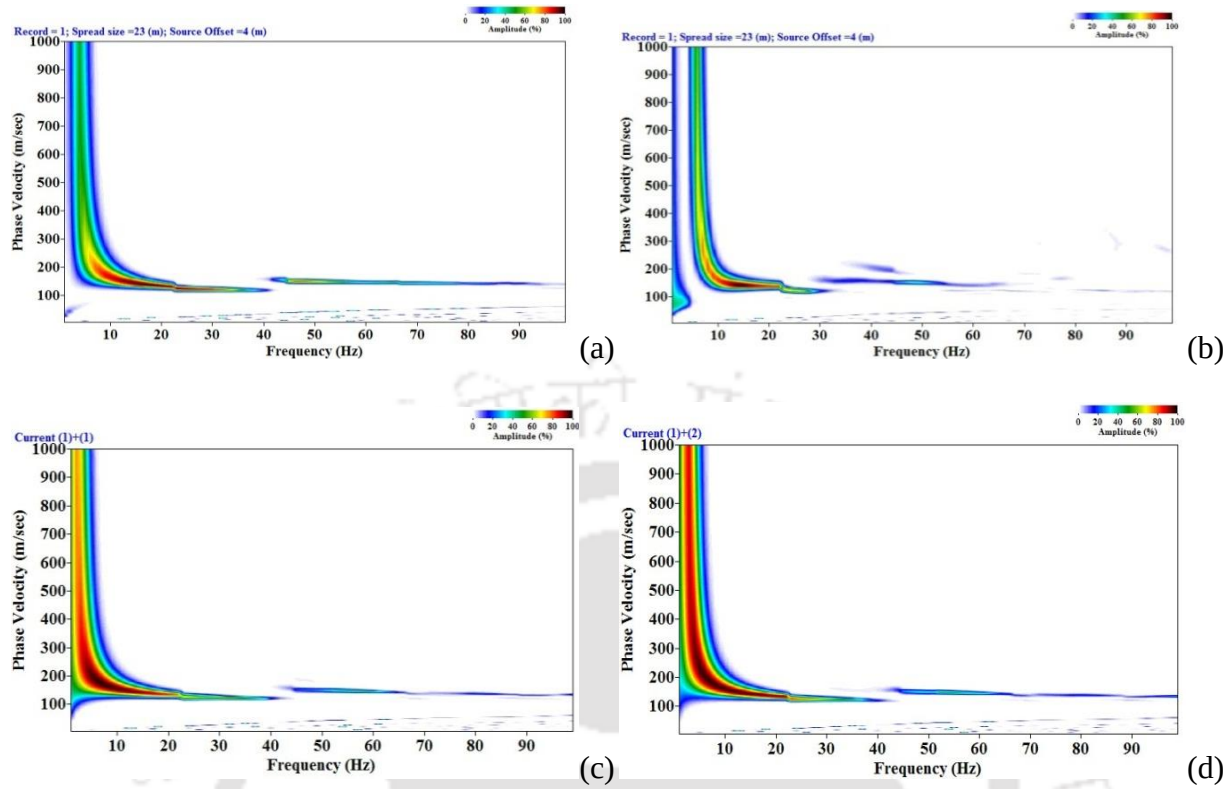

Fig. 8.13: Dispersion images for varying stacks (a) 0 stack (b) 1 stack (c) 2 stack (d) 3 stack (Sampling frequency – 15000 Hz, Numbers of samples – 5120, Offset distance – 4 m, Inter-receiver spacing – 1 m, Numbers of channels – 24)

8.3.7 Extraction of Dispersion Curve

8.3.7.1 Manual Extraction

In SURFSEIS, dispersion curves is extracted by manually selecting the dispersion points having the best possible visual of highest energy. The darkest points are the supposed to be representation of highest energy points as shown in the color legend bar in the top right hand side of a dispersion image. Since , the selection is based on the user's discretion, the reliability and repeatability is in question as described in Chapter 7. Figure 8.14 shows the dipersion curve extraction based on manual selection methods and the corresponding extraction.

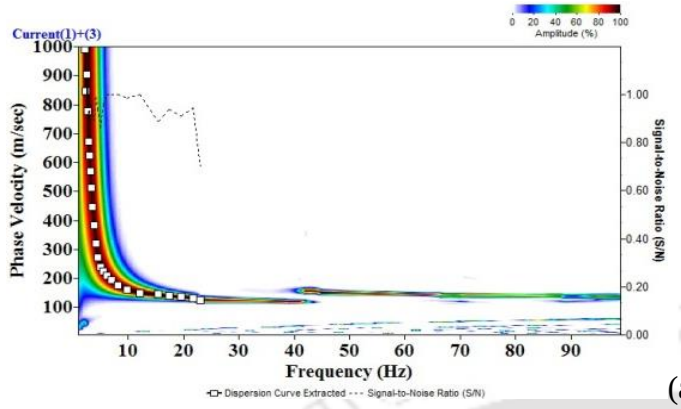

(a)

```
>>Start
ndata 24 1
DATA    2.130000        990.269000      0.998000
DATA    2.335000        846.736000      0.971000
DATA    2.438000        905.122000      0.983000
DATA    2.644000        776.186000      0.954000
DATA    2.755000        673.723000      0.922000
DATA    2.916000        624.917000      0.903000
DATA    3.097000        570.811000      0.975000
DATA    3.302000        511.565000      0.961000
DATA    3.536000        448.097000      0.935000
DATA    3.806000        382.810000      0.892000
DATA    4.120000        321.015000      0.991000
DATA    4.491000        271.769000      0.939000
DATA    4.935000        239.833000      0.862000
DATA    5.476000        223.245000      0.962000
DATA    6.151000        209.583000      0.999000
DATA    7.016000        193.382000      0.999000
DATA    8.164000        175.809000      1.000000
DATA    9.761000        160.954000      0.988000
DATA    12.135000       148.118000      1.000000
DATA    15.484000       146.100000      0.888000
DATA    17.436000       138.802000      0.940000
DATA    19.593000       136.369000      0.910000
DATA    21.751000       131.504000      0.947000
DATA    23.086000       126.638000      0.700000
>>End
```

(b)

Fig. 8.14: (a) Typical representation of manual selection of the dispersion points in SURFSEIS (b) Screenshot of the data obtained from the manual selection

8.3.7.2 Automated extraction

Based on the variation of the energy content in the dispersion image, represented by different colour concentrations, Fig. 8.15a shows a typical 3D representation of the dispersion image developed with the aid of the MatLab code (as described in Chapter 7). Further, the MatLab code has been used to extract this highest energy trend, to be subsequently used as input to inversion analysis. Figure 8.15b shows the extracted fundamental mode. Figure 8.16 shows the partical screenshot of the data obtained by the automated extraction of the dispersion curve using MATLAB. It can be observed that the SNR values of chosen points are substantially high indicating superior quality of the extracted dispersion curve. The obtained dispersion curve is then imported to the *.txt file in SURFSEIS, and is further used for inversion analysis.

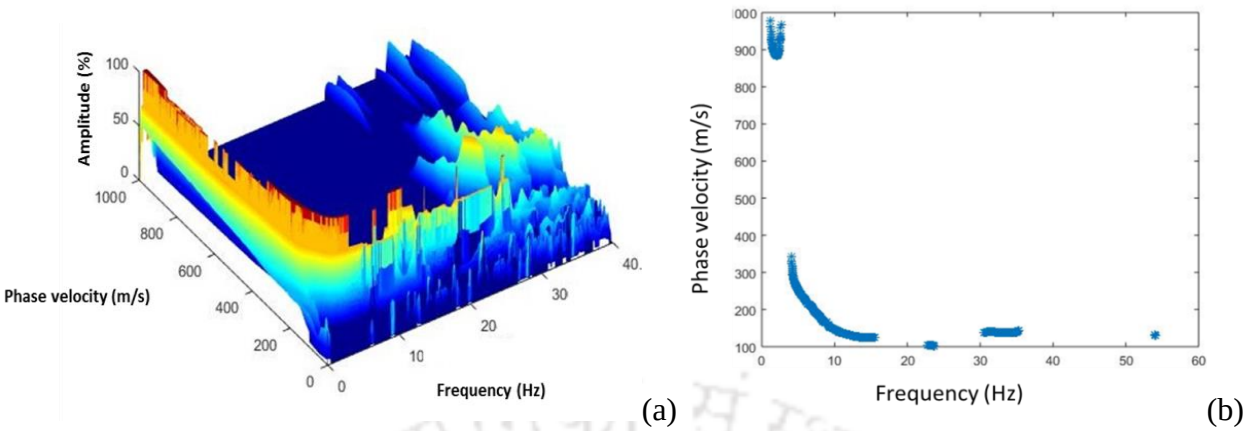

Fig. 8.15: (a) 3D dispersion image representation obtained from MATLAB based coding related to color / energy concentrations (b) Identification of the fundamental and higher modes of the dispersion image (local highest energy peaks)

```
>>Start    747
DATA    1.2     979     0.99    0
DATA    1.225   962     0.99    0
DATA    1.25    950     0.99    0
DATA    1.275   940     0.99    0
DATA    1.3     934     0.99    0
DATA    1.325   928     0.99    0
DATA    1.35    924     0.99    0
DATA    1.375   920     0.99    0
DATA    1.4     915     0.99    0
DATA    1.425   912     0.99    0
DATA    1.45    908     0.99    0
DATA    1.475   905     0.99    0
DATA    1.5     902     0.99    0
DATA    1.525   899     0.99    0
DATA    1.55    898     0.99    0
DATA    1.575   896     0.99    0
DATA    1.6     895     0.99    0
DATA    1.625   894     0.99    0
DATA    1.65    893     0.99    0
DATA    1.675   892     0.99    0
DATA    1.7     891     0.99    0
DATA    1.725   891     0.99    0
DATA    1.75    890     0.99    0
DATA    1.775   889     0.99    0
DATA    1.8     889     0.99    0
DATA    1.825   888     0.99    0
DATA    1.85    888     0.99    0
DATA    1.875   887     0.99    0
DATA    1.9     886     0.99    0
DATA    1.925   886     0.99    0
DATA    1.95    885     0.99    0
DATA    1.975   885     0.99    0
DATA    2       885     0.99    0
```

Fig 8.16: Screenshot of the data obtained from the automated extraction of dispersion curve

Figure 8.17 exhibits the shear wave velocity profiles obtained from the dispersion curves obtained using manual and automated extractions. It can be observed that the precision of the

points selected using automated extraction mode leads to higher depth of investigation. This is attributed to the precise identification of the dispersion points at the low frequency range; such precision is not possible with the manual extraction as it would lead to the selection of low energy points. Automated extraction of the dispersion curve leads to the higher depth of investigation with greater accuracy. The RMSE error in the present case of automated extraction was found to only 0.95 %, which is significantly low.

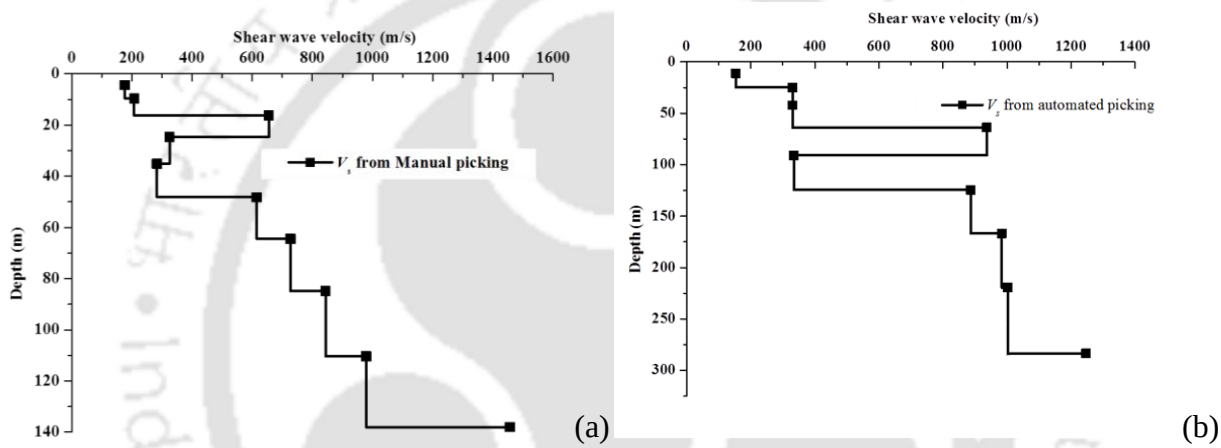

Fig 8.17: Shear wave velocity profiles obtained using dispersion curves from (a) Manual extraction (b) Automated extraction

8.4 Shear Wave Velocity Profile along the Bridge Alignment

Based on the methodology adopted as described for a typical wavefield as shown in Section 8.3, likewise, the shear wave velocity at all the piers and abutments have been estimated. It is observed that in the locations ranging from Abutment 1 - Pier 7 and Pier 23 – Abutment 2, the shear wave velocity have exceeded the magnitude of 300 m/s beyond a depth of 25-30 m, indicating the presence of denser and stiffer soils. Some locations exhibit the presence of soft patches of soils in deeper strata (e.g. P9, P17, P18, and P22). Caution should be exercised in the

design of the well foundations in these locations. The soils at various depths of the subsurface can be categorized as per the NEHRP soil profile type classification (BSSC, 2003), which is provided in Table 8.1: The shear wave velocity (V_s) profiles at different abutment and pier locations in the alignment of the proposed bridge over the Jia Bharali river is shown in Fig. 8.18(a-v).

Table 8.1: NEHRP soil profile type classifications (BSSC, 2003)

Soil Profile Type	Average Shear-Wave Velocity to 30-m depth ($\overline{V}_{s30}$)
A	$\overline{V}_{s30}$ > 1500 m/s, hard rock
B	760 m/s < $\overline{V}_{s30}$ ≤ 1500 m/s, rock
C	360 m/s < $\overline{V}_{s30}$ ≤ 760 m/s, very dense soil and soft rock
D	180 m/s < $\overline{V}_{s30}$ ≤ 360 m/s, stiff soil
E	$\overline{V}_{s30}$ < 180 m/s

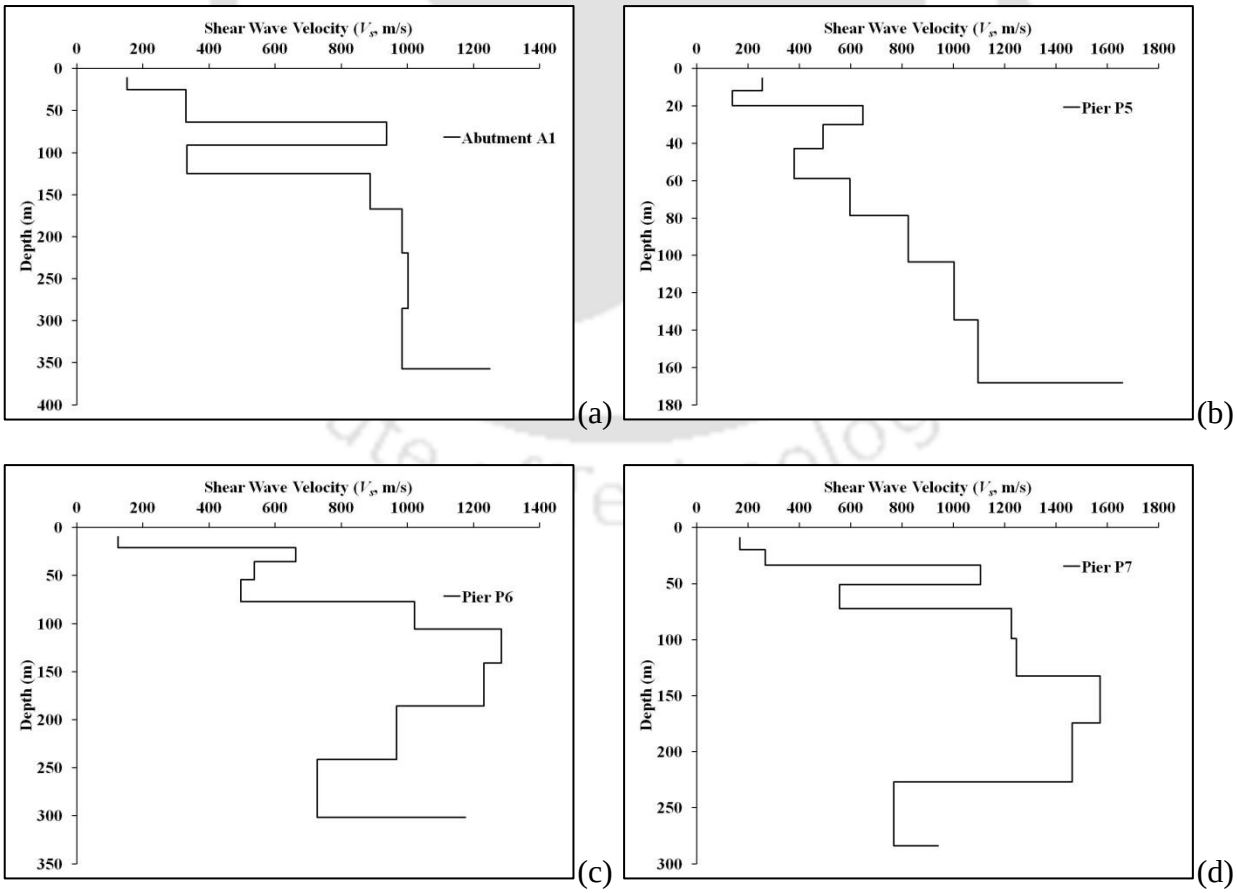

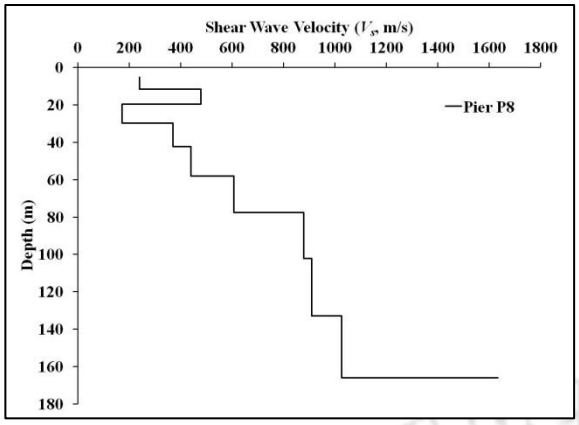
Shear Wave Velocity (V_s, m/s)
0 200 400 600 800 1000 1200 1400 1600 1800
Depth (m)
0 20 40 60 80 100 120 140 160 180
Pier P8

(e)

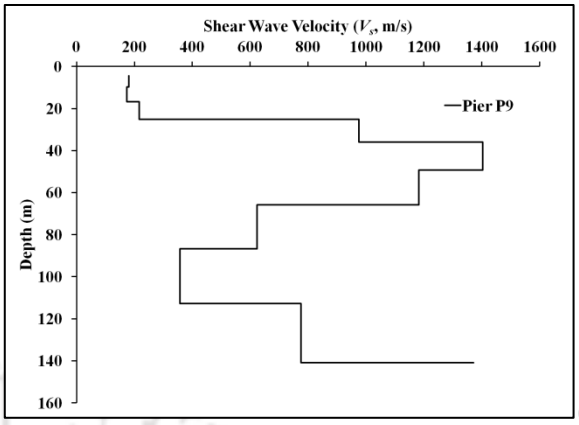
Shear Wave Velocity (V_s, m/s)
0 200 400 600 800 1000 1200 1400 1600
Depth (m)
0 20 40 60 80 100 120 140 160
Pier P9

(f)

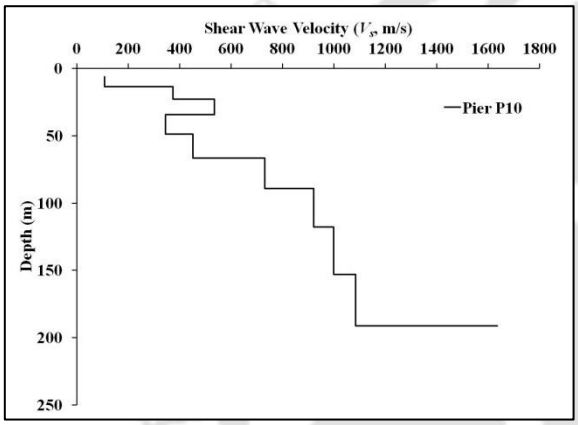
Shear Wave Velocity (V_s, m/s)
0 200 400 600 800 1000 1200 1400 1600 1800
Depth (m)
0 50 100 150 200 250
Pier P10

(g)

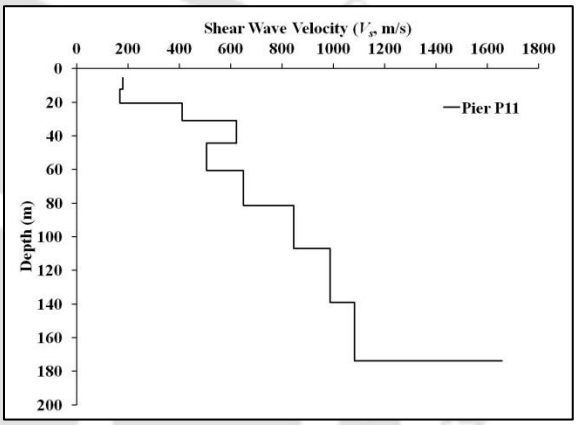
Shear Wave Velocity (V_s, m/s)
0 200 400 600 800 1000 1200 1400 1600 1800
Depth (m)
0 20 40 60 80 100 120 140 160 180 200
Pier P11

(h)

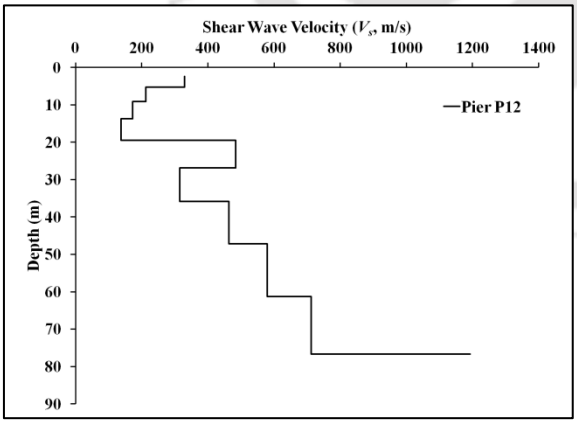
Shear Wave Velocity (V_s, m/s)
0 200 400 600 800 1000 1200 1400
Depth (m)
0 10 20 30 40 50 60 70 80 90
Pier P12

(i)

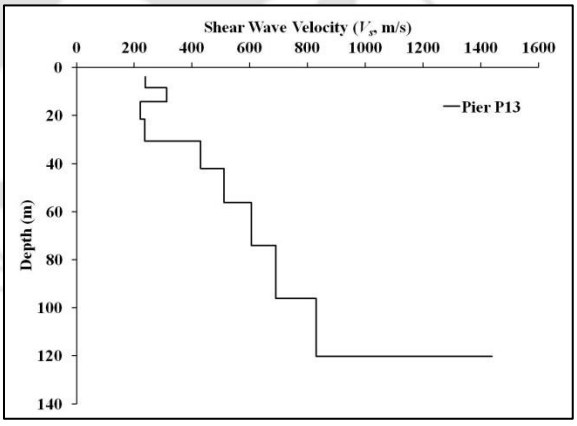
Shear Wave Velocity (V_s, m/s)
0 200 400 600 800 1000 1200 1400 1600
Depth (m)
0 20 40 60 80 100 120 140
Pier P13

(j)

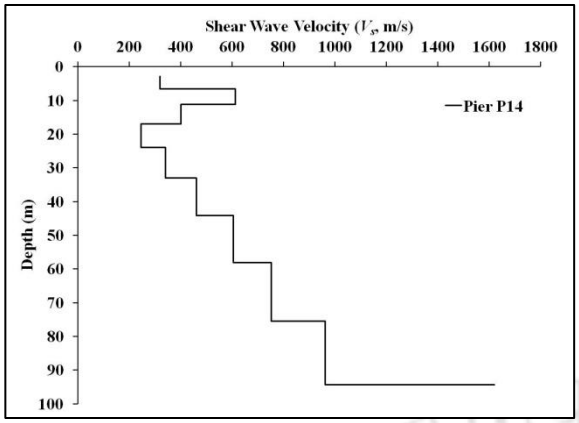
Shear Wave Velocity (V_s, m/s)
0 200 400 600 800 1000 1200 1400 1600 1800
Depth (m)
0 10 20 30 40 50 60 70 80 90 100
Pier P14

(k)

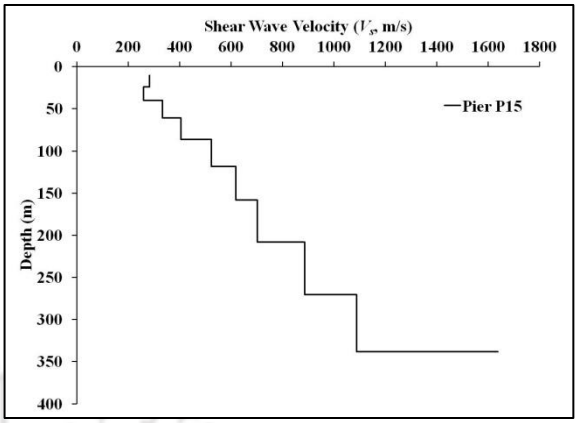
Shear Wave Velocity (V_s, m/s)
0 200 400 600 800 1000 1200 1400 1600 1800
Depth (m)
0 50 100 150 200 250 300 350 400
Pier P15

(l)

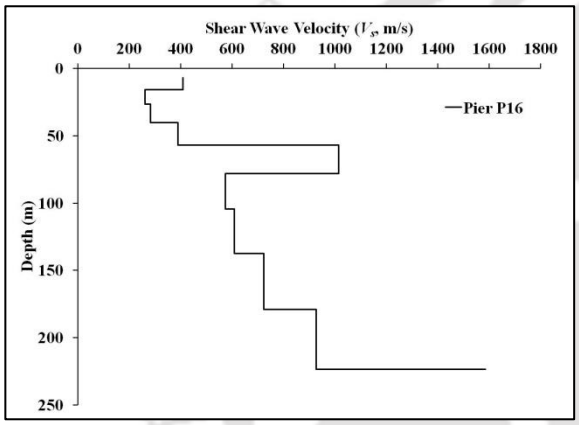
Shear Wave Velocity (V_s, m/s)
0 200 400 600 800 1000 1200 1400 1600 1800
Depth (m)
0 50 100 150 200 250
Pier P16

(m)

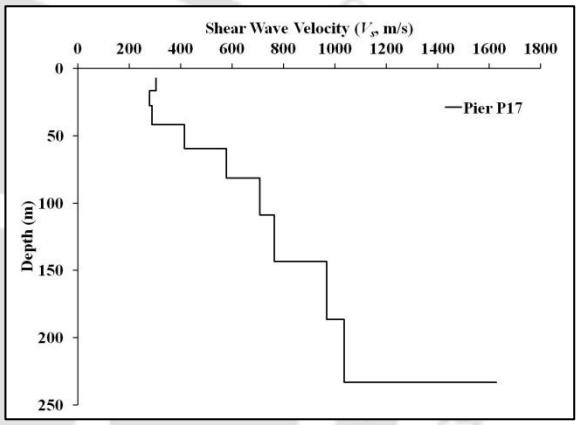
Shear Wave Velocity (V_s, m/s)
0 200 400 600 800 1000 1200 1400 1600 1800
Depth (m)
0 50 100 150 200 250
Pier P17

(n)

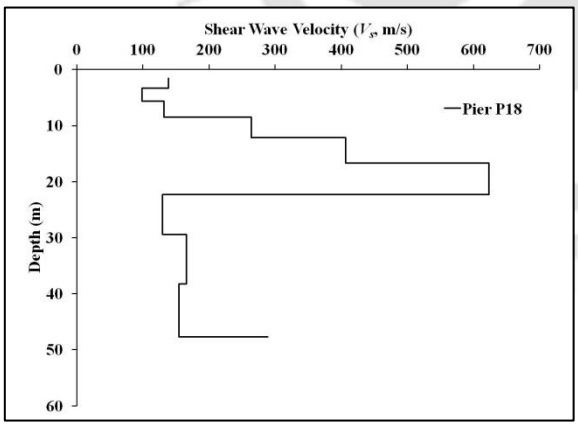
Shear Wave Velocity (V_s, m/s)
0 100 200 300 400 500 600 700
Depth (m)
0 10 20 30 40 50 60
Pier P18

(o)

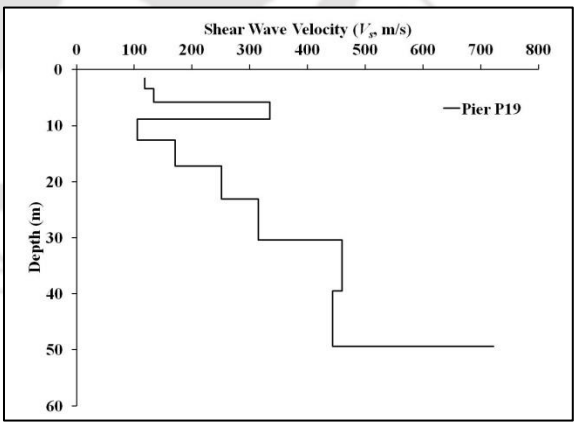
Shear Wave Velocity (V_s, m/s)
0 100 200 300 400 500 600 700 800
Depth (m)
0 10 20 30 40 50 60
Pier P19

(p)

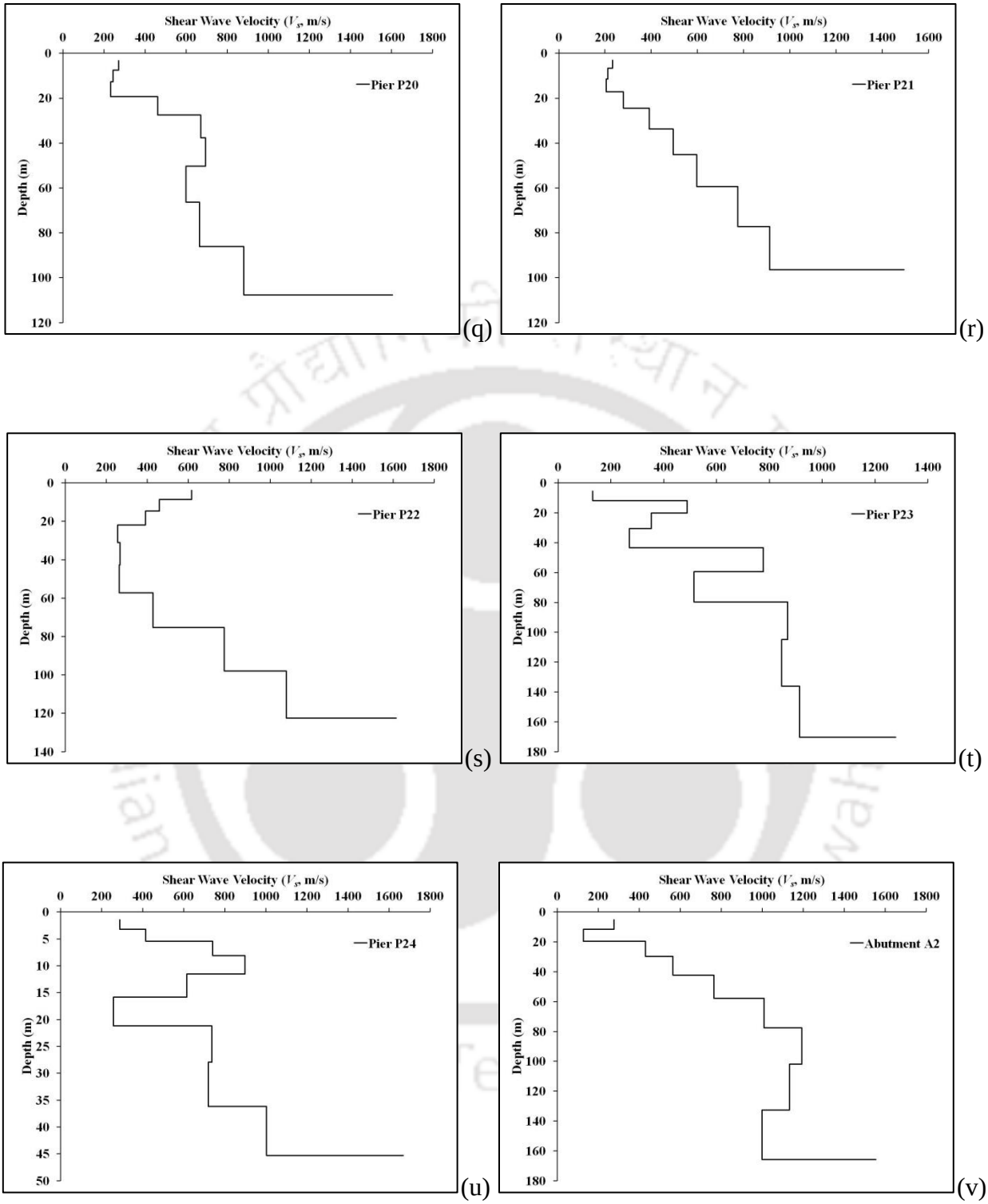

Fig. 8.18: Shear wave velocity profiles at different abutment and pier locations in the alignment of the proposed bridge over the Jia Bharali River bed

Figure 8.19 shows a typical comparative between the Vs obtained for Pier-18 using MASW test with that obtained from borehole exploration data of SPT-N values. The outcomes are in appreciable agreement with each other, thus depicting the efficacy of the automated extraction in deciphering the subsurface stratification. Moreover, the outcomes also depict that the even through the physical exploration technique can get prohibited from progressing to larger depths due to the presence of hard or stiff subsurface layers, geophysical exploration can be an effective tool in determining the subsurface stratifications.

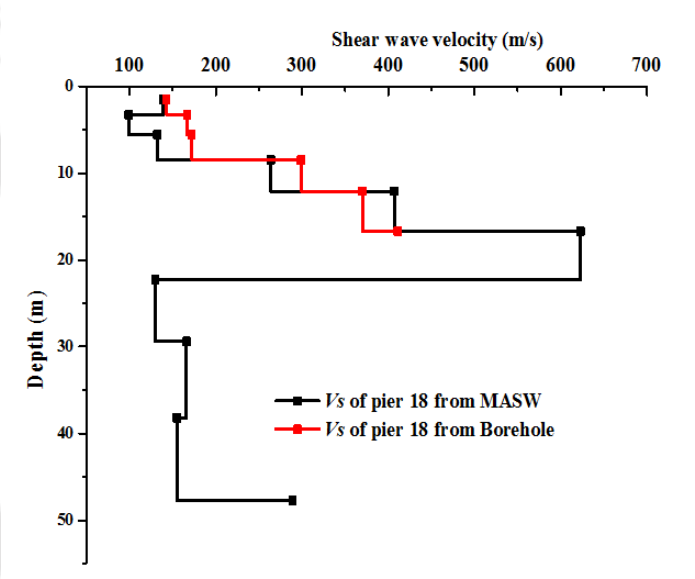

Fig. 8.19: Typical comparative of the shear wave velocity profile obtained using borehole exploration and MASW tests at the location of Pier P-18

Roll-along active MASW survey had been carried out between the locations of Pier-5 to Abutment-2. The outcome of the survey is provided as the 2-D variation of shear wave velocity profile along the length of the investigation, as exhibited in Fig. 8.20. It can be observed that a relatively soft patch of soil stratum (V_s < 250 m/s, approx.) is sandwiched between sufficiently stiffer strata (V_s > 600 m/s, approx), all along the river bed at a depth of around 30-35 m from the

ground surface. It is advised to avoid this particular layer of soil and locate the base of the well foundation beyond this layer.

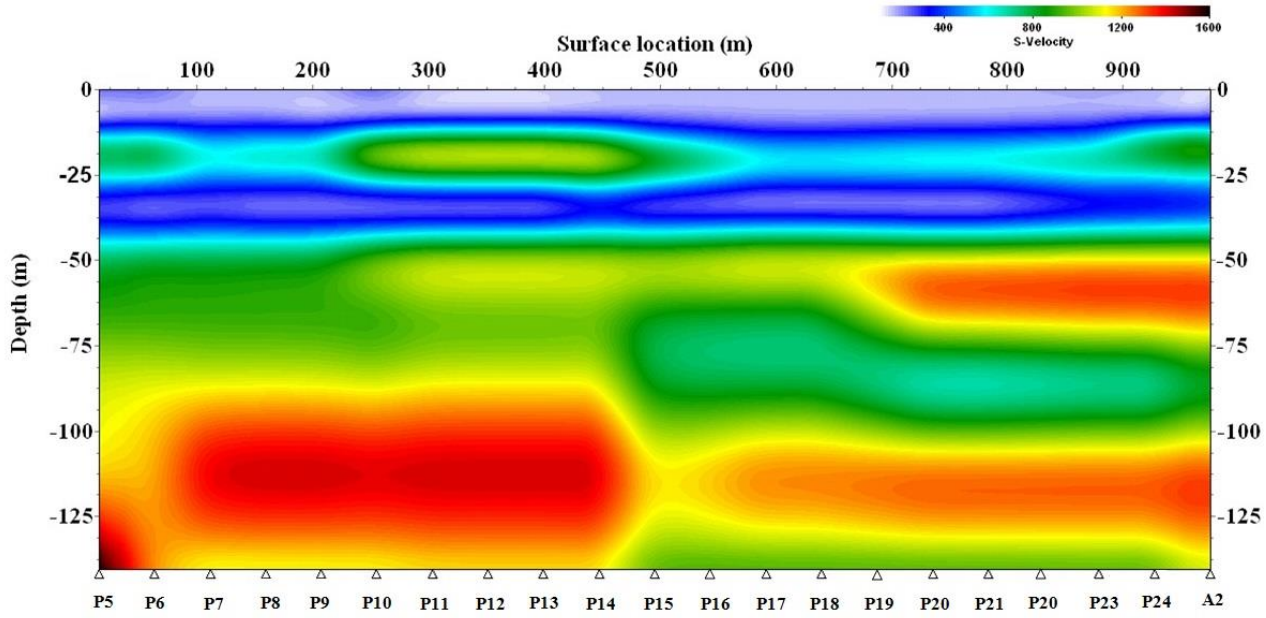

Fig. 8.20: 2-D shear wave velocity profile obtained from a roll-along active MASW conducted along the alignment of the proposed bridge over Jia-Bharali (P5-A2)

8.5 Summary

This chapter illustrates a case study wherein active MASW survey had been conducted along athe Jia Bharali river bed (a tributary of River Brahmaputra) for the proposed construction work of a 1.2 km long bridge along the new 4-lane road from Dolabari to Jamuguri connecting NH-37A with NH-52 in Tezpur, Assam. Both spot and roll-along active MASW survey have been carried out. The experience developed from the understands, as discussed in the previous chapters, have been utilized to adjudge the proper choices of various factors affecting the resolution of dispersion image. Apart from manual extraction dispersion curve aleady provided with SURFSEIS, the automated dispersion curve extraction has been carried out with the

indigenously developed MatLab codes as described in the earlier chapters. The shear wave velocity profiles at each of the pier and abutment locations have been deciphered, and the presence of perched hard and soft strata were discovered. The 2D image from the roll-along active survey exhibited the presence of soft patches along the entire length of the proposed bridge alignment, along with the presence of perched hard stratum. Very hard stratum, possibly bedrock, can be identified below 100 m. Based on the observations for the shear wave velocity profiles, the stifness variaton in the subsurface can be identified, and accordingly, cautionary notes related to the placement of the base of the well foundation were decided.

CHAPTER 9

CONCLUSIONS AND RECOMMENDATIONS

9.1 Brief Summary of the Dissertation

This dissertation reports about the identification of the subsurface from active MASW survey. The field investigations have been conducted at different location having different subsurface characteristics. Influence of several data acquisition and data preprocessing parameters have been deciphered. The shortcomings of the conventional approach of extraction and dispersion curve and quantification of resolution have been elucidated. In this regard, indigenous MatLab codes based on image processing have been developed to provide a quantification of the resolution of the dispersion image and automated extraction of the dispersion curves. The influences of the automations have been suitably explored by integrating the same in the inversion analysis conducted through SURFSEIS. A case study related to successfully conducting active MASW survey along Jia Bharali river bed (a tributary of River Brahmaputra) for the proposed construction work of a 1.2 km long bridge along the new 4-lane road from Dolabari to Jamuguri connecting NH-37A with NH-52 in Tezpur, Assam, has been vividly described.

9.2 Conclusions and Recommendations

Based on the analysis and results obtained in the present study in lieu of the active MASW survey conducted at various sites with varying substrata, the conclusions and recommendations can be listed as follows:

Conclusions and Recommendations related to Preprocessing Parameters

- The filtering frequency range for soil sites underlain by a shallow depth stiffer stratum is higher (approx. 5-300 Hz) in comparison to that of softer sites (approx. 5-40 Hz).
- Band-pass filter with proper choice of filtering frequency range results in the best resolution of the dispersion image.
- Best suitable muting should be adopted so that the significant energy of the propagating wavefield is not lost. Excessive muting results in loss of information and resolution of the dispersion images. Application of muting on unfiltered wavefields produces aliasing effects on the low frequency range of the dispersion images.
- For active MASW survey conducted at any site, combined application of band-pass filtering with best suitable muting is recommended to obtain the best resolution dispersion images.

Conclusions and Recommendations related to Data Acuisition Parameters

- The optimal sampling frequency is site dependent. For sites comprising of softer strata ($N \leq 25$), sampling frequency of 7500 Hz is recommended, while for sites having stiffer stratum located at shallow depth ($N > 40$), sampling frequency of 15000 Hz is recommended.
- Optimum sampling time depends on the completion of phase propagation through the receiver array without inducing noise adulteration in the wavefield record. Based on the present study on various sites, a sample length of 5120 samples is recommended.
- Out of the several combinations sampling frequency and sampling time which allows for the optimal completion of phase propagation, the maximum sampling frequency is recommended.

- Sampling frequency less than 1000 Hz is recommended to be avoided for soil sites due to excessive sampling time and accumulation of noise.
- The offset distance should be so chosen that the requirement of planar wave propagation is satisfied and the best resolution dispersion image is obtained. Smaller offset distance induces high accumulation of energy at low frequencies resulting in indistinct dispersion trends and shallow depth shear wave velocity profiles (near-offset effect). Large offset distance results in dominant adulteration of the records due to the prevalent noises, resulting in dispersion curves with low SNR (far-offset effect).
- The choice of best suitable offset distance is site dependent. For sites possessing an average shear wave velocity less than 200 m/s, 6-10 m offset distance is recommended for obtaining higher resolution dispersion images. Similarly, for sites having an average shear wave velocity greater than 200 m/s, 4-6 m offset are recommend for obtaining the best resolution dispersion images.
- Large receiver spacing should be avoided as it leads to significant attenuation of active energy traversing the array, leading to incomplete wave propagation through the array. Based on the present study, it is recommended to maintain an inter-receiver spacing of 1 m for an active MASW survey to obtain the best resolution dispersion image.
- Inter-receiver spacing and the numbers of receivers used in active MASW survey governs the total length of array. It is found that in contrary to the conventional notion, merely increasing the length of the array will not enhance the depth of investigation.
- The depth of investigation, governed by the maximum wavelength recorded by the receiver, is primarily dependent on frequency characteristics of the site substrata and the wave generating source. Even if the source generates long wavelengths, the same can get curtailed

depending on the site characteristics, and the receivers will be left with shorter wavelength records leading to shallow investigation depths.

- Mere increase in the number of receivers will not enhance the resolution of the dispersion image. An increase in the array length accompanied by an increase in the number of receivers will provide higher resolution dispersion images. Based on the present study, a 24 channel configuration is recommended while satisfying the best suitable offset distance and inter-receiver spacing.
- The spectrum of the recorded wavefield, generated during an active MASW due to the usage of a specific impact source, is primarily site dependent. The spectral energy obtained from sites comprising of relatively stiffer substrata ($V_{s,avg}$>200 m/s) is nearly 3-6 times higher than the sites comprising of less stiffer substrata ($V_{s,avg}$<200 m/s). Correspondingly, the effective frequency bandwidth of the energy distribution for the stiff sites is approximately 2-4 times higher than the otherwise.
- Heavier source such as 40 kg PEG imparts higher impulse energy, nearly 3-4 times that produced by a 10 kg sledgehammer, thus generating wavefields containing longer wavelengths, allowing for higher depths of investigation.
- Since stacking results in the enhancement in the energy of the frequency spectra, dispersion image stacking should be used as an effective means of achieving higher depths of investigation using low weight 10 kg sledgehammers, thus overcoming the difficulty of portability of heavy weight drops for the purpose of active MASW survey.
- In order to obtain a good resolution dispersion image, it is recommended to use 3-4 dispersion image stacks for sites with $V_{s,avg}$<200 m/s, while single stack is recommended tobe sufficient for sites with $V_{s,avg}$>200 m/s.

- Wavefields generated from a single strike on a rubber base plate produces waves of low frequency content (<15 Hz), and hence is recommended for large-depth investigations. Cast steel plates are recommended for high resolution shallow depth investigations, since the wavefield generated from a single strike on cast steel plate favorably consists of significant high frequency content (till 50 Hz).
- Owing to the rapid degradation of the rubber strike plate and for avoiding the recurring replacement, cast steel plate is recommended to be used for all practical purposes. Large depth investigations can be effectively achieved when recommended dispersion image stacking is adopted, the numbers of stacks will depend on the site substrata characteristics.

Outcomes of the Study based on Dispersion Curve Extraction and Inversion Analysis

- For manual extraction of dispersion curve from dispersion image, it is recommended to select the dispersion points, as precise as possible from the darkest dispersion band, the points being uniformly distributed over the entire frequency band of the fundamental dispersion mode. The extraction should incorporate the best possible points from the low frequency region for obtaining shear wave velocity information for the deeper substrata.
- In case of manual extraction of the dispersion curve, an initial earth model comprising of a minimum 10 layers of varying thickness is recommended for obtaining the shear wave velocity profile from inversion analysis.
- The automated dispersion curve extraction sequence as developed using the MatLab image processing schemes and proper integration with the SURFSEIS modules have been instrumental in successful delineation of the exact dispersion curve from the dispersion image. The application of this technique aptly eliminates the subjectivity and concerns of

reliability and repeatability of the entire exercise arising due to user discretion in the conventional approach.

- The automated extraction successfully encompasses several points from the entire frequency band of the dispersion, all of them having high SNR (> 0.9), and hence, the accuracy and reliability of the obtained shear wave velocity profile of the subsurface increases manifold in comparison to that obtained using manual extraction of dispersion curves. It is recommended to use the automated extraction technique to achieve reliable and repeatable subsurface identification.
- The image processing scheme used in the indigenously developed MatLab code have been efficient in quantifying the resolution of the dispersion image, and is recommended to be used to successful identification of the optimal parametric configuration for an active MASW survey.

9.3 Limitation and Scope of Future Research

Any research work conducted has its own limitations and thus paves the way and scope for future research. Some of them, as applicable for the present study, are listed as follows:

- In all the analysis conducted and reported in the present study, only the fundamental mode of dispersion have been considered in the subsequent analysis to obtain the shear wave velocity profile. It is imperative that most of the cases, there would be presence of multimodal dispersion exhibited by the image, and the cumulative energy from the higher mode might significantly govern the dispersion characteristics. Hence, such multimodal inversion should be attempted considering higher dispersion modes in the inversion analysis. This case might be particularly important when comparatively thin soft or hard

strata remain perched in the subsurface and create a different mode of wave propagation within the medium.

- The initial earth model used for the inversion analysis comprise of uniform stratifications. The shear wave velocity profiles obtained from such analysis are further used in a roll along mode, with suitable interpolations, lead to the development of 2D Vs profiles. However, as the earth model remains uniformly stratified, the variations encountered in the 2D profile is only due to interpolation, and does not necessarily includes the changes in the features actually prevalent in the site. Under such circumstance, a technique should be frames how direct 2D images can be produced using 'Arbitrary earth models' as initial feed to the inversion analysis.
- The presently developed automated dispersion curve extraction scheme still needs user discretion and intervention in order to delineate the fundamental dispersion curve, and the developed method cannot automatically identify and remove the problems of mode misidentification and mode mixing. Hence, advanced dispersion curve extraction schemes have to be developed to tackle such complexities.
- The inversion process used in these studies is deterministic, and has every possibility that the final outcome gets trapped into any local minima. A technique to overcome such a pitfall is to try with several different initial earth models, however without any scientific guideline. In this regard, application of evolutionary algorithms should be the aim of future so that the global minima, thus the final shear wave velocity profile, can be successfully and unambiguously identified.
- In all the present studies, only the fundamental dispersion mode has been used to decipher the subsurface profile. It is understandable that only the fundamental mode comprises of

only 67% (approximately) of the total wave energy propagating through the medium. Hence, under such scenario, the information carried by the waves with lower energy are lost, which might lead to the loss of valuable information about the substrata. Hence, in this regard, 'Total Dispersion Image Inversion' or 'Raw Wavefield Inversion' should be explored for better efficacies.

- It has been already appraised in the literature, Passive MASW survey can provide information about deeper substrata (> 30 m) with better resolution, while Active MASW survey provides higher resolution for shallow depths (< 30 m). The limitation has been overcome in the present study by using dispersion image stacking. However, it would be wise to attempt further 'Combined Active and Passive MASW Survey' in order to obtain better resolution subsurface profiles for both shallow and deeper layers.

REFERENCES

1. Aki, K. **1957**. Space and time spectra of stationary stochastic waves, with special reference to micro-tremors. ***Bulletin of Earthquake Research Institute***. 35, 415-456.

2. Andrus, R. D., and Stokoe II, K. H. **2000.** Liquefaction resistance of soils from shear-wave velocity. ***Journal of Geotechnical and Geoenvironmental Engineering, ASCE***. 126(11), 1015-1025.

3. Baker, G. S., Steeples, D. W., and Drake, M. **1998**. Muting the noise cone in near-surface reflection data: an example from southeastern Kansas. ***Geophysics***. 63(4), 1332-1338

4. Beaty, K. S., Schmitt, D. R., and Sacchi, M. **2002**. Simulated annealing inversion of multimode rayleigh wave dispersion curves for geological structure. ***Geophysical Journal International***. 151(2), 622-631.

5. Building Seismic Safety Council. **2003**. ***NEHRP Recommended Provisions for seismic regulations for new buildings and other Structures, Part 1: Provisions***, FEMA 450, Federal Emergency Management Agency, BSSC, National Institute of Building Sciences, Washington, DC.

6. Capon, J. **1969**. High-resolution frequency-wave number spectrum analysis. ***Proceedings of the IEEE***. 57(8), 1408-1418.

7. Dikmen, U., Arisoy, M., and Akkaya, I. **2010**. Offset and linear spread geometry in the MASW method. ***Journal of Geophysics and Engineering***. 7, 211-222.

8. Dzienwonski, A., Bloch, S., and Landisman, M., **1969**. A technique for the analysis of transient seismic signals. ***Bulletin of Seismological Society of America***. 59(1), 427-444.

9. Eker, A. M., H. Akgun., and Koçkar. M. K. **2012**. Local site characterization and seismic zonation study by utilizing active and passive surface wave methods: A case study for the northern side of Ankara, Turkey. ***Engineering Geology***. 151, 64–81.

10. Forbriger, T. **2003a**. Inversion of shallow seismic wavefields: I. Wavefield transformation. ***Geophysical Journal International***, 153, 719-734.

11. Forbriger, T. **2003b**. Inversion of shallow seismic wavefields: II. Inferring subsurface properties from wavefield transforms. ***Geophysical Journal International***, 153, 735-752.

12. Foti, S., Lai, C. G., Rix, G.J., and Strobbia, C. **2015**. ***Surface Wave Methods for Near-Surface Site Characterization***, 1st Edition, CRC press, Boca Raton.

13. Gabriels, P., Snieder, R., and. Nolet. G. **1987**. In-situ measurements of shear wave velocity in sediments with higher-mode Rayleigh waves. ***Geophysical Prospecting***. 35, 187-196.

14. Ganji, V., Gucunski, V., and Nazarian, S., **1998**. Automated inversion procedure for spectral analysis of surface waves. ***Journal of Geotechnical and Geoenvironmental Engineering, ASCE***. 124(8), 757-770.

15. Gordon, M. A. **1997**. Application of Field Seismic Geophysics to the Measurement of Geotechnical Stiffness Parameters. ***PhD Thesis***, University of Surrey.

16. Gosar, A., Stopar, R., and Roser, J. **2008**. Comparative test of active and passive multichannel analysis of surface waves (MASW) methods and microtremor HVSR method. ***RMZ - Materials and Geoenvironment***. 55(1), 41-66.

17. Grandjean, G., and Bitri, A. **2006**. 2M-SASW: Multifold multichannel seismic inversion of local dispersion of Rayleigh waves in laterally heterogeneous subsurface: Application to the Super-Sauze earthflow, France. ***Near Surface Geophysics***. 4, 367-375.

18. Griffin, S., and Pippett, T. **2002**. Ground penetrating radar. ***Geophysical and Remote Sensing Methods for Regolith Exploration CRCLEME File Report 144***, 80-89.

19. Haeni, F. P. **1986**. Application of seismic refraction methods in groundwater modeling studies in New England. ***Geophysics***. 51, 236-249.

20. Heisey, J. S., Stokoe II, K. H., and Meyer. A. H. **1982**. Moduli of pavement systems from Spectral Analysis of Surface Waves. ***Transportation Research Record***. 652, 22-31.

21. Herrmann, R. B. **1973**. Some aspects of bandpass filtering of surface waves. ***Bulletin of Seismological Society of America***. 63(2), 663-667.

22. Imai, T., and Tonouchi, K. **1982**. Correlation of N-value with S-wave velocity and shear modulus: ***Proceedings of the 2nd European Symposium of Penetration Testing***, Amsterdam. 67-72.

23. Ivanov, J., Miller, R. D., Xia, J and Peterie, S. **2010.** Multi-mode inversion of multi-channel analysis of surface waves (MASW) dispersion curves and high-resolution linear radon transform (HRLRT). ***80th Annual International Meeting, Society of Exploration Geophysicist***. Expanded Abstracts. 29, 1902-1907.

24. Ivanov, J., Park, C. B., Miller, R. D., and Xia, J. **2005**. Analysing and Filtering Surface-Wave Energy By Muting Shot Gathers. ***Journal of Environmental and Engineering Geophysics***. 10, 307-322.

25. Johnson. G., and J. M. S. Hutchison. **1985**. The limitations of NMR recalled-echo imaging techniques. ***Journal of Magnetic Resonance***. 63, 14-30.

26. Jones, R. **1955**. A vibration method for measuring the thickness of concrete slab in-situ. ***Magazine of Concrete Research***. 7, 97-102.

27. Kanli, A. I., Tildy, P., Pronay, Z., Pinar, A., and Hermann, L. **2006**. V_s^{30} mapping and soil classification for seismic site effect evaluation in Dinar region, SW Turkey. ***Geophysical Journal International***. 165, 223-235.

28. Kaufmann, R. D., Xia, J., Benson, R. C., Yuhr, L. B., Casto, D. W., and Park. C. B. **2005**. Evaluation of MASW data acquired with a hydrophone streamer in a shallow marine environment. ***Journal of Environmental and Engineering Geophysics***. 10, 87-98.

29. Kayen, R., Moss, R. E. S., Thompson, E. M., Seed, R. B., Cetin, K. O., der Kiureghian, A., Tanaka, Y., and Tokimatsu, K. **2013.** Shear-wave velocity-based probabilistic and deterministic assessment of seismic soil liquefaction potential. ***Journal of Geotechnical and Geoenvironmental Engineering, ASCE***, 139(3), 407-419.

30. Ke, G., Dong, H., Kristensen, A., and Thompson, M. **2011**. Modified Thomson–Haskell matrix methods for surface-wave dispersion-curve calculation and their accelerated root-searching schemes. ***Bulletin of the Seismological Society of America***. 101(4), 1692-1703.

31. Kumar, J., and Naskar, T. **2015**. Effects of site stiffness and source to receiver distance on surface wave tests' results. ***Soil Dynamics and Earthquake Engineering***. 77, 71-82.

32. Kumar, J., and Naskar, T. **2017**. A fast and accurate method to compute dispersion spectra for layered media using a modified Kausel-Roësset stiffness matrix approach. ***Soil Dynamics and Earthquake Engineering***. 92, 176-182.

33. Kumar, J., and Rakaraddi, P. G. **2013**. SASW evaluation of asphaltic and cement concrete pavements using different heights of fall for a spherical mass. ***International Journal of Pavement Engineering***, 14(4), 354-363.

34. Lai, C. G., Rix, G. J., Foti, S., and Roma, V. **2002**. Simultaneous measurement and inversion of surface wave dispersion and attenuation curves. ***Soil Dynamics and Earthquake Engineering***, 22, 923-930.

35. Lin, C. P., Chang, C. C., and Chang, T. S. **2004**. The use of MASW method in the assessment of soil liquefaction potential. ***Soil Dynamics Earthquake Engineering***. 24, 689-698.

36. Lin, S. **2014**. Advancements in active surface wave methods: Modeling, testing and inversion. ***Ph.D. Thesis***, Iowa State University.

37. Liu, J., Xia, J., Luo. Y., Li, X., and Xu, S. **2004**. Extracting transient Rayleigh wave and its application in detecting quality of highway roadbed. ***Progress in Environment. and Engineering Geophysics. Proceedings of the International Conference on Environment and Engineering Geophysics*** (***ICEEG***).

38. Louie, J. N. **2001**. Faster, better: shear-wave velocity to 100 meters depth from refraction microtremor arrays. ***Bulletin of the Seismological Society of America***. 91(2), 347-364.

39. Lu, L., and Zhang, B. **2006**. Inversion of Rayleigh waves using a genetic algorithm in the presence of a low-velocity layer. ***Acoustical Physics***, 52(6), 701-712.

40. Luke, B. A., Calderon-Macias, C., Stone, R. C., and Huynh, M. **2003**. Non-uniqueness in inversion of seismic surface-wave data. ***Proceedings of the Symposium on the Application of Geophysics to Engineering and Environmental Problems***. 1342-1347.

41. Luo, Y., Xia, J., Miller, R. D., Xu, Y., Liu, J., and Liu, Q. **2008**. Rayleigh-wave dispersive energy imaging using a high-resolution linear radon transforms. ***Pure and Applied Geophysics***. 165(5), 903-922.

42. Luo, Y., Xia, J., Miller, R. D., Xu, Y., Liu, J., and Liu, Q. **2009.** Rayleigh-wave mode separation by high-resolution linear Radon transform. ***Geophysical Journal International***. 179, 254-264.

43. Marks II, R. **1991**. ***Introduction to Shannon Sampling and Interpolation Theory***. 1st Edition, Springer Verlag, New York, USA.

44. Matheron, G. **1967**. Kriging or Polynomial Interpolation Procedures-a Contribution to Polemics in Mathematical Geology. ***Canadian Mining and Metallurgical Bulletin.*** 60, 1041-1045.

45. Matthews, M. C., Hope, V. S., and Clayton. C. R. **1996**. The usage of surface waves in the determination of ground stiffness profiles. ***Proceedings of the Institution of Civil Engineers, Geotechnical Engineering***. 119, 84-95.

46. McMechan, G., and Yedlin, M. J. **1981**. Analysis of dispersive waves by wave field transformation. ***Geophysics***. 46(3), 869-874.

47. Menke, W., Abbott, D. **1989**. ***Geophysical Theory***. Columbia University Press, New York.

48. Michaels, T. E., Michaels, J. E., and Ruzzene, M. **2011**. Frequency-wavenumber domain analysis of guided wavefields. ***Ultrasonics***. 51, 452-466.

49. Miller, R. D., Anderson, T.S., Ivanov, J., Davis, J. C., Olea, R. A., Park, C. B., Steeples, D.W., Moran, M. L., and Xia, J. **2003**. 3-D Characterization of seismic properties at the smart weapons test range, YPG. ***Proceedings of the 73rd Annual International Meeting, Society of Exploration Geophysicist Expanded Abstracts***. 1195-1198.

50. Miller, R. D., Xia, J., Park, C. B., and Ivanov, J. M. **1999**. Multichannel analysis of surface waves to map bedrock. ***The Leading Edge***. 18(12), 1392-1396.

51. Mitchell, B. J. **1973**. Radiation and attenuation of Rayleigh waves from the southeastern Missouri earthquake of October 21, 1965. ***Journal of Geophysical Research***. 78(5), 886-899.

52. Mitra, S. **2013**. ***Digital Signal Processing: A Computer Based Approach***. McGraw Hill Education, New York, USA.

53. Morlet, J., Arensz, G., Fourgeau, F., and Giard, D. **1982**. Wave propagation and sampling theory-Part II: Sampling theory and complex waves. ***Geophysics***. 47(2), 222-236.

54. Moro, G., Pipan, M., Forte, E., and Finetti. I. **2003**. Determination of Rayleigh wave dispersion curves for near surface applications in unconsolidated sediments. ***International Meeting of the Society of Exploration Geophysicists*** (Extended Abstracts). 1247-1250.

55. Mukherjee, M., and Prashant, A. **2009**. Evaluation of SASW test configurations and associated data uncertainties in generating site specific dispersion curves. ***Soils and Foundations***. 49(5), 699-709.

56. Mukherjee, M., and Prashant, A. **2013**. SASW analysis through inversion of combined dispersion curve using reliability of data from several receiver-configurations. ***International Journal of Geotechnical Engineering***. 7(1), 10-20.

57. Nazarian, S., Stokoe II, K. H., and Hudson, W. R. **1983**. Use of spectral analysis of surface waves method for determination of moduli and thicknesses of pavement systems. ***Transportation Research Record***. 930, 38-45.

58. Nazarian, S., Stokoe II, K. H., Briggs, R. C., and Rogers. R. **1987**. Determination of Pavement Layer Thicknesses and Moduli by SASW Method. ***Transportation Research Record***. 1196, 133-150.

59. Neducza, B. **2007**. Stacking of surface waves. ***Geophysics***. 72(2), 51-58.

60. Ohrnberger, M., Schissele, E., Cornou, C., Bonnefoy-Claudet, S., Wathelet, M., Savvaidis, A., Scherbaum, F., and Jongmans, D. **2004**. Frequency wavenumber and spatial autocorreltation methods for dispersion curve determination from ambient vibration recordings. ***Proceedings of the 13th World Conference on Earthquake Engineering***, Vancouver, Canada, pp. 1-15.

61. Okada, H. **2003**. The microtremor survey method. ***Geophysical Monograph Series***. Society of Exploration Geophysicists (SEG), Tulsa.

62. Okada, H., and Sakajiri, N. **1983**. Estimates of an S-wave velocity distribution using long-period microtremors. ***Geophysical Bulletin of Hokkaido University***. 42, 119–143.

63. Okada, H., Matsushima, T., Moriya, T., and Sasatani. T. **1990**. An exploration technique using long-period microtremors for determination of deep geological structures under urbanized areas. ***Geophysical Exploration***. 43, 402–417.

64. Olea, R. A**. 1974**. Optimal contour mapping using universal kriging**. Journal of Geophysical Research.** 79(5), 695-702.

65. Park, C. B. **2011**. Imaging dispersion of MASW data-full *vs.* selective offset scheme. ***Journal of Environmental and Engineering Geophysics***. 16(1), 13-23.

66. Park, C. B., and Miller, R. D. **2008**. Roadside passive multichannel analysis of surface waves (MASW). ***Journal of Environmental and Engineering Geophysics***. 13(1), 1-11.

67. Park, C. B., Miller, R. D., and Miura, H. **2002a**. Optimum field parameters of an MASW survey. ***Japanese Society of Exploration Geophysics (SEG-J)***, Extended Abstracts. 1-6.

68. Park, C. B., Miller, R. D., and Ivanov, J. **2002b**. Filtering surface waves. ***Symposium on the Application of Geophysics to Engineering and Environmental Problems***. Society of Exploration Geophysicists. SEI9, 1-10.

69. Park, C. B., Miller, R. D., and Ryden, N. **2006**. Roadside seismic survey utilizing traffic noise. ***Proceedings of the NDE Conference on Civil Engineering***, St. Louis, MO. 317-324.

70. Park, C. B., Miller, R. D., and Xia, J. **1998**. Imaging dispersion curves of surface waves on multi-channel record. ***Proceedings of the 68th Annual International Meeting of Society of Exploration Geophysics***, Expanded Abstract. 1377-1380.

71. Park, C. B., Miller, R. D., and Xia, J. **1999**. Multichannel analysis of surface waves. ***Geophysics***. 64(3), 800-808.

72. Park, C. B., Miller, R. D., and Xia, J. **2001**. Offset and resolution of dispersion curve in Multichannel analysis of surface waves (MASW). ***Proceeding of the SAGEEP***. SSM4. 1-6.

73. Park, C. B., Miller, R. D., Laflen, D., Neb, C., Ivanov, J., Bennett, B., and Huggins, R. **2004**. Imaging dispersion curves of passive surface waves. ***74th Annual International Meeting, SEG Technical Program Expanded Abstracts***. 1357-1360.

74. Park, C. B., Miller, R. D., Ryden, N., Xia, J., and Ivanov, J. **2005**. Combined use of active and passive surface waves. ***Journal of Environmental and Engineering Geophysics***. 10(3), 323-333.

75. Park, C. B., Miller, R. D., Xia, J., and Ivanov, J. **2007**. Multichannel analysis of surface waves (MASW)-Active and passive methods. ***The Leading Edge***. 26, 60-64.

76. Proakis, J. G., and Manolakis, D. G. **2007**. ***Digital Signal Processing: Principles, Algorithms and Applications***. 4th Edition, Prentice-Hall/Pearson Education, Englewood Cliffs.

77. Roesset, J. M., Chang, D. W., Stokoe II, K. H., and Aouad, M. **1989**. Modulus and thickness of the pavement surface layer from SASW tests. ***Transportation Research Record***. 1260, 53-63.

78. Ryden, N., and Lowe, M. J. **2004**. Guided wave propagation in three-layer pavement Structures. ***Journal of the Acoustical Society of America***. 116, 2902-2913.

79. Ryden, N., and Park, C. B. **2006**. Inversion of surface waves using phase velocity spectra. ***Geophysics***, 71(4), 49-58.

80. Ryden, N., Park, C. B., Ulriksen, P., and Miller, R. D. **2004**. Multimodal approach to seismic pavement testing. ***Journal of Geotechnical and Geoenvironmental Engineering, ASCE***, 130, 636-645.

81. Sanchez-Salinero, I., Roesset, J. M., Shao, K. Y., Stokoe II, K. H., and Rix, G. J. **1987**. Analytical Evaluation of Variables Affecting Surface Wave Testing of Pavements. ***Transportation Research Record***. 1136, 86–95.

82. Sauvin, G., Vanneste, M., O'Connor, P., O'Rourke, S., O'Connell, Y., Lombard, T., and Long, M. **2016**. Impact of data acquisition parameters and processing techniques on S-wave velocity profiles from MASW- Examples from Trondheim, Norway. ***Proceedings of the 17th Nordic Geotechnical Meeting Challenges in Nordic Geotechnic***, Reykjavik. 1-10.

83. Schultz, P. S., and Claerbout, J. F. **1978**. Velocity estimation and downward continuation by wavefront synthesis. ***Geophysics***. 43, 691-714.

84. Schwab, F., and Knopoff, L. **1972**. Fast Surface Wave and Free Mode Computations. ***Methods of Computational Physics***. 11, 87-180.

85. Shtivelman, V. **2002**. Surface wave sections as a tool for imaging subsurface in homogeneities. ***European Journal of Environmental and Engineering Geophysics***. 7, 121-138.

86. Shtivelman, V. **2003**. Using surface waves for studying the shallow subsurface. ***Bollettino di Geofisica Teorica ed Applicata***. 44, 223-236.

87. Socco, L. V. and Boiero, D. **2008**. Improved Monte Carlo inversion of surface wave data. ***Geophysical Prospecting***, 56, 357-371.

88. Socco, L.V., Boiero, D., Foti, S., and Wisen. R. **2009**. Laterally constrained inversion of ground roll from seismic reflection records. ***Geophysics***. 74, 35-45.

89. Socco, L.V., Foti, S., and Boiero, D. **2010**. Surface-wave analysis for building near-surface velocity models -Established approaches and new perspectives. ***Geophysics***. 75, 75A83-75A102.

90. Song, X., Gu, H., Liu, J., and Zhang, X. **2007**. Estimation of shallow subsurface shear-wave velocity by inverting fundamental and higher-model Rayleigh waves. ***Soil Dynamics and Earthquake Engineering***, 27, 599-607.

91. Song, Y. Y., Castagna, J. P., Black, R. A., and Knapp, R. W. **1989**. Sensitivity of near surface shear wave velocity determination from Rayleigh and Love waves. ***Proceedings of the 59th Annual International Meeting, Society of Exploration Geophysicist***. Expanded Abstracts. PoS5, 509-512.

92. Srinivas, G. S., Govardhan, K., Narsimhulu, C. H., and Seshunarayana, T. **2014**. Estimation of shear wave velocity in drifts using multichannel analysis of surface wave (MASW) technique-A case study from Jammu & Kashmir, India. ***Journal of the Geological Society of India***. 84, 174-180.

93. Stephenson, W. J., Louie, J. N., Pullammanappallil, S., Williams, R. A., and Odum, J. K. **2005**. Blind shear-wave velocity comparison of ReMi and MASW results with boreholes to 200 m in Santa Clara Valley: Implications for Earthquake Ground-Motion Assessment. ***Bulletin of the Seismological Society of America***. 95(6), 2506-2516.

94. Stokoe II, K. H., and Nazarian, S. **1983**. Effectiveness of Ground Improvement from Spectral Analysis of Surface Waves. ***Proceedings of the 8th European Conference on Soil Mechanics and Foundation Engineering***, Helsinki, Finland. 1, 91-94.

95. Stokoe II, K. H., Wright, S. G., Bay, J. A., and Roesset, J. M. **1994**. Characterization of geotechnical sites by SASW method, in Geophysical characterization of sites. ***ISSMFE Technical Committee#10 by R. D Woods***, Oxford Publishers .15-25.

96. Tarantola, A. **2005**. ***Inverse Problem Theory and Methods of Model Parameter Estimation***. SIAM, Philadelphia.

97. Tian, G., Steeples, D. W., Xia, J., and Spikes, K. T. **2003b**. Useful resorting in surface wave method with the autojuggie. ***Geophysics***. 68(6), 1906-1908.

98. Tian, G., Steeples, D. W., Xia, J., Miller, R.D., Spikes, K. T., and Ralston, M. D. **2003a**. Multichannel analysis of surface wave method with the autojuggie. ***Soil Dynamics and Earthquake Engineering***. 23, 243-247.

99. Van der Poel, C. **1951**. Dynamic testing of road constructions. ***Journal of Applied Chemistry***. 1, 281-290.

100. Wood, C.M., and Cox, B. R. 2012. A comparison of MASW dispersion uncertainty and bias for impact and harmonic sources: ***Proceedings of the GeoCongress, ASCE***. 2756-2765.

101. Xia, J. H., Xu, Y. X., and Miller, R. D. **2007**. Generating an image of dispersive energy by frequency decomposition and slant stacking. ***Pure and Applied Geophysics***. 164, 941-956.

102. Xia, J., Miller, R. D., and Park, C.B. **1999**. Estimation of near-surface shear-wave velocity by inversion of Rayleigh waves. ***Geophysics***. 64(3), 691-700.

103. Xia, J., Miller, R. D., Park, C. B., and Ivanov, J. **2004**. Utilization of high-frequency Rayleigh waves in near-surface geophysics. ***The Leading Edge***. 23(8), 753-759.

104. Xia, J., Miller, R. D., Park, C. B., and Tian, G. **2003**. Inversion of high frequency surface waves with fundamental and higher modes. ***Journal of Applied Geophysics***. 52, 45-57.

105. Xia, J., Miller, R. D., Park, C.B., and Ivanov, J. **2000**. Construction of 2-D vertical shear-wave velocity field by the Multichannel Analysis of Surface Wave technique. ***Proceedings of the Symposium on the Application of Geophysics to Engineering and Environmental Problems (SAGEEP 2000)***, Arlington. 1197-1206.

106. Xia, J., Miller, R. D., Xu, Y., Luo, Y., Chen, C., Liu, J., Ivanov, J., and Zeng, C. **2009.** High-frequency Rayleigh-wave method. ***Journal of Earth Science***, 20(3), 563-579.

107. Xu, Y., Xia, J., and Miller, R. D. **2006**. Quantitative estimation of minimum offset for multichannel surface-wave survey with actively exciting source. ***Journal of Applied Geophysics***. 59, 117-125.

108. Yamanaka, H., and Ishida, H. **1996**. Application of genetic algorithms to an inversion of surface-wave dispersion data. ***Bulletin of the Seismological Society of America***. 86(2), 436-444.

109. Yilmaz, O., and Eser, M. **2002**, A unified workflow for engineering seismology. ***Proceedings of the 72nd Annual Meeting SEG***, Salt Lake City UT. 1496-1499.

110. Yuan, D., and Nazarian, S. **1993**. Automated surface wave method: Inversion Technique. ***Journal of Geotechnical Engineering, ASCE***, 119(7), 1112-1126.

111. Zhang, S. X., Chan, L. S., and Xia, J. **2004**. The Selection of Field Acquisition Parameters for Dispersion Images from Multichannel Surface Wave Data. ***Pure and Applied Geophysics***. 161, 185-201.

Web Resources

112. https://en.wikipedia.org/wiki/Image_resolution (Last accessed: 28.08.2018)

113. http://www.dadisp.com/webhelp/dsphelp.htm#mergedprojects/refman2/FncrefAE/BESSEL.htm (Last accessed: 28.08.2018)

114. http://masw.com/ACQParaTables.html (Last accessed: 28.08.2018)

115. www.masw.com (Last accessed: 28.08.2018)

LIST OF PUBLICATIONS

Manuscript Published:

Journals

1. Taipodia, J., Dey, A. and Baglari, D. (**2018**) "Influence of signal preprocessing parameters on the resolution of dispersion image in active MASW survey" ***Journal of Geophysics and Engineering***. (Manuscript Accepted) (DOI: 10.1088/1742-2140/aaaf4c)

2. **Taipodia, J**., Baglari, D. and Dey, A. (**2018**) "Recommendations for generating dispersion images of optimal resolution from Active MASW survey" ***Innovative Infrastructure Solutions***, Vol. 3, Article 14, pp. 1-19. (DOI: 10.1007/s41062-017-0120-5)

3. **Taipodia, J.,** Baglari, D. and Dey, A. (**2017**). **"**Resolution of dispersion image obtained from active MASW survey" ***Disaster Advances***, Vol. 10(11), pp 34-45.

Book Sections

1. **Taipodia, J.** and Dey, A. (**2018**) "Impact of strike energy on the resolution of dispersion images in active MASW survey" ***Multi-physics Processes in Soil Mechanics and Advances in Geotechnical Testing***, Proceedings of the GeoShanghai 2018, Shanghai, China, Ed. L. Hu, X. Gu, J. Tao and A. Zhao, Springer, Singapore, pp. 419-427: ISBN No. 978-981-13-0094-3.

Conferences

1. **Taipodia, J.** and Dey, A. (**2018**) "Impact of data preprocessing parameters on the accuracy of the inverted Vs profile in MASW" ***International Conference on Advances in Concrete, Structural & Geotechnical Engineering (ACSGE - 2018)***, BITS Pilani, India, pp. 1-6.

2. **Taipodia, J.** and Dey, A. (**2017**) "Impact of offset on the resolution of dispersion image in active MASW survey" *Geotechnics for Natural and Engineered Sustainable Technologies:* ***Indian Geotechnical Conference (GeoNEst: IGC-2017)***, Guwahati, India, pp. 1-4.

3. **Taipodia, J.** and Dey, A. (**2017**) "Impact of frequency filtering and temporal muting on the resolution of dispersion image" ***13th International Conference on Vibration Problems (13ICOVP)***, Guwahati, India, pp. 1-11.

4. Dey, A., Mukherjee, M., **Taipodia, J**., Baglari, D. and Biswas, S. (**2017**). "Non-invasive Geophysical Investigation for Subsurface Profiling in Urbanized Megacities" Extended Abstract: ***Proceedings of the 2nd Korea-India Joint Geotechnical Workshop***, Seoul, South Korea, pp. 9-10.

5. **Taipodia, J.,** Baglari, D., Biswas, S. and Dey, A. (**2015**). "Dispersion analysis using active MASW survey data" ***Indian Geotechnical Conference: IGC 2015***, Pune, India, pp. 1-9.

6. **Taipodia, J.,** Bishnoi, B. R., Baglari, D., Murali Krishna, A. and Dey, A. (**2014**). "Geophysical investigations for identification of subsurface stratigraphy at IIT Guwahati" ***Indian Geotechnical Conference (IGC-2014)***, Kakinada, India, pp. 219-226.

7. **Taipodia, J.,** Prakash Babu, K., Kiran, B. and Dey, A. (**2014**). "Subsurface Characterization using MASW: Preliminary Experimentation and Analysis" ***National Conference on Recent Advances in Civil Engineering: NCRACE-2013***, Nirjuli, pp. 1-7.

8. **Taipodia, J.** and Dey, A. (**2012**). "A Review of Active and Passive MASW Techniques" ***EGCEG 2012, National Workshop on Engineering Geophysics for Civil Engineering and GeoHazards***, Roorkee, India, pp. 1-12.

Manuscript under Review

Journals

1. **Taipodia, J.,** Dey, A. and Baglari, D. (…). "Effect of source characteristics on the resolution of dispersion image from active MASW survey", ***Indian Geotechnical Journal***, Springer. (Revised Manuscript Communicated)

2. **Taipodia, J.**, Madhulatha, B., Dey, A., Acharyya, R. and Sarma, C. P. (…) "1-D and 2-D active MASW survey for subsurface profiling of Jia Bharali riverbed for a proposed 1.2 km road bridge" ***Geoscience Frontiers***. (Manuscript communicated).

3. **Taipodia, J.**, Dey, A., Gaj, S. and Baglari, D. (…) "Quantification of the resolution of dispersion image in active MASW survey and automated extraction of dispersion curve" ***Computers and Geosciences***. (Manuscript communicated).

4. **Taipodia, J.**, Dey, A. and Baglari, D. (…) "Influence of receiver layout on active masw survey conducted at different sites having varying substrata characteristics" *Journal of* ***Arabian Journal of Geosciences***. (Manuscript communicated).

Conferences

1. **Taipodia, J.**, Madhulatha, B. and Dey, A. (2018) "Influence of stacking on the resolution of the dispersion image in Active MASW survey" *Indian Geotechnical Conference,* Bangalore, India (Full Manuscript Communicated).

2. Boga, M., **Taipodia, J.** and Dey, A. (2019) "Active MASW Roll-along Survey and 2D Ground Response Analysis of a Bridge Site" ***IACMAG Symposium***, Gandhinagar, India. (Abstract Communicated)

Manuscript under Preparation

Journals

1. **Taipodia, J.** and Dey, A. (…). "Impact of extraction and inversion parameters on the accuracy of inverted V_S profile in active MASW survey", ***Near Surface Geophysics***, EAGE

2. **Taipodia, J.** and Dey, A. (2017). "Optimal parameters for generating dispersion images from Active MASW survey in soft soil sites" ***Pure and Applied Geophysics***, Springer

3. **Taipodia, J.,** Madhulatha, B., Talukdar, P., Jana, A. and Dey, A. (…). "Investigation of stiffness characteristics of earth embankment using Active MASW survey" ***Journal of Performance of Constructed Facilities***, ASCE

4. **Taipodia, J.,** Acharyya, R., Sarma, C. P., Murali Krishna, A. and Dey, A. (…). "Estimation of shear wave velocity profile of a failed slope using Active MASW and Cross-Hole surveys" ***International Journal of Geotechnical Engineering***, Taylor and Francis

APPENDIX-I

WORKING STEPS OF SURFSEIS

This following sections lists the working steps of SURFSEIS for carrying out dispersion analysis on the collected wavefields, and subjecting to further inversion analysis to obtain the 1-D or 2-D shear wave velocity profiles of the subsurface.

A1 Step 1: Data acquisition and Format (SEG-2)

MASW requires a multichannel record with at least 12 traces to produce reliable results. A weight drop, specifically a sledge hammer, is normally employed as the seismic source. Although its weight and impact velocity can vary, a hammer of 5 to 10 kilograms is usually sufficient for investigations within a few tens of meters of the ground surface. Low-frequency geophones (from an engineering perspective) are essential. Usually 4.5 Hz geophones are adequate for investigation in the few tens of meters. The source offset (X_1) (distance between source and the first closest geophone) needs to be large enough (X_n) to assure efficient generation of surface waves that extend down to the primary depth range of interest. Fig.A.1 shows the main window display once SURFSEIS is opened. The data acquired in the field is in the format of SEG in the seismogram. Once the utility button is clicked, a pop up window appears where the SEG file can be opened as shown in Fig. A.2.

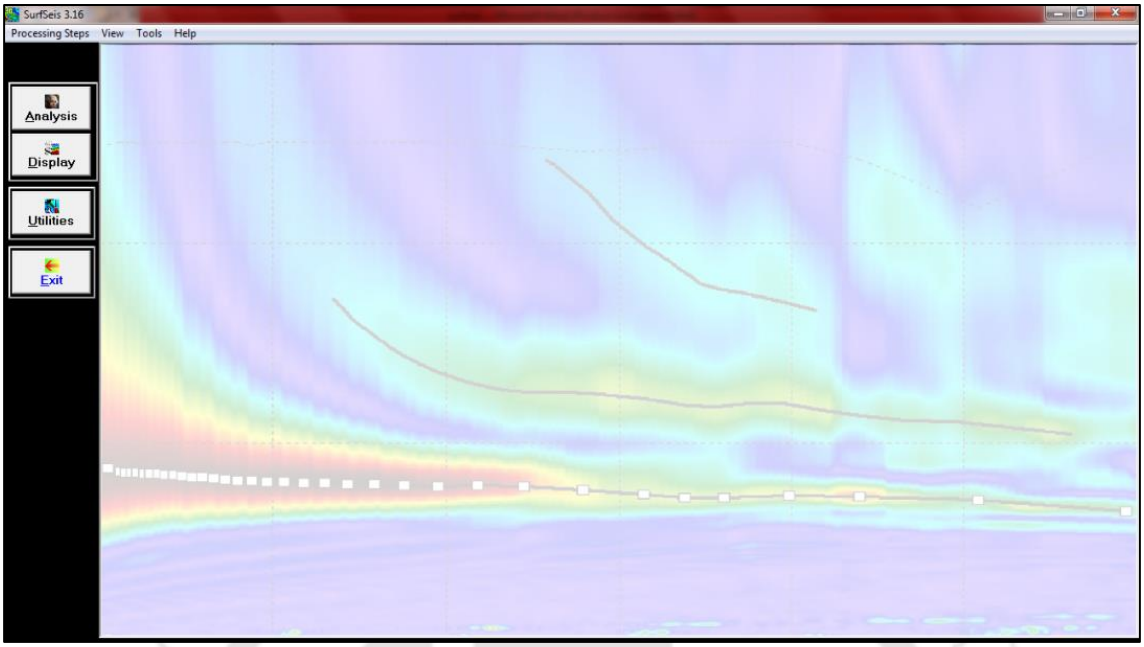

Fig. A.1: Main window display of SURFSEIS

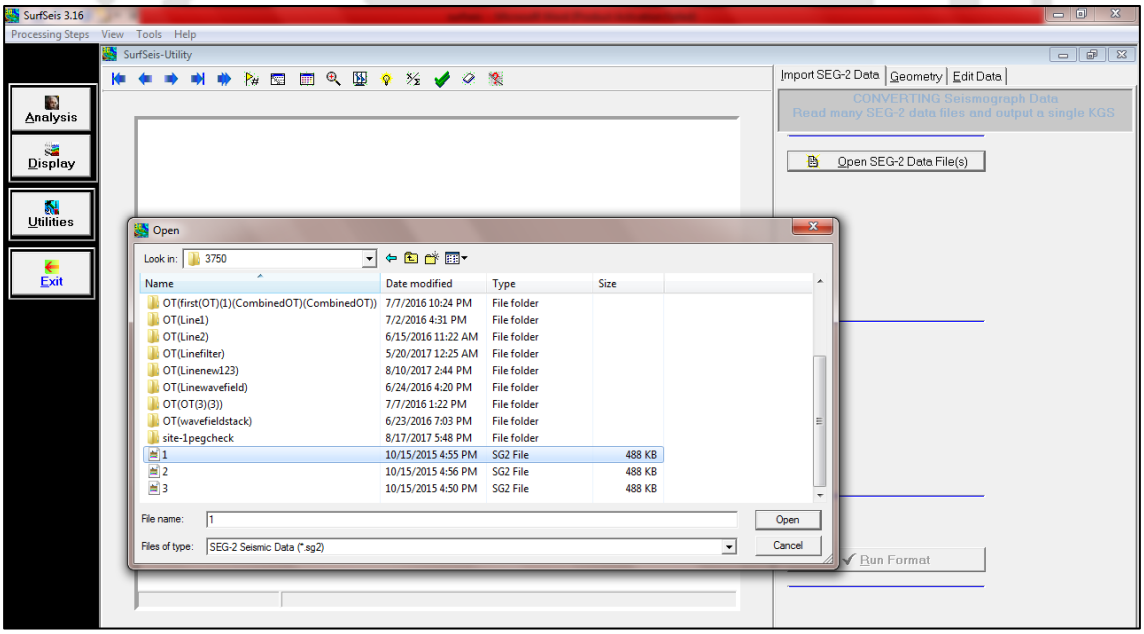

Fig. A.2: Pop-up window facilitating to open the SEG files.

A1.1 Data Format

Most engineering seismographs give output in SEG-2 format. Other output options will generally be SEG-Y. Processing of seismic data requires organization of the information within the trace in a very structured form. Most seismic processing packages use data in SEG-Y or a slightly modified version of SEG-Y. SURFSEIS uses the same modified SEG-Y data format used by WINSEIS and WINSEIS TURBO. This modified form of SEG-Y is a trace-by-trace sequential and possesses a fixed header length followed by the recorded data. Conversion routines and processing formats are available for most seismographs.

Trace headers, sample resolution, and data order designate the format of a seismic data file. SURFSEIS reads and writes data in the KGS-modified SEG-Y format. This data format is unique and requires conversion before anything can be done with or to the data, regardless of whether it came directly from a seismograph or other processing software. Several data formats are presently being used by commercial seismograph manufacturers. The engineering "standard" is designated as SEG-2. Conversion of data files requires the user to double click the format/header icon and select the appropriate conversion routine. Since the majority of modern engineering seismographs are using SEG-2, reference will be made primarily to that format. The general flow of all conversion routines is the same, so little would be gained by going through each individually. Information required from the user includes input file names (usually one file name for each shot gather or field file), output file name (SURFSEIS, as most processing routines, handles all the field files from a particular line as a single file), and source sequence number (SSN).

A2 Step 2: Field Geometry Encoding

The station number, offset distance and the receiver spacing is numbered in the field geometry encoding, as shown in Fig. A.3. Offset distance is the distance between the source and first geophone, and receiver spacing signifies the inter-receiver spacing. The station number is the number allotted to geophone or traces for better identification of the location of traces. After the geometry is applied, the data can be visualized and is ready for next step of dispersion analysis, as shown in Fig. A.4.

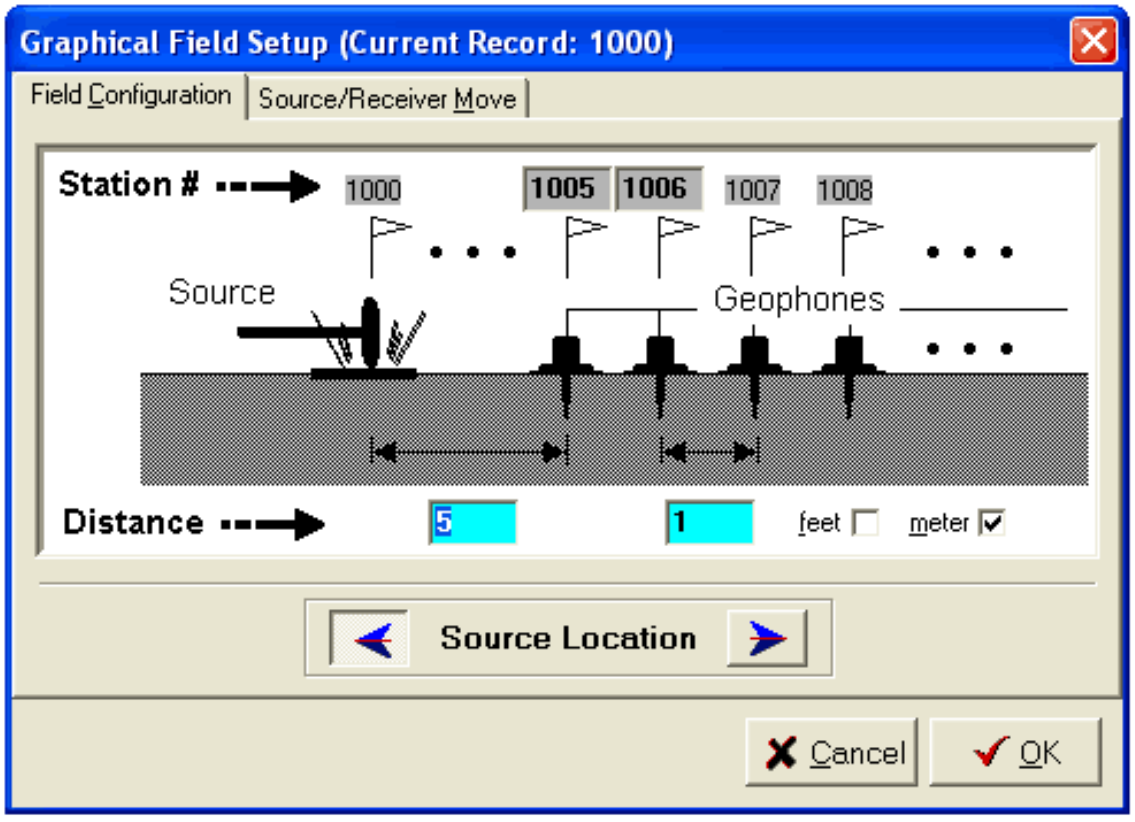

Fig. A.3: Pop-up window for field geometry encoding

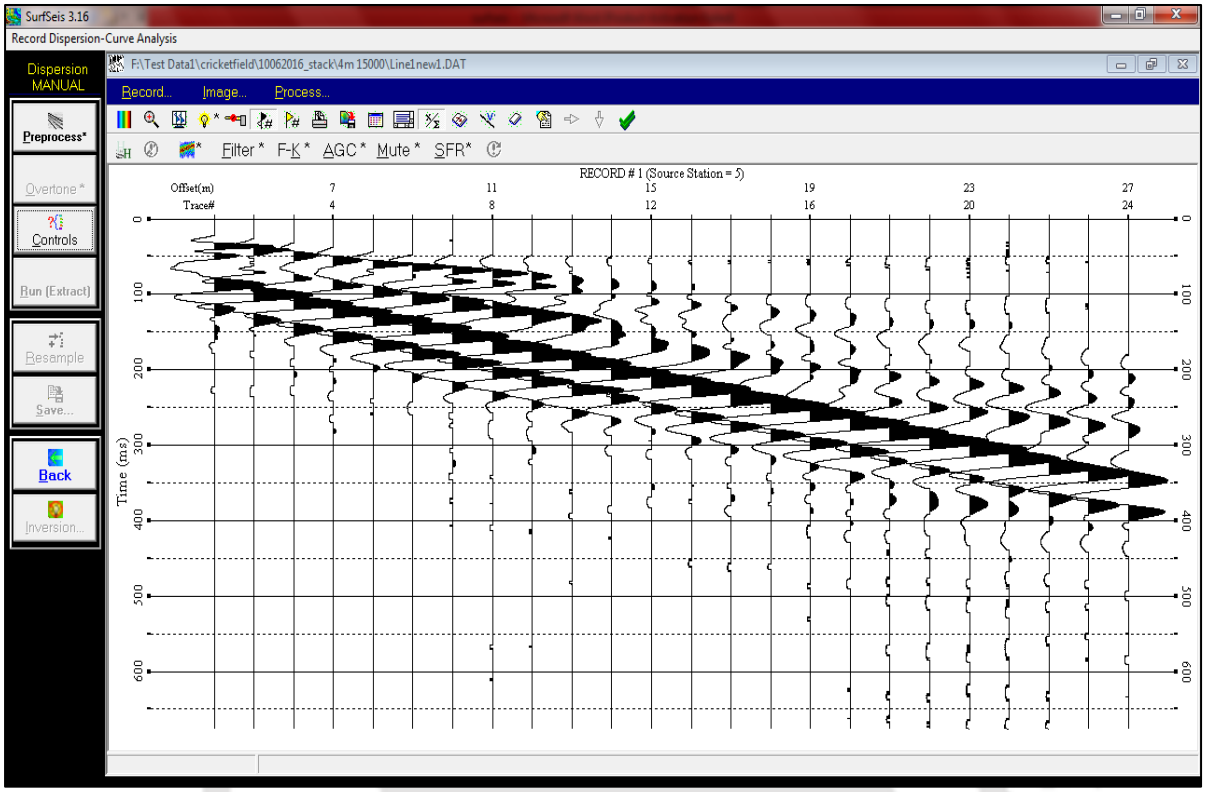

Fig. A.4. Visualization of raw data after encoding field geometry

A3 Step 3: Generation of Dispersion Image or Overtone Data

The "***Dispersion***" option in the analysis section gives complete flexibility to determine key processing parameters. It also provides a way to construct dispersion images considering all types of propagating dispersive waves, regardless of whether they are body or surface waves. Contamination by higher-mode surface waves and body waves can be clearly examined using these images. When the "***Dispersion***" button is pressed, a dialog box pops up that allows selecting a file containing multichannel seismic record(s). The file may contain one or more records and can process one record at a time, or sequentially as a group.

A3.1 Data Preprocessing

When the ***Preprocess*** button is clicked, the program tries to estimate the following two data characteristics:

1. Optimum range and increment of frequency.
2. Optimum (upper and lower) bounds of phase velocity.

Figure 3.14 shows the raw amplitude spectra. Below the amplitude spectra, four variants of filter namely, Band-cut, Low-cut, High-cut and Band-pass, are highlighted. There are radio buttons to select the range of frequency and phase velocity as overtone generator as shown in Fig. A.5. After the application o suitable filtering, the same set of data can undergo muting operation, and then the data is processed as shown in Fig. A.6. After preprocessing, the data is ready for overtone, where dispersion images will be created the data will be saved as the OT file in .dat format.

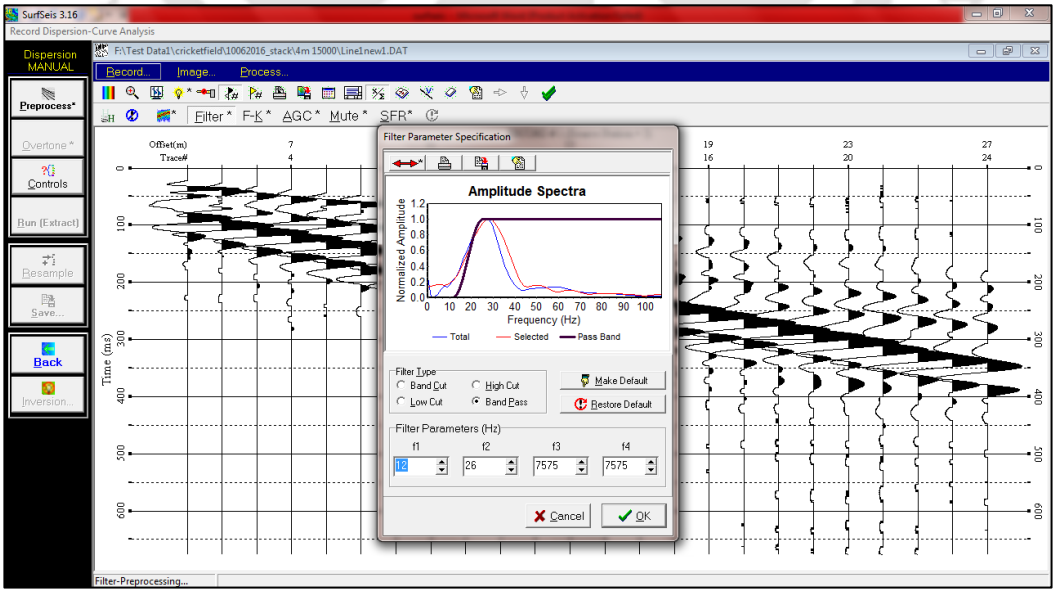

Fig. A.5: Visualization of amplitude spectra and choice of suitable filter

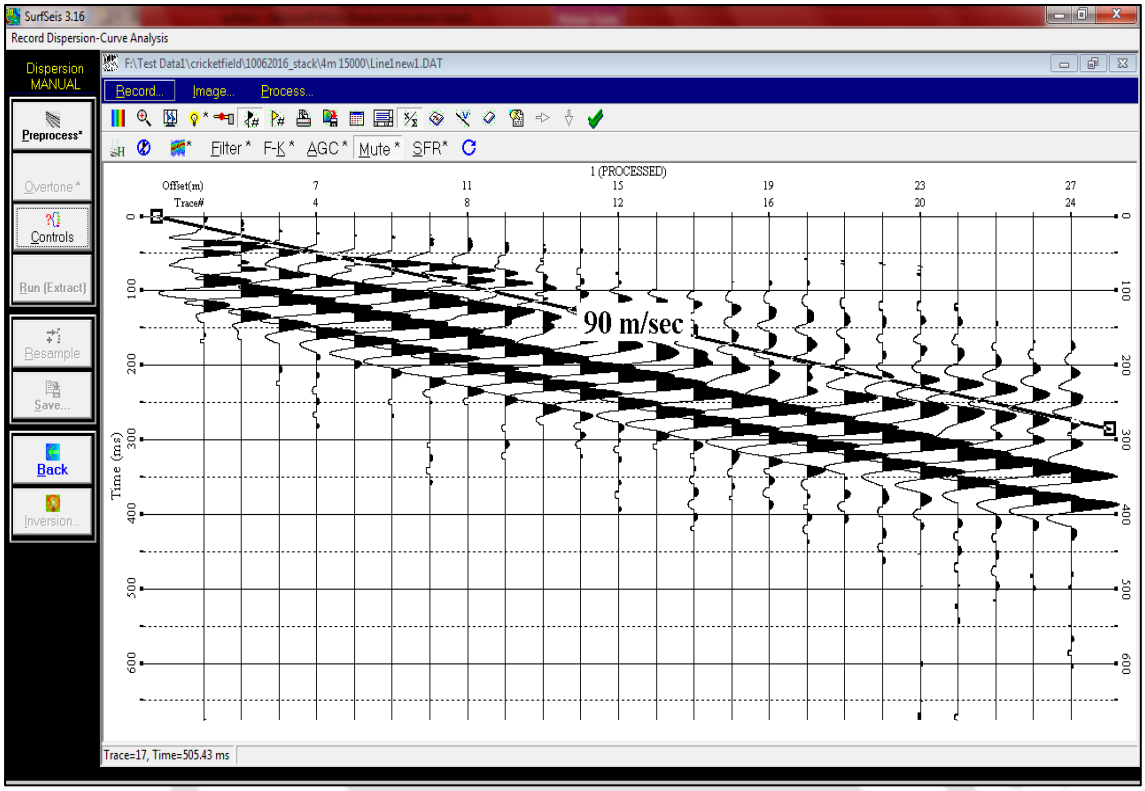

Fig. A.6: Muting of raw or filtered records

A3.2 Overtone

Overtone analysis is a tool for identifying changing propagation velocity patterns with frequency for all types of seismic events (both signal and noise events). This method is based on 2-D pattern recognition (Park *et al*. 1999) and is by far the most-unbiased way of delineating phase velocity information. It is probably most useful in identifying surface wave of higher modes (overtones). A seismic record contains surface waves and body waves. A good quality record is defined as a record in which the surface wave energy dominates body wave energy. However, there is always the presence of body-wave energy coincident with the surface waves, however insignificant it may be.

Overtone analysis is the best way to observe the dispersive nature of any type of seismic wave without the bias associated with event interpretations. Fundamental principles of this analysis (Park *et al*. 1999) are quite straightforward. This type of analysis basically attempts to construct a wiggle-trace image where local amplitude maxima trends represent possible dispersive energy (i.e., fundamental and higher modes). This is accomplished by examining all possible phase velocities for all frequencies being considered. Figure A.7 shows the pre-processed data which is ready for overtone. Before clicking the overtone button, there are control parameters (Fig. A.8) for the processing such as frequency and the phase velocity range which need to be addressed first. Figure A.9 shows the typically obtained dispersion images. The obtained images show normalized amplitude of different percentage which is represented in color bar. The darkest color consist the 100 % amplitude which means that the dark black color is the representation of the highest energy.

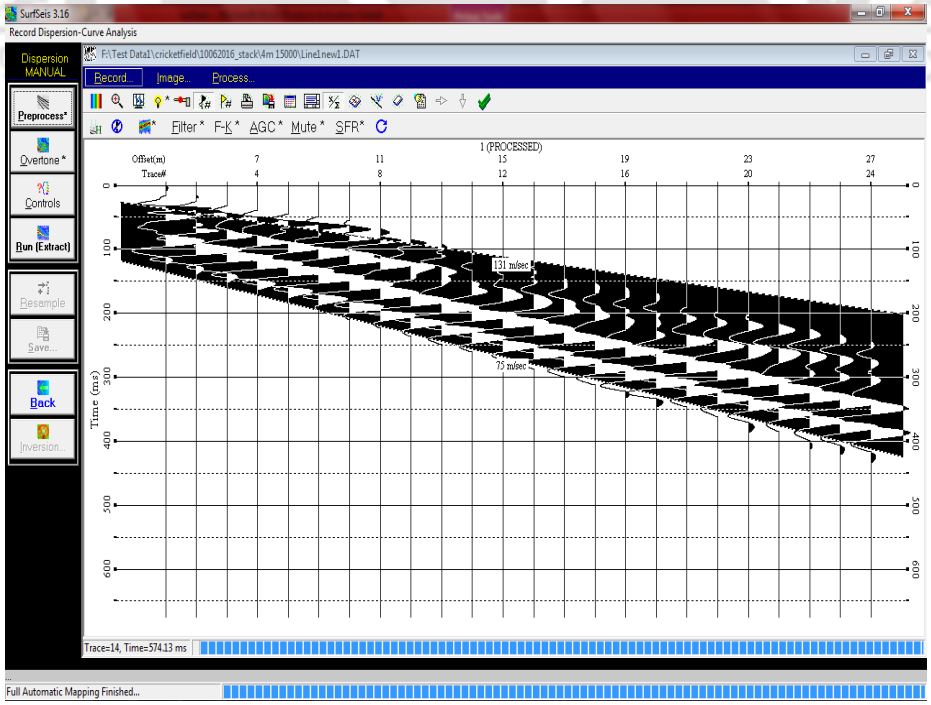

Fig. A.7: Overtone processing and muting by noise-cone technique

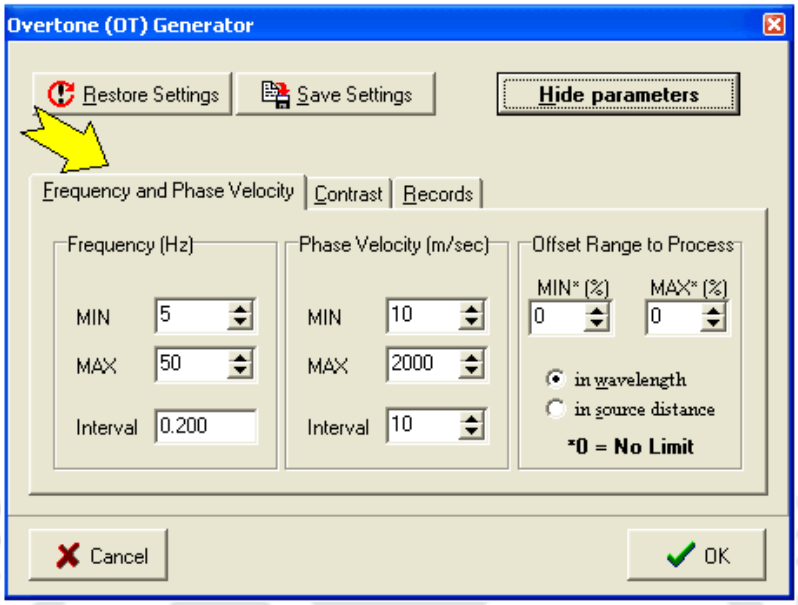

Fig. A.8: Parameters controlling overtone processing

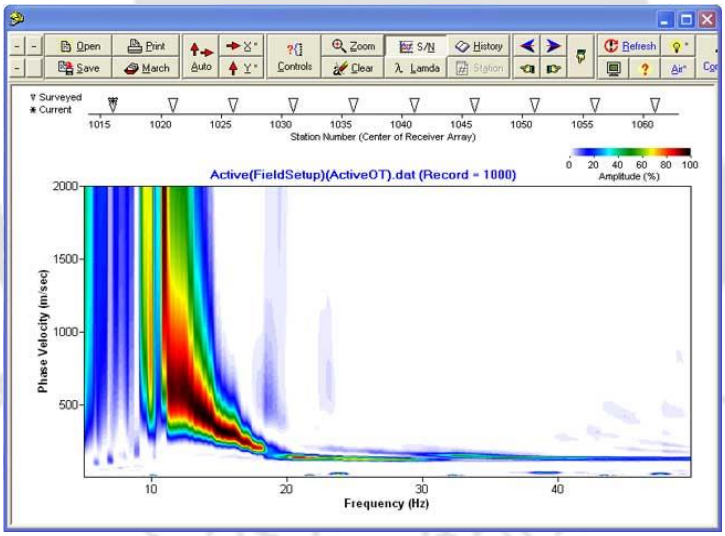

Fig. A.9: A typical dispersion image obtained after overtone analysis

A4. Step 4: Extraction of Dispersion Curve(s)

Dispersion points are manually selected from the darkest color band, as shown in Fig. A.10, to be representing the dispersion curve, and the same is used as input for initial layer model in the

subsequent inversion analysis to obtain the shear wave velocity profile. The number points picked and curve smoothening can be carried out as shown in Fig. A.11.

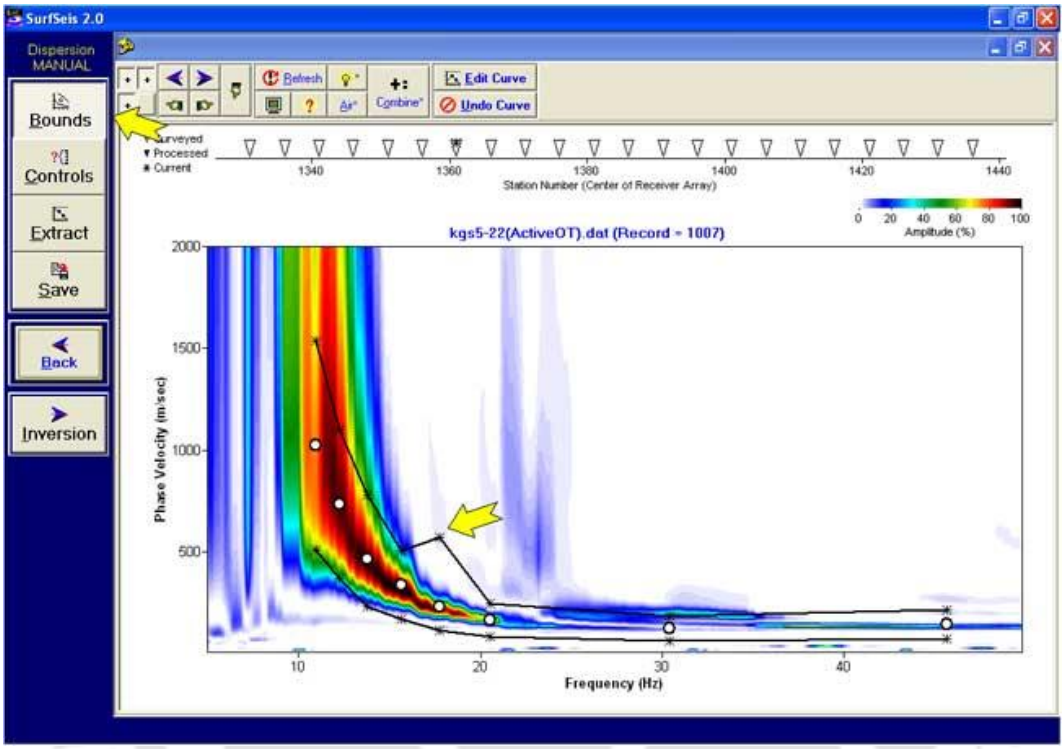

Fig. A.10: Extraction of points from dispersion curve by manual selection of dispersion points

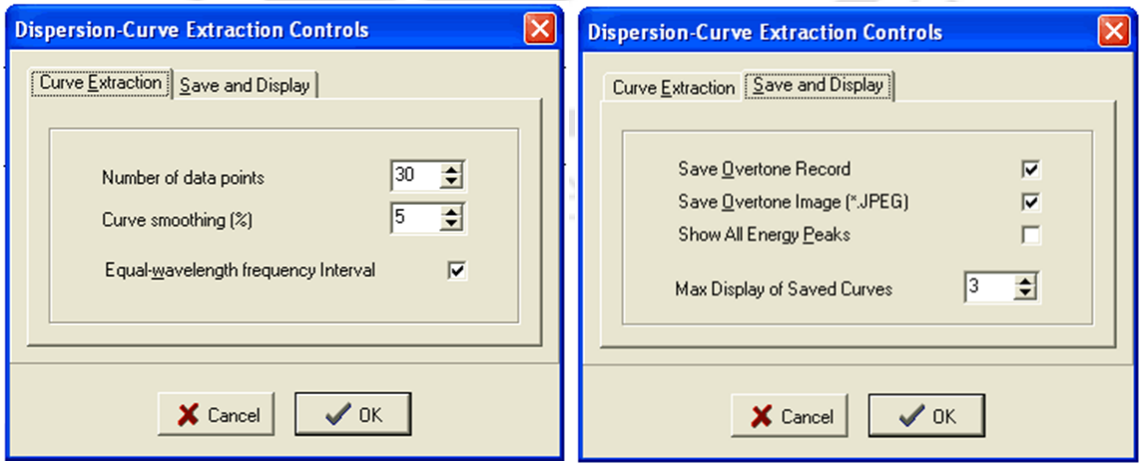

Fig. A.11: Parameters controlling extraction of the dispersion curve

A5. Step 5: Inversion of Extracted Dispersion Curves

Inversion of the extracted dispersion curve uses the phase velocity with frequency curve as a reference to estimate the vertical shear wave velocity (V_s) structure of near-surface materials. The inversion algorithm in SURFSEIS has been adopted from Xia *et al*. (1999). The most commonly used inversion method uses an initial model before actually beginning to search (iterate) for the convergent solution. An initial model consists of several key parameters: shear wave velocity (V_s), primary wave velocity (Vp), density (ρ), and the stratum thickness (h) of the various layers in the earth model. Using this set of parameters, the program begins searching for a solution, continuously converging in an iterative fashion on the most probable values. The S-wave velocity (V_s) is most sensitive and influential to the surface wave phase velocity. Influence of all other types of parameters can usually be neglected as long as they have been reasonably estimated.

The initial S-wave velocity (Vs) model is approximated from the measured dispersion curve. The initial P-wave velocity (Vp) model is determined using this Vs model and a constant Poisson's ratio of 0.4. A density of 2.0 g/cc is assigned to all layers of the earth model. The maximum depth of investigation is determined from the longest surface wave wavelength measured from the dispersion curve. The stratification thickness, or the layer model, is then created by successively increasing the thickness of each layer as its depth increases, to the maximum depth of investigation. A ten-layer model is initially assigned. The iterative inversion procedure can continue uninterrupted unless a stopping criterion is imposed. Two types of termination criteria are commonly used: maximum number of iteration (I_{max}) and maximum root-mean-square error (RMSE).

When the "***Inversion***" button is selected, a dialog box appears, allowing selection of dispersion curve file(s). A single file or multiple files to be processed in succession can be defined. Once an input file is selected, an initial model is created using phase velocities in the input file and the preset parameters. The initial S-wave velocity (*Vs*) model is displayed along with the input dispersion curve. The dispersion curve is also displayed, but with an inverted frequency axis so that general trend in the S-velocity (V_s) model and dispersion curve match in an approximate sense. The P-wave velocity (*Vp*) model and other parameters (e.g., density) can be displayed using appropriate buttons and tabs. Actual values of the parameters can be viewed and changed using the "***Layer Model***" option. Radio buttons available at this stage of the process include *Run*, *Controls*, *Layer Model*, and *Back*.

A5.1 Stopping Criteria

The inversion is terminated when one of the criteria is met: the root-mean-square error (RMSE) or maximum number of iteration (I_{max}). The default setting of RMSE is 3.0, but the optimum value may change based on the input dispersion curve. The default value of I_{max} is set to 30, which will usually exceed the number of iterations necessary to obtain a reasonable solution for S-wave velocity (V_s) profile.

A5.2 Initial Vs Model

The initial V_s model is usually calculated from phase velocities in the input dispersion curve ("***Dispersion Data***" option). This is the only option available if only one dispersion curve is to be inverted. However, if multiple consecutive dispersion-curve files have been selected, the inversion results of a previous record can be used as a "good" approximation of the initial model

for the current inversion. Using a previous profile ("***Previous V_s Inverted***" option) as an initial V_s model, a more accurate result is more likely with fewer examinations (i.e., iterations). If the "Previous V_s Inverted" option is selected, it is necessary that all input dispersion curve files be selected in the consecutive order of acquisition.

A5.3 Run

"***Run***" starts the searching algorithm for a V_s profile whose theoretical dispersion curve matches the experimental dispersion curve obtained from the "Dispersion" analysis. The "match" will be evaluated on the basis of root-mean-square error (RMSE) between the two curves (Xia *et al*. 1999). The inversion algorithm first calculates the theoretical curve using the initial V_s profile (along with other layer parameters previously explained), and subsequently compares the theoretical curve with the experimental curve (from the RMSE perspective). If the estimated RMSE is greater than the minimum RMSE (E_{min}) specified in the "***Controls***" dialog (Fig. A.12), the inversion algorithm will automatically modify the V_s profile (Xia *et al*. 1999) and repeat the procedure by calculating a new theoretical curve. Each round of this searching procedure is called "iteration", and the iterations continue until either E_{min} or maximum number of iterations (I_{max}) is reached.

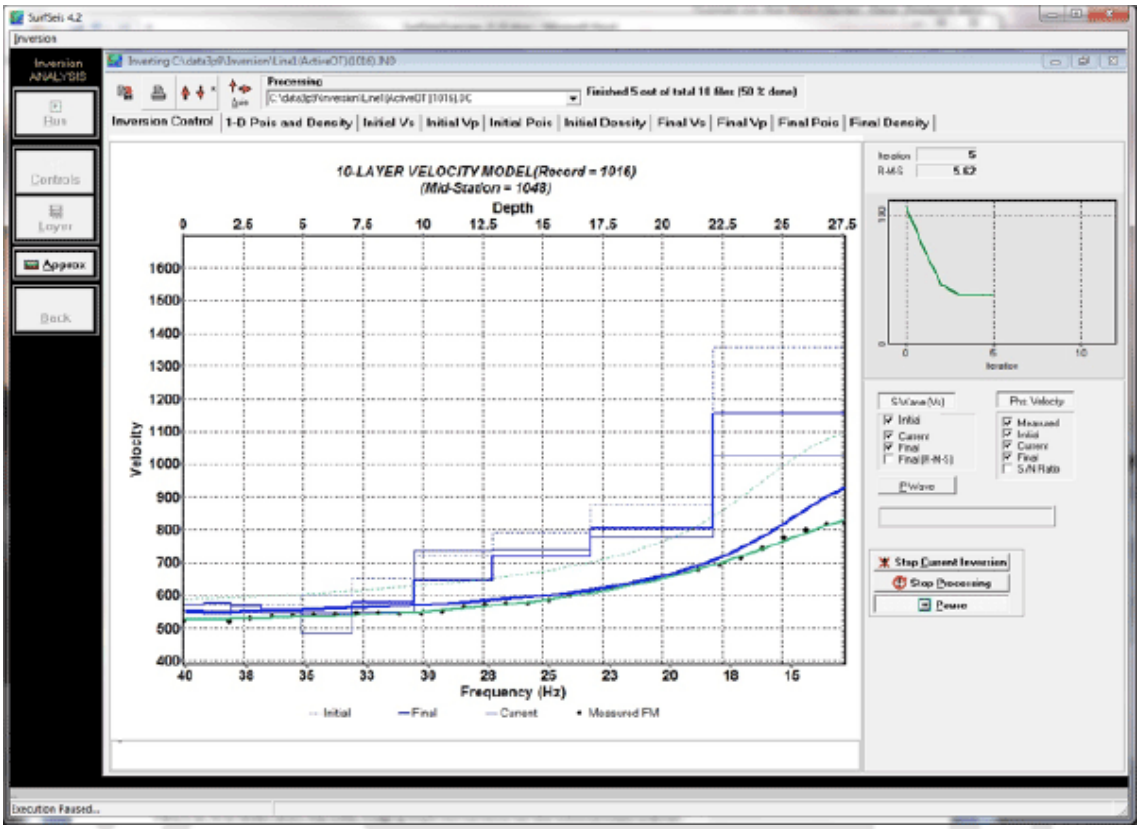

Fig. A.12: Inversion of extracted dispersion curve to obtain the V_S profile with depth

A5.4 Deterministic Inversion of Dispersion Curves

If all extracted dispersion-curves are of the fundamental mode of the Rayleigh wave only, this is the fastest, simplest, and most researched inversion approach to be utilized. When using dispersion curves that have more than one modes (e.g., fundamental mode and one or more higher modes), possible inversion difficulties may arise (i.e., poor fit between observed and calculated curves, high RMS error) as a result of inaccurate mode interpretation (Ivanov *et al*., 2010).

A6 Step 6: Inversion of Curves for 2-D Vs Profile

A typical 2-D V_s model (Fig. A.13) is created when multiple dispersion curves are imported. The output V_s data are calculated based on the wavelength-dependent ratio. This can be a useful tool to quickly evaluate the approximate 2-D V_s distribution over the surveyed and analyzed zone. The 1-D profiles, obtained at regular intervals, are interpolated to produce a 2-D profile. In general, there are many interpolation algorithms available; however, three of them considered in SURFSEIS are bilinear interpolation, simple Kriging and normal Kriging interpolations. There is always a possibility of interpolating externally with the 1-D profiles obtained.

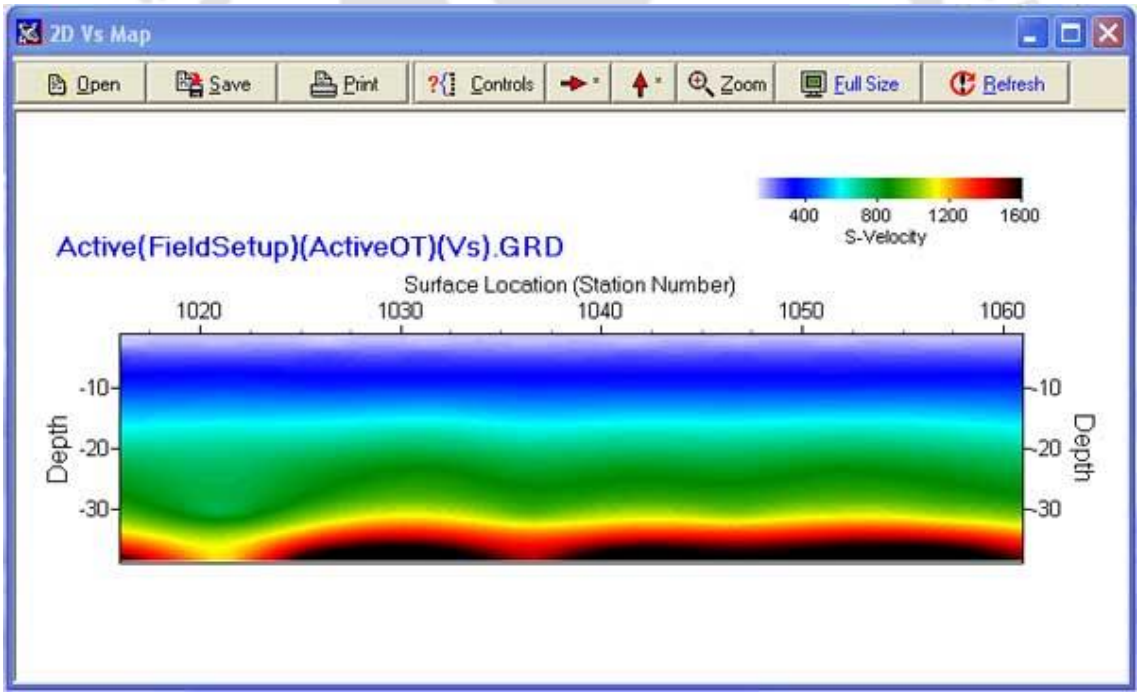

Fig. A.13: A typical 2D V_s profile from inversion analysis